Return of the first inflammasome

Elucidation of NLRP1 inflammasome activation by p38-mediated phosphorylation and ubiquitination

Doctoral thesis

to obtain a doctorate (PhD)

from the Faculty of Medicine

of the University of Bonn

Lea-Marie Jenster

from Emmerich am Rhein, Germany

2024

Written with authorization of

the Faculty of Medicine of the University of Bonn

First reviewer: Prof. Dr. Florian Ingo Schmidt

Second reviewer: Prof. Dr. Natalio Garbi

Day of oral examination: 11.01.2024

From the Institute of Innate Immunity

Director: Prof. Dr. Dagmar Wachten

Table of contents

List of abbreviations

β-TrCP:	β-transducin repeats-containing protein
aa:	Amino acid
AID:	Auxin-inducible degron
AIM2:	Absent in melanoma 2
ALR:	AIM2-like receptor
Aniso:	Anisomycin
ASC:	Apoptosis-associated speck-like protein containing CARD
ATP:	Adenosin triphosphate
BafA:	Bafilomycin A1
BeMeEs:	Bestatin methyl ester
BFV:	Barmah Forest virus
BHK:	Baby hamster kidney
Borte:	Bortezomib
BPE:	Bovine pituitary extract
BSA:	Bovine serum albumin
C1C:	Caspase-1^{CARD}
CARD:	Caspase activating and recruitment domain
CD:	Catalytic domain
cDNA:	Complementary DNA
CDR:	Complementarity-determining regions
CHIKV:	Chikungunya virus
CI:	Confidence interval
CRL:	Cullin-RING E3 ligase
Ctrl:	Control
DAMP:	Danger-associated molecular pattern
DC:	Dendritic cell
DHL:	Downstream hairpin loop
DLP:	Double-layered particle
DMEM:	Dulbecco's Modified Eagle's medium
DMSO:	Dimethyl sulfoxide
DNA:	Deoxyribonucleic acid
Dora:	Doramapimod
Dox:	Doxycycline
DPP:	Dipeptidyl peptidase
ds:	Double-stranded
dTAG:	Degradation TAG
DTT:	Dithiothreitol
E. coli:	*Escherichia coli*
ECL:	Enhanced chemiluminescence
EDTA:	Ethylenediaminetetraacetic acid
EEEV:	Eastern equine encephalitis virus
EGF:	Epidermal growth factor
EGFP:	Enhanced green fluorescent protein
eIF2α:	Eukaryotic initiation factor 2α
ELISA:	Enzyme-linked immunosorbent assay

ER:	Endoplasmic reticulum
FBS:	Fetal bovine serum
FIIND:	Function to find domain
FKCL:	Familial keratosis lichenoides chronica
GCN2:	General control nonderepressible 2
GFP:	Green fluorescent protein
GSDM:	Gasdermin
GST:	Glutathione S-transferase
HBSS:	Hanks' balanced salt solution
HEK:	Human embryonic kidney
HEPES:	4-(2-hydroxyethyl)-1-piperazineethanesulfonic acid
HIV-1:	Human immunodeficiency virus-1
HMW:	High molecular weight
HRP:	Horseradish peroxidase
HRV:	Human rhinovirus
HT-DNA:	Herring testis-DNA
HTRF:	Homogeneous Time-Resolved Fluorescence
IFN:	Interferon
Ig:	Immunoglobulin
IL:	Interleukin
Iono:	Ionomycin
IPTG:	Isopropyl-β-D-thiogalactopyranosid
IRF:	Interferon regulatory factor
ISR:	Integrated stress response
JNK:	C-Jun N-terminal kinase
Jnk:	Jnk-In-8
KSHV:	Kaposi´s sarcoma-associated herpesvirus
Lacti:	Lactimidomycin
LDH:	Lactate dehydrogenase
LF:	Lipofectamine
LMW:	Low molecular weight
LPS:	Lipopolysaccharides
LRR:	Leucine-rich repeat
MAP2K:	Mitogen-activated protein kinase kinase
MAP3K:	Mitogen-activated protein kinase kinase kinase
MAPK:	Mitogen-activated protein kinase
MAYV:	Mayaro virus
MBP:	Maltose-binding protein
MDP:	Muramyl-dipeptide
MEM:	Minimum Essential medium
MLN4:	MLN4924
MLN7:	MLN7243
MOI:	Multiplicity of infection
mRNA:	Messenger RNA
NACHT:	Domain present in NAIP, CIITA, HET-E and TP-1
NAIAD:	NLRP1-associated autoinflammation with arthritis and dyskeratosis
NAIP:	NLR family apoptosis inhibitory protein
NBD:	Nucleotide-binding domain

NEDD8: Neural precursor cell expressed, developmentally down-regulated 8
NF-κB: Nuclear factor κ-light-chain-enhancer of activated B cells
NFDM: Non-fat dry milk
Nig: Nigericin
NINJ1: Ninjurin 1
NLR: Nucleotide-binding domain and leucine-rich repeat containing receptors
NLRC: NLR family CARD containing
NLRP: NLR family PYD containing
NLRX1: NLR family member X1
NOD: Nucleotide-binding oligomerization domain containing
NR100: N-terminal domain of rodent Nlrp1 proteins approximately 100 amino acids
NSP: Non-structural protein
OD: Optical density
ONNV: O'nyong-nyong virus
PAGE: Polyacrylamide gel electrophoresis
Pam3: Pam3CSK4
PAMP: Pathogen-associated molecular pattern
PARP: Poly-ADP-ribose-polymerase
PBMCs: Peripheral blood mononuclear cells
PBS: Phosphate-buffered saline
PCR: Polymerase chain reaction
PEI: Polyethylenimine
PERK: PKR-like endoplasmic reticulum kinase
PF: PF3644022
PI: Propidium iodide
PKR: Protein kinase R
PMA: Phorbol myristate acetate
PRR: Pattern recognition receptor
pUbC: Ubiquitin C promoter
PYD: Pyrin domain
RIG-I: Retinoic acid-inducible gene I
RNA: Ribonucleic acid
ROS: Reactive oxygen species
RPMI: Roswell Park Memorial Institute
RRV: Ross River virus
RSR: Ribotoxic stress response
RV: Rotavirus
RVA: Rotavirus species A
SB: SB202190
SDS: Sodium dodecyl sulfate
SFV: Semliki Forrest virus
sgRNA: Single guide RNA
SINV: Sindbis virus
ss: Single-stranded
Tal: Talabostat
TAOK2: TAO kinase 2
TBS: Tris-buffered saline
TCEP: Tris(2-carboxyethyl)phosphine

TCR:	T cell receptor
Th:	T helper
TLP:	Triple-layered particle
TLR:	Toll-like receptor
TMB:	3,3′,5,5′-Tetramethylbenzidin
TNF:	Tumor necrosis factor
T_{reg}:	Regulatory T cell
TRX:	Thioredoxin
UPA:	Conserved in UNC5, PIDD and Akirins
UT:	Untreated
UV:	Ultraviolet
VEEV:	Venezuelan equine encephalitis virus
VHH:	Variable domain of heavy-chain antibodies
VHL:	Von Hippel-Lindau
VSV:	Vesicular stomatitis virus
VX:	Vx-765
WEEV:	Western equine encephalitis virus
Wt:	Wild type
Z-VAD:	Z-VAD(OMe)-FMK
ZAK:	Leucine zipper- and sterile alpha motif-containing kinase
ZU5:	Found in ZO-1 and UNC5

1. Introduction

1.1 Inflammasomes mediate inflammation as part of the innate immune response

1.1.1 Inflammasome sensors are innate immune receptors that detect cytosolic danger signals

The innate immune system represents the first line of defense in the continuous fight of our bodies against potential threats like invading pathogens or cell damage. Specialized innate immune cells like granulocytes, macrophages, and dendritic cells (DCs), but also non-hematopoietic cells like epithelial and endothelial cells, guard the different tissues and raise the alarm whenever they detect danger signals (Takeuchi & Akira, 2010). Innate immune responses are then rapidly induced, involving for example the release of cytokines and chemokines, as well as antigen presentation to adaptive immune cells. The innate immune system is therefore essential for the induction of an adaptive immune response, which represents a slower but more specific immune reaction that relies on antigen-specific T and B lymphocytes. While adaptive immune cells generate a nearly unlimited number of antigen-specific receptors by gene recombination, cells of the innate immune system rely on the expression of a limited number of germline-encoded receptors to detect potential threats (Beutler, 2004; Netea et al., 2020). These so-called pattern recognition receptors (PRRs) recognize conserved microbial structures (pathogen-associated molecular patterns (PAMPs)) or endogenous molecules in the context of damaged cells (danger-associated molecular patterns (DAMPs)). On the one hand, some PRRs are expressed at the plasma membrane or within intracellular endosomes, like Toll-like receptors (TLRs) and C-type lectin receptors, thus detecting threats from the extracellular space. On the other hand, cytosolic retinoic acid-inducible gene I (RIG-I)-like receptors, absent in melanoma 2 (AIM2)-like receptors (ALRs), nucleotide-binding domain and leucine-rich repeat-containing receptors (NLRs), and other sensors like cGAS/STING enable the detection of intracellular pathogens and danger signals (Brubaker et al., 2015; Faenza & Blalock, 2022; Takeuchi & Akira, 2010). Stimulation of PRRs usually leads to the transcriptional upregulation of proinflammatory cytokines, type I interferons (IFN), chemokines, and antimicrobial molecules. Furthermore, activation of some ALRs and

NLRs leads to the formation of proinflammatory multi-protein complexes called inflammasomes (Meunier & Broz, 2017; Takeuchi & Akira, 2010).

1.1.2 Inflammasome formation leads to the release of proinflammatory cytokines and pyroptotic cell death

The majority of inflammasome sensors belong to the NLR family. All NLRs share a nucleotide-binding domain (NBD), which is part of the NACHT (domain present in NAIP, CIITA, HET-E, and TP-1), followed by a leucine-rich repeat (LRR) domain for most of them. The human NLR family includes amongst others the caspase activating and recruitment domain (CARD)-containing proteins NOD1-2 and NLRC3-5, as well as the pyrin domain (PYD)-containing proteins NLRP1-14 (see Table 1).

Name	Family members
NLR family apoptosis inhibitory protein (NAIP)	NAIP
Nucleotide-binding oligomerization domain containing (NOD)	NOD1-2
NLR family, CARD containing (NLRC)	NLRC3-5
NLR family, PYD containing (NLRP)	NLRP1-14
NLR family member X (NLRX)	NLRX1

Table 1: Designation of human NLR family members that are relevant to this thesis. Adapted from (Ting et al., 2008).

Out of the listed NLR family members, especially NAIP/NLRC4, NLRP1, and NLRP3 represent established inflammasome sensors (Meunier & Broz, 2017; Ting et al., 2008). Stimulation of these sensors leads to oligomerization and subsequent recruitment of the adaptor protein apoptosis-associated speck-like protein containing CARD (ASC). As ASC exhibits a PYD and CARD, its recruitment can occur via homotypic PYD-PYD or CARD-CARD interactions with the sensor. ASC^{PYD} forms filaments that are cross-linked by ASC^{CARD}, inducing the formation of a single micron-sized ASC speck in the cytosol (Dick et al., 2016; Schmidt, Lu, et al., 2016; Stutz et al., 2013). ASC^{CARD} then recruits the endoprotease caspase-1 via CARD-CARD interaction, leading to the autoproteolytic activation of proinflammatory caspase-1 (Srinivasula et al., 2002). Thus, ASC specks represent “potent caspase-1-activating platforms” (Fernandes-Alnemri et al., 2007).

Dimerization of caspase-1 at the ASC speck induces cleavage between the large (p20) and the small (p10) subunit of the catalytic domain, leading to the formation of $(p33/p10)_2$ homodimers, which remain bound to the ASC speck and show the highest activity. Cleavage between CARD and p20 releases rather unstable $(p20/p10)_2$ dimers that rapidly lose their activity (Boucher et al., 2018; Van Opdenbosch & Lamkanfi, 2019; Walsh et al., 2011). Active caspase-1 executes its inflammatory function by processing the proinflammatory cytokines pro-interleukin (IL)-1β and pro-IL-18 (Puren et al., 1999), and by inducing a lytic form of cell death called pyroptosis. Pyroptotic cell death is enabled by caspase-dependent cleavage of pore-forming proteins of the gasdermin family. In the context of canonical inflammasomes, caspase-1 cleaves gasdermin D (GSDMD) allowing the N-terminal GSDMD fragment to bind the inner leaflet of the plasma membrane, forming pores that lead to cellular swelling and membrane permeabilization (J. Ding et al., 2016; Galluzzi et al., 2018; X. Liu et al., 2016; Shi et al., 2015). Pyroptotic cells release small cytosolic proteins through the GSDMD pores, including processed IL-1β and IL-18. GSDMD is critical for the release of these cytokines since they lack signal peptides that normally regulate cytokine secretion (Evavold et al., 2018; Phulphagar et al., 2021; Puren et al., 1999). In fact, even though neutrophils do not undergo pyroptosis after inflammasome activation, they still require GSDMD for sufficient IL-1β release (K. W. Chen et al., 2014; Heilig et al., 2018). Eventually, pyroptotic cells will undergo cell membrane rupture mediated by ninjurin 1 (NINJ1) (Kayagaki et al., 2021).

Processed IL-1β and IL-18 bind their respective IL-1 and IL-18 receptors and induce transcriptional upregulation of proinflammatory genes similar to TLR signaling. IL-1β is a critical regulator of local and systemic inflammation. It induces fever, vasodilatation, and upregulation of adhesion molecules and chemokines amongst other things, thereby promoting immune cell infiltration at the site of inflammasome stimulation. Many autoinflammatory diseases are caused by dysregulated IL-1β activity. IL-18 induces IFN-γ production by natural killer cells and cytotoxic T cells and seems to play a role in metabolic syndrome and obesity (Dinarello, 2009, 2018; H. Zhang et al., 2023).

1.1.3 Inflammasome sensors react to a variety of stimuli

Different ALRs and NLRs represent inflammasome sensors, enabling the detection of distinct stimuli:
ALR member AIM2 senses cytosolic double-stranded deoxyribonucleic acid (dsDNA) in the context of intracellular infection or mitochondrial damage and nucleates ASC specks via its PYD (Fernandes-Alnemri et al., 2009; Hornung et al., 2009; Próchnicki et al., 2023).

The NLR member NAIP (different Naip proteins in mice) detects needle proteins of the bacterial type III secretion system or flagellin. Following detection, NAIP requires interaction with NLRC4 to form an inflammasome (Kortmann et al., 2015; Rauch et al., 2016; J. Yang et al., 2013; Y. Zhao et al., 2011). NLRC4 recruits ASC via its CARD but can also directly interact with caspase-1. The formation of these ASC-independent inflammasomes induces only weak caspase-1 activity which is sufficient to induce pyroptosis. However, ASC speck formation is necessary for optimal caspase-1 processing and subsequent cytokine maturation (Broz et al., 2010; Dick et al., 2016; Schmidt, Lu, et al., 2016).

In contrast to AIM2 and NAIP, the inflammasome sensor pyrin detects no defined PAMP or DAMP but instead recognizes homeostasis-altering molecular processes (Liston & Masters, 2017). During homeostasis, pyrin is phosphorylated and inhibited via a Rho GTPase-regulated process. Rho-GTPase-inactivating toxins disturb this inhibition and therefore induce pyrin activation, even though altered microtubule dynamics might play a role as well (W. Gao et al., 2016; Magnotti et al., 2019; Y. H. Park et al., 2016; H. Xu et al., 2014).

The exact mechanism of activation of the probably most studied inflammasome sensor, NLRP3, is still unknown despite extensive research since its discovery (Agostini et al., 2004). NLRP3 can be activated by extracellular adenosine triphosphate (ATP), pore-forming toxins, and crystalline substances. Many of these stimuli, but not all of them, induce potassium efflux, hence alternative underlying NLRP3 triggers like reactive oxygen species (ROS), lysosomal damage, different ionic fluxes, and organelle dysfunction are

discussed (Akbal et al., 2022; Groß et al., 2016; Kelley et al., 2019; Muñoz-Planillo et al., 2013). NLRP3 requires priming to form functional inflammasomes, which is commonly performed by lipopolysaccharide (LPS)-induced TLR4 stimulation in experimental setups. Priming leads to the activation of the nuclear factor κ-light-chain-enhancer of activated B cells (NF-κB) transcription factor complex, inducing the transcriptional upregulation of NLRP3. In addition, it also induces post-translational modifications like deubiquitination of the LRR domain and multiple phosphorylations (Bauernfeind et al., 2009; McKee & Coll, 2020).

As already mentioned in the context of NAIP/NLRC4 inflammasomes, there are also ASC-independent inflammasomes. Intracellular LPS can directly be detected by guanylate-binding proteins and inflammatory caspase-4/5 (caspase-11 in mice), which leads to the cleavage of GSDMD and pyroptosis (Casson et al., 2015; Kayagaki et al., 2011, 2015; Santos et al., 2020; Shi et al., 2014; Wandel et al., 2020). This non-canonical inflammasome activation can still result in the release of mature IL-1β and IL-18, caused by subsequent activation of NLRP3 following GSDMD pore-induced potassium efflux (Rühl & Broz, 2015; Schmid-Burgk et al., 2015).

1.2 NLRP1: An inflammasome sensor like no other

1.2.1 Human and rodent NLRP1 have different domain structures

Compared to all inflammasome sensors described so far, human NLRP1 exhibits a unique domain structure, as it is the only NLR family member that contains both an N-terminal PYD and a C-terminal CARD (Martinon et al., 2002; Ting et al., 2008). Moreover, it has a function to find domain (FIIND), consisting of a ZU5 (found in ZO-1 and UNC5)- and a UPA (conserved in UNC5, PIDD, and Akirins)-like subdomain, close to the C-terminal CARD (Fig. 1.1 A). In humans, the FIIND is only found in NLRP1 and the inflammasome sensor CARD8, which will be described later in this chapter. The NLRP1 FIIND undergoes autoproteolytic cleavage at F1212/S1213, involving at least one of the three conserved histidine residues in this domain. The cleavage results in the C-terminal NLRP1$^{\text{UPA-CARD}}$ fragment that remains non-covalently connected with the bigger N-terminal fragment.

NLRP1 mutations that impair FIIND autoprocessing inhibit inflammasome formation (D'Osualdo et al., 2011; Finger et al., 2012).

Rodent and human NLRP1 share the C-terminal FIIND and CARD domains, as well as the autoproteolytic cleavage mechanism (Frew et al., 2012). However, rodent Nlrp1 completely lacks the N-terminal PYD (Fig. 1.1 A). Instead, it exhibits an NR100 (N-terminal domain of rodent Nlrp1 proteins approximately 100 amino acids) region at the N-terminus (Moayeri et al., 2012). Mice express three Nlrp1 paralogs (Nlrp1a-c). Nlrp1a is highly conserved in different mouse strains, implying an important but yet unknown function for this protein. In contrast, Nlrp1b is highly polymorphic. Indeed, Nlrp1b is expressed from five alleles in different inbred mouse strains, out of which alleles 3 and 4 are not functional due to impaired FIIND processing or CARD deletion. Nlrp1c also lacks the CARD and is no longer functional (Boyden & Dietrich, 2006; Frew et al., 2012; Sastalla et al., 2013).

1.2.2 NLRP1 is activated by N-terminal degradation

The first studies dealing with NLRP1 activation revolved around the finding that lethal factor of *Bacillus anthracis* lethal toxin activates certain sensitive Nlrp1(b) alleles in murine and rat macrophages (Boyden & Dietrich, 2006; Newman, Printz, et al., 2010), but not human NLRP1 (Moayeri et al., 2012; Newman, Crown, et al., 2010). Activation of Nlrp1(b) and subsequent pyroptosis was dependent on functional proteasomal degradation (Fink et al., 2008; Newman, Crown, et al., 2010; Squires et al., 2007; G. Tang & Leppla, 1999) and N-degron pathways (Wickliffe et al., 2008), but how the toxin actually stimulated the inflammasome response was long unknown. The elucidation of this mode of activation began with the discovery that lethal factor cleaves all sensitive Nlrp1(b) alleles at the N-terminus and that this cleavage is sufficient for inflammasome activation (Chavarría-Smith & Vance, 2013; Hellmich et al., 2012; Levinsohn et al., 2012). Moreover, murine Nlrp1a and lethal factor-insensitive Nlrp1b alleles, as well as human NLRP1 (which all cannot be cleaved and activated by lethal factor) formed inflammasomes after artificial N-terminal cleavage in human embryonic kidney (HEK) cells. Based on these observations, the concept of "proteolysis as a general mechanism for NLRP1 inflammasome activation" was proposed (Chavarría-Smith et al., 2016). A few years later, three groups developed this concept into the model of "functional degradation" (Sandstrom et al., 2019). They showed

that Nlrp1b is degraded after cleavage by lethal factor, dependent on an Ubr2-mediated N-degron pathway (Chui et al., 2019; H. Xu et al., 2019) and that targeted N-terminal degradation of Nlrp1b is sufficient for its activation (Sandstrom et al., 2019). N-terminal degradation leads to the release of the C-terminal NLRP1$^{UPA\text{-}CARD}$ fragment, which then recruits ASC to form inflammasomes (Fig. 1.1 B). This model explains why NLRP1 activation requires functional proteasomal degradation and preceding cleavage of the FIIND. Since human NLRP1 exhibits both a PYD and a CARD domain, both domains could be responsible for ASC recruitment. By now, many experiments in reconstituted cell lines have proven that NLRP1$^{UPA\text{-}CARD}$ alone forms inflammasomes and that NLRP1 CARD but not PYD interacts with ASC (Chui et al., 2019; Finger et al., 2012; Sandstrom et al., 2019; Z. Xu et al., 2021; Zhong et al., 2016).

Thus, the functional degradation model explained all observations regarding lethal factor-mediated Nlrp1(b) inflammasome activation in rodents, but at that time no proteolytic stimulus for human NLRP1 was known. However, soon after, Robinson et al. and Tsu, Beierschmitt et al. reported the N-terminal cleavage of NLRP1 by Enterovirus 3C proteases, the subsequent degradation by the glycine-specific N-degron pathway, and inflammasome activation. They showed that 3C proteases of human rhinovirus (HRV) 14/16, coxsackie virus B3, enterovirus 71/D68, and poliovirus 1 activate NLRP1 by cleavage at Q130/G131 in the linker region between PYD and NBD. This suggested that NLRP1 contains a conserved enterovirus polyprotein cleavage site (Fig. 1.1 B) (Robinson et al., 2020; Tsu et al., 2021). Tsu and Beierschmitt also tested additional picornavirus 3C proteases and found that different viral proteases cleave NLRP1 but not all of them lead to activation (Tsu et al., 2021). The repertoire of human NLRP1 proteolytic stimuli was complemented with SARS-CoV-2 3C-like protease non-structural protein (NSP) 5 which cleaves NLRP1 at Q333 (Planès et al., 2022).

1.2.3 The CARD8 inflammasome is similarly activated by N-terminal degradation

As already mentioned, NLRP1 is not the only human protein that undergoes autoproteolytic processing in the FIIND. CARD8 is encoded by 13 exons out of which exons 7-13 show an identical gene structure to NLRP1 (Bagnall et al., 2008). Hence, it is impossible to discuss NLRP1 without mentioning CARD8. Instead of further NLR and PYD

domains, CARD8 exhibits a 160 amino acid-long unstructured region at its N-terminus (Fig. 1.1 A) (Chui et al., 2020). CARD8 is also expressed in at least five different splicing isoforms (T47, T48, T51, T54, T60) which differ in the length of the N-terminus, with T48 representing the canonical isoform. Transcriptomic analyses revealed that these isoforms are differentially expressed in various human tissues (Bagnall et al., 2008; Z. Xu et al., 2022). Similar to NLRP1, CARD8 is autoproteolytically processed in the FIIND at S297 (D'Osualdo et al., 2011). CARD8 is not expressed in rodents but is for example found in primates and carnivores (Bagnall et al., 2008). The first descriptions of CARD8 proposed an inhibitory and regulatory role in general inflammasome (Razmara et al., 2002), NLRP3 (Agostini et al., 2004; Ito et al., 2014; Mao et al., 2018), or NOD2 signaling (von Kampen et al., 2010). Later, it was demonstrated that CARD8 is indeed an inflammasome sensor itself (D. C. Johnson et al., 2018). Given the fact that CARD8 and NLRP1 share the same C-terminus, it is not surprising that CARD8 is activated by functional degradation as well. Indeed, human immunodeficiency virus (HIV)-1 proteases cleave and activate the CARD8 inflammasome in infected T cells (Moore et al., 2022; Q. Wang et al., 2021). Coxsackie virus B3 3C proteases cleave and activate not only NLRP1 but also CARD8. CARD8 is also cleaved by the viral 2A proteases of the same virus (Nadkarni et al., 2022) (Fig. 1.1 B).

1.2.4 NLRP1 and CARD8 inflammasomes are activated by inhibition of DPP8/9

NLRP1 and CARD8 not only share functional degradation as an activation mechanism, but they both can be activated by inhibition of dipeptidyl peptidases (DPP) 8/9. DPP enzymes are involved in the processing and degradation of proline-containing (poly-)peptides, as they cleave peptides with free N-termini after second-position prolines (XP). DPP8 and 9 are homologous proteins and both are ubiquitously expressed in human tissues and different cell lines (Griswold, Cifani, et al., 2019; H. K. Tang et al., 2009). Inhibition of DPP8/9 by the potential anti-cancer drug talabostat (also called Val-boroPro) leads to the activation of both CARD8 and NLRP1 inflammasomes, with a more prominent role for DPP9 in this mode of activation (D. C. Johnson et al., 2018; Okondo et al., 2017; Zhong et al., 2018). The different isoforms of CARD8 (T48, T54, T60) all respond to talabostat (Chui et al., 2020). Moreover, all functional murine Nlrp1b alleles, murine

Nlrp1a, and rat Nlrp1 form inflammasomes after stimulation with talabostat, which makes DPP8/9 inhibition the first common stimulus of human and rodent NLRP1 (Gai et al., 2019; Okondo et al., 2018). Cryo-EM structures of DPP9-NLRP1 and DPP9-CARD8 complexes revealed why inhibition of these enzymes leads to inflammasome formation. The ternary complexes consist of DPP9 dimers in which each DPP9 binds two NLRP1 or CARD8 molecules. One of the NLRP1 or CARD8 proteins is still in its full-length form, while the other protein is the UPA-CARD fragment (Fig. 1.1 B). The full-length proteins bind DPP9 via the FIIND. In the case of NLRP1, NLRP1$^{\text{UPA-CARD}}$ inserts into the active site of the enzyme and is directly replaced by talabostat. In contrast, CARD8$^{\text{UPA-CARD}}$ is not interacting with the active site and there is no direct displacement by the drug, but the complex is still sensitive to talabostat treatment (Hollingsworth, Sharif, et al., 2021; Sharif et al., 2021). The enzymatic activity of DPP9 seems to play a role in the sequestration of NLRP1 (Zhong et al., 2018) and CARD8 (Griswold, Ball, et al., 2019). However, although human NLRP1$^{\text{UPA-CARD}}$ inserts into the active site, the UPA-CARD fragments of human and murine NLRP1 are no direct substrate of DPP9 (Griswold, Cifani, et al., 2019; Hollingsworth, Sharif, et al., 2021). Even though the DPP9-NLRP1 and DPP9-CARD8 complexes are very similar, the regulation of NLRP1 and CARD8 by DPP9 differs regarding binding and requirement of enzymatic activity. In line with these differences, inhibiting DPP8/9 by the accumulation of XP peptides is sufficient to activate CARD8 but not NLRP1 (Rao et al., 2022). Although the exact mechanisms of NLRP1 and CARD8 regulation by DPP8/9 are not completely understood, the resolved complexes give us a general idea of how these inflammasomes are activated after DPP8/9 inhibition and functional degradation: Both sensors release free NLRP1$^{\text{UPA-CARD}}$ or CARD8$^{\text{UPA-CARD}}$ fragments during cell homeostasis which are sequestered by DPP9. Inhibition of DPP9 activity leads to the release of these active sensors and formation of inflammasomes (Fig. 1.1 B). Functional degradation of both sensors leads to an accumulation of free UPA-CARD fragments, with a concomitant decrease of full-length sensor protein. This results in an excess of UPA-CARD fragments that can no longer be sequestered by DPP9, causing inflammasome activation (Hollingsworth, Sharif, et al., 2021). A similar Dpp9 complex was described for rat Nlrp1 and murine Nlrp1b, suggesting a comparable mode of activation by DPP8/9 inhibition in humans and rodents (Fig. 1.1 B) (Griswold, Ball, et al., 2019; Huang et al., 2021). Orth-He et al. and Wang et al. also reported that DPP8/9

inhibition not only releases sequestered NLRP1$^{UPA\text{-}CARD}$ or CARD8$^{UPA\text{-}CARD}$ fragments, but also induces further N-terminal degradation of both sensors (Orth-He et al., 2023; Q. Wang et al., 2023). This is in line with reports that talabostat-induced activation of Nlrp1b and CARD8 still requires functional proteasomal degradation (D. C. Johnson et al., 2018; Okondo et al., 2018).

1.2.5 NLRP1 and CARD8 differ in their dependency on ASC

NLRP1 and CARD8 share the same C-terminus and they can both be activated by functional degradation and inhibition of DPP8/9. But if these two inflammasome sensors are that similar, how can they be distinguished? The two sensors differ in their dependency on the inflammasome adaptor protein ASC. The first description of CARD8 already mentioned that CARD8^{CARD} directly interacts with caspase-1 (Razmara et al., 2002). Later reports about CARD8 inflammasomes confirmed that CARD8 forms ASC-independent inflammasomes (D. C. Johnson et al., 2018; Okondo et al., 2017). In contrast, NLRP1 needs ASC to form functional inflammasomes (Fig. 1.1 B). This was proven in endogenous and overexpression systems (Ball et al., 2020; Zhong et al., 2018). CARD8, but not NLRP1, causes pyroptosis in HEK cells expressing caspase-1 and GSDMD. On the other hand, only NLRP1 can form ASC specks in HEK cells (Ball et al., 2020). This exclusive binding of NLRP1^{CARD} to ASC^{CARD} and CARD8^{CARD} to caspase-1^{CARD} was substantiated by structures of NLRP1$^{UPA\text{-}CARD}$ and CARD8$^{UPA\text{-}CARD}$ filaments. In both cases, the UPA-like domain mediates CARD oligomerization, leading to the formation of two-layered UPA-CARD filaments consisting of an inner filament of CARDs surrounded by a UPA spiral. However, the filaments differ in their charge distribution, causing a distinct preference for the recruitment of either ASC^{CARD} or caspase-1^{CARD}. NLRC4^{CARD} can recruit either ASC or caspase-1, which does not seem to be the case for NLRP1^{CARD} (Gong et al., 2021; Hollingsworth, David, et al., 2021). However, both NLRC4 and NLRP1 require additional bridging ASC molecules to enable ASC^{CARD} and caspase-1^{CARD} interaction after ASC recruitment to the oligomerized sensor (Finger et al., 2012).

Similar to NLRC4-nucleated ASC-independent inflammasomes, CARD8 activation is associated with only weak caspase-1 processing, which is sufficient to induce pyroptosis but not cytokine maturation (D. C. Johnson et al., 2018; Okondo et al., 2017). NLRP1

inflammasome activation, on the other hand, depends on ASC and therefore leads to optimal caspase-1 and cytokine processing (Fig. 1.1 B) (Zhong et al., 2018). In contrast to human NLRP1, murine Nlrp1b seems to be able to bind both Asc^{CARD} and caspase-1^{CARD}. Indeed, Asc knockout macrophages still undergo pyroptosis after Nlrp1b stimulation. Some studies even show Asc-independent IL-1β processing and release, contradicting the model in which ASC specks are required for optimal caspase-1 activity (Ball et al., 2020; Broz et al., 2010; Chavarría-Smith et al., 2016; Guey et al., 2014; Van Opdenbosch et al., 2014).

1.2.6 Other reported stimuli of NLRP1 inflammasomes

Next to the two main modes of NLRP1 activation by functional degradation and DPP8/9 inhibition, there is a variety of other potential NLRP1 stimuli:
Infection with the alphavirus Semliki Forrest virus (SFV) and transfection of the double-stranded ribonucleic acid (dsRNA) analog poly(I:C) leads to NLRP1 inflammasome formation, concomitant with binding of dsRNA to $NLRP1^{LRR}$ (Bauernfried et al., 2021). Zhou et al. reported NLRP1 activation by the DNA analog poly(dA:dT) (J. Y. Zhou et al., 2023). Interestingly, both stimuli require functional proteasomal degradation, suggesting that the nucleic acids (analogs) somehow induce degradation and activation of NLRP1 (Fig. 1.1 B). Moreover, ultraviolet B (UVB) irradiation activates NLRP1 in human but not murine keratinocytes (Feldmeyer et al., 2007; Fenini, Grossi, Contassot, et al., 2018; Sand et al., 2018; Sollberger et al., 2015). The exact mechanism of activation or the role of NLRP1 degradation is unknown (Fig. 1.1 B). NLRP1 activation by SFV, nucleic acids (analogs), and UVB irradiation will be discussed in more detail in chapter 3.

Rat macrophages undergo Nlrp1-induced pyroptosis after infection with *Toxoplasma gondii* (Cavailles et al., 2014; Cirelli et al., 2014). Others proposed murine Nlrp1b (Ewald et al., 2014; Gorfu et al., 2014) and human NLRP1 (Gov et al., 2013; Witola et al., 2011) as sensors of *Toxoplasma gondii* infection as well, but they did not show direct evidence of Nlrp1b/NLRP1 inflammasome formation after infection with the intracellular parasite.

In addition, Kaposi´s sarcoma-associated herpesvirus (KSHV) protein ORF45 was reported to interfere with a DPP9-independent complex formed by the NLRP1 linker region (between PYD and NBD) and the UPA-like subdomain of the FIIND. Binding of ORF45 to the linker region disrupts the complex and induces NLRP1 inflammasome activation. The DPP9-dependent complex seems to be disrupted by ORF45 as well (X. Yang et al., 2022).

Next to DPP8/9 as regulators of NLRP1 activity, the oxidoreductase thioredoxin (TRX) 1 was shown to bind human and rodent NLRP1 at the NACHT-LRR domains, but only in its oxidized form. It was suggested that this binding negatively regulates NLRP1, enabling the sensor to detect reductive cellular stress. However, knockdown of TRX1 was not sufficient to induce NLRP1 inflammasome formation, but it increased NLRP1 activation after talabostat treatment (Ball et al., 2022). Similarly, ferroptosis inhibitors that act as antioxidants and protein folding-interfering drugs were reported to boost talabostat-induced NLRP1 and CARD8 activation by increasing N-terminal degradation of both sensors (Orth-He et al., 2023; Q. Wang et al., 2023). The authors propose that NLRP1 and CARD8 sense protein folding stress in combination with the accumulation of proline-containing peptides. Thus, different stimuli seem to enhance the degradation of NLRP1 and CARD8, but they are not sufficient to overcome the sequestration of $NLRP1^{UPA\text{-}CARD}$ and $CARD8^{UPA\text{-}CARD}$ fragments by DPP8/9.

1.2.7 Epithelial cells express NLRP1 inflammasomes

Transcriptome analyses reveal a broad expression of NLRP1 in different human tissues (Z. Xu et al., 2022) but it seems to be especially highly expressed in the skin and the brain (Chu et al., 2001; Kummer et al., 2007). Epithelial cells in general seem to have functional NLRP1 inflammasomes, as they were found in human airway epithelial cells (Planès et al., 2022; Robinson et al., 2020), corneal epithelial cells (Griswold et al., 2022), and keratinocytes (Zhong et al., 2016; J. Y. Zhou et al., 2023). In addition, functional NLRP1 inflammasomes were reported in human aortic endothelial cells (Nadkarni et al., 2022). Importantly, in contrast to NLRP3, NLRP1 does not need priming to be functional (Guey et al., 2014; Zhong et al., 2016).

There are some known NLRP1 gain-of-function mutants in humans and the affected

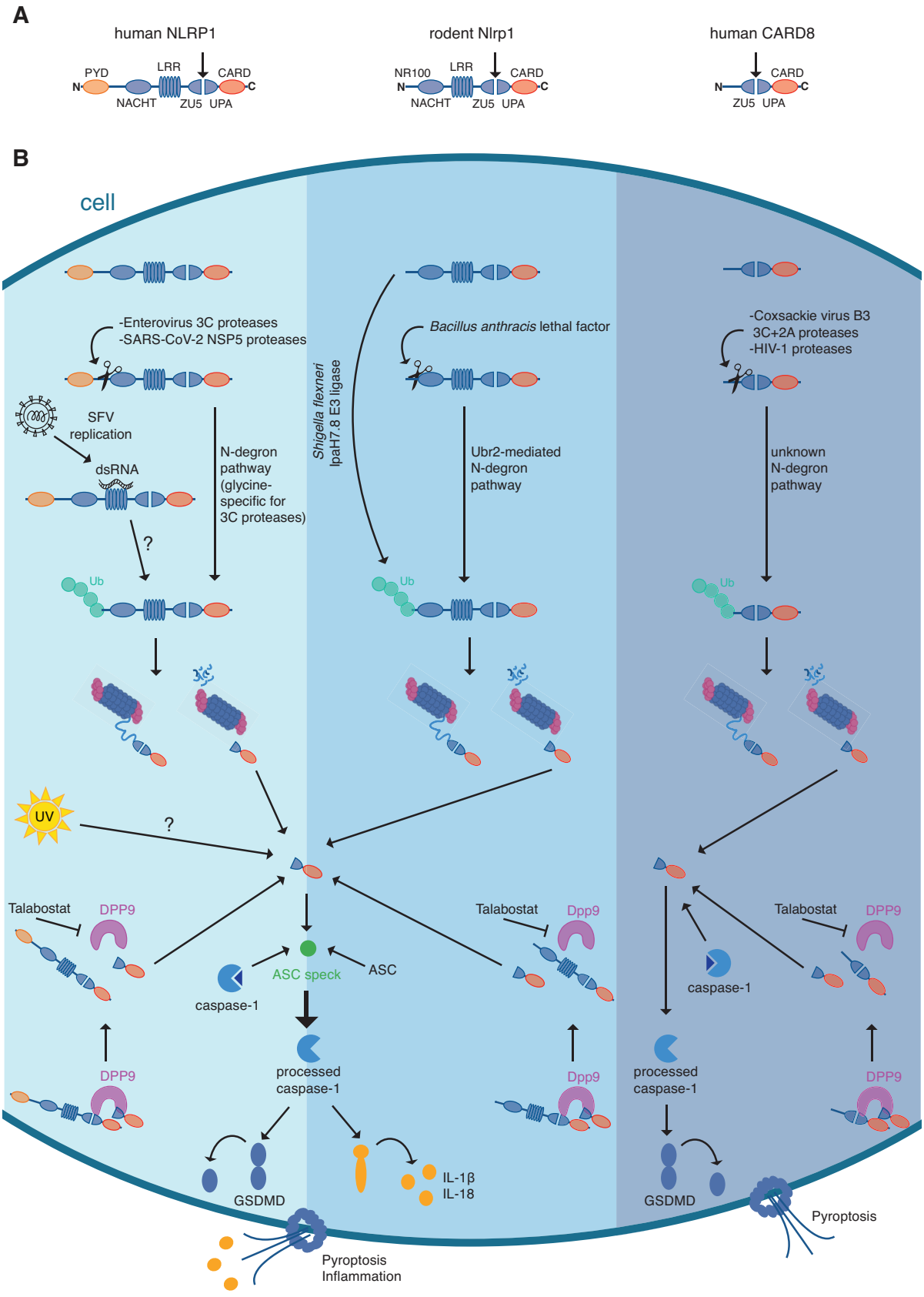

Figure 1.1: Overview of human NLRP1 inflammasome activation in comparison to rodent Nlrp1 and human CARD8. (**A**) Domain structure of human NLRP1, rodent Nlrp1, and human CARD8 (**B**) Schematic overview of NLRP1/Nlrp1 and CARD8 inflammasome activation by N-terminal cleavage and degradation, DPP8/9 inhibition (Talabostat), Semliki Forest virus (SFV) infection/dsRNA, and ultraviolet (UV) irradiation. Detailed explanation in the text.

patients show a variety of symptoms. In line with the strong expression of NLRP1 in the skin and epithelium, many patients present with skin pathologies including multiple self-healing palmoplantar carcinoma, familial keratosis lichenoides chronica (FKCL), NLRP1-associated autoinflammation with arthritis and dyskeratosis (NAIAD) and autoinflammatory dyskeratosis (Grandemange et al., 2017; Herlin et al., 2020; Zhong et al., 2016), or abnormal papilloma growth in the respiratory tract as seen in FKCL, NAIAD, and Juvenile-onset recurrent respiratory papillomatosis patients (Drutman et al., 2019; Grandemange et al., 2017; M. Li et al., 2023). The underlying mutations are found in the PYD, the LRR, or the FIIND and all lead to NLRP1 autoactivation or a reduction in the activation threshold. The NAIAD-associated P1214R mutation in the FIIND impairs the binding to DPP9 (Zhong et al., 2018). Some patients also express mutated DPP9 variants which fail to repress NLRP1, causing skin pathologies amongst other things (Harapas et al., 2022).

There are many association studies linking different NLRP1 mutations to a variety of human diseases. For example, NLRP1 L155H and M1184V are associated with the development of vitiligo and additional autoimmune diseases (Levandowski et al., 2013; Tupik et al., 2020), and perilesional skin samples from vitiligo patients show increased NLRP1 levels in immunostainings (Marie et al., 2014).

1.3 Aim of this thesis

Although NLRP1 was the first inflammasome sensor to be described (Martinon et al., 2002), it took more than ten years until the first concepts about its mode of activation were developed. Within the five years that I worked on this thesis, many studies contributed to our present understanding of human NLRP1 inflammasomes and especially the concepts of functional degradation and the sequestration of free NLRP1$^{UPA\text{-}CARD}$ fragments by DPP9 provided a completely new perspective on this inflammasome sensor. Nevertheless, there are still many aspects of NLRP1 biology that we do not understand: Does NLRP1 activation always require N-terminal degradation and what is the function of the N-terminal domains if they are degraded most of the time? How do stimuli like dsRNA and SFV infection induce N-terminal degradation of the sensor? Are there additional stimuli that activate NLRP1? Which cells can form functional NLRP1 inflammasomes and what are the consequences of activation?

To address and discuss all of these questions, the following aims were pursued in this thesis:

- To generate and validate experimental systems to study human NLRP1 in reporter cell lines and primary cells.
- To identify NLRP1-specific nanobodies that enable further analyses of NLRP1 inflammasome activation.
- To elucidate the mechanisms upstream of NLRP1 activation after the proposed stimuli UVB irradiation, SFV infection, and intracellular dsRNA.
- To screen additional viruses for potential NLRP1 activation
- To reveal new NLRP1 inflammasome-forming cells in human blood.

2. Nanobodies selectively activate the human NLRP1 inflammasome by targeted ubiquitination

2.1 Introduction

In this chapter, I will validate NLRP1 reporter cell lines and identify NLRP1-specific nanobodies. I will further use $NLRP1^{PYD}$ nanobodies to prove that targeted ubiquitination and degradation of human endogenous NLRP1 is sufficient for activation.

Nanobodies represent the variable domain of heavy chain-only antibodies (VHHs). They can be derived from camelids, which express heavy chain-only antibodies that lack both light chains and the first constant domain (Arbabi Ghahroudi et al., 1997; Hamers-Casterman et al., 1993). Novel nanobodies can be generated by immunization of llamas (R. van der Linden et al., 2000) and alpacas (Maass et al., 2007), followed by cloning of VHH libraries and selection of target binders by phage display (Arbabi Ghahroudi et al., 1997). Single VHH domains are soluble due to mutations at sites that normally interact with the variable domain of the light chain. Yet, they show antigen-specific binding with high affinities. Nanobody paratopes are formed by three complementarity-determining region (CDR) loops, embedded in a more conserved framework. The most variable and exposed CDR3 loop forms convex antigen-binding sites that permit binding of epitopes inside clefts such as catalytic centers of enzymes (Arbabi Ghahroudi et al., 1997; Lauwereys et al., 1998; Muyldermans, 2021). Compared to conventional antibodies, nanobodies have several advantages: they are stable at high temperatures, they are small, they are encoded in a single gene, and they can be recombinantly expressed in *Escherichia coli* (*E. coli*) (Arbabi Ghahroudi et al., 1997; Sheriff & Constantine, 1996; R. H. J. van der Linden et al., 1999). VHHs are also a great tool to study target molecules in living cells, as they are properly folded and functional in the reducing environment of the cytosol. They can be labeled with fluorophores to visualize targets, they can stabilize alternative protein confirmations and thereby activate or inhibit protein functions, and they can be easily cloned into fusion constructs to specifically manipulate targets (Ashour et al., 2015; Kirchhofer et al., 2010; Muyldermans, 2021; Rothbauer et al., 2006).

As described in the previous chapter, proteasomal degradation is a key element in NLRP1 inflammasome activation. During cell homeostasis, proteasomal degradation is important

to maintain protein and amino acid homeostasis, remove misfolded proteins, and control pathways by degradation of regulatory proteins (Bard et al., 2018). Proteins are marked for degradation by modification with ubiquitin, mediated by an isopeptide bond between glycines of ubiquitin C-terminus and lysines of the target protein. Ubiquitin itself contains seven lysines (K6, K11, K27, K29, K33, K48, K63), which enable the formation of different homo- or heterogenous polyubiquitin chains that determine the outcome of protein ubiquitination. In this “ubiquitin-code”, K48 chains present the main degradation signal but K11, K29, and K63 chains can induce degradation as well (Bard et al., 2018; Nandi et al., 2006; Rousseau & Bertolotti, 2018; Tracz & Bialek, 2021). The modification of target proteins with ubiquitin requires the transfer of ubiquitin from E1 activating enzymes via E2 conjugating enzymes to E3 ubiquitin ligases, which then mediate specific ubiquitination (Nandi et al., 2006; Scheffner et al., 1995). Humans express two E1, more than 35 E2, and over 600 different E3 enzymes. The largest family of E3 ubiquitin ligases are the Cullin-RING E3 ligases (CRLs) with over 200 members. They are responsible for around 20 % of proteasomal degradation within the cell. CRLs consist of a scaffold cullin protein (cullin 1, 2, 3, 4A, 4B, 5, 7) and a RING protein (most cullins bind Rbx1, except for cullin 5 which binds Rbx2) that recruits E2 enzymes. Substrate-specificity is mediated by an adaptor (Skp1 for cullin 1/7, elongin B/C for cullin 2/5, BTB for cullin 3, and DDB1 for cullin 4) and a substrate-specific receptor (for example F-box proteins for cullin 1+Skp1 and BC-box proteins for cullin 2+elongin B/C). Hundreds of substrate receptors enable the ubiquitination of thousands of substrates. CRL complexes are named after the cullin scaffold and the substrate receptor protein, for example, $CRL2^{VHL}$ for the cullin 2 complex with the von Hippel-Lindau (VHL) receptor (Bulatov & Ciulli, 2015; Harper & Schulman, 2021). All cullins, except cullin 7, require modification with the ubiquitin-like protein NEDD8 (neural precursor cell expressed, developmentally down-regulated 8) to form CRL complexes. This is why only cullins 1-5 are termed canonical cullins. NEDD8 modification, also called neddylation, provides cullins more flexibility to interact with E2 enzymes and substrates (Baek et al., 2021; Bulatov & Ciulli, 2015). After successful ubiquitination, proteins are unfolded and degraded by 26S proteasomes which consist of 19S caps and 20S proteolytic cores. The 19S cap recruits ubiquitinated proteins into the internal 20S chamber and recycles the polyubiquitin chains (Bard et al., 2018).

Some E3 ligases detect N- or C-terminal degron sequences, inducing N-/C-degron pathway-mediated degradation. These degrons are short linear motifs that are found in disordered regions of protein termini. These detected motifs can be, for example, acetylated N-termini, N-terminal prolines, or C-terminal arginines but all amino acids can be part of a degron in the right sequence context (Sherpa et al., 2022; Timms & Koren, 2020). N-degron pathways mediate the degradation of rodent Nlrp1(b) after cleavage by lethal factor and human NLRP1 after cleavage by HRV14 3C proteases. Cleavage by lethal factor induces the Ubr2-mediated N-degron pathway (Chui et al., 2019; H. Xu et al., 2019). UBR E3 ligases can have a RING or a HECT domain and recognize mostly aberrant N-termini to induce the Arg/N-degron pathway (Sherpa et al., 2022; Timms & Koren, 2020). Cleavage by HRV14 3C induces the N-terminal glycine N-degron pathway mediated by $CRL2^{ZYG11B}$ or $CRL2^{ZER1}$ complexes (Robinson et al., 2020; Timms et al., 2019). CRLs participate in both N- and C-degron pathways, but most C-degrons are recognized by CRLs (Sherpa et al., 2022; Timms & Koren, 2020).

Endogenous murine Nlrp1b can be activated by targeted ubiquitination by ubiquitin ligases of the human pathogen *Shigella flexneri* (Sandstrom et al., 2019). However, targeted ubiquitination and subsequent N-terminal degradation of human NLRP1 was so far only achieved in auxin-inducible degron (AID) (Sandstrom et al., 2019) and degradation TAG (dTAG) (Hollingsworth, Sharif, et al., 2021) systems. The dTAG system was later also used to induce targeted degradation of CARD8 (Hsiao et al., 2022; Sharif et al., 2021; Q. Wang et al., 2023). The degradation of AID-tagged proteins is induced by the addition of auxin hormones which mediate the binding of $CRL1^{TIR1}$ to the AID-tag. In the dTAG system, the recognition of the target protein by different CRL complexes is mediated by heterobifunctional dTAG molecules that interact with the tagged target and CRL substrate receptors (Prozzillo et al., 2020). Both techniques require reconstituted cell systems and overexpression of AID- or dTAG-NLRP1. In the AID system, the F-box protein TIR1 has to be co-expressed as well since auxin hormones and TIR1 are only expressed in plants. Nanobodies were already successfully used to degrade cellular proteins. Caussinus et al. fused a yeast F-box substrate receptor domain to a green fluorescent protein (GFP)-binding VHH and were able to degrade GFP-tagged proteins by recruitment of CRL1 complexes (Caussinus et al., 2012). Fulcher et al. used GFP-binding VHHs but this time

fused to the human VHL substrate receptor to recruit CRL2 complexes. VHL initiates the ubiquitination of the transcription factor hypoxia-inducible factor-1α under normoxic conditions (Fulcher et al., 2016; Kamura et al., 2004; Yu et al., 2001). Fulcher et al. later succeeded in degrading endogenous ASC using VHL fusions of ASC-specific VHHs (Fulcher et al., 2017). Siepe et al. used bivalent nanobodies, in which one VHH binds transmembrane E3 ligases, to specifically degrade murine and human membrane receptors (Siepe et al., 2023).

2.2 Results

Contributions

The HEK 293T and N/TERT-1 reporter cell lines were generated by Karl Elmar Lange. The fluorescence microscopy pictures in Fig. 2.1 B and Fig. 2.2 C were taken and processed by Florian Gohr. The experiments to quantify ASC speck formation in Fig. 2.1 D/E were performed by Sabine Normann. The immunoblots in Fig. 2.2 B/F were performed by Lisa Schiffelers. All were members of the Institute of Innate Immunity (Florian Schmidt Lab) in Bonn when the experiments were performed. All other experiments and further analyses of the provided data were performed by myself.

Modified versions of the results and figures were published in:
Journal of Experimental Medicine (2023) 220 (1): e20220837 (doi.org/10.1084/jem.20220837)

P38 kinases mediate NLRP1 inflammasome activation after ribotoxic stress response and virus infection

Lea-Marie Jenster[1], Karl-Elmar Lange[1], Sabine Normann[1], Anja vom Hemdt[2], Jennifer D. Wuerth[1], Lisa D.J. Schiffelers[1], Yonas M. Tesfamariam[1], Florian N. Gohr[1,3], Laura Klein[1], Ines H. Kaltheuner[4], Stefan. Ebner[1], Dorothee J. Lapp[1], Jacob Mayer[1], Jonas Moecking[4], Hidde L. Ploegh[5], Eicke Latz[1], Felix Meissner[1], Matthias Geyer[4], Beate M. Kümmerer[2,6], Florian I. Schmidt[1,7]

[1] Institute of Innate Immunity, Medical Faculty, University of Bonn, 53127 Bonn, Germany

[2] Institute of Virology, Medical Faculty, University of Bonn, 53127 Bonn, Germany

[3] Department of Microbiology and Immunology, The University of Melbourne, Parkville, VIC, 3010, Australia

[4] Institute of Structural Biology, Medical Faculty, University of Bonn, 53127 Bonn, Germany

[5] Program in Cellular and Molecular Medicine, Boston Children's Hospital, Boston, MA 02115, USA

[6] German Centre for Infection Research (DZIF), partner site Bonn-Cologne, 53127 Bonn, Germany

[7] Core Facility Nanobodies, Medical Faculty, University of Bonn, 53127 Bonn, Germany

2.2.1 Reporter cells enable the analysis of human NLRP1 inflammasome activation

To study the details of human NLRP1 inflammasome activation, I used two complementary cellular systems: On the one hand, HEK 293T cells, which do not express inflammasome-related proteins (Agostini et al., 2004; Chavarría-Smith et al., 2016), were reconstituted with NLRP1 and ASC, the latter fused to enhanced green fluorescent protein (EGFP), to analyze ASC speck assembly in a controlled bottom-up approach (Fig. 2.1). On the other hand, immortalized N/TERT-1 keratinocytes, which express all relevant NLRP1 inflammasome components endogenously (Zhong et al., 2016), were used to analyze NLRP1 activation and its outcomes in a physiologically relevant cell type (Fig. 2.2). In both models, detection of ASC speck formation was used as the main readout for inflammasome activation, as ASC specks allow easy detection and quantification of inflammasome formation on a single cell level (Stutz et al., 2013) and as all downstream effects of NLRP1 activity rely on the formation of these macromolecular assemblies.

To generate HEK 293T inflammasome reporter cells, first monoclonal HEK 293T cells expressing ASC-EGFP under control of a weak ubiquitin C promoter (pUbC) were selected for low ASC speck background. These cells were then equipped with either HA-tagged NLRP1 or the control NLR sensor NLRP3, both also under control of pUbC. Single clones were selected based on the optimal signal-to-noise ratio, resulting in $HEK^{NLRP1+ASC}$ and $HEK^{NLRP3+ASC}$ reporter cells (Fig. 2.1 A). $HEK^{NLRP1+ASC}$ cells were validated by stimulation with the well-studied NLRP1 activator talabostat (Tal), which stimulates the inflammasome by inhibition of DPP8/9. The expression of ASC-EGFP in the reporter cells enabled easy visualization and quantification of ASC speck formation by fluorescence microscopy (Fig. 2.1 B) or flow cytometry (Fig. 2.1 C). For the latter, I utilized the altered height and width signal of the reporter in a speck-forming cell to quantify inflammasome

activation, as described before (Sester et al., 2015). More than 40 % of HEK$^{NLRP1+ASC}$ cells

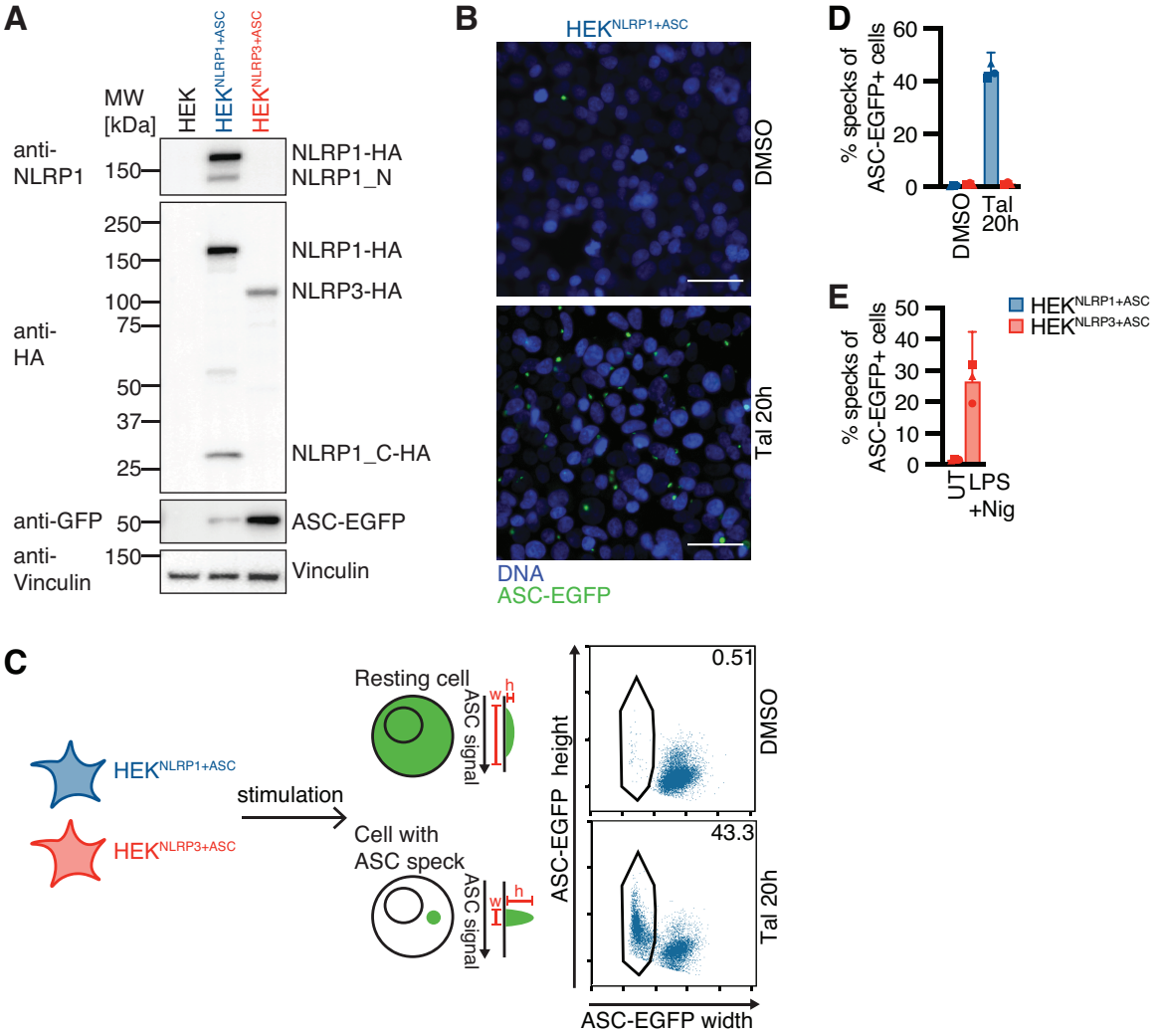

Figure 2.1: HEK 293T reporter cells recapitulate NLRP1 inflammasome assembly. (**A**) Lysates of HEK 293T (HEK), HEK$^{NLRP1+ASC}$, and HEK$^{NLRP3+ASC}$ cells were analyzed by immunoblot with the indicated antibodies to confirm expression of NLRP1-HA, NLRP3-HA and ASC-EGFP. (**B-D**) HEK$^{NLRP1+ASC}$ and HEK$^{NLRP3+ASC}$ cells were stimulated with DMSO or 30 µM talabostat (Tal) for 20 h. ASC speck formation was detected by wide-field fluorescence microscopy (B) or flow cytometry (C,D). For microscopy, cells were seeded on cover slips prior to stimulation. Fixed cells were stained for DNA. Scale bars represent 50 µm. For flow cytometry, the altered height and width signal of ASC-EGFP was utilized to quantify cells with specks, as illustrated. (**E**) HEK$^{NLRP3+ASC}$ cells were stimulated with 200 ng/mL LPS for 3 h and 10 µM nigericin (Nig) for 1 h, or left untreated (UT), followed by quantification of ASC-EGFP specks by flow cytometry. Data represents average values (with individual data points) from three independent experiments ± 95 % confidence interval (CI). Immunoblot in (A) and microscopy images in (B) display experiment representatives of two independent experiments.

assembled ASC specks after talabostat stimulation (Fig. 2.1 C,D). HEK$^{NLRP3+ASC}$ cells did not respond, but they formed ASC specks after treatment with LPS and the potassium ionophore nigericin (Nig), validating functional NLRP3 inflammasomes (Fig. 2.1 E).

To assess human NLRP1 inflammasome assembly in keratinocytes at endogenous levels of NLRP1 and ASC, N/TERT-1 keratinocytes were equipped with a reporter construct composed of the caspase-1^{CARD} (C1C) fused to EGFP, resulting in N/TERT-1$^{C1C\text{-}EGFP}$ reporter cells (Fig. 2.2 A,B). Similarly to caspase-1, C1C-EGFP was efficiently recruited to ASC specks, allowing detection of inflammasome assembly after talabostat stimulation by fluorescence microscopy (Fig. 2.2 C) and flow cytometry (Fig. 2.2 D), utilizing the characteristic redistribution of fluorescence into a single speck per cell as for ASC-EGFP. Unlike HEK 293T cells, N/TERT-1 keratinocytes release processed IL-1β and undergo pyroptosis as a consequence of inflammasome activation. Since pyroptotic cells lose their mechanical resilience and rupture easily (M. A. Davis et al., 2019), all experiments for the quantification of ASC specks in keratinocytes were performed in the presence of the caspase-1 inhibitor Vx-765 (VX) to prevent loss of responding pyroptotic cells during the experimental procedure (Fig. 2.2 E). I was further able to complement the ASC speck readout by quantifying caspase-1-dependent IL-1β release and (pyroptotic) cell death in parallel experiments omitting Vx-765.

To validate NLRP1-dependent inflammasome assembly, polyclonal NLRP1 knockout N/TERT-1$^{C1C\text{-}EGFP}$ derivatives were generated, followed by the selection of monoclonal cell lines by limiting dilutions (Fig. 2.2 F). Wild type (wt) but not NLRP1 knockout N/TERT-1$^{C1C\text{-}EGFP}$ cells assembled ASC specks and released IL-1β after stimulation with talabostat. IL-1β release was completely inhibited in the presence of caspase-1 inhibitor Vx-765, confirming caspase-1-dependent processing and release of the proinflammatory cytokine (Fig. 2.2 G). The response rates were low compared to the engineered HEK 293T reporter system, revealing inflammasome formation in less than 5 % of all reporter cells. This may be attributed to endogenous protein levels or a higher threshold of activation. In line with the weak inflammasome response, no talabostat-induced cell death was detected by quantification of lactate dehydrogenase (LDH) release or uptake of the non-cell permeable DNA dye DRAQ7 (Fig. 2.2 G,H). However, the few dying cells showed the characteristic ballooning phenotype of pyroptotic cells (Fig. 2.2 I).

Thus, both reporter cells enable the direct analysis of human NLRP1 inflammasome

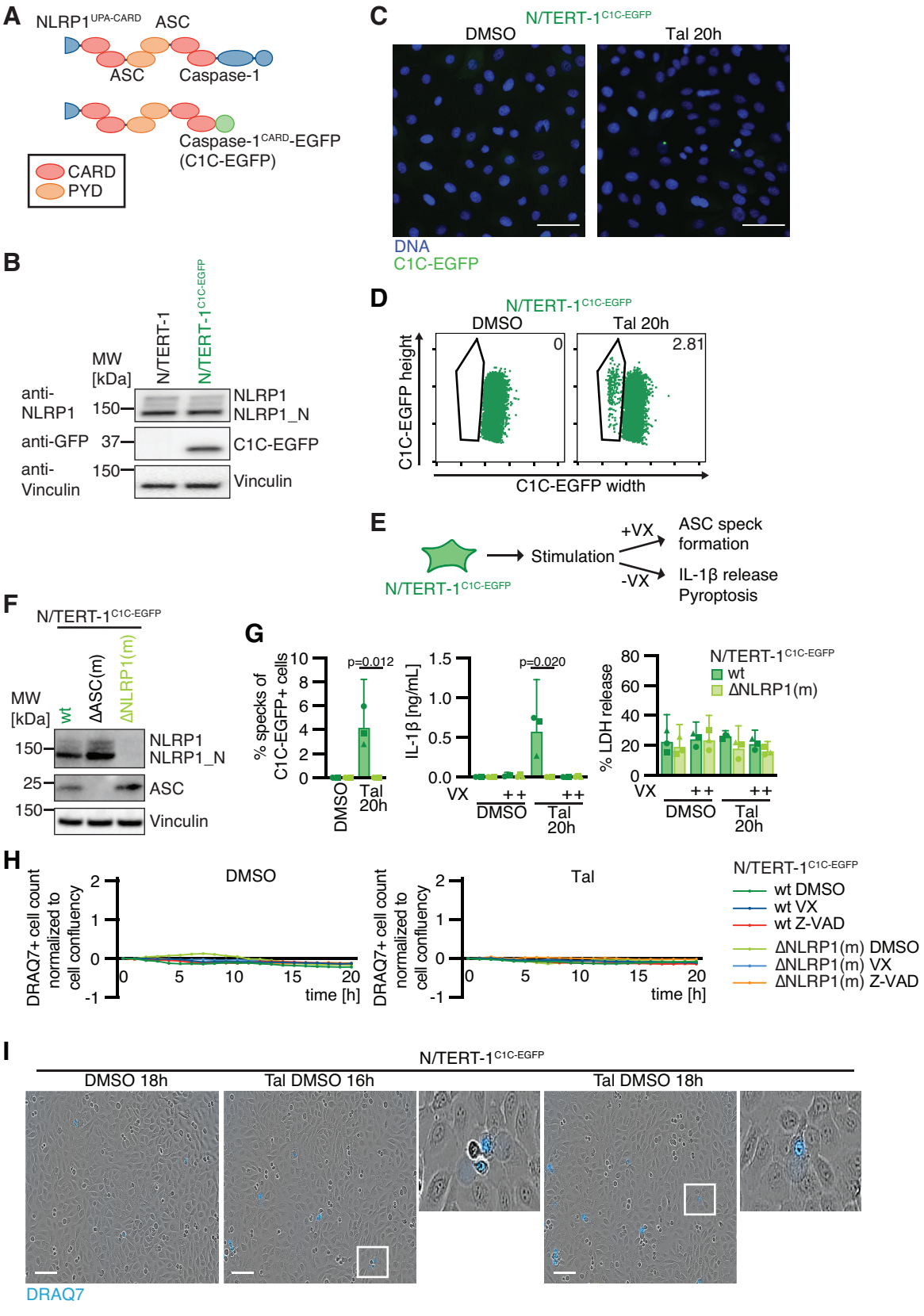

Figure 2.2: N/TERT-1 keratinocyte reporter cells recapitulate NLRP1 inflammasome activation. (**A**) Scheme of Caspase-1^{CARD}-EGFP (C1C-EGFP) reporter recruited to the ASC speck via CARD-CARD interaction, similar to Caspase-1. (**B**) Lysates of N/TERT-1 and N/TERT-1$^{C1C\text{-}EGFP}$ cells were analyzed by immunoblot with the indicated antibodies to confirm expression of NLRP1 and C1C-EGFP. (**C,D**) N/TERT-1$^{C1C\text{-}EGFP}$ cells were stimulated with DMSO or 30 µM Tal for 20 h. ASC speck formation was detected by wide-field fluorescence microscopy (C) or flow cytometry (D), as described in Fig. 2.1. Scale bars represent 50 µm. (**E**) ASC speck formation in N/TERT-1 cells was detected in the presence of 100 µM Vx-765 (VX). Caspase-1-dependent IL-1β release and pyroptosis were detected in the absence of VX. (**F**) Monoclonal ASC and NLRP1 knockout derivatives of N/TERT-1$^{C1C\text{-}EGFP}$ cells were confirmed by immunoblot with the indicated antibodies. (**G-I**) N/TERT-1$^{C1C\text{-}EGFP}$ cells and their monoclonal NLRP1 knockout derivatives were stimulated with Tal, where indicated in the presence of 100 µM VX, 50 µM Z-VAD(OMe)-FMK (Z-VAD), or DMSO. (G) ASC speck formation was quantified by flow cytometry and supernatants from the same cells were collected. IL-1β release was quantified by Homogeneous Time Resolved Fluorescence (HTRF). Cell death was quantified by detection of lactate dehydrogenase (LDH) release. (H) Cell death was quantified by uptake of non-cell permeable DNA dye DRAQ7 over 20 h. (I) Representative microscopy images of DRAQ7 uptake and pyroptotic cells. Scale bars represent 100 µm. Data represents average values (with individual data points) from three independent experiments ± 95 % CI, p-values were calculated using unpaired t-test. Immunoblots in (B,F) and microscopy images in (D) display experiment representatives of two independent experiments. Quantifications of DRAQ7 uptake over time in (G) and microscopy images in (I) display experiment representatives of three independent experiments.

assembly, especially combined with the simple quantification of ASC specks by flow cytometry. While HEK-based reporter cells show high response rates within a minimal inflammasome setting, the N/TERT-1 cells reflect endogenous protein levels and recapitulate the entire inflammatory signaling pathway. This makes them a useful tool to screen for potential NLRP1 activators and delineate the mechanisms of NLRP1 activation.

2.2.2 Identification of human NLRP1^{PYD}-specific nanobodies

To complement my toolbox for studying human NLRP1 inflammasome activation, I decided to produce NLRP1-specific nanobodies as they are promising tools to specifically manipulate the inflammasome sensor in living cells. I used NLRP1^{PYD}, NLRP1^{LRR}, and NLRP1^{CARD} as potential targets for the nanobodies. All domains represent possible targets for manipulation or inhibition of NLRP1, as ubiquitination and degradation of the NLRP1 N-terminus seem to be key events in activation (Chui et al., 2019; Sandstrom et al., 2019),

NLRP1^{LRR} was reported to bind dsRNA (Bauernfried et al., 2021) and NLRP1^{CARD} is the ASC-recruiting domain of the active NLRP1$^{UPA\text{-}CARD}$ fragment (Finger et al., 2012; Gong et al., 2021). VHH libraries for all three NLRP1 domains had already been generated after immunization of one alpaca with His-NLRP1^{PYD} and His-NLRP1^{CARD}, as well as one llama with His-NLRP1^{LRR}. Moreover, an earlier selection by phage display resulted in some hits for potential NLRP1^{PYD} and NLRP1^{CARD} nanobodies. To verify these hits by enzyme-linked immunosorbent assay (ELISA), I purified new NLRP1^{PYD}, NLRP1^{LRR}, and NLRP1^{CARD} proteins. I produced recombinant proteins for all three domains in bacteria as a fusion to glutathione S-transferase (GST) and purified them by affinity- and size-exclusion chromatography. Unfortunately, I could not completely separate the fusion proteins from GST-only fragments, which were still present in the final products for all expressed domains (Fig. 2.3 A).

I used the GST fusion proteins to confirm the binding of two potential NLRP1-specific nanobodies, one against NLRP1^{PYD} (VHH$_{PYD\ 1}$ or VHH AF-F08a) and one against NLRP1^{CARD} (VHH$_{CARD}$ or VHH AG-C03). VHH$_{PYD\ 1}$ showed strong binding to GST-NLRP1^{PYD} in ELISA, whereas the binding of VHH$_{CARD}$ to GST-NLRP1^{CARD} was rather weak (Fig. 2.3 B). When I performed the same ELISA with full-length NLRP1-SH, extracted from cell lysates using Streptactin, only VHH$_{PYD\ 1}$ was able to bind its target (Fig. 2.3 C). This suggests that VHH$_{CARD}$ cannot bind the natural configuration of NLRP1^{CARD} within the folded full-length protein, either because the recognized epitope is blocked in this conformation or because the nanobody detects an artificial epitope based on structures only formed by purified NLRP1^{CARD}.

To identify more nanobodies against NLRP1, I performed new selections by phage display using the existing phagemid libraries. Infection of phagemid plasmid-containing bacteria with helper phages generated nanobody-presenting phages, which I used to perform two rounds of phage display assay to select phages that specifically bound GST-NLRP1^{PYD}, GST-NLRP1^{LRR}, or GST-NLRP1^{CARD} (Fig. 2.3 D). I finally obtained 45 hits for GST-NLRP1^{PYD} and 35 hits for GST-NLRP1^{CARD}, which were divided into 5 and 4 clusters based on their sequence similarity. There were no hits for GST-NLRP1^{LRR}, even though I performed an additional phage display selection using biotinylated NLRP1^{LRR} (data not shown). When I compared the sequences of the cluster representatives of VHH$_{PYD}$ and VHH$_{CARD}$, I noticed that all VHH$_{CARD}$ hits cluster with VHH$_{PYD}$ hits, suggesting that these

nanobodies actually bind the shared fusion partner GST but not the NLRP1 domains. This

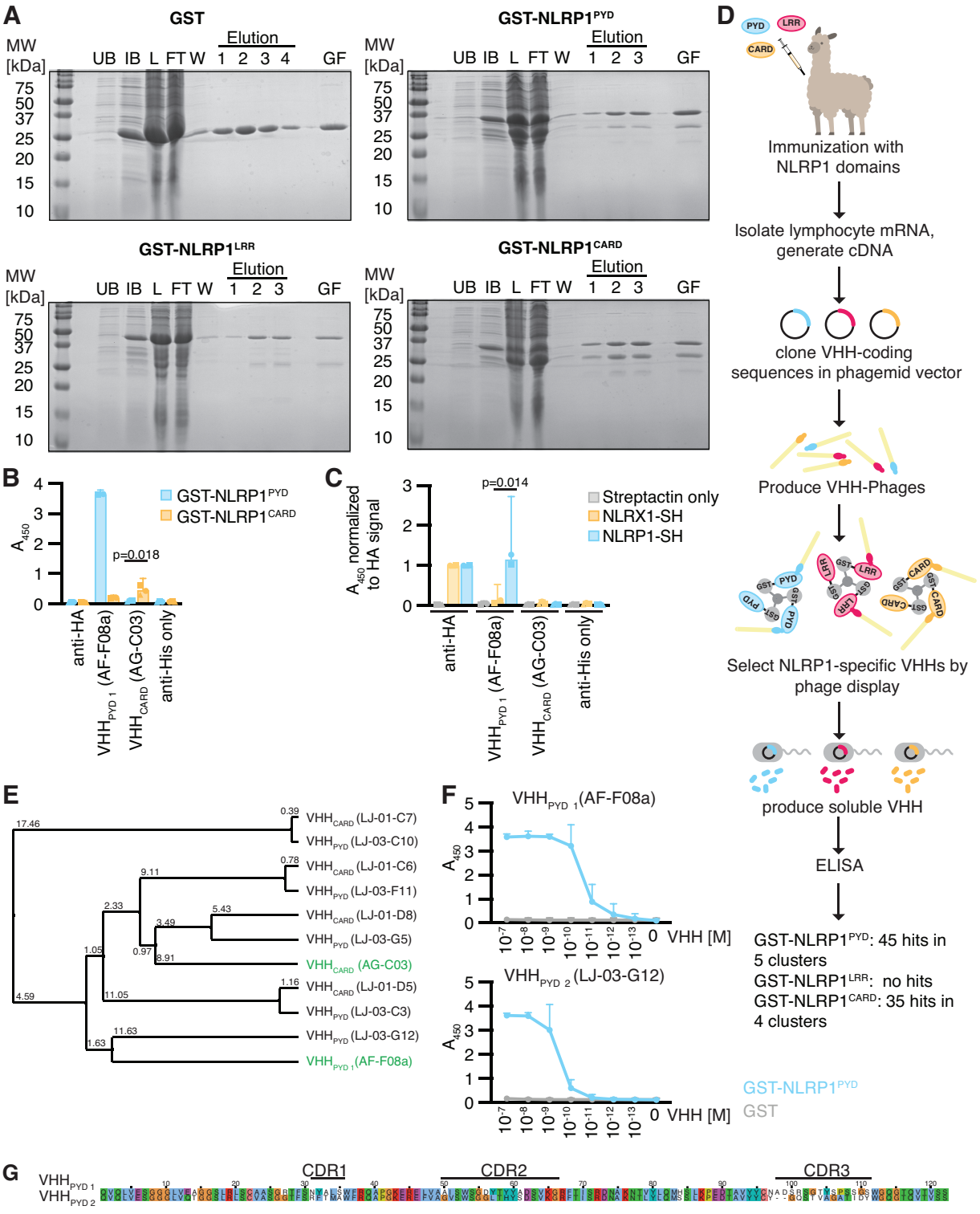

Figure 2.3: Identification of NLRP1-specific nanobodies. (**A**) Purification process of recombinant GST, GST-NLRP1^{PYD}, GST-NLRP1^{LRR}, and GST-NLRP1^{CARD} was analyzed by SDS-PAGE and Coomassie staining. *Escherichia coli* BL21 were transformed with corresponding expression constructs (uninduced bacteria [UB]) and expression was induced by addition of 0.2 M IPTG (induced bacteria [IB]). Bacteria were lysed by sonification [L] and GST proteins were enriched by affinity chromatography using glutathione beads (flow through [FT], wash [W], elutions [E]). Pooled elutions were further purified by gel filtration [GF]. (**B**) Binding of indicated His-tagged nanobodies (VHHs) and anti-HA antibodies to immobilized GST-NLRP1^{PYD} or GST-NLRP1^{CARD} was quantified by ELISA. (**C**) Binding of indicated His-tagged VHHs and anti-HA antibodies to immobilized full-length NLRP1-SH or control protein NLRX1-SH was quantified by ELISA. Target proteins were extracted from target-overexpressing cell lysates using Streptactin-coated plates. (**D**) Schematic overview of VHH identification process. Camelids were immunized with NLRP1^{PYD}, NLRP1^{LRR}, or NLRP1^{CARD}. VHH-coding sequences were extracted from lymphocyte mRNA and cloned into phagemid vector libraries, which were used to produce VHH-presenting phages. Phages that encode NLRP1-binding VHHs were selected by two rounds of phage display using GST-NLRP1^{PYD}-, GST-NLRP1^{LRR}-, and GST-NLRP1^{CARD}-loaded magnetic beads. Bacteria were infected by the selected phages to generate single clones encoding specific VHH sequences in the phagemid vector. 95 clones per target were screened for binding by ELISA. All positive hits were sequenced and divided into clusters based on their sequence similarity in Average Distance Tree. (**E**) Average Distance Tree for all GST-NLRP1^{PYD} and GST-NLRP1^{CARD} cluster representatives, as well as the known binders VHH$_{CARD}$ and VHH$_{PYD\ 1}$ in green. (**F)** Binding of indicated concentration of His-tagged VHHs to immobilized GST-NLRP1^{PYD} or control protein GST was quantified by ELISA. (**G**) Alignment of NLRP1^{PYD} VHHs with indicated complementarity determining regions (CDRs). Data in (B,C,F) represents average values (with individual data points) from two (VHH$_{PYD\ 1}$ data in B,C) or three independent experiments ± 95 % CI, p-values were calculated using unpaired t-test.

was also confirmed in additional ELISA experiments (data not shown). Only one VHH$_{PYD}$ hit (VHH LJ-03-G12) clustered separately and the binding of VHH LJ-03-G12 to GST-NLRP1^{PYD} was confirmed by ELISA, where it showed only slightly lower affinity than VHH$_{PYD\ 1}$ (Fig. 2.3 F). Importantly, neither of the nanobodies bound the GST-only control. The detailed sequence comparison showed that the two NLRP1^{PYD} binders mostly differ in the CDR1 and CDR3 regions, while their CDR2 regions revealed more than 70 % sequence homology (Fig. 2.3 G). From here on, VHH LJ-03-G12 will be named VHH$_{PYD\ 2}$.

In summary, I identified two nanobodies binding human NLRP1^{PYD}. In contrast, NLRP1^{LRR} and NLRP1^{CARD} seem to be difficult targets for nanobodies, as there were no new reproducible hits after phage display and the confirmed binder VHH$_{CARD}$ did not bind the full-length protein.

2.2.3 Targeted ubiquitination of NLRP1^{PYD} by VHL-VHH$_{PYD}$ is sufficient for NLRP1 inflammasome activation

After the discovery of two NLRP1^{PYD}-specific nanobodies, I could study the activation of endogenous NLRP1 by N-terminal ubiquitination and degradation. So far, targeted degradation of human NLRP1 was based on overexpression of N-terminal tagged NLRP1 that allowed inducible degradation in HEK 293T cells (Hollingsworth et al., 2021; Sandstrom et al., 2019). Here, I used the NLRP1^{PYD} nanobodies to overcome these limitations and specifically ubiquitinate endogenous human NLRP1 at the N-terminus.

To do this, I first generated expression vectors for fusions of nanobodies to the human CRL2 substrate receptor VHL, as previously described by Fulcher et al. (Fulcher et al., 2016, 2017), and transiently transfected the FLAG-tagged constructs in the HEK$^{NLRP1+ASC}$

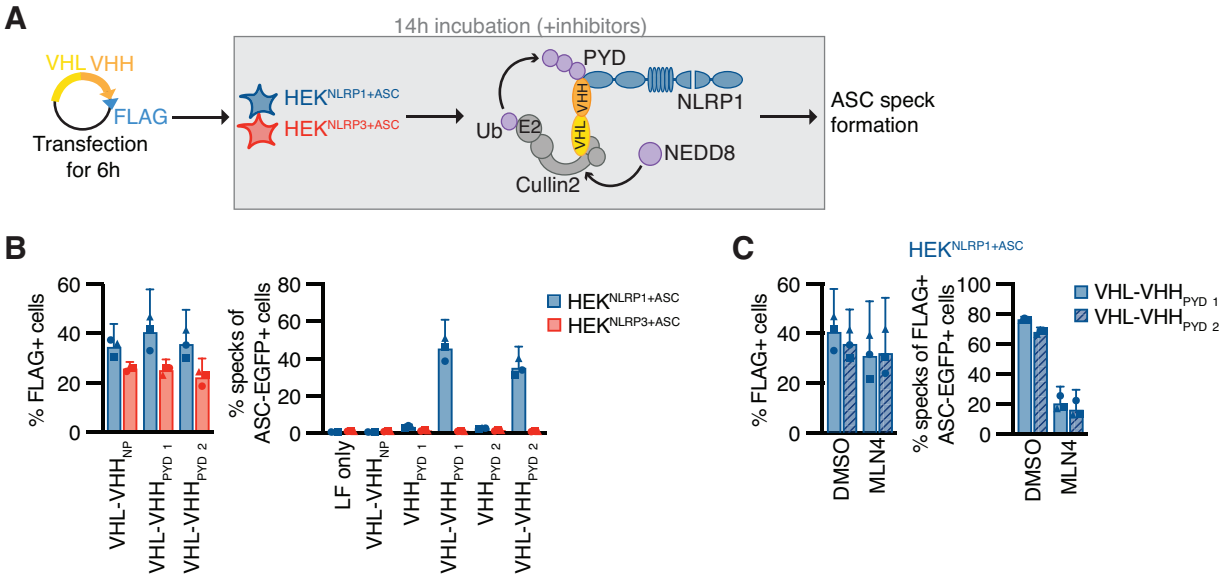

Figure 2.4: Targeted ubiquitination of NLRP1^{PYD} by VHL-VHH$_{PYD}$ is sufficient for NLRP1 inflammasome assembly in HEK 293T reporter cells. (**A**) Schematic overview of the experimental setup and VHH-mediated ubiquitination of NLRP1. HEK$^{NLRP1+ASC}$ and HEK$^{NLRP3+ASC}$ cells were transiently transfected with expression vectors for FLAG-tagged Von Hippel Lindau (VHL)-VHH fusions or HA-tagged VHHs alone for 6 h. Lipofectamine (LF) only treated cells served as controls. Cells were further incubated for 14 h, where indicated in the presence of 1 µM MLN4924 (MLN4) or DMSO. VHL-VHH$_{PYD}$ expression leads to the recruitment of Cullin2 Ring E3-ligase complexes, ubiquitination of NLRP1^{PYD}, and NLRP1 activation by degradation, observable by ASC speck formation. (**B,C**) FLAG-tagged VHL-VHH expression and ASC speck formation were quantified by flow cytometry, as described in Fig. 2.1. Quantification of specks was limited to FLAG-positive cells in (C). Data represents average values (with individual data points) from three independent experiments ± 95 % CI. Ub indicates ubiquitin.

and HEK$^{NLRP3+ASC}$ reporter cells (Fig. 2.4 A). VHL-VHH$_{PYD\ 1}$ and VHL-VHH$_{PYD\ 2}$, as well as the VHL fusion to a control nanobody targeting influenza A virus NP (Ashour et al., 2015) (VHL-VHH$_{NP-1}$), were similarly expressed but only the NLRP1^{PYD}-specific nanobody fusions induced ASC speck formation in more than 40 % of HEK$^{NLRP1+ASC}$ cells (Fig. 2.4 B). In line with the affinities measured by ELISA, VHL-VHH$_{PYD\ 1}$ was the stronger activator of the two nanobodies. Expression of NLRP1^{PYD} nanobodies alone did not stimulate an inflammasome response. When I specifically gated for VHL-VHH$_{PYD}$-expressing cells, almost 80 % of the cells exhibited ASC specks (Fig. 2.4 C), indicating nearly complete activation of NLRP1 in these cells. Inhibition of neddylation with the NEDD8-activating enzyme inhibitor MLN4924 (MLN4) blocked NLRP1 inflammasome activation by VHL-VHH$_{PYD}$, in line with the recruitment of CRL2 complexes by VHL and the critical role of NEDD8 for the activity of canonical CRLs (Fig. 2.4 C) (Soucy et al., 2009).

Next, I generated N/TERT-1 keratinocyte cell lines expressing C1C-EGFP as well as VHHs or VHL-VHH fusions under the control of a bidirectional doxycycline (dox)-inducible promoter (Fig. 2.5 A). Induction of expression led to a similar expression of C1C-EGFP in all cell lines, suggesting that nanobodies and their fusions were similarly transcribed as well (Fig. 2.5 B). Only induced expression of VHL-VHH$_{PYD\ 1}$ and VHL-VHH$_{PYD\ 2}$ triggered

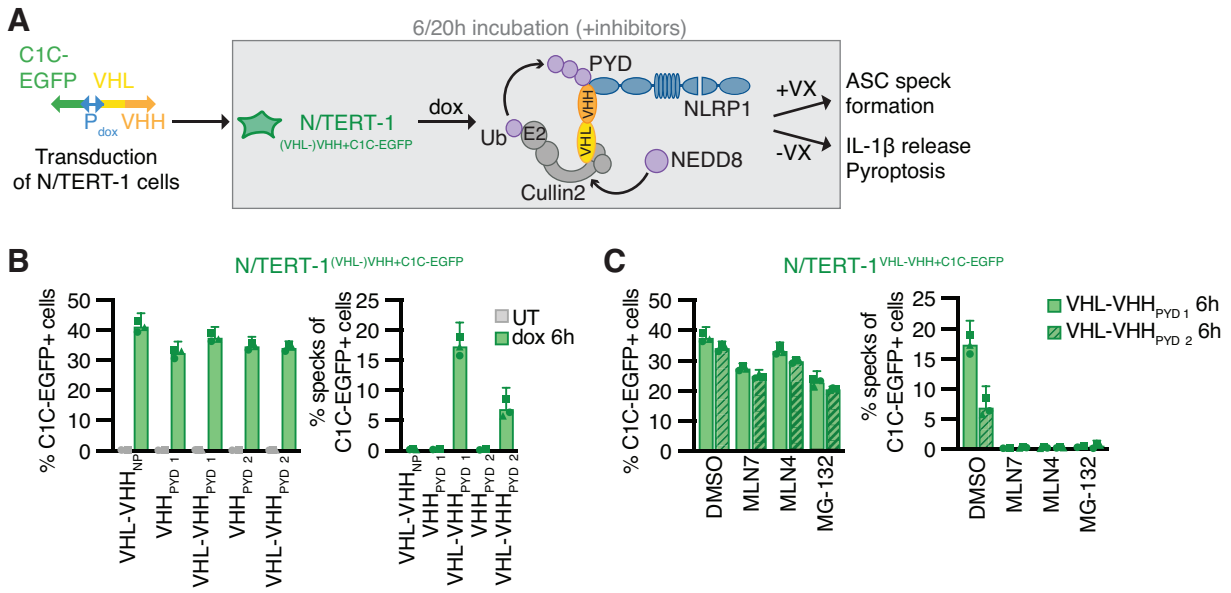

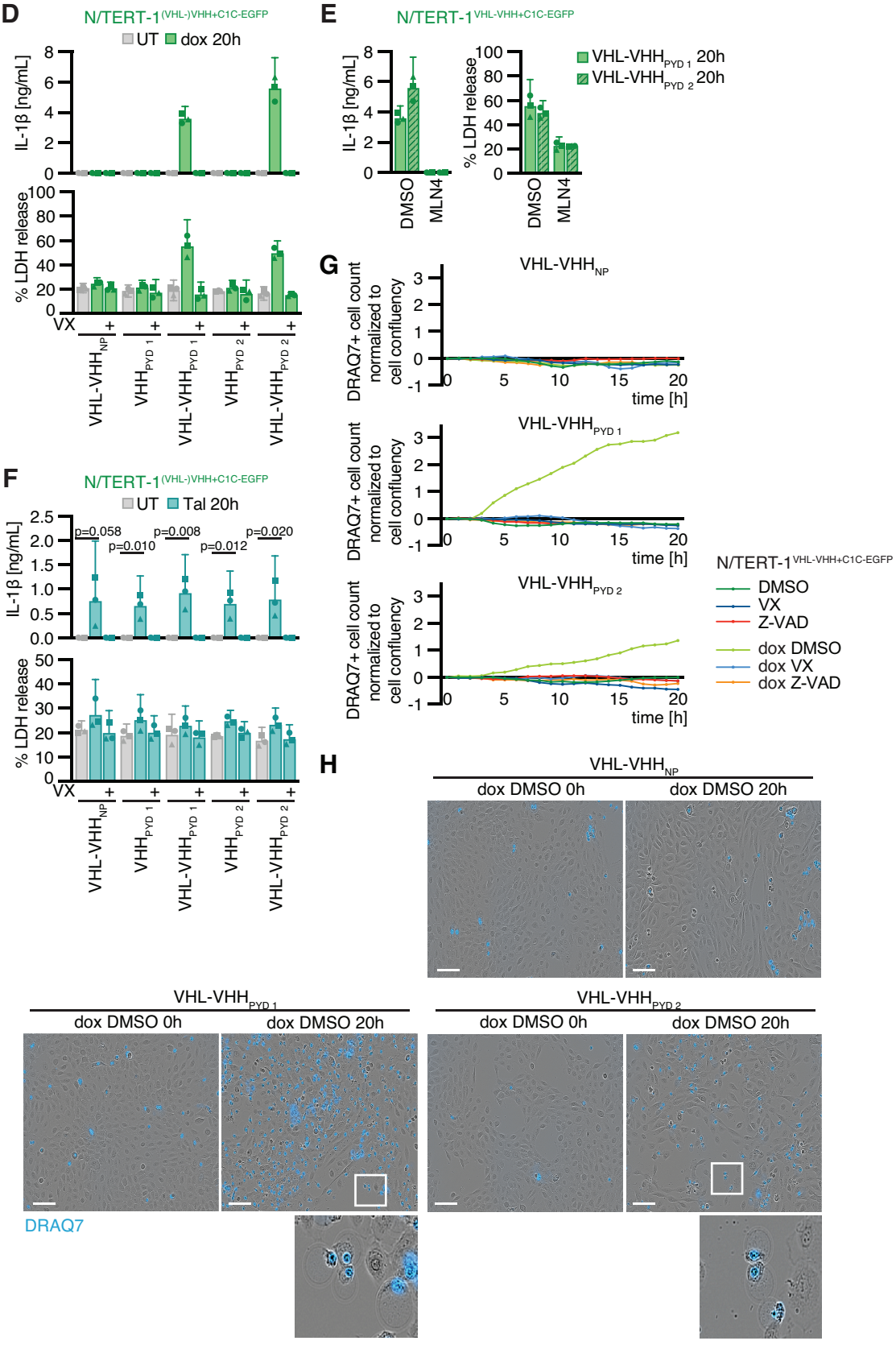
D
N/TERT-1 (VHL-)VHH+C1C-EGFP
UT
dox 20h
IL-1β [ng/mL]
% LDH release
VX
VHL-VHH NP
VHH PYD 1
VHL-VHH PYD 1
VHH PYD 2
VHL-VHH PYD 2
E
N/TERT-1 VHL-VHH+C1C-EGFP
VHL-VHH PYD 1 20h
VHL-VHH PYD 2 20h
DMSO
MLN4
F
N/TERT-1 (VHL-)VHH+C1C-EGFP
UT
Tal 20h
p=0.058
p=0.010
p=0.008
p=0.012
p=0.020
G
VHL-VHH NP
VHL-VHH PYD 1
VHL-VHH PYD 2
DRAQ7+ cell count normalized to cell confluency
time [h]
N/TERT-1 VHL-VHH+C1C-EGFP
DMSO
VX
Z-VAD
dox DMSO
dox VX
dox Z-VAD
H
VHL-VHH NP
dox DMSO 0h
dox DMSO 20h
VHL-VHH PYD 1
VHL-VHH PYD 2
DRAQ7

Figure 2.5: Targeted ubiquitination of NLRP1^{PYD} by VHL-VHH$_{PYD}$ is sufficient for NLRP1 inflammasome activation in N/TERT-1 keratinocyte reporter cells. (**A**) Schematic overview of the experimental setup and VHH-mediated ubiquitination of NLRP1. N/TERT-1 cells were transduced with lentiviral vectors encoding C1C-EGFP and (VHL-)VHH controlled by a bidirectional doxycycline (dox)-inducible promoter. N/TERT-1$^{(VHL-)VHH+C1C-EGFP}$ cells were treated with 1 µg/mL dox for 6 h or 20 h to induce expression, where indicated in the presence of 1 µM MLN7243 (MLN7), 1 µM MLN4, 1 µM MG-132, 100 µM VX, 50 µM Z-VAD, or DMSO. Untreated cells (UT) served as a control. ASC speck formation was detected in the presence of caspase-1 inhibitor VX. (**B,C**) C1C-EGFP expression and ASC speck formation in C1C-EGFP+ cells were quantified after 6 h dox treatment by flow cytometry, as described in Fig. 2.1. (**D,E**) Supernatants were collected after 20 h dox treatment. IL-1β release was quantified by HTRF. Cell death was quantified by detection of LDH release. (**F**) Supernatants from cells stimulated with 30 µM Tal for 20 h, in the absence of dox, were analyzed for IL-1β and LDH release as above. (**G**) Cell death was quantified by uptake of non-cell permeable DNA dye DRAQ7 over 20 h. (**H**) Representative microscopy images of DRAQ7 uptake and pyroptotic cells. Scale bars represent 100 µm. Data represents average values (with individual data points) from three independent experiments ± 95 % CI, p-values were calculated using unpaired t-test. Quantifications of DRAQ7 uptake over time in (G) and microscopy images in (H) display experiment representatives of three independent experiments. Ub indicates ubiquitin.

inflammasome assembly, which was already detectable 6 h post-induction, with faster activation by VHH$_{PYD\ 1}$ than by VHH$_{PYD\ 2}$. Inflammasome responses were substantially higher than after talabostat treatment with ASC speck formation in nearly 20 % of VHH$_{PYD\ 1}$-expressing cells already after 6 h. Neither nanobody expression alone, nor VHL fusions to the control nanobody VHH$_{NP-1}$ induced inflammasome assembly. The fast inflammasome activation allowed me to quantify responses in the presence of inhibitors of E1 ubiquitin-activating enzyme (MLN7243, here MLN7) and the proteasome (MG-132), which are toxic during prolonged incubations, next to the less toxic neddylation inhibitor MLN4924. I found that inflammasome assembly was completely blocked by either inhibitor, indicating that VHL fusions of NLRP1^{PYD} nanobodies indeed rely on the activation of ubiquitin, CRLs, as well as the proteasome to mediate ubiquitination and N-terminal degradation of NLRP1 (Fig. 2.5 C). Assembly of ASC specks was accompanied by caspase-1-dependent IL-1β release and cell death, which were likewise substantially higher than after talabostat treatment and inhibited by neddylation inhibitors (Fig. 2.5 D,E). In contrast to ASC speck formation, cells expressing VHL-VHH$_{PYD\ 2}$ released more IL-1β. All generated cell lines exhibited comparable levels of IL-1β and LDH release when treated with talabostat in the absence of transgene expression, confirming functional

NLRP1 inflammasomes in all cell lines (Fig. 2.5 F). When I quantified cell death over time by uptake of the non-cell permeable DNA dye DRAQ7, I saw a continuous increase in caspase-1-dependent cell death for both VHL-VHH$_{PYD}$, starting already 4 h post-induction (Fig. 2.5 G). VHL-VHH$_{PYD\ 2}$ induced less cell death, which is probably why the cells can process and release more IL-1β. Microscopy analyses revealed that VHL-VHH$_{PYD}$-expressing cells show the characteristic ballooning phenotype of pyroptotic cells (Fig. 2.5 H).

Thus, I succeeded in specifically activating human NLRP1 using the NLRP1^{PYD}-specific nanobodies in combination with the VHL system. Thereby, I also prove that targeted ubiquitination of human NLRP1^{PYD} is sufficient for its activation by N-terminal degradation. This well-controlled system allows the precise and direct activation of endogenous NLRP1 in the absence of any upstream signals.

2.3 Discussion

Reporter cells enable the analysis of human NLRP1 inflammasome activation

I first validated HEK 293T and N/TERT-1 NLRP1 reporter cell lines which had been generated in the lab to study human NLRP1 inflammasome activation. HEK 293T cells are a useful system to reconstitute different inflammasomes in a bottom-up approach, as they lack most inflammasome-relevant proteins (Agostini et al., 2004; Chavarría-Smith et al., 2016). Recently, Yang et al. were able to detect NLRC4 and pyrin in HEK cell lysates but NLRP1 and NLRP3 were not expressed (X. Yang et al., 2022). Many groups used similar reconstituted HEK cell systems to study rodent and human NLRP1 inflammasomes. Some reconstituted the cells with NLRP1, ASC, caspase-1, pro-IL-1β, and GSDMD to analyze NLRP1-induced pyroptosis and cytokine release (Ball et al., 2020; Chavarría-Smith et al., 2016; Chui et al., 2019, 2020; Gai et al., 2019; Hollingsworth, Sharif, et al., 2021; Sandstrom et al., 2019; Tsu et al., 2021). Others also used ASC-EGFP-expressing HEK cells to detect NLRP1-dependent ASC speck formation (Ball et al., 2020, 2022; Gai et al., 2019; Gong et al., 2021; Moecking et al., 2021; Robinson et al., 2020, 2022; Zhong et al., 2016, 2018). Most of the mentioned NLRP1 assays in HEK cells were based on transient transfections of the required inflammasome components.

However, inflammasome sensors and ASC are prone to oligomerization even in the absence of stimuli, causing high baseline levels of inflammasome assembly in unregulated overexpression systems. I observed ASC speck formation in more than 50 % of NLRP1-transfected ASC-EGFP-expressing HEK cells without additional stimulation, even when I reduced the amount of transfected NLRP1 expression plasmid drastically (data not shown). If most of the cells activate NLRP1 just by overexpression, it is difficult to differentiate between baseline and stimulus-induced signals. Furthermore, transfections lead to variable expression levels, compromising the reproducibility of experiments. Therefore, we decided to generate cell lines that express the NLR sensors and ASC-EGFP under control of the weak pUbC promoter to minimize baseline inflammasome formation as much as possible. The selection of monoclonal ASC-EGFP-expressing cells with a low ASC speck background and NLRP1/NLRP3-expressing cells with an optimal signal-to-noise ratio generated $HEK^{NLRP1+ASC}$ and $HEK^{NLRP3+ASC}$ cell lines with a baseline inflammasome response of maximally 2 %. These reporter cells enable the sensitive detection of inflammasome assembly and the stable expression of all components permits high reproducibility. Another advantage of the HEK 293T cell system is the possibility to express different inflammasome sensor mutants or variants to study the influence of certain domains or amino acids on sensor activity. I will use HEK 293T cells expressing murine and mutant forms of NLRP1 in chapters 3 and 4. In addition, $HEK^{NLRP1+ASC}$ and $HEK^{NLRP3+ASC}$ cells do not undergo pyroptosis after inflammasome activation as they lack the required components. This allows the analysis of ASC speck formation by flow cytometry without additional caspase-1 inhibitor treatment.

To complement the reconstituted cell line approach, immortalized N/TERT-1 keratinocytes were used to analyze the activation of endogenous NLRP1 and its outcomes in a physiologically relevant cell type. N/TERT keratinocytes were generated by expression of the telomerase subunit hTERT, combined with the spontaneous loss of cell cycle control mechanisms (Dickson et al., 2000). Compared to primary keratinocytes, N/TERT cells show similar differentiation and formation of epidermal equivalents at air interfaces (Smits et al., 2017). Primary keratinocytes express NLRP1, ASC, caspase-1, and pro-IL-1β, without the need for additional priming (Mizutani et al., 1991; Zhong et al., 2016) and the same was shown for N/TERT keratinocytes (Bauernfried et al., 2021). Transcriptional

analyses of primary keratinocytes showed that they do not express AIM2, NLRP3, and NLRC4 (J. Y. Zhou et al., 2023). AIM2 expression can be induced by IFN-γ priming of primary and N/TERT keratinocytes (Dombrowski et al., 2011; J. Y. Zhou et al., 2023) and there was also a report about IFN-γ-induced NLRP3 expression (Fenini, Grossi, Contassot, et al., 2018). However, Bauernfried et al. detected no inflammasome response in N/TERT cells after priming and stimulation with nigericin (Bauernfried et al., 2021). By now, N/TERT cells are an accepted and widely used model to study endogenous NLRP1 inflammasomes (Ball et al., 2022; Bauernfried et al., 2021; Robinson et al., 2020, 2022; Q. Wang et al., 2023; Zhong et al., 2016, 2018; J. Y. Zhou et al., 2023). It is also important to mention that N/TERT keratinocytes show no activation of CARD8 after inhibition of DPP8/9 by talabostat (Bauernfried et al., 2021). Since NLRP1 and CARD8 share processing of the FIIND, stimuli like talabostat and viral protease cleavage can potentially activate both inflammasome sensors. Thus, inflammasome responses in cells that express both CARD8 and NLRP1 cannot be easily allocated to one or the other. This was shown in primary human aortic endothelial cells, in which both sensors contribute to talabostat- and Coxsackie virus B3-induced pyroptosis and IL-18 release (Nadkarni et al., 2022). Another example is the human monocytic THP-1 cell line which is widely used in inflammasome studies. Even though these cells express NLRP1, inhibition of DPP8/9 induces only CARD8-dependent pyroptosis (D. C. Johnson et al., 2018; X. Yang et al., 2022). Thus, N/TERT keratinocytes, which seem to lack functional CARD8 inflammasomes, are a good model to specifically study NLRP1 activity.

ASC-dependent inflammasomes like NLRP1 require the adaptor protein ASC to recruit and activate caspase-1 (Fernandes-Alnemri et al., 2007). Therefore, ASC speck assembly is a sufficient readout for NLRP1 inflammasome formation, as all downstream readouts like pyroptosis and IL-1β release depend on ASC speck-mediated caspase-1 activation (Ball et al., 2020; Zhong et al., 2018). ASC speck formation also discriminates between NLRP1 and CARD8 stimulation because CARD8 cannot recruit ASC and only induces ASC-independent caspase-1 activation (Ball et al., 2020; Gong et al., 2021; Hollingsworth, David, et al., 2021), a fact that I confirmed in CARD8- and ASC-EGFP expressing HEK cells (data not shown). Moreover, ASC speck detection allows the analysis of inflammasome responses on a single cell level, enabling the exact quantification of

responsive cells in contrast to analyses based on whole cell lysates or supernatants. ASC speck assembly is also irreversible and the specks are highly stable, even showing extracellular proinflammatory activity (Bertheloot et al., 2022; Franklin et al., 2014). Therefore, they persist in cells as long as pyroptosis is blocked, enabling the detection of accumulated inflammasome responses over longer periods of time (Stein et al., 2016). To detect ASC speck formation in N/TERT keratinocytes, the cells were equipped with the inflammasome reporter C1C-EGFP. Caspase-1^{CARD} leads to efficient recruitment of EGFP to ASC specks, allowing the quantification of specks similar to ASC-EGFP but without altering the endogenous levels of ASC. This way, C1C-EGFP reporter cells have no background inflammasome formation at all, enabling the precise quantification of even weaker inflammasome responses. Endogenous caspase-1 can also still be activated in inflammasome-forming reporter cells, as I observed caspase-1-dependent IL-1β release in talabostat-treated N/TERT-$1^{C1C\text{-}EGFP}$ cells.

Both $HEK^{NLRP1+ASC}$ and N/TERT-$1^{C1C\text{-}EGFP}$ cells formed NLRP1 inflammasomes after inhibition of DPP8/9 by talabostat. NLRP1 is functional in HEK 293T cells because the FIIND is autoproteolytically processed even after reconstituted expression (Chavarría-Smith et al., 2016; D'Osualdo et al., 2011). This was also confirmed in fibroblasts and U2O2 cells reconstituted with NLRP1 (Finger et al., 2012; Liao & Mogridge, 2009). However, the immunoblots of NLRP1 from $HEK^{NLRP1+ASC}$ cell lysates show less processing than the ones of endogenous NLRP1 from N/TERT-1 keratinocyte lysates (compare Fig. 2.1A and Fig. 2.2B). Hence, despite the overexpression of NLRP1 in the HEK 293T cells, the amount of processed NLRP1 is comparable in the two cell types. Interestingly, while more than 40 % of $HEK^{NLRP1+ASC}$ cells assembled ASC specks after talabostat stimulation, only around 5 % of N/TERT-$1^{C1C\text{-}EGFP}$ cells responded to the same stimulus. The HEK 293T reporter cells represent an engineered overexpression system and therefore perhaps lack additional regulations of NLRP1 activity that are present in the endogenous keratinocyte system. Moreover, the monoclonal $HEK^{NLRP1+ASC}$ cells were selected based on a high NLRP1 response to talabostat. The cells may thus be selected for properties that promote NLRP1 responses, like alterations in DPP8/9 sequestration.
In line with the low number of inflammasome-forming N/TERT-1 cells, talabostat-treated keratinocytes released only low levels of IL-1β. In contrast, quantification of pyroptotic cell

death revealed no increase in membrane permeability at all. Low levels of talabostat-induced pyroptosis in N/TERT keratinocytes were reported before (Bauernfried et al., 2021; Robinson et al., 2022; Zhong et al., 2018). Nevertheless, the few dying N/TERT-1 cells showed the characteristic phenotype of pyroptotic cells, confirming that NLRP1 activation leads to cytokine processing and pyroptosis in these cells. Therefore, detection of ASC speck formation and IL-1β release are more sensitive readouts for weak NLRP1 responses in keratinocytes.

Even though the N/TERT keratinocytes are a useful cellular system to study NLRP1 inflammasomes, they still are an immortalized cell line that underwent spontaneous mutations, and are therefore not completely comparable to primary cells (Dickson et al., 2000). Therefore, all findings in N/TERT cells should be confirmed in primary keratinocytes, as done by others (Bauernfried et al., 2021; Robinson et al., 2022; Zhong et al., 2018). My lab is currently working on the generation and optimization of primary keratinocyte cultures to overcome these limitations. The next step will be to use human skin explants or 3D organotypic skin cultures in which the keratinocytes show the natural differentiation and epidermal structure as found at air-liquid interfaces (Robinson et al., 2022; Smits et al., 2017). These models reflect the most natural conditions of inflammasome responses in the human skin. It was for example shown that terminally differentiated keratinocytes in the stratum granulosum layer express the inflammasome sensor NLRP10, which cannot be observed in undifferentiated N/TERT cells (Próchnicki et al., 2023).

Challenges in the identification of human NLRP1^{CARD}-specific nanobodies

Next to the validation of NLRP1 reporter cell lines, I aimed to identify NLRP1-specific nanobodies that allow specific manipulation of the inflammasome sensor in living cells. I performed phage display assays to find nanobodies that bind NLRP1^{PYD}, NLRP1^{LRR}, and NLRP1^{CARD}. As we still lack NLRP1-specific inhibitors, inhibitory nanobodies would be a great tool to analyze the role of NLRP1 in different inflammatory conditions. NLRP1^{CARD} is the ASC-recruiting domain of the active NLRP1$^{UPA\text{-}CARD}$ fragment (Finger et al., 2012; Gong et al., 2021) and NLRP1^{CARD} nanobodies that directly interfere with the sensor oligomerization and the recruitment of ASC would probably be the most promising

candidates for potential NLRP1 inhibitory nanobodies. Unfortunately, there were no hits for $NLRP1^{LRR}$ and $NLRP1^{CARD}$, and the validation of an $NLRP1^{CARD}$ nanobody hit previously identified in the lab showed that it could only bind the purified GST-$NLRP1^{CARD}$ and not full-length NLRP1. The fact that VHH_{CARD} cannot bind the natural configuration of $NLRP1^{CARD}$ within the folded full-length protein could be explained by an artificial epitope based on structures only formed by purified $NLRP1^{CARD}$. It was shown that $NLRP1^{CARD}$ alone does not oligomerize because the UPA-like domain within the $NLRP1^{UPA\text{-}CARD}$ fragment mediates this process. Overexpression of $NLRP1^{CARD}$ alone can induce filament formation but the filaments differ from $NLRP1^{UPA\text{-}CARD}$ and other known CARD filament structures. $NLRP1^{CARD}$ seems to be prone to dimer formation and therefore forms thicker filaments than other CARD proteins (Gong et al., 2021; Hollingsworth, David, et al., 2021). Therefore, it is possible that overexpression of $NLRP1^{CARD}$ led to the formation of these unusual CARD dimers/filaments and the immunized camelids developed antibodies against these structures. In line with this hypothesis, in my experiments, only GST-$NLRP1^{CARD}$ showed an additional oligomer peak in size-exclusion chromatography. Another explanation would be that the recognized $NLRP1^{CARD}$ epitope is blocked in full-length NLRP1. Yang et al. describe a DPP9-independent NLRP1 complex in which the linker region (between PYD and NBD) and UPA-like domain of the FIIND interact (X. Yang et al., 2022). This interaction could also happen intramolecularly, causing a protein fold that interferes with the binding of VHH_{CARD}. Inactive NLRP3 forms a cage structure that switches into an active disk structure after priming and stimulation (Fu & Wu, 2023; Hochheiser et al., 2022). As there is no known structure of full-length NLRP1, it cannot be excluded that $NLRP1^{CARD}$ is kept in a similar inhibitory structure to prevent autoactivation of the inflammasome.

If the problem to find $NLRP1^{CARD}$ nanobodies is based on artificial dimer/filament formation, one could perform another immunization or phage display campaign using mutated $NLRP1^{CARD}$ that cannot oligomerize (Hollingsworth, David, et al., 2021). Another option would be the utilization of synthetic nanobody libraries (Muyldermans, 2021). The phage display selections could also be performed by directly using $NLRP1^{UPA\text{-}CARD}$. This way, potential $NLRP1^{CARD}$-blocking conformations of full-length NLRP1 could be avoided. To increase the chance of identifying inhibitory nanobodies, the oligomerization of

$NLRP1^{UPA\text{-}CARD}$ should again be prevented, to gain nanobodies that interfere with oligomerization instead of binding the oligomerized filaments.

Targeted ubiquitination of $NLRP1^{PYD}$ by $VHL\text{-}VHH_{PYD}$ is sufficient for NLRP1 inflammasome activation

In contrast to $NLRP1^{LRR}$ and $NLRP1^{CARD}$, I successfully identified and validated two $NLRP1^{PYD}$-specific nanobodies. This allowed me to specifically induce the ubiquitination of human endogenous NLRP1 at the N-terminal PYD, thereby inducing N-terminal degradation and inflammasome activation. So far, targeted degradation attempts of human NLRP1 were only achieved in HEK cell systems overexpressing AID- or dTAG-NLRP1 (Hollingsworth et al., 2021; Sandstrom et al., 2019). I achieved N-terminal ubiquitination of endogenous untagged NLRP1 by fusing the $NLRP1^{PYD}$-specific nanobodies to the human CRL2 receptor VHL, as described by Fulcher et al. (Fulcher et al., 2016, 2017). Targeted ubiquitination of NLRP1 by $VHL\text{-}VHH_{PYD}$ induced strong inflammasome activation in both $HEK^{NLRP1+ASC}$ cells and N/TERT-1 keratinocytes. Especially in the N/TERT-1 cells, the response rates were much higher than after inhibition of DPP8/9, causing robust IL-1β release and pyroptosis. This suggests that either the targeted degradation overcomes existing regulations of NLRP1 activity or talabostat is just a weak NLRP1 stimulus in keratinocytes. Importantly, $VHL\text{-}VHH_{PYD}$-induced NLRP1 inflammasome formation proves for the first time that targeted ubiquitination of $NLRP1^{PYD}$ is sufficient to activate endogenous human NLRP1.

Moreover, $VHL\text{-}VHH_{PYD}$ fusions represent strong NLRP1-specific stimuli that enable direct activation of human NLRP1 without disturbance of other cellular pathways. Therefore, it will be a useful tool to screen different cell types for functional NLRP1 inflammasomes. In contrast to talabostat, $VHL\text{-}VHH_{PYD}$ fusions will not activate CARD8 inflammasomes. The only requirement is that the fusions have to enter the cell to reach cytosolic NLRP1. Not every cell type can be lentivirally transduced to express $VHL\text{-}VHH_{PYD}$ fusions. A more universal strategy would be to purify the fusion protein and treat the cells extracellularly. It was shown that fusions of nanobodies to cell-penetrating peptides enable endocytosis-independent uptake (Herce et al., 2017; Sun et al., 2023), but it has to be tested whether this system is suitable for $VHL\text{-}VHH_{PYD}$ delivery. The $VHL\text{-}VHH_{PYD}$ system could also be

used to help identify inhibitory NLRP1^{CARD}-specific nanobodies. One could generate lentiviral VHH libraries (Schmidt, Hanke, et al., 2016) and transduce NLRP1-expressing and pyroptosis-competent cells to express VHL-VHH$_{PYD}$ and different VHH$_{CARD}$ under a bidirectional promotor. If most of the cells undergo VHL-VHH$_{PYD}$-mediated pyroptosis, the surviving cells should be enriched in inhibitory VHH$_{CARD}$ nanobodies.

It has to be mentioned that I neither confirmed ubiquitination nor degradation of NLRP1 in this setup. I proved that all readouts of NLRP1 inflammasome activation are inhibited by inhibitors of E1 enzymes, neddylation, and proteasomes, confirming that ubiquitination by canonical CRL complexes and subsequent proteasomal degradation are necessary for this mode of activation. NEDD8 executes cullin-independent functions as well (Enchev et al., 2015) but in the context of the other proteasomal degradation inhibitors, it is safe to assume that inhibition by MLN4924 is based on interference with the neddylation of CRL complexes. I tried to detect N-terminal degradation of NLRP1 in the context of other NLRP1 stimuli using immunoblots and NLRP1^{PYD}-specific antibodies. However, I found it difficult to show clear N-terminal degradation using this method. Small amounts of released NLRP1$^{UPA\text{-}CARD}$ are sufficient for inflammasome formation and only a small fraction of NLRP1 is likely degraded in inflammasome-forming cells, impeding the detection of degradation in bulk lysate assays (Hollingsworth, Sharif, et al., 2021; Sandstrom et al., 2019). The VHL-VHH$_{PYD}$ fusions recruit CRL2 complexes specifically to NLRP1^{PYD}, so it should be the N-terminus of NLRP1 that is ubiquitinated and subsequently degraded. Nevertheless, it was reported that ubiquitination of adaptor proteins is sufficient to degrade proteins in close proximity that exhibit unstructured regions (Prakash et al., 2009). Thus, it is possible that not NLRP1 but a potential negative regulator binding to the NLRP1^{PYD} is degraded, leading to inflammasome formation. Several arguments contradict this hypothesis: Firstly, NLRP1 mutants that exhibit GFP or mScarlet fluorescent proteins instead of NLRP1^{PYD} are not autoactive, arguing against an NLRP1^{PYD}-specific regulator (Bauernfried et al., 2021; Chavarría-Smith et al., 2016). Secondly, HRV14 3C proteases cleave the complete NLRP1^{PYD} off, but inflammasome activation still requires N-degron pathway-mediated proteasomal degradation (Robinson et al., 2020). Most importantly, many studies support the model in which NLRP1 has to be processed and degraded to release the active NLRP1$^{UPA\text{-}CARD}$ to form inflammasomes (Chui et al., 2019; Finger et al.,

2012; Sandstrom et al., 2019; Z. Xu et al., 2021; Zhong et al., 2016). Therefore presumably NLRP1 itself is degraded after VHL-VHH_{PYD}-mediated ubiquitination. As already mentioned, unstructured regions are important initiation sites for proteasomal degradation (Prakash et al., 2004). The linker region between $NLRP1^{PYD}$ and $NLRP1^{NBD}$ is predicted to be disordered, and thus ubiquitination of $NLRP1^{PYD}$ close to the disordered linker region may lead to efficient degradation by the proteasome (Chui et al., 2020). I also tried to detect ubiquitination of immunoprecipitated NLRP1 from VHL-VHH_{PYD}-transfected $HEK^{NLRP1+ASC}$ cells in preliminary experiments, but I observed no ubiquitin signal for NLRP1 in immunoblots. Many labs perform ubiquitination analyses in reconstituted cells that express tagged ubiquitin as this simplifies the detection. The analysis of endogenous ubiquitin requires experimental optimizations which I did not further pursue. Nevertheless, the VHL-VHH_{PYD} system represents an excellent tool to establish assays that detect ubiquitination of NLRP1 as the VHL-mediated CRL2 recruitment should induce a strong signal. Mass spectrometry is a promising method to detect specific ubiquitination sites in proteins. Tools like the UbiSite antibody allow the enrichment of ubiquitin remnant-containing peptides, before the exact sites can be identified by mass spectrometry (Akimov et al., 2018). Approaches like this can help to confirm VHL-VHH_{PYD}-mediated NLRP1 ubiquitination and explore if and where NLRP1 is ubiquitinated in the context of different stimuli.

In summary, I confirmed that $HEK^{NLRP1+ASC}$ and N/TERT-$1^{C1C-EGFP}$ cells are useful reporter cells that enable the direct analysis of human NLRP1 inflammasome activation. Detection of ASC speck formation in these cells is a sufficient readout for NLRP1 inflammasome activity, as NLRP1 forms a critically ASC-dependent inflammasome in contrast to CARD8. While the HEK-based reporter cells allow easy manipulations within a minimal inflammasome setting, the N/TERT-1 cells reflect endogenous protein levels and potential inflammasome regulations. In addition, I used $NLRP1^{PYD}$-specific nanobodies in combination with the VHL system to prove for the first time that targeted ubiquitination of human $NLRP1^{PYD}$ is sufficient for its activation by N-terminal degradation. The VHL-VHH_{PYD} system induces strong and NLRP1-specific inflammasome responses that can help to identify NLRP1 ubiquitination sites and to screen potential NLRP1 inflammasome-

competent cells. The reporter cells and the VHL-VHH_{PYD} system will be used throughout this thesis to analyze human NLRP1 inflammasome activation.

2.4 Material and Methods

Cells

Cell culture

HEK 293T cells (ATCC Cat# CRL-3216, RRID: CVCL_0063) were cultivated in Dulbecco's Modified Eagle's Medium (DMEM) containing 10 % fetal bovine serum (FBS) and GlutaMax (all Thermo Fisher Scientific). Human N/TERT-1 keratinocytes (a kind gift of James Rheinwald, Harvard Medical School) were cultivated in Keratinocyte serum-free medium (Thermo Fisher Scientific) supplement with 0.5x bovine pituitary extract (BPE), 0.2 mg/mL epidermal growth factor (EGF), 1x penicillin/streptomycin, and 0.3 mM $CaCl_2$ (resulting in a final concentration of 0.4 mM $CaCl_2$).

Generation of genetically modified cell lines

$2.5 \cdot 10^5$ HEK 293T (or HEK 293T derivatives) or $7 \cdot 10^4$ N/TERT-1 (or N/TERT-1 derivatives) cells were seeded per well in 24 well-plates. Genetically modified cell lines were generated by lentiviral transduction in the presence of 10 µg/mL polybrene (Sigma-Aldrich) for 6-8 h. The next day, transduced cells were transferred into 10 cm dishes and selected by addition of required antibiotics.

Lentiviral vectors for constitutive expression under control of pUbC were constructed by Gateway cloning (Thermo Fisher Scientific) using vectors modified from pRRL (a kind gift of Susan Lindquist, Whitehead Institute of Biomedical Research). HEK 293T cells expressing ASC-EGFP under control of pUbC (HEK^{ASC}) were generated by transduction with a dilution series of lentivirus to achieve single insertions. Individual clones were cultivated in medium supplemented with 1 µg/mL puromycin and tested for minimal background of ASC-EGFP specks. Derivatives of HEK^{ASC} expressing NLRP1-HA ($HEK^{NLRP1+ASC}$; cell line H8-1), or NLRP3-HA ($HEK^{NLRP3+ASC}$; cell line H98) under the control of pUbC from single insertions were generated using the same protocol and cultivated in the presence of 1 µg/mL puromycin and 50 µg/mL hygromycin B. Clones were selected based on optimal signal-to-noise ratio (after talabostat or LPS+nigericin

stimulation) and background. Polyclonal N/TERT-1 cells expressing caspase-1^{CARD}-EGFP (C1C-EGFP) controlled by pUbC (N/TERT-1$^{C1C\text{-}EGFP}$, cell line K14), were generated by lentiviral transduction with virus multiplicities of infection (MOIs) that permit multiple insertions and selection with 1 µg/mL puromycin. Lentiviral vectors for knockout generation were constructed by ligation of annealed oligonucleotides that encode single guide RNA (sgRNA) target sequences with vectors modified from pLenti CRISPR v2 (a kind gift of Feng Zhang, Broad Institute). The sgRNA target sequences were designed using CRISPick (Broad Institute, see Table 2 for sgRNA target sequences). Monoclonal knockout derivatives of N/TERT-1$^{C1C\text{-}EGFP}$ cells were generated using limiting dilutions of polyclonal cell lines generated by lentiviral transduction, and selection with 5 µg/mL blasticidin S. OutKnocker analyses were used to identify clones that have only two frameshift mutations in the target sequence, proving that these clones were derived from a single cell (Schmid-Burgk et al., 2014). The knockouts were additionally confirmed by immunoblot (N/TERT-1$^{C1C\text{-}EGFP}$ ΔASC (m), cell line K17-1 and N/TERT-1$^{C1C\text{-}EGFP}$ ΔNLRP1 (m), cell line K20-6). Lentiviral vectors for expression of C1C-EGFP and VHHs or VHL-VHH fusions under a bidirectional doxycycline-inducible promoter were constructed by Gibson cloning (New England Biolabs) based on lentiviral vector pInducer20bi-NA, a derivative of pInducer20-NA (Schmidt, Hanke, et al., 2016), using the promoter from pTRE3G-BI (Takara Bio). Polyclonal derivatives of N/TERT-1 cells were generated by lentiviral transduction with virus MOIs that permit multiple insertions and selection with 500 µg/mL geneticin (N/TERT-1$^{(VHL\text{-})VHH+C1C\text{-}EGFP}$, cell lines K44-K48). Flp-In 293 T-REx cells (Thermo Fisher Scientific Cat# R78007, RRID:CVCL_U427) inducibly expressing NLRP1 (cell line HFT9) or NLRX1 (cell lines HFT44) with a C-terminal Strep-HA tag were generated using the Flp-In system (Thermo Fisher Scientific) according to the manufacturer´s recommendations, and cultivated in DMEM supplemented with 10 % FBS, Glutamax, 4 µg/mL blasticidin S, and 50 µg/mL hygromycin B.

Target gene	sgRNA name	Target sequence
ASC	ASC sg5	GCTGGATGCTCTGTACGGGA
NLRP1	NLRP1 sg2	CAGGCCCAATAGGAAACGTG

Table 2: sgRNA target sequences used for the generation of monoclonal ASC and NLRP1 knockout N/TERT-1 cell lines

Viruses

Lentivirus production

All experiments involving lentiviruses were conducted in a Biosafety Level 2 laboratory. For lentivirus production $2.5 \cdot 10^5$ (24 well-plate) or $1 \cdot 10^6$ (6 well-plate) HEK 293T cells were seeded per well. Lentiviruses for transduction of N/TERT-1 cells were always generated in 6 well-plates. The next day, cells were co-transfected with 0.3 µg lentiviral vector, 0.13 µg psPax2, and 0.07 µg pMD2.G per 24 well, or 5 times the amounts per 6 well, using Polyethylenimine (PEI) Max (Polysciences). Packaging vectors psPax2 and pMD2.G were kind gifts from Didier Trono (École polytechnique fédérale de Lausanne). HEK 293T cells were transfected for 6-8 h, before addition of 600 µL (24 well) or 2 mL (6 well) full medium and further cultivation for 48 h. For generation of HEK 293T cell lines, lentivirus-containing supernatants were harvested, filtered using 0.45 µm polyethersulfon filter (Millipore) and directly used for transduction. For generation of N/TERT-1 cell lines, lentivirus-containing supernatants were similarly harvested and filtered but lentiviruses were additionally precipitated using Lenti-X™ Concentrator (Takara Bio). Pelleted lentiviruses were resuspended in keratinocyte serum-free medium to avoid contact of N/TERT-1 cells with serum during the transduction.

Proteins

Expression and purification of GST, GST-NLRP1^{PYD}, GST-NLRP1^{LRR} and GST-NLRP1^{CARD}

Expression vectors for human GST-NLRP1^{PYD} (amino acids (aa) 1-92), GST-NLRP1^{LRR} (aa 808-973), and GST-NLRP1^{CARD} (aa 1374-1463) were generated by Gateway cloning with a customized destination vector based on pGEX-2T (a kind gift of Mikko Taipale, Whitehead Institute of Biomedical Research). Proteins were expressed in *E. coli* BL21 cells in Terrific Broth induced with 0.2 mM Isopropyl-β-D-thiogalactopyranosid (IPTG) at an optical density (OD)600 of 0.6. Cells were cultivated for 24 h at 18 °C, and lysed by sonication (Bandelin Sonopuls HD2070 with TT13 tip) in phosphate-buffered saline (PBS), supplemented with 1 µM Dithiothreitol (DTT), Ethylenediaminetetraacetic acid (EDTA)-free protease inhibitor (Roche), 1 mg/mL lysozyme, and 5 µg/mL DNAse I. Clarified lysates were further purified by affinity chromatography using glutathione resin and 3-4 elutions were collected in elution buffer containing 50 mM Tris pH 8.0, 150 mM NaCl,

1 mM DTT, and 10 mM reduced glutathione. The pooled elutions were purified by gel filtration with a HiLoad 16/600 Superdex 75 pg column in buffer containing 20 mM 4-(2-hydroxyethyl)-1-piperazineethanesulfonic acid (HEPES) pH 7.4, 150 mM NaCl, and 10 % glycerol. All collected fractions were tested by sodium dodecyl sulfate (SDS)-polyacrylamide gel electrophoresis (PAGE) and colloidal Coomassie staining, and fractions containing the desired protein were pooled and concentrated to 1 mg/mL.

Expression and purification of nanobodies

Nanobody-coding sequences were cloned into pHEN6-based bacterial, periplasmic expression vectors with C-terminal HA-His tags using Gibson cloning. Nanobodies were expressed in *E. coli* WK6 cells in Terrific Broth induced with 1 mM IPTG at an OD600 of 0.6. Cells were cultivated for 16 h at 30 °C. Bacterial pellets were resuspended in TES buffer (200 mM Tris-HCl pH 8.0, 0.65 mM EDTA, 0.5 M sucrose) supplemented with protease inhibitor (Roche), and periplasmic extracts were generated by osmotic shock in 0.25x TES. Nanobodies were purified by Ni-NTA purification and desalting by PD MiniTrap G-25 columns (GE Healthcare Life Sciences).

Antibodies

The following antibodies were used: rabbit polyclonal anti-ASC (AdipoGen Cat# AG-25B-0006, RRID:AB_2490440), rabbit polyclonal anti-E-tag-HRP (Bethyl Cat# A190-133P, RRID:AB_345222), rabbit anti-FLAG clone D6W5B (Cell Signaling Technology Cat# 14793, RRID:AB_2572291), mouse anti-GFP clone JL-8 (Takara Bio Cat# 632380, RRID:AB_10013427), mouse anti-HA clone 16B12 (Biolegend Cat# 901533, RRID:AB_2801249), mouse anti-HA-HRP clone 6E2 (Cell Signaling Technology Cat# 2999S, RRID:AB_1264166), mouse anti-His-HRP clone J099B12 (Biolegend Cat# 652504, RRID:AB_2563555), mouse anti-NLRP1 clone 9F9B12 (BioLegend Cat# 679802, RRID:AB_2566263), mouse anti-vinculin clone hVIN-1 (Sigma-Aldrich Cat# V9131, RRID:AB_477629), goat polyclonal anti-rabbit IgG (H+L)-Alexa Flour™ Plus 647 (Invitrogen Cat#A32733, RRID:AB_2633282), goat polyclonal anti-rabbit IgG (H+L)-HRP (Invitrogen Cat#31460, RRID:AB_228341), goat polyclonal anti-mouse IgG (H+L)-HRP (Invitrogen Cat#31430, RRID:AB_228307)

Small compound inhibitors and reagents

The following small compound inhibitors and reagents were used: doxycycline (Thermo Fisher Scientific), LPS-EK Ultrapure (Invivogen), MG-132 (Selleckchem), MLN4924 (MedChem Express), MLN7243 (ChemieTek), Nigericin sodium salt (Biomol), talabostat mesylate (MedChemExpress), Vx-765 (Selleckchem), and Z-VAD(Ome)-FMK (MedChemExpress).

Nanobody library generation

To raise heavy chain-only antibodies against NLRP1^{PYD}, NLRP1^{LRR}, and NLRP1^{CARD} one alpaca and one llama were five times immunized with 200 µg His-NLRP1^{PYD}/His-NLRP1^{CARD} and His-NLRP1^{LRR} using Imject™ Alum Adjuvant (Thermo Fisher Scientific) or Gerbu Fama adjuvant (Gerbu Biotechnik) according to locally authorized protocols. Nanobody plasmid libraries in the M13 phagemid vector pD (pJSC) were generated as described before (Schmidt, Lu, et al., 2016) In brief, RNA from peripheral blood lymphocytes was extracted and used as a template to generate complementary DNA (cDNA) using three sets of primers (random hexamers, oligo(dT), and primers specific for the constant region of the alpaca heavy chain gene). Nanobody-coding sequences were amplified by polymerase chain reaction (PCR) using VHH-specific primers, cut with AscI and NotI, and ligated into pJSC linearized with the same restriction enzymes. *E. coli* TG1 cells (Agilent) were electroporated with the ligation reactions and the obtained ampicillin-resistant colonies were harvested, pooled, and stored as glycerol stocks.

Nanobody identification

NLRP1-specific nanobodies were identified by phage display and panning with a protocol modified from Schmidt et al. (Schmidt, Lu, et al., 2016). *E. coli* TG1 cells containing the VHH library were infected with helper phage VCSM13 (10^{13} pfu per 100 mL) in SOC medium (Super Optimal Broth with 20 mM glucose) at an OD600 of 0.6 to produce phages displaying the encoded nanobodies as pIII fusion proteins. After 2 h infection, phage-producing bacteria cultures were cultivated for 16 h at 30 °C in 2YT medium with 0.1 % glucose. Phages in the supernatant were purified and concentrated by two rounds of precipitation using 20 % polyethylene glycol 6000 in 2.5 M NaCl. To exclude phages that present nanobodies binding to the selection beads or GST, all phages were negatively

selected using empty beads and cell culture flasks coated with 1 mg/mL purified GST in PBS. Phages presenting NLRP1-specific nanobodies were enriched using GST-NLRP1^{PYD}, GST-NLRP1^{LRR}, or GST-NLRP1^{CARD} immobilized to magnetic Pierce glutathione beads (Thermo Fisher Scientific, 1 µg protein per 1 µL beads). The retained phages were eluted using 50 mM reduced glutathione in PBS and used to infect *E. coli* ER2738. Bacteria containing the enriched nanobody sequences were subjected to a second round of panning. The second round was performed using less protein-loaded beads (0.25 µg protein per 1 µL beads) and phages, without prior negative selection. *E. coli* ER2738 infected with the retained phages were plated in 10-fold dilutions to obtain single colonies, each encoding one enriched nanobody sequence in the phagemid vector. 95 colonies per nanobody target were grown in 2YT medium in 96 well-plates and nanobody expression was induced with IPTG for 16 h at 30 °C, leading to leakage of nanobodies into the supernatant. The specificity of nanobodies was tested using ELISA plates coated with 1 µg/mL control protein GST or GST fusion proteins in PBS. Bacterial supernatants were incubated with the immobilized antigen in 2 % bovine serum albumin (BSA) in PBS. Bound VHHs were detected with horseradish peroxidase (HRP)-coupled rabbit anti-E-Tag antibodies (1:10,000 in 4 % milk/PBS with 0.1 % Tween-20), and the chromogenic substrate 3,3′,5,5′-Tetramethylbenzidin (TMB). Reactions were stopped with 1 M HCl and absorption at 450 nm was recorded using a SpectraMax i3 instrument and the SoftMax Pro 6.3 Software (Molecular Devices). ELISA signals were normalized to medium- and GST-only controls, and nanobodies presenting values >3 on the target plate and <2 on the GST control plate were defined as hits to be sequenced for further analyses. Sequences were analyzed using Jalview 2.11.2.6 software (Waterhouse et al., 2009). Sequences were aligned using Clustal algorithm and Average distance trees (Percentage Identity) were generated. All nanobodies within a branch length of 3 were clustered and the nanobody with the highest ELISA signal was defined as the cluster representative. Relevant nanobodies were cloned into bacterial expression vectors and purified for further analysis.

Nanobody ELISA

To test nanobody binding to purified NLRP1 domains, ELISA plates were coated with 1 µg/mL GST-NLRP1^{PYD}, GST-NLRP1^{CARD}, or GST in PBS and blocked with 10 % FBS

in PBS. To test nanobody binding to full-length NLRP1, ELISA plates were coated with 10 µg/mL streptactin in PBS and blocked with 10 % FBS in PBS. Flp-In 293 T-REx cells were treated with 1 µg/mL doxycycline for 24 h to induce expression of Strep-HA tagged-NLRP1 or NLRX1. Four confluent 15 cm dishes per protein were lysed in 1 mL lysis buffer (0.2 % NP-40, 10 mM Tris pH 7.5, 10 mM KCl, 1.5 mM $MgCl_2$) supplemented with protease inhibitor (Roche), and clarified lysates were added to the streptactin-coated ELISA plates for 1 h. His-tagged nanobodies were incubated with the immobilized antigen at a concentration of 1 µg/mL or a 10-fold dilution series in 10 % FBS/PBS, followed by HRP-coupled anti-His (1:1000), and the chromogenic substrate TMB. Incubation with 1 µg/mL anti-HA antibody, followed by HRP-coupled anti-mouse Immunoglobulin (Ig)G served as a positive control for the detection of Strep-HA tagged proteins. Reactions were stopped with 1 M HCl and absorption was measured at 450 nm using a SpectraMax i3 instrument and the SoftMax Pro 6.3 Software (Molecular Devices).

Flow cytometry-based quantification of inflammasome assembly

To quantify the assembly of ASC-EGFP specks or recruitment of C1C-EGFP to ASC specks (‘C1C specks’), cells were typically treated in 24-wells or 48-wells and analyzed by flow cytometry. $2.5 \cdot 10^5$ (24 well-plate)/$1.25 \cdot 10^5$ (48 well-plate) $HEK^{NLRP1+ASC}$ (or other derivatives of HEK 293T), or 0.5-$1 \cdot 10^5$ (48 well-plate) N/TERT-$1^{C1C\text{-}EGFP}$ (or other derivatives of N/TERT-1) cells were seeded per well and cultivated overnight in the absence of antibiotics. Cells were stimulated in DMEM/10 % FBS (HEK 293T) or keratinocyte serum-free medium (BPE, EGF, $CaCl_2$) (N/TERT-1). Importantly, N/TERT-$1^{C1C\text{-}EGFP}$ cells were stimulated in the presence of 100 µM Vx-765 for all flow cytometry experiments to prevent loss of responding cells by caspase-1-dependent pyroptosis.

For drug-induced inflammasome stimulation, cells were treated with 200 ng/mL LPS for 3 h followed by 10 µM nigericin for 1 h, or 30 µM talabostat for 20 h. Cells treated with the solvent dimethyl sufoxide (DMSO) only served as controls.

For inflammasome stimulation by transient overexpression of HA- or FLAG-tagged VHHs and VHL-VHH fusions, expression vectors based on pCAGGS (Hitoshi et al., 1991) were constructed by Gibson cloning. HEK-based reporter cells in 24-wells were transfected with 500 ng total expression vectors using Lipofectamine 2000 (Thermo Fisher Scientific).

Medium was replaced with full medium after 6 h and cells were cultivated for another 14 h. Cells treated with Lipofectamine 2000 only served as controls.
For induction of doxycycline-inducible expression in lentivirus-generated cell lines, cells were cultivated in medium containing 1 µg/mL doxycycline for 6 or 20 h.
In case of additional inhibitor treatments, small compound inhibitors were added 30 min before and during the stimulation, with the following concentrations: 1 µM MG-132, 1 µM MLN4924, 1 µM MLN7243, 100 µM Vx-765, or 50 µM Z-VAD(Ome)-FMK. In the case of stimulation by transient overexpression of HA- or FLAG-tagged VHHs and VHL-VHH fusions, inhibitors were only added with the medium change after 6 h transfection.
After stimulation, cells were harvested by trypsinization, fixed in 4 % formaldehyde, and analyzed using BD FACSCanto flow cytometers, recording area, width, and height of the EGFP signal of single cells. Flow cytometers were provided and serviced by the Flow Cytometry Core Facility (University Hospital, Bonn, Germany). Where indicated, fixed and permeabilized cells were stained with anti-FLAG (1:300) in Intracellular Staining Permeabilization Wash Buffer (Biolegend) combined with Alexa Flour™ Plus 647-coupled, highly cross-absorbed secondary antibodies (1:500). Flow Cytometry data was analyzed using FlowJo 10.8.1 software. To determine the frequency of cells with ASC specks, cell debris and doublets were excluded based on forward and sideward scatter signals. Only cells expressing the ASC speck reporter ASC-EGFP or C1C-EGFP were included in the analysis of the ASC speck response based on height and width of the reporter signals.

Cytokine quantification by HTRF

To quantify IL-1β release, N/TERT-1-derived cells were seeded (10^5 cells in 300 µL per 48 well-plate) and stimulated as described for flow cytometry experiments in the absence and presence of Vx-765. Supernatants for the quantification of IL-1β levels after inducible expression of (VHL)-VHH fusions were collected from $5 \cdot 10^4$ cells in 200 µL per well in 96 well-plates. IL-1β was quantified using the Human IL1 beta Homogeneous Time-Resolved Fluorescence (HTRF) kit (Ciscbio) according to the manufacturer's instructions. Emissions at 620 nm and 665 nm were measured using a SpectraMax i3 instrument and IL-1β levels were calculated by the SoftMax Pro 6.3 Software (Molecular Devices) based on the standard curve.

Cell death quantification by LDH release

To quantify cell death by pyroptosis, the same cell supernatants as for the IL-1β quantification were used. Release of LDH was quantified using the LDH Cytotoxicity Detection Kit (Takara Bio) according to the manufacturer's instructions. Absorption at 490 nm was measured using a SpectraMax i3 instrument and the SoftMax Pro 6.3 Software (Molecular Devices). Control samples, in which cells were lysed in 1 % Triton X-100, were used to normalize LDH release, after subtraction of medium background signal.

Cell death quantification by DRAQ7 uptake

To quantify cell death over time, the uptake of the non-cell permeable DNA dye DRAQ7 (Biolegend) was analyzed using the Incucyte Live-Cell Imaging system (Sartorius). N/TERT-1-derived cells were seeded ($1.5 \cdot 10^4$ cells in 96 well-plate) and stimulated as described for flow cytometry experiments using DRAQ7-containing medium (1:3000). Stimulation was performed in the absence and presence of Vx-765 or Z-VAD(Ome)-FMK. The cells were imaged every hour for a total of 20 h using the Incucyte SX5 instrument, taking 9 images per well. The number of DRAQ7-positive nuclei (cell death count) and the cell confluency were analyzed using the Incuycyte 2021C software. For every single image, the cell death count was corrected by subtraction of the value at the beginning of the experiment. The corrected cell death count was further normalized to the cell confluency by division, before the average value for all 9 images was calculated and plotted over time.

Microscopy

To generate microscopy samples, cells were seeded on 12 mm cover slips in 24 well-plates and otherwise stimulated as described for flow cytometry experiments. Cells were fixed in 4 % formaldehyde and stained for DNA using Hoechst 33342 (1:5000; Thermo Fisher Scientific). Images were recorded with a Zeiss Observer.Z1 wide field microscope, provided and serviced by the Microscopy Core Facility (University Hospital, Bonn, Germany). Images were processed using ImageJ 2.3.0 software.

Immunoblot

To confirm expression or knockout of proteins in cell lines, 10^6 cells were lysed in 200 µL 1x SDS-PAGE buffer (50 mM Tris pH 6.8; 0.01 % Bromophenol blue, 10 % glycerol, 2 % SDS, 100 mM DTT) to generate immunoblot samples. Proteins were separated by SDS-PAGE using 4–15 % Criterion™ TGX™ Precast Midi protein gels (Bio-Rad). Separated proteins were transferred to polyvinylidene difluoride membranes (0.45 µm, Merck) by semi-dry transfer. All immunoblots were blocked in 5 % non-fat dry milk (NFDM) solution in Tris-buffered saline (TBS) with 0.05 % Tween-20 (TBS-T) and probed with the following primary antibody dilutions: anti-ASC 1:1000, anti-GFP 1:1000, anti-HA-HRP 1:1000, anti-NLRP1 1:1000, and anti-vinculin 1:1000. All primary antibodies were added in NFDM solution. After overnight incubation at 4 °C, the immunoblots were probed with HRP-coupled secondary antibodies in NFDM solution (1:5000) for 2 h. Chemiluminescent signal was induced by Western Lightning Plus enhanced chemiluminescence (ECL) substrate (Perkin Elmer), except for immunoblots of ASC and NLRP1, which required Western Lightning Ultra-ECL (Perkin Elmer). The signal was detected using a Fusion Advancer imaging system (Vilber) and images were taken using the EvolutionCapt SL6 software (Vilber).

Statistical analyses

The generated data was analyzed using GraphPad Prism 9.5.1 software. All shown error bars represent the mean with 95 % confidence interval (CI). P-values were reported whenever the error bars show no clear separation and the difference between two groups is important for the statements in this thesis. P-values were calculated using an unpaired t-test assuming individual variance for each treatment.

3. P38 kinases mediate human NLRP1 inflammasome activation after ribotoxic stress response and virus infection

3.1 Introduction

In this chapter, I will use the NLRP1 reporter cells, as well as VHL-VHH_{PYD}-mediated targeted NLRP1 degradation, to demonstrate that p38 kinases mediate NLRP1 activation by direct phosphorylation of the N-terminal linker region after UVB irradiation, SFV infection, and dsRNA transfection.

The UV radiation of sunlight consists of 95 % UVA and 5 % UVB. While UVA damages cells mainly through the generation of ROS, UVB induces strong damage of cellular DNA and RNA (Karran & Brem, 2016). UVB-induced ribosomal RNA and messenger RNA (mRNA) damage causes ribosome stalling which activates the ribotoxic stress response (RSR) (Iordanov et al., 1998; Wu et al., 2020). The RSR can be activated by other stimuli that impair ribosome function such as ribotoxins and bacterial translation inhibitors. For example, the antibiotic anisomycin represents an established inducer of the RSR pathway by interfering with peptide-bond formation in the peptidyl transferase center (Garreau de Loubresse et al., 2014; Iordanov et al., 1997; Vind, Genzor, et al., 2020). RSR induction is dependent on mitogen-activated protein kinase kinase kinase (MAP3K) leucine zipper- and sterile alpha motif-containing kinase α (ZAKα). ZAKα is the longer of two splicing isoforms, directly binding to ribosomes to detect ribosome stalling and collisions. Activation leads to ZAKα autophosphorylation and initiation of subsequent mitogen-activated protein kinase (MAPK) signaling cascades (Mathea et al., 2016; Vind, Snieckute, et al., 2020; X. Wang et al., 2005; Wu et al., 2020).

Activation of ZAKα leads to the activation of MAPK p38 and C-Jun N-terminal kinase (JNK) via different MAP kinase kinases (MAP2K). P38 is phosphorylated by MAP2K MKK3 and MKK6, whereas MKK4 and MKK7 phosphorylate JNK. Both p38 and JNK are stress-activated protein kinases whose activity is initiated by diverse MAP3 kinases after various environmental stress and proinflammatory stimuli, like oxidative stress, UV irradiation, and cytokine signaling (Canovas & Nebreda, 2021; Cargnello & Roux, 2011; Raingeaud et al., 1996; Vind, Genzor, et al., 2020).

P38 exhibits four isoforms: P38α/β are ubiquitously expressed, in contrast to p38γ/δ, which show tissue-specific expression. Active p38 acts as a proline-directed serine/threonine kinase with more than 100 reported substrates. Thereby, p38 can regulate transcription, mRNA stability, protein degradation, endocytosis, metabolism, and more. P38α/β activate, for example, MAPK-activated protein kinases like MK2/3 which control especially cytokine mRNA stability to boost proinflammatory cytokine responses. Depending on the upstream signals and the cell type, p38 activity can result in pro-survival or inflammatory/cell death signaling (Canovas & Nebreda, 2021; Cargnello & Roux, 2011; Gaestel, 2006; J. L. Johnson et al., 2023).

It was reported that UV- and anisomycin-induced ZAKα activation also plays a role in the general control nonderepressible 2 (GCN2)-mediated integrated stress response (ISR) (Wu et al., 2020). The ISR is mediated by four kinases which all phosphorylate eukaryotic initiation factor 2α (eIF2α) after recognition of different stress signals, thereby inhibiting translation: GCN2 detects amino acid deficiency, heme-regulated inhibitor detects heme deprivation, protein kinase R (PKR) detects dsRNA, and PKR-like endoplasmic reticulum (ER) kinase (PERK) detects ER stress. GCN2 is also activated in the context of impaired ribosome function, resulting in parallel activation of the RSR and ISR (Vind, Genzor, et al., 2020).

UVB irradiation activates NLRP1 in human but not murine keratinocytes. The first studies only reported that primary human keratinocytes undergo caspase-1-dependent cell death and release IL-1β after UVB irradiation (Feldmeyer et al., 2007; Sollberger et al., 2015). Later, it was shown that these responses are caused by NLRP1 inflammasomes (Fenini, Grossi, Contassot, et al., 2018; Sand et al., 2018). Sand et al. were not able to detect similar inflammasome activities in murine keratinocytes, arguing that UV irradiation is no real threat for nocturnal animals with fur. The exact mechanism of UVB-induced NLRP1 activation or the role of sensor degradation in this process were not examined. In a follow-up report, Fenini et al. indicated that the activity of p38 is important for UVB-induced NLRP1 activation, but the authors did not explore how the kinase regulates the inflammasome (Fenini, Grossi, Gehrke, et al., 2018).

SFV is an alphavirus, a genus that belongs to the family of Togaviridae. Alphaviruses form small, enveloped viruses with a 12 kb linear positive-sense single-stranded RNA (ssRNA)

genome. They are transmitted via arthropods (mostly mosquitos) and rodents, birds and non-human primates act as virus-maintaining hosts. Alphaviruses are classified into old- or new-world viruses, depending on the continent where they were first isolated. The old-world alphaviruses SFV, Sindbis virus (SINV), and o'nyong-nyong virus (ONNV) are mostly found in Africa. Ross River virus (RRV) and Barmah Forest virus (BFV) cause infections in Oceania, and Chikungunya virus (CHIKV) is endemic to Asia, South Europe, and the Caribbean. Even though it is classified as an old-world virus, Mayaro virus (MAYV) is mainly found in America. Prominent representatives of new-world alphaviruses are Eastern, Venezuelan, and Western equine encephalitis virus (EEEV, VEEV, WEEV) (Acosta-Ampudia et al., 2018; Fros & Pijlman, 2016; Kafai et al., 2022; Powers et al., 2001; Skidmore & Bradfute, 2023). Old-world alphaviruses replicate in joint-associated and musculoskeletal tissues, causing mostly fever and arthralgia with sometimes long-lasting symptoms in the cases of CHIKV, MAYV, and RRV. New-world viruses can replicate in the nervous system and cause encephalitis. These viruses induce severe pathologies and death in livestock, whereas most humans show asymptomatic infections (Acosta-Ampudia et al., 2018; Kafai et al., 2022; Skidmore & Bradfute, 2023). SFV and SINV are widely used alphavirus models as they are less pathogenic than other family members and replicate well in cell culture (Atkins et al., 1999).

Alphaviruses exhibit a broad cellular tropism, as they can bind to multiple receptors, which differ for distinct viruses. They enter the host cell via endocytosis and escape the endosome by membrane fusion induced by decreased pH. The nucleocapsid is disassembled, leading to the release of the genome into the cytosol. As the genome is capped and poly-A-tailed, translation of the non-structural polyprotein nsP1234 is initiated by the host machinery. The intermediate nsP1234 complex produces negative-sense genomic RNA before the polyprotein is cleaved by nsP2. The cleaved nsP1/2/3/4 replicase complex can then synthesize new positive-sense genomic and subgenomic RNA based on the negative-sense template. Importantly, this replication causes the generation of dsRNA intermediates. The subgenomic RNA encodes the structural proteins, which form new virions that bud from the host cell membrane (Jose et al., 2009; Marsh et al., 1983; Skidmore & Bradfute, 2023).

Infection with the alphavirus SFV and transfection of dsRNA longer than 500 bp leads to NLRP1 inflammasome formation in N/TERT keratinocytes (Bauernfried et al., 2021).

Neither of the stimuli activates CARD8 or murine Nlrp1b. Furthermore, binding of dsRNA to $NLRP1^{LRR}$ induces ATP hydrolysis in the $NLRP1^{NACHT}$ and the authors propose that binding of dsRNA to NLRP1 (also in the course of SFV infection) induces conformational changes of the sensor and subsequent inflammasome activation. Functional proteasomal degradation was required for this mode of NLRP1 activation.

3.2 Results

Contributions

The NLRP1, ASC, and p38 knockout N/TERT-1 reporter cell lines were generated by Karl Elmar Lange. The experiments to quantify ASC speck formation in Fig. 3.1 B/F/G, as well as the immunoblots in Fig. 3.3 F, were performed by Lisa Schiffelers. The experiments to quantify ASC speck formation in Fig. 3.2 E/F/H, Fig. 3.5 A-F, Fig. 3.8 B, as well as the immunoblots in Fig. 3.1 E, Fig. 3.2 A/B/C, Fig. 3.3 D/E, Fig. 3.6 H, Fig. 3.7 D, were performed by Sabine Normann. The experiments to quantify ASC speck formation in Fig. 3.2 I, Fig. 3.6 J, Fig. 3.7 A/B/F, as well as the immunoblots in Fig. 3.7 E, were performed by rotation student Laura Klein under my supervision. The experiments to quantify ASC speck formation in Fig. 3.3 G were performed by Jennifer Wuerth and Dorothee Lapp. The fluorescence microscopy pictures in Fig. 3.2 G/J were taken and processed by Florian Gohr. All were members of the Institute of Innate Immunity (Florian Schmidt lab) in Bonn when the experiments were performed and many of the experiments were coordinated by me to speed up the finalization of the manuscript.

Infection experiments in Fig. 3.9 A,B were performed by Anja vom Hemdt, then a member of the Institute of Virology (Beate Kümmerer Lab) in Bonn. Production of recombinant p38 kinase and *in vitro* kinase assays in Fig. 3.12 D were performed by Ines Kaltheuner. Recombinant NLRP1 for *in vitro* kinase assays was produced by Jonas Moecking. Both were members of the Institute of Structural Biology (Matthias Geyer lab) in Bonn, when the experiments were performed. Mass spectrometry experiments to identify NLRP1 phosphorylation in Fig. 3.13 A were performed by Stefan Ebner, at that time member of the Institute of Innate Immunity (Felix Meissner lab) in Bonn. All other experiments and further analyses of the provided data were performed by myself.

Modified versions of the results and figures were published in:
Journal of Experimental Medicine (2023) 220 (1): e20220837 (doi.org/10.1084/jem.20220837)

P38 kinases mediate NLRP1 inflammasome activation after ribotoxic stress response and virus infection

Lea-Marie Jenster[1], Karl-Elmar Lange[1], Sabine Normann[1], Anja vom Hemdt[2], Jennifer D. Wuerth[1], Lisa D.J. Schiffelers[1], Yonas M. Tesfamariam[1], Florian N. Gohr[1,3], Laura Klein[1], Ines H. Kaltheuner[4], Stefan. Ebner[1], Dorothee J. Lapp[1], Jacob Mayer[1], Jonas Moecking[4], Hidde L. Ploegh[5], Eicke Latz[1], Felix Meissner[1], Matthias Geyer[4], Beate M. Kümmerer[2,6], Florian I. Schmidt[1,7]

[1] Institute of Innate Immunity, Medical Faculty, University of Bonn, 53127 Bonn, Germany
[2] Institute of Virology, Medical Faculty, University of Bonn, 53127 Bonn, Germany
[3] Department of Microbiology and Immunology, The University of Melbourne, Parkville, VIC, 3010, Australia
[4] Institute of Structural Biology, Medical Faculty, University of Bonn, 53127 Bonn, Germany
[5] Program in Cellular and Molecular Medicine, Boston Children's Hospital, Boston, MA 02115, USA
[6] German Centre for Infection Research (DZIF), partner site Bonn-Cologne, 53127 Bonn, Germany
[7] Core Facility Nanobodies, Medical Faculty, University of Bonn, 53127 Bonn, Germany

3.2.1 UV irradiation activates NLRP1 inflammasomes through p38 kinase activity

After establishing HEK 293T- and N/TERT-1-based NLRP1 inflammasome reporter cells, as well as the VHL-VHH_{PYD} system to specifically activate human NLRP1 (see chapter 2), I wanted to use these tools to further analyze the mechanisms of NLRP1 activation. As a start, I followed up on the reported NLRP1 activation by UVB irradiation (Fenini, Grossi, Contassot, et al., 2018; Sand et al., 2018), as this is a relevant environmental stimulus of inflammation, especially for human keratinocytes which are regularly exposed to UV radiation. I stimulated the reporter cells with UVB for 3 min and analyzed the inflammasome response after 20 h (Fig. 3.1 A). Both $HEK^{NLRP1+ASC}$ and $HEK^{NLRP3+ASC}$ showed some level of ASC speck formation after UVB stimulation, but the response was substantially more pronounced in the NLRP1-expressing cells, with around 15 % of

HEK$^{NLRP1+ASC}$ cells forming ASC specks (Fig. 3.1 B). Similarly, UVB-stimulated N/TERT-1$^{C1C-EGFP}$ cells showed inflammasome assembly and caspase-1-dependent IL-1β release. Yet, with ASC speck levels around 1 %, the response rates were even lower than after talabostat treatment (see chapter 2, Fig. 2.2 G), and the response therefore hardly distinguishable from the NLRP1 knockout derivatives (Fig. 3.1 C). Immunoblot analyses showed no UVB-induced release of processed IL-1β, whereas the weak response to talabostat was sufficient to identify the cleaved p33 fragment of caspase-1 and p17 fragment of IL-1β in the supernatant of stimulated N/TERT-1$^{C1C-EGFP}$ cells (Fig. 3.1 E). While talabostat did not trigger cell death in the earlier experiments, UVB irradiation caused substantial cell death as quantified by LDH release (Fig. 3.1 C) or uptake of the non-cell permeable DNA dye DRAQ7 (Fig. 3.1 D). In line with the weak inflammasome responses to UVB, knockout of NLRP1 did not alter cell death. Yet, UVB-induced cell death was completely blocked by pan-caspase inhibitor Z-VAD(OMe)-FMK (Z-VAD). I further observed apoptosis-related cleavage of caspase-3 and poly-ADP-ribose-polymerase (PARP) in immunoblots (Fig. 3.1 E), which was also independent of NLRP1. I thus conclude that NLRP1 activation by UVB irradiation does not dominate the cell death response, but promotes inflammation by inflammasome-mediated IL-1β release.

After recapitulation of UVB-induced NLRP1 activation in the reporter cells, I was wondering which upstream pathways are involved. As described before, UVB irradiation damages mostly cellular DNA and RNA, the latter causing induction of the RSR. DNA damage and ROS as possible factors in UVB-induced NLRP1 activation had already been excluded, as no response had been observed after treatment with DNA-damaging agents and H_2O_2 (data not shown). I next tested whether UVB-induced inflammasome assembly relies on the RSR and p38 signaling. Therefore, ASC speck formation was quantified in HEK$^{NLRP1+ASC}$ and N/TERT-1$^{C1C-EGFP}$ cells treated with the p38α/β inhibitor SB202190 (SB) (Kumar et al., 1997), or the pan-p38 inhibitor doramapimod (Dora) (Kuma et al., 2005) (Fig. 3.1 F,G). Assembly of ASC specks was completely abrogated by both inhibitors, suggesting that UVB-induced NLRP1 activation was indeed critically dependent on p38 kinase activity. Inflammasome assembly was not sensitive to ISRIB, a small molecule that reverses the effects of eIF2α phosphorylation after ISR induction (Sidrauski et al., 2013) or PF3644022 (PF), which inhibits the MAPK-activated protein kinase MK2 downstream

of p38. Thus, changes in mRNA stability, regulated by MK2, seem not to be involved in NLRP1 inflammasome activation after UVB irradiation, although p38-dependent gene

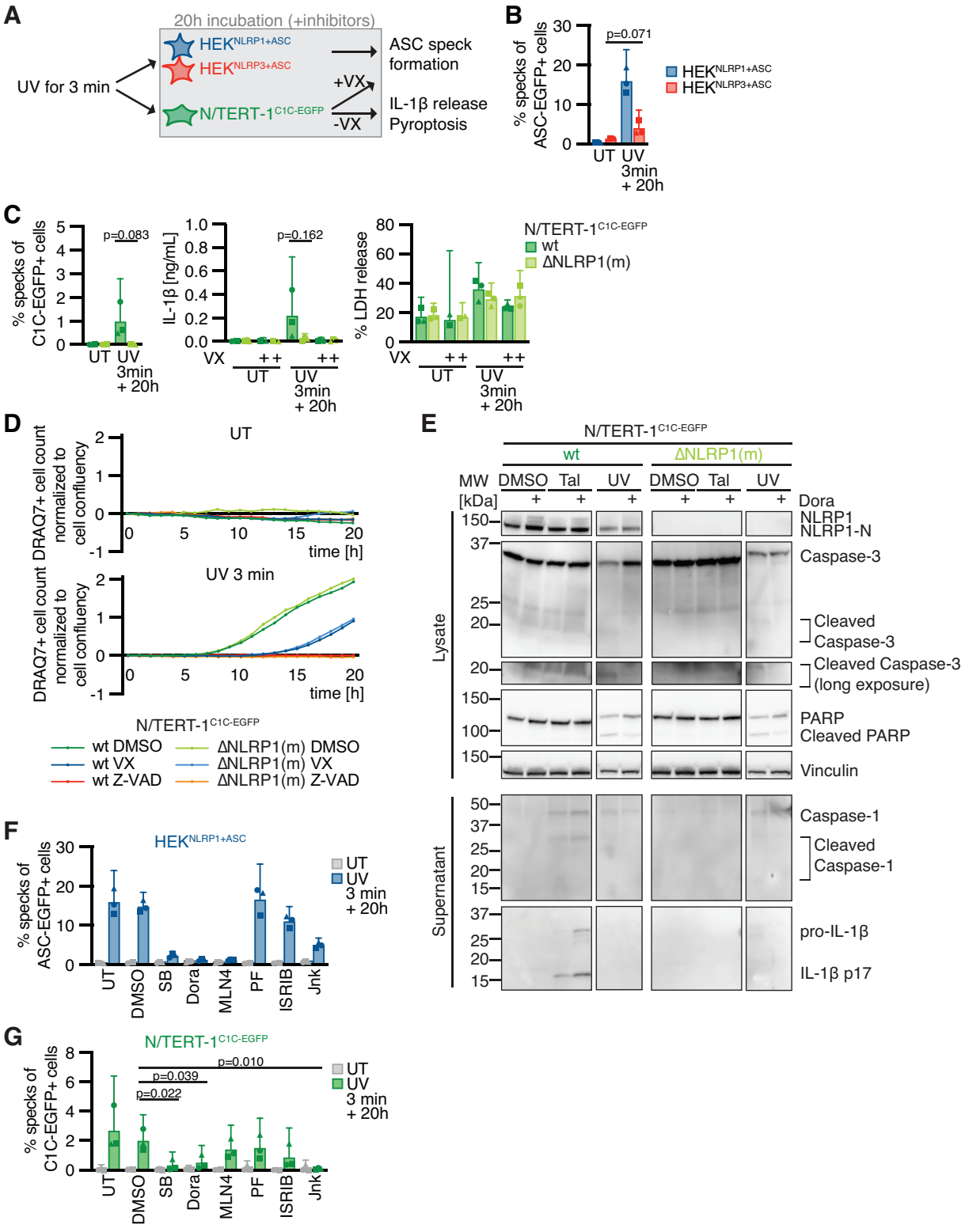

Figure 3.1: NLRP1 inflammasome activation by UV irradiation is dependent on p38 activity. (**A**) Schematic overview of the experimental setup. HEK$^{NLRP1+ASC}$, HEK$^{NLRP3+ASC}$, and N/TERT-1$^{C1C-EGFP}$ cells were stimulated with UV for 3 min, or left untreated (UT), and further incubated for 20 h, where indicated in the presence of 100 µM VX, 50 µM Z-VAD, 20 µM SB202190 (SB), 10 µM doramapimod (Dora), 1 µM MLN4, 1 µM PF3644022 (PF), 200 nM ISRIB, 3 µM Jnk-In-8 (Jnk), or DMSO. ASC speck formation in N/TERT-1 cells was detected in the presence of caspase-1 inhibitor VX. (**B**) ASC speck formation in HEK$^{NLRP1+ASC}$ and HEK$^{NLRP3+ASC}$ cells was quantified by flow cytometry, as described in Fig. 2.1. (**C**) ASC speck formation in N/TERT-1$^{C1C-EGFP}$ cells and their monoclonal NLRP1 knockout derivatives was quantified by flow cytometry and supernatants from the same cells were collected. IL-1β release was quantified by HTRF. Cell death was quantified by detection of LDH release. (**D**) Cell death of N/TERT-1$^{C1C-EGFP}$ cells and their monoclonal NLRP1 knockout derivatives was quantified by uptake of non-cell permeable DNA dye DRAQ7 over 20 h. (**E**) Lysates and precipitated supernatants of N/TERT-1$^{C1C-EGFP}$ cells and their monoclonal NLRP1 knockout derivatives were analyzed by immunoblot with the indicated antibodies. Cells treated with 30 µM Tal served as control. (**F,G**) ASC speck formation in HEK$^{NLRP1+ASC}$ and N/TERT-1$^{C1C-EGFP}$ cells was quantified by flow cytometry. Data represents average values (with individual data points) from two (C, LDH release, UT+VX) or three independent experiments ± 95 % CI, p-values were calculated using unpaired t-test. Quantifications of DRAQ7 uptake over time in (D) display experiment representatives of three independent experiments. Immunoblots in (E) display experiment representatives of two independent experiments.

regulation could not be ruled out. The inflammasome response in N/TERT-1$^{C1C-EGFP}$ cells was also completely abrogated by Jnk-In-8 (Jnk), a reversible inhibitor of JNK1, JNK2, and JNK3, whereas the response in HEK$^{NLRP1+ASC}$ was only partially affected. As only p38 inhibitors robustly abrogated UVB-induced NLRP1 inflammasome assembly in both reporter cell lines, I decided to focus on the role of p38 in NLRP1 inflammasome activation.

3.2.2 The ribotoxic stress response activates NLRP1 inflammasomes

NLRP1 activation by UVB was dependent on p38 activity and in line with that, I observed robust phosphorylation of p38 after UVB irradiation (Fig. 3.2 A). P38 is activated through UVB-triggered RNA damage in the course of the RSR (Iordanov et al., 1998; Wu et al., 2020). Thus, I next evaluated whether other activators of the RSR were also able to activate NLRP1 inflammasomes. I first tested anisomycin (Aniso), an antibiotic produced by *Streptomyces griseolus* and a strong inducer of the RSR pathway (Vind, Snieckute, et

al., 2020). I confirmed robust phosphorylation and thus activation of p38 in HEK 293T cells

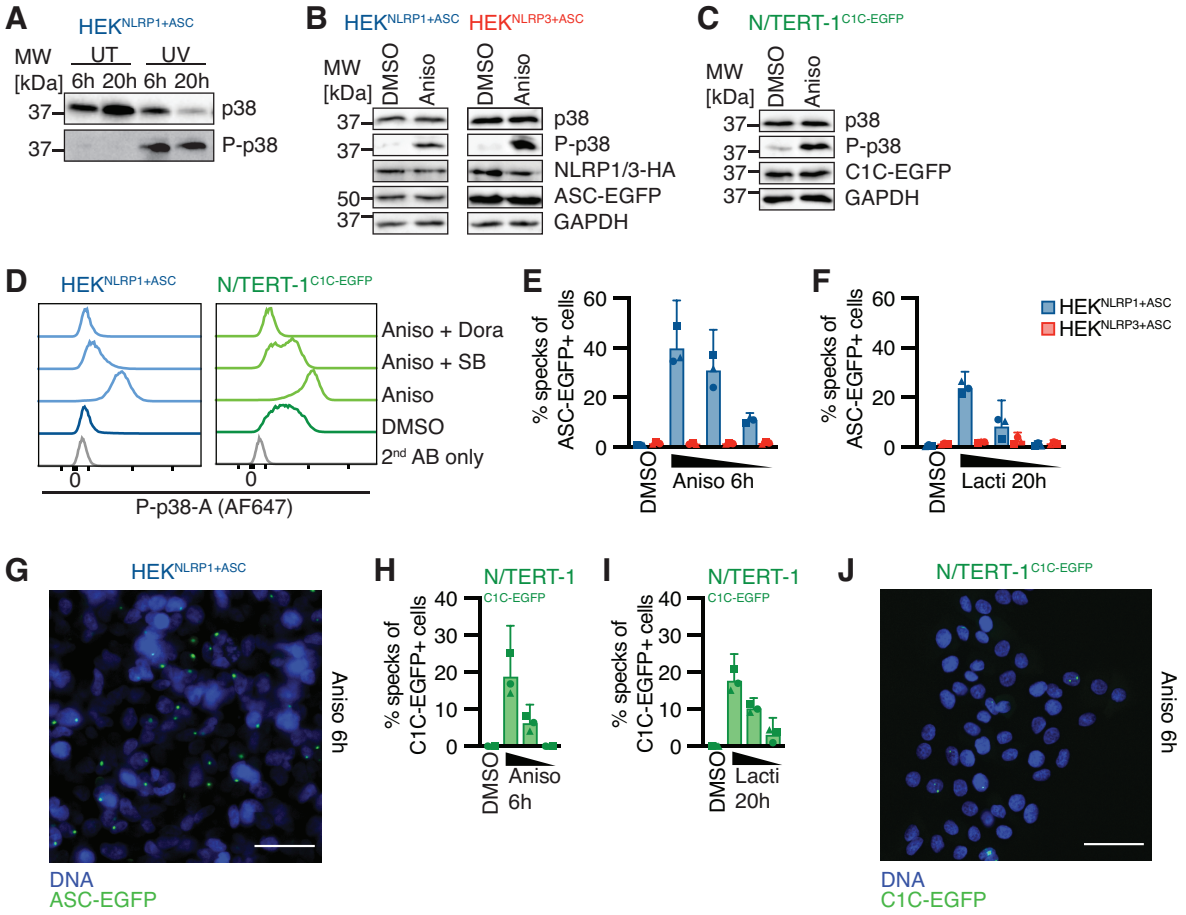

Figure 3.2: Induction of the ribotoxic stress response activates the NLRP1 inflammasome. (**A**) HEK$^{NLRP1+ASC}$ cells were stimulated with UV for 3 min, or left untreated (UT), and further incubated for 6 or 20 h. Lysates were analyzed by immunoblot with the indicated antibodies to confirm the phosphorylation of p38 (P-p38). (**B-D**) HEK$^{NLRP1+ASC}$, HEK$^{NLRP3+ASC}$, and N/TERT-1$^{C1C-EGFP}$ cells were treated with 15 µM anisomycin (Aniso) or DMSO for 1 h, where indicated in the presence of 20 µM SB or 10 µM Dora. (B,C) Lysates were analyzed by immunoblot with the indicated antibodies. (D) Fixed cells were stained for P-p38 and analyzed by flow cytometry. (**E,H**) HEK$^{NLRP1+ASC}$, HEK$^{NLRP3+ASC}$, and N/TERT-1$^{C1C-EGFP}$ cells were stimulated with DMSO or 15/1.5/0.15 µM Aniso for 6 h. (**F,I**) HEK$^{NLRP1+ASC}$, HEK$^{NLRP3+ASC}$ and N/TERT-1$^{C1C-EGFP}$ cells were stimulated with DMSO or 2.5/0.5/0.1 µM lactimidomycin (Lacti) for 20 h. ASC speck formation was quantified by flow cytometry, as described in Fig. 2.1. ASC speck formation in N/TERT-1 cells was detected in the presence of caspase-1 inhibitor VX. (**G,J**) HEK$^{NLRP1+ASC}$ and N/TERT-1$^{C1C-EGFP}$ cells were stimulated with 15 µM Aniso for 6 h. ASC speck formation was detected by wide-field fluorescence microscopy, as described in Fig. 2.1. Scale bars represent 50 µm. Data represents average values (with individual data points) from three independent experiments ± 95 % CI. Immunoblots in (A-C), flow cytometry histograms in (D) and microscopy images in (G,J) display experiment representatives of two independent experiments.

and N/TERT-1 keratinocytes after anisomycin treatment by immunoblot (Fig. 3.2 B,C) and flow cytometry (Fig. 3.2 D) using phospho-p38-specific antibodies, suggesting that the RSR is functional in the inflammasome reporter cells. I was excited to see that anisomycin treatment activated NLRP1 inflammasomes in HEK$^{NLRP1+ASC}$ and N/TERT-1$^{C1C-EGFP}$ cells in a dose-dependent manner (Fig. 3.2 E,G,H,J). With 40 % ASC speck formation in HEK$^{NLRP1+ASC}$ cells, the fraction of responding cells was comparable to talabostat stimulation. In contrast, responses in N/TERT-1 keratinocytes were substantially stronger than after talabostat treatment, with more than 15 % of the cells assembling ASC specks already after 6 h.

Next, I tested lactimidomycin (Lacti) produced by *Streptomyces amphibiosporus*, which inhibits ribosomes by interfering with polypeptide translocation (Garreau de Loubresse et al., 2014). Similarly, lactimidomycin activated NLRP1 inflammasomes in a dose-dependent manner in HEK$^{NLRP1+ASC}$ and N/TERT-1$^{C1C-EGFP}$ cells (Fig. 3.2 F,I). In comparison to anisomycin, the lactimidomycin-induced NLRP1 response was weaker and started later in both reporter cells. Importantly, neither of the antibiotics activated inflammasomes in HEK$^{NLRP3+ASC}$ cells.

Worth noting, I also observed weak NLRP1 inflammasome activation after stimulation with cycloheximide, which inhibits ribosomes similar to lactimidomycin, and blasticidin S, which impairs the termination of translation at the ribosome (data not shown). However, I focused further analyses on the stronger NLRP1 activators anisomycin and lactimidomycin (Fig. 3.3 A). In both cases, ASC speck assembly depended on NLRP1 and ASC, as neither NLRP1 nor ASC knockout derivatives of N/TERT-1$^{C1C-EGFP}$ cells assembled inflammasomes in response to both stimuli (Fig. 3.3 B). Remarkably, more than 50 % of the N/TERT-1 reporter cells responded to anisomycin after 20 h stimulation. ASC speck formation was also accompanied by caspase-1-dependent IL-1β release in the wild type keratinocytes. NLRP1-dependent cleavage of caspase-1 and IL-1β was additionally confirmed by immunoblot (Fig. 3.3 D,E). To test whether NLRP1 activation by anisomycin and lactimidomycin was indeed initiated by the RSR, I again quantified inflammasome assembly in the presence of p38 inhibitors SB202190 and doramapimod (Fig. 3.3 C). I also tested compound 6p (ZAKi), an inhibitor of the RSR-inducing MAP3K ZAKα (J. Yang et al., 2020). Inflammasome assembly and IL-1β release were completely

blocked by both p38 inhibitors as well as by the ZAKα inhibitor. This was not the case for

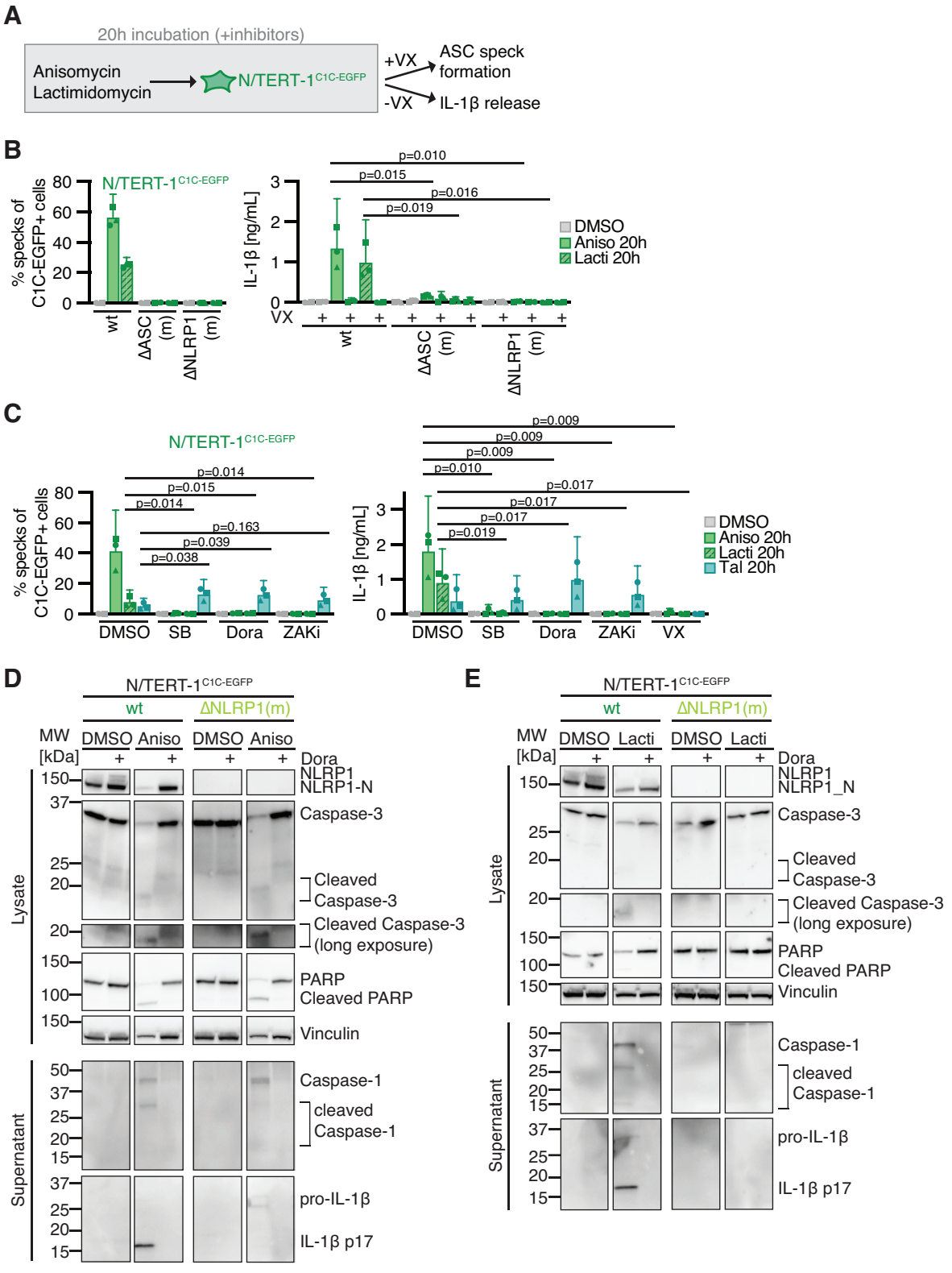

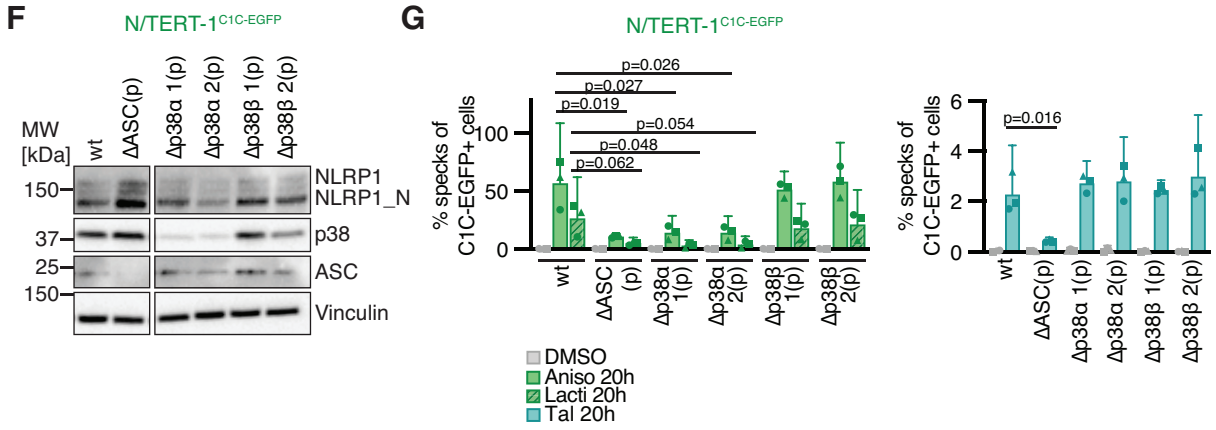

Figure 3.3: NLRP1 inflammasome activation by the ribotoxic stress response is dependent on p38 activity. (**A**) Schematic overview of the experimental setup. N/TERT-1$^{C1C\text{-}EGFP}$ cells were stimulated with 15 µM Aniso, 2 µM Lacti, DMSO, or 30 µM Tal as a control, for 20 h, where indicated in the presence of 20 µM SB, 10 µM Dora, 100 nM ZAKα inhibitor 6p (ZAKi), or DMSO. ASC speck formation was detected in the presence of caspase-1 inhibitor VX. (**B,C**) ASC speck formation in N/TERT-1$^{C1C\text{-}EGFP}$ cells and their monoclonal ASC and NLRP1 knockout derivatives was quantified by flow cytometry, as described in Fig. 2.1, and supernatants from the same cells were collected. IL-1β release was quantified by HTRF. (**D,E**) Lysates and precipitated supernatants of N/TERT-1$^{C1C\text{-}EGFP}$ cells and their monoclonal NLRP1 knockout derivatives were analyzed by immunoblot with the indicated antibodies. The DMSO control in (D) is the same as shown in Fig. 3.1 E. (**F**) Polyclonal ASC, p38α, and p38β knockout derivatives of N/TERT-1$^{C1C\text{-}EGFP}$ cells were confirmed by immunoblot with the indicated antibodies. (**G**) ASC speck formation in N/TERT-1$^{C1C\text{-}EGFP}$ cells and their polyclonal ASC, p38α, and p38β knockout derivatives was quantified by flow cytometry. Data represents average values (with individual data points) from three independent experiments ± 95 % CI, p-values were calculated using unpaired t-test. Immunoblots in (D-F) display experiment representatives of two independent experiments.

talabostat-induced NLRP1 responses, which were even slightly boosted by the p38 inhibitors. Doramapimod also inhibited cleavage of caspase-1 and IL-1β as confirmed by immunoblot (Fig. 3.3 D,E).

To evaluate the role of the different p38 isoforms in the activation of NLRP1 inflammasomes, polyclonal p38α and p38β knockout derivatives of N/TERT-1$^{C1C\text{-}EGFP}$ cells were generated and compared to polyclonal ASC knockouts (expecting similar knockout efficiencies) (Fig. 3.3 F). Analysis of p38 levels by immunoblot using a p38 antibody recognizing p38α, β, and γ isoforms revealed that p38 signals were substantially diminished in p38α knockout keratinocytes, suggesting that p38α is the most abundant

isoform in these cells. In line with these results, knockout of p38α inhibited anisomycin- and lactimidomycin-induced NLRP1 speck assembly to similar levels as ASC knockouts, whereas responses in knockouts of p38β were unchanged (Fig. 3.3 G). NLRP1 inflammasome assembly triggered by talabostat was not impaired in p38α knockouts, in line with the p38 inhibitor experiments. This suggests that activation of NLRP1 by the RSR follows a mechanism independent of DPP9 complex perturbations.

Next, I wondered whether NLRP1 activation by the RSR controls subsequent cell death (Fig. 3.4 A). Similar to UVB irradiation, anisomycin and lactimidomycin induced high levels of cell death as shown by strong release of LDH (Fig. 3.4 B) and uptake of DNA dye DRAQ7 in N/TERT$^{C1C\text{-}EGFP}$ cells (Fig. 3.4 C). In the case of lactimidomycin, cell death was largely abrogated in NLRP1 knockout derivatives, whereas anisomycin-induced cell death was only delayed. Microscopy analyses of cells at earlier time points (6 h for anisomycin, 12 h for lactimidomycin) revealed that wild type N/TERT-1 cells look clearly pyroptotic, whereas the NLRP1 knockout cells looked round and shriveled but did not undergo pyroptosis (Fig. 3.4 D). This shows that both antibiotics cause NLRP1-dependent pyroptosis at earlier time points. However, at later time points, especially the anisomycin-treated cells revealed similar morphologies and levels of cell death, independent of NLRP1. DRAQ7 uptake after anisomycin and lactimidomycin treatment was completely inhibited by pan-caspase inhibitor Z-VAD(OMe)-FMK. In addition, immunoblot analyses revealed NLRP1-independent cleavage of caspase-3 and PARP (Fig. 3.3 D,E), demonstrating that anisomycin and lactimidomycin also cause apoptosis, as described before (Y. Liu et al., 2012; X. Wang et al., 2005; Wu et al., 2020). Cell death and apoptosis were largely prevented by p38 inhibitor doramapimod, suggesting that apoptosis and cell death were additional consequences of p38 MAPK signaling. Thus, NLRP1-induced pyroptosis partially contributes to RSR-induced cell death at the beginning of the stimulation, but is dominated by apoptosis at later time points.

To define the cellular activities required for NLRP1 activation by the RSR, inflammasome responses were quantified in the presence of different inhibitors in HEK$^{NLRP1+ASC}$ and N/TERT-1$^{C1C\text{-}EGFP}$ cells (Fig. 3.5 A-D). As controls, activation of NLRP1 by anisomycin and lactimidomycin was consistently inhibited by p38 inhibitors SB202190 and doramapimod

in both reporter cells. To analyze the role of proteasomal degradation, the proteasome

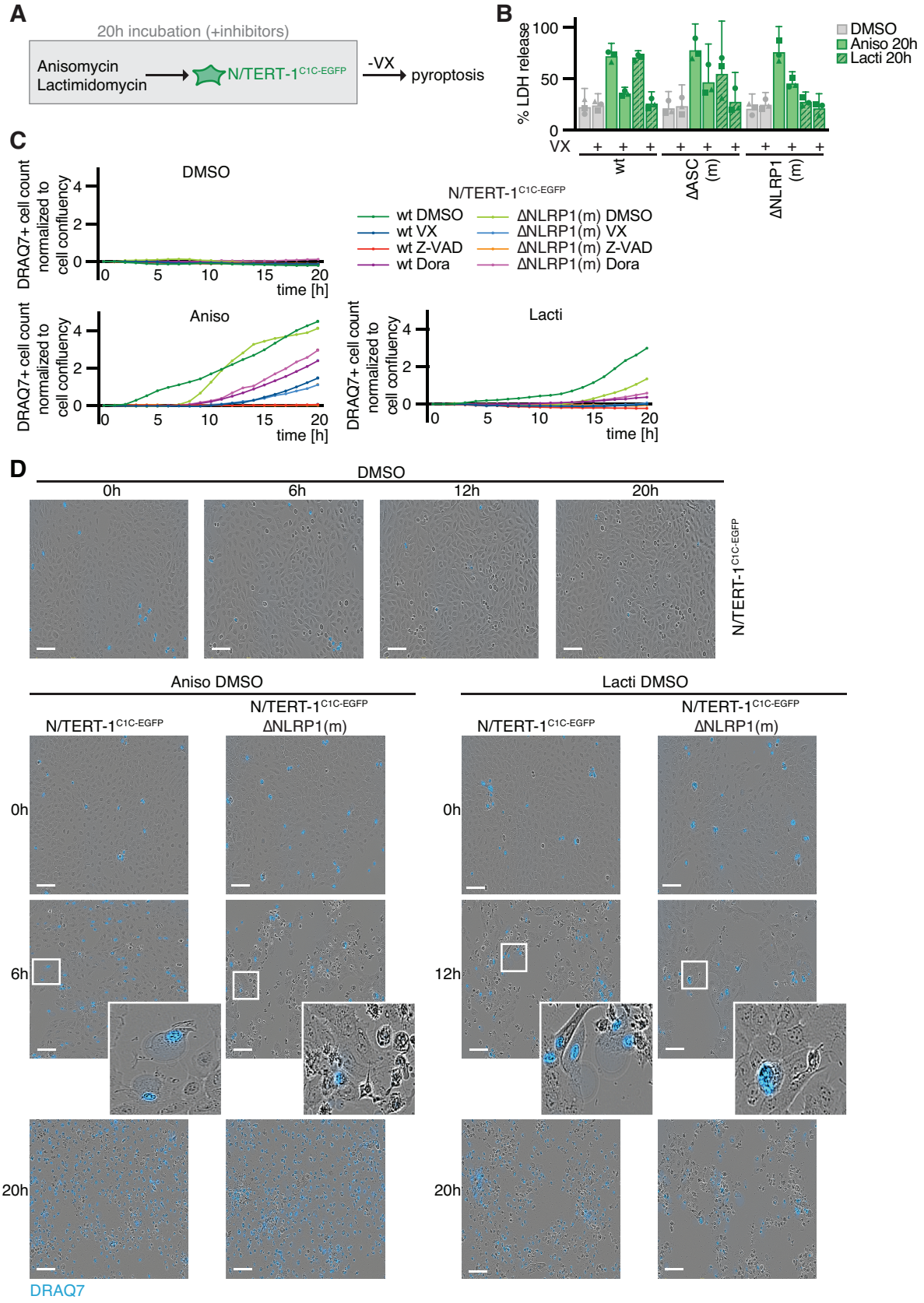

Figure 3.4: NLRP1 inflammasome activation only partially contributes to ribotoxic stress response-induced cell death. (**A**) Schematic overview of the experimental setup. N/TERT-1$^{C1C\text{-}EGFP}$ cells were stimulated with 15 µM Aniso, 2 µM Lacti, or DMSO for 20 h, where indicated in the presence of 100 µM VX, 50 µM Z-VAD, 10 µM Dora, or DMSO. (**B**) Cell death of N/TERT-1$^{C1C\text{-}EGFP}$ cells and their monoclonal ASC and NLRP1 knockout derivatives was quantified by detection of LDH release. The same supernatants as in Fig. 3.3 B were used. (**C)** Cell death of N/TERT-1$^{C1C\text{-}EGFP}$ cells and their monoclonal NLRP1 knockout derivatives was quantified by uptake of non-cell permeable DNA dye DRAQ7 over 20 h. Values shown for DMSO are the same as in Fig. 2.2 H. (**D**) Representative microscopy images of DRAQ7 uptake and pyroptotic cells. Scale bars represent 100 µm. Data represents average values (with individual data points) from three independent experiments ± 95 % CI. Quantifications of DRAQ7 uptake over time in (C) and microscopy images in (D) display experiment representatives of three independent experiments.

inhibitors MG-132 and bortezomib (Borte), as well as the E1 enzyme inhibitor MLN7243 (MLN7), were used for 6 h activation experiments, complemented with the less toxic neddylation inhibitor MLN4924 (MLN4) for 20 h stimulations, as already described in chapter 2. NLRP1 activation by the RSR was consistently shut down by all mentioned inhibitors of proteasomal degradation in both reporter cells, implying that NLRP1 degradation, involving E1 enzymes, CRL complexes, and the proteasome, is necessary to activate NLRP1 after ribotoxic stress. Inhibition of MAPK-activated protein kinase MK2 (PF) or the integrated stress response (ISRIB) did not inhibit NLRP1 activation by either activator. Bestatin methyl esters (BeMeEs) are non-specific inhibitors of metallo-aminopeptidases, which were reported to interfere with N-degron pathway-mediated Nlrp1b activation after lethal factor-mediated cleavage (Chui et al., 2019; Orth-He et al., 2023; Wickliffe et al., 2008). However, addition of bestatin methyl esters did not impair RSR-induced NLRP1 activation. Inhibition of JNK kinases (Jnk) affected NLRP1 activation in variable degrees, similar to the results after UVB irradiation. Importantly, inhibition of p38, neddylation, E1, or the proteasome for the same time duration did not inhibit NLRP3 activation by LPS and nigericin in HEK$^{NLRP3+ASC}$ cells (Fig. 3.5 E,F); E1 and proteasome inhibitors even enhanced NLRP3 responses. This indicates that the requirement for these cellular activities is specific for NLRP1, and not inflammasomes in general. As before, activation of NLRP1 by talabostat (Fig. 3.5 B,D) did not require p38 activity. Interestingly, inhibition of neddylation abolished talabostat-induced NLRP1 inflammasome assembly in N/TERT-1 keratinocytes but not in the more artificial HEK cell system.

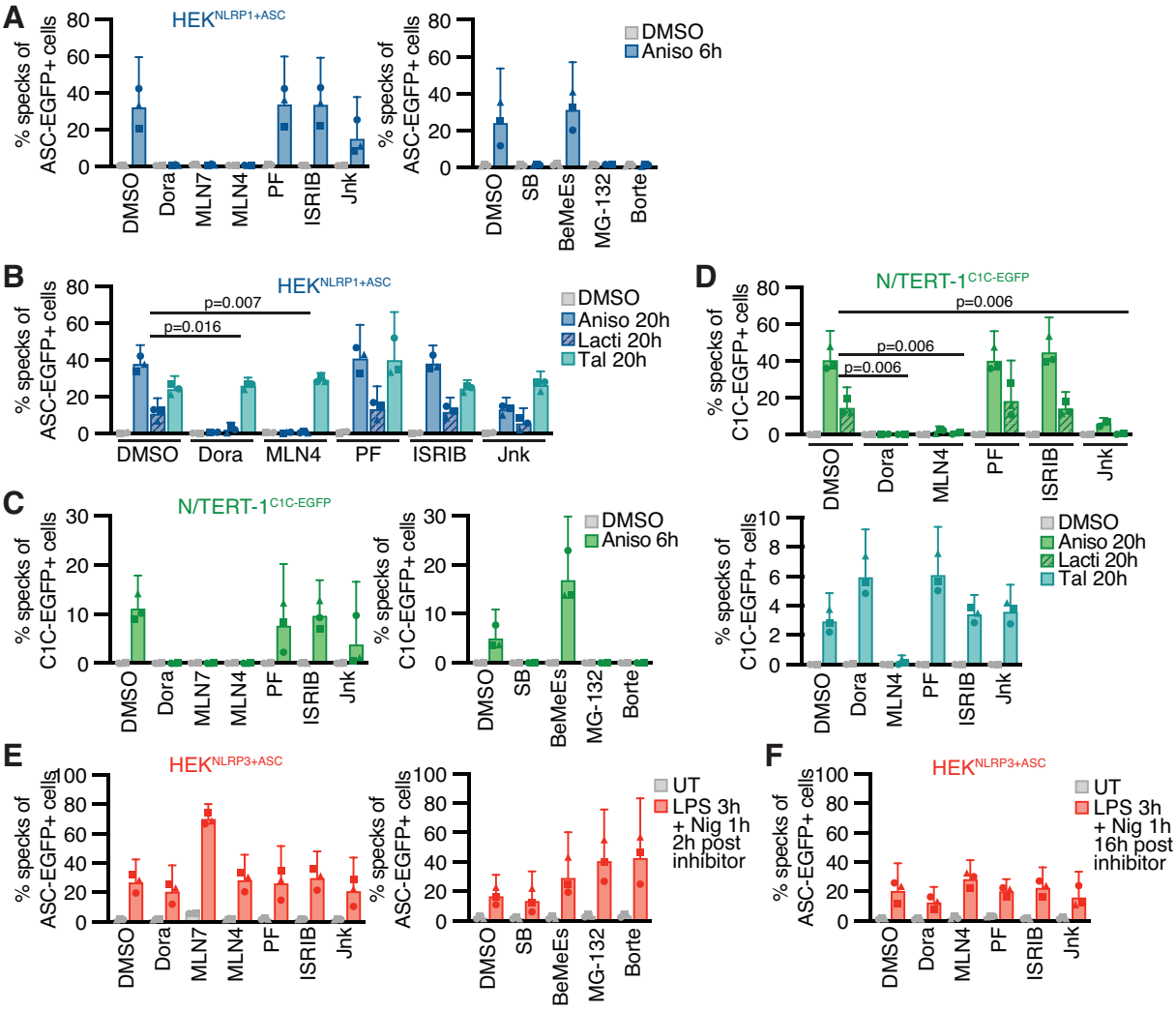

Figure 3.5: NLRP1 inflammasome activation by the ribotoxic stress response relies on the ubiquitination machinery and proteasomes. (**A-D**) HEK$^{NLRP1+ASC}$ or N/TERT-1$^{C1C-EGFP}$ cells were stimulated with 15 µM Aniso, 2 µM Lacti, 30 µM Tal, or DMSO for 6 or 20 h. (**E,F**) HEK$^{NLRP3+ASC}$ cells were stimulated with 200 ng/mL LPS for 3 h and 10 µM Nig for 1 h, or left untreated (UT). Stimulations were performed in the presence of 10 µM Dora, 1 µM MLN7, 1 µM MLN4, 1 µM PF, 200 nM ISRIB, 3 µM Jnk, 20 µM SB, 20 µM bestatin methyl ester (BeMeEs), 1 µM MG-132, 1 µM bortezomib (Borte), or DMSO, as indicated. Note that LPS+Nig stimulation was performed towards the end of inhibitor treatment to evaluate NLRP3 responses after 6 or 20 h of inhibitor effect. ASC speck formation was quantified by flow cytometry, as described in Fig. 2.1. ASC speck formation in N/TERT-1 cells was detected in the presence of caspase-1 inhibitor VX. Data represents average values (with individual data points) from three independent experiments ± 95 % CI, p-values were calculated using unpaired t-test.

Taken together, I show that diverse activators of the RSR activate human NLRP1. This response is distinct from NLRP1 activation by inhibition of DPP8/9, as it depends on p38 kinase activity. Since several of the described NLRP1 activators also efficiently inhibit

translation, NLRP1 activation does probably not depend on p38-dependent gene upregulation, but rather directly on the kinase activity of p38. As described for other NLRP1 stimuli, NLRP1 activation through the RSR required E1 activity, neddylation, and proteasome activity. The ubiquitin-proteasome pathway likely contributes to the N-terminal degradation of NLRP1 itself, followed by the release of the C-terminal $NLRP1^{UPA\text{-}CARD}$.

3.2.3 Activation of NLRP1 by alphavirus infection is also dependent on p38 kinase activity

Since I had found that activators of the RSR activate human NLRP1 in a p38-dependent manner, I was curious whether other reported stimuli of NLRP1 also depend on p38 activity. Thus, I tested NLRP1 activation by the model alphavirus SFV (Bauernfried et al., 2021). To study NLRP1 activation in response to viral infection, I infected $HEK^{NLRP1+ASC}$, $HEK^{NLRP3+ASC}$, and N/TERT-$1^{C1C\text{-}EGFP}$ cells with SFV, the closely related SINV, as well as vesicular stomatitis virus (VSV), a negative-sense ssRNA virus, and analyzed the inflammasome response after 20 h (Fig. 3.6 A). Infection was quantified by staining of dsRNA (SFV, SINV) or the VSV G protein, and only infected cells were included in the flow cytometry analysis of inflammasome activation. Nearly all of the cells were infected with the respective viruses, but only SFV and SINV induced a detectable assembly of ASC specks in $HEK^{NLRP1+ASC}$ and N/TERT-$1^{C1C\text{-}EGFP}$ cells (Fig. 3.6 B,D). With less than 10 % ASC speck formation in $HEK^{NLRP1+ASC}$ cells, the inflammasome response was weak compared to talabostat or anisomycin stimulation. Around 10 % of SFV-infected N/TERT-$1^{C1C\text{-}EGFP}$ cells showed inflammasome formation, so the responses were higher than after talabostat treatment but also clearly weaker than after anisomycin stimulation. As SFV was the stronger inflammasome activator in both reporter cell lines, I focused further analyses on this alphavirus. Treatment of the cells with the V-ATPase inhibitor bafilomycin A1 (BafA) completely abolished SFV infection, as alphaviruses require endosomal acidification to fuse with the membrane of endosomes (Marsh et al., 1983) (Fig. 3.6 C,E). The treatment also abrogated ASC speck formation, demonstrating that cytosolic delivery of viral genomes was critical to activate NLRP1 in the reporter cells. Alphavirus-infected N/TERT-$1^{C1C\text{-}EGFP}$ cells released IL-1β in a caspase-1-dependent

manner, which was also inhibited by bafilomycin A1 (Fig. 3.6 F). ASC speck formation and

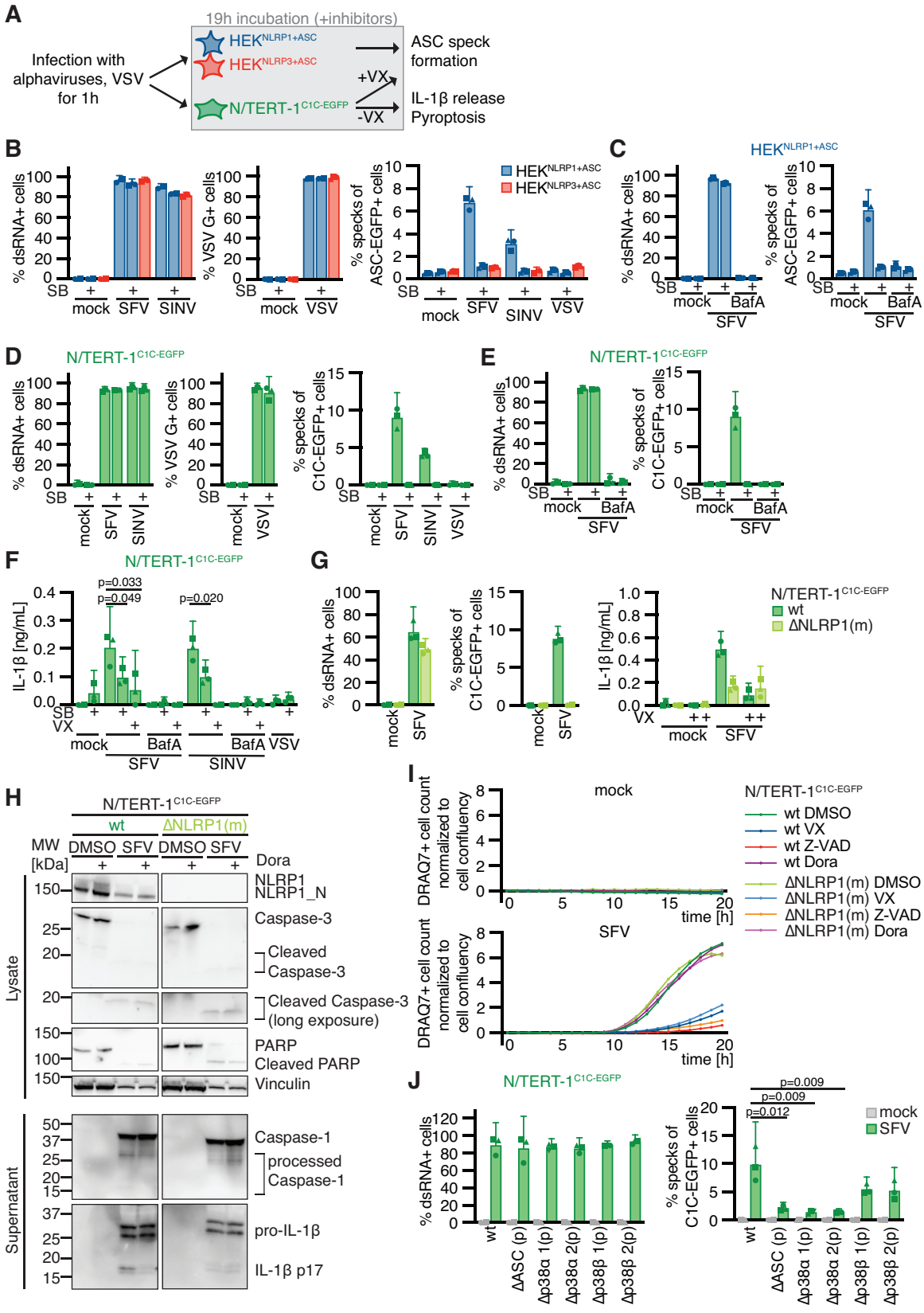

Figure 3.6: NLRP1 inflammasome activation by alphavirus infection is dependent on p38 activity. (**A**) Schematic overview of the experimental setup. HEK$^{NLRP1+ASC}$, HEK$^{NLRP3+ASC}$, or N/TERT-1$^{C1C-EGFP}$ cells were infected with Semliki Forest virus (SFV), Sindbis virus (SINV), or vesicular stomatitis virus (VSV) as control, at multiplicity of infection (MOI) 1 (HEK) or 5 (N/TERT-1) for 1 h. Cells were further incubated for 19 h, where indicated in the presence of 20 µM SB, 100 µM VX, 10 µM Dora, 50 µM Z-VAD, or DMSO. 100 nM bafilomycin A1 (BafA) was added before, during, and after infection. ASC speck formation in N/TERT-1 cells was detected in the presence of caspase-1 inhibitor VX. Infection was confirmed by staining of double-stranded RNA (dsRNA) (SFV, SINV) or VSV G (VSV). Quantification of specks was limited to infected cells, with exception of mock controls and BafA-treated cells. (**B,C**) Infection and ASC speck formation in HEK$^{NLRP1+ASC}$ and HEK$^{NLRP3+ASC}$ cells were quantified by flow cytometry, as described in Fig. 2.1. (**D,E**) Infection and ASC speck formation in N/TERT-1$^{C1C-EGFP}$ cells were quantified by flow cytometry and supernatants from the same cells were collected. (**F**) IL-1β release was quantified by HTRF. (**G**) Infection and ASC speck formation in N/TERT-1$^{C1C-EGFP}$ cells and their monoclonal NLRP1 knockout derivatives were quantified by flow cytometry and supernatants from the same cells were collected. IL-1β release was quantified by HTRF. (**H**) Lysates and precipitated supernatants of N/TERT-1$^{C1C-EGFP}$ cells and their monoclonal NLRP1 knockout derivatives were analyzed by immunoblot with the indicated antibodies. The DMSO control is the same as shown in Fig. 3.3 E. (**I**) Cell death of N/TERT-1$^{C1C-EGFP}$ cells and their monoclonal NLRP1 knockout derivatives was quantified by uptake of non-cell permeable DNA dye DRAQ7 over 20 h. (**J**) Infection and ASC speck formation in N/TERT-1$^{C1C-EGFP}$ cells and their polyclonal ASC, p38α, and p38β knockout derivatives were quantified by flow cytometry. Data represents average values (with individual data points) from three independent experiments ± 95 % CI, p-values were calculated using unpaired t-test. Immunoblots in (H) display experiment representatives of two independent experiments. Quantifications of DRAQ7 uptake over time in (I) display experiment representatives of three independent experiments.

release of IL-1β after SFV infection were abrogated in NLRP1 knockout N/TERT-1$^{C1C-EGFP}$ cells (Fig. 3.6 G). NLRP1-dependent processing of IL-1β was also confirmed by immunoblot (Fig. 3.6 H). Similar to the RSR stimuli, SFV infection led to caspase-3 and PARP cleavage, as well as strong NLRP1-independent DRAQ7 uptake (Fig. 3.6 I). This suggests that apoptosis dominated the observed cell death after infection with cytotoxic SFV. However, as for the RSR initiated by UV and anisomycin, activation of NLRP1 inflammasomes substantially alters the physiological response because it triggers the release of the strong pro-inflammatory cytokine IL-1β.

As I was able to recapitulate NLRP1 activation by SFV in both reporter cells, I next analyzed the role of p38 in this response. ASC speck formation in HEK$^{NLRP1+ASC}$ and

N/TERT-1$^{C1C\text{-}EGFP}$ cells infected with SFV and SINV was completely inhibited by the p38α/β inhibitor SB202190 (Fig. 3.6 B,D). In line with this, IL-1β release by alphavirus-infected keratinocytes was substantially reduced by SB202190 and pan-p38 inhibitor doramapimod (Fig 2.6 F,H). In contrast, inhibition of p38 did not rescue N/TERT-1$^{C1C\text{-}EGFP}$ from SFV-induced cell death (Fig. 3.6 I), in line with unaltered cleavage of caspase-3 and PARP in the presence of doramapimod in immunoblots (Fig. 3.6 H). Polyclonal p38α knockout derivatives of N/TERT-1$^{C1C\text{-}EGFP}$ cells exhibited impaired SFV-induced NLRP1 speck assembly to similar levels as ASC knockouts (Fig. 3.6 J), confirming a crucial role of p38 activity for alphavirus-induced NLRP1 activation.

Not only p38 inhibitors SB202190 and doramapimod inhibited SFV-induced NLRP1 activation, but also neddylation (MLN4) and JNK (Jnk) inhibitors completely abrogated inflammasome assembly in HEK$^{NLRP1+ASC}$ and N/TERT-1$^{C1C\text{-}EGFP}$ cells after infection with SFV (Fig. 3.7 A,B). Since NLRP1 inflammasome activation by alphavirus infection depends on p38 kinase activity and neddylation, virus infection likely activates NLRP1 by a mechanism that resembles activation by the RSR. To test whether NLRP1 activation by alphaviruses engages a similar signaling cascade relying on MAP3K ZAKα, I infected N/TERT-1$^{C1C\text{-}EGFP}$ cells with SFV in the presence of p38 or ZAKα inhibitors (Fig. 3.7 C). While inflammasome assembly was completely abrogated by both p38 inhibitors, ZAK inhibition blocked the formation of ASC specks substantially, but not completely. The same trend was observed for the release of IL-1β. To verify the specificity of the used kinase inhibitors, I wanted to confirm that the pan-p38 inhibitor doramapimod does not interfere with the anisomycin-induced phosphorylation of MAP2K MKK3 (Fig. 3.7 D). Indeed, immunoblots with phospho-specific antibodies revealed that doramapimod did not inhibit phosphorylation of MKK3, suggesting that the MAP3K ZAKα is still active in presence of the p38 inhibitor. As expected, inhibition of ZAKα completely blocked anisomycin-induced phosphorylation of MKK3 and the downstream kinase p38. I can thus be confident that the inhibition of SFV-induced NLRP1 activation by p38 inhibitors is not caused by indirect interference with ZAKα activity. To further study the contribution of ZAKα, I generated knockouts of ZAK as well as control MAP3K TAO kinase 2 (TAOK2), in the background of N/TERT-1$^{C1C\text{-}EGFP}$ cells (Fig. 3.7 E). As expected, NLRP1 activation by talabostat was not affected by either of the knockouts (Fig. 3.7 F). Anisomycin-induced

ASC speck assembly was completely abrogated in ZAK-knockout cells, validating the critical role of ZAKα for the RSR and the resulting p38-dependent NLRP1 activation. In comparison, SFV-induced NLRP1 inflammasome activation was reduced by around 70 % in ZAK-knockout cells, but the response was not completely abrogated, resembling the ZAK inhibitor experiments. This suggests that other MAP3 kinases can contribute to p38 activation in the context of alphavirus infections, even though ZAKα seems to play a substantial role in this inflammasome activation pathway.

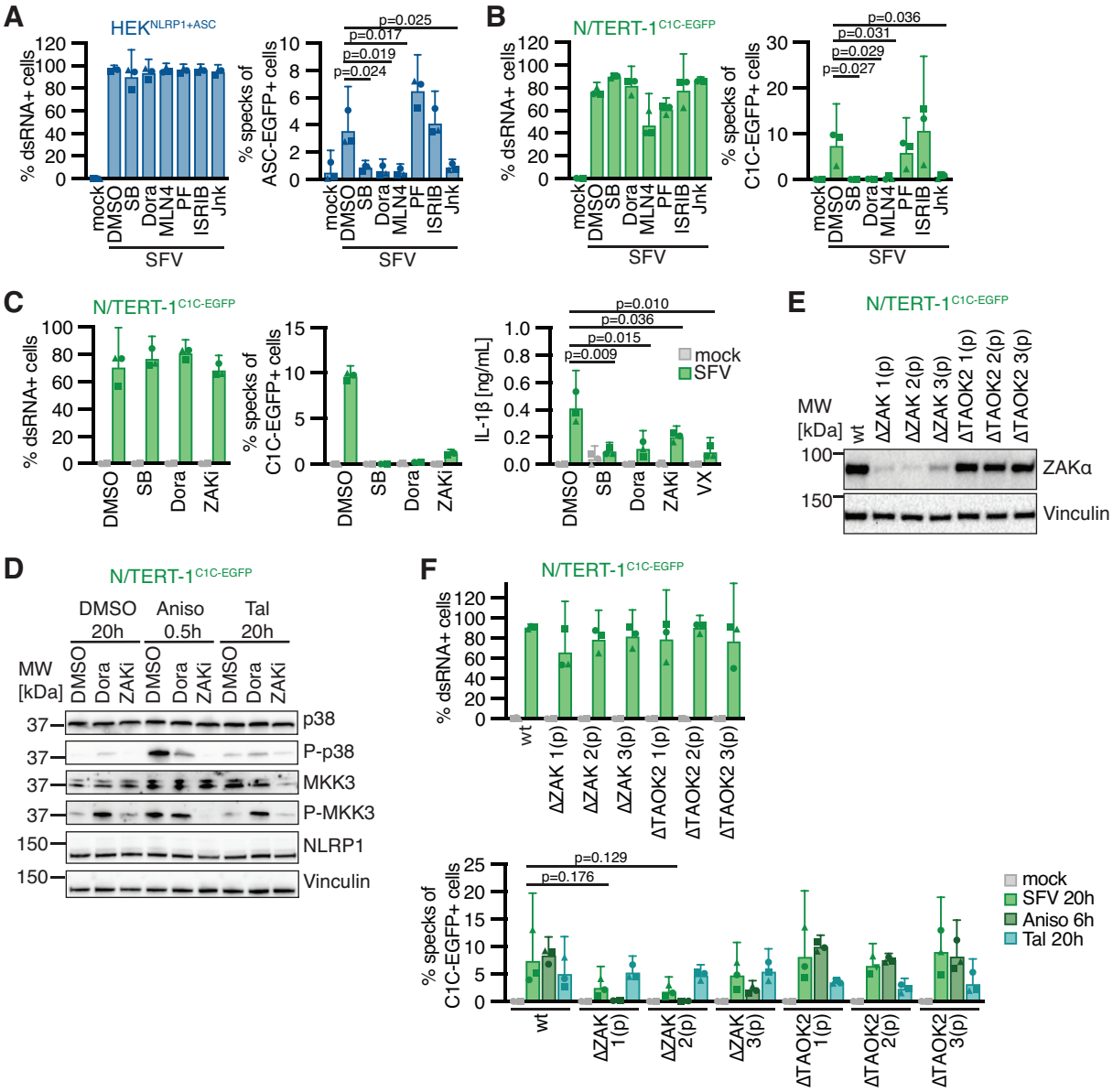

Figure 3.7: NLRP1 inflammasome activation by alphavirus infection is dependent on p38 and ZAKα activity. (**A-C**) HEK$^{NLRP1+ASC}$ or N/TERT-1$^{C1C-EGFP}$ cells were infected with SFV at MOI 1 (HEK) or 5 (N/TERT-1) for 1 h. Cells were further incubated for 19 h, where indicated in the presence of 20 µM SB, 10 µM Dora, 1 µM MLN4, 1 µM PF, 200 nM ISRIB, 3 µM Jnk, 100 nM ZAKi, 100 µM VX, or DMSO. ASC speck formation in N/TERT-1 cells was detected in the presence of caspase-1 inhibitor VX. Infection was confirmed by staining of dsRNA. Quantification of specks was limited to infected cells, with exception of mock controls. Infection and ASC speck formation in HEK$^{NLRP1+ASC}$ (A) or N/TERT-1$^{C1C-EGFP}$ (B) cells were quantified by flow cytometry, as described in Fig. 2.1. Infection and ASC speck formation in N/TERT-1$^{C1C-EGFP}$ cells (C) was quantified by flow cytometry and supernatants from the same cells were collected. IL-1β release was quantified by HTRF. (**D**) N/TERT-1$^{C1C-EGFP}$ cells were stimulated with 15 µM Aniso for 0.5 h, 30 µM Tal, or DMSO for 20 h, where indicated in the presence of 10 µM Dora, 100 nM ZAKi, or DMSO. Lysates were analyzed by immunoblot with the indicated antibodies to confirm phosphorylation of p38 (P-p38) and MKK3 (P-MKK3). (**E**) Polyclonal ZAK knockout derivatives of N/TERT-1$^{C1C-EGFP}$ cells were confirmed by immunoblot with the indicated antibodies. (**F**) N/TERT-1$^{C1C-EGFP}$ cells and their polyclonal ZAK and TAOK2 knockout derivatives were infected with SFV at MOI 5, or stimulated with 15 µM Aniso for 6 h, or 30 µM Tal for 20 h. Infection and ASC speck formation were quantified by flow cytometry. Quantification of specks was limited to infected cells in SFV samples. Data represents average values (with individual data points) from three independent experiments ± 95 % CI, p-values were calculated using unpaired t-test. Immunoblots in (D,E) display experiment representatives of two independent experiments.

It was proposed that dsRNA intermediates of SFV are the relevant trigger for NLRP1 (Bauernfried et al., 2021). I therefore transfected the HEK 293T and N/TERT-1 reporter cells with either synthetic dsRNA poly(I:C), low or high molecular weight (LMW/HMW), synthetic DNA poly(dA:dT), or herring testis-DNA (HT-DNA). Inflammasome activation was analyzed 20 h post-transfection (Fig. 3.8 A). Although proposed as a direct NLRP1 ligand, transfection of poly(I:C) did not induce inflammasome activation above background levels in HEK$^{NLRP1+ASC}$ cells, and neither did poly(dA:dT) or HT-DNA (Fig. 3.8 B). In contrast, N/TERT-1$^{C1C-EGFP}$ assembled inflammasomes and released IL-1β in a caspase-1-dependent manner when transfected with dsRNA, which was not observed in NLRP1 knockout cells (Fig. 3.8 C). This suggests that additional factors absent in HEK 293T cells contributed to NLRP1 activation in N/TERT-1 keratinocytes. Transfection of poly(dA:dT), but not HT-DNA, induced minor inflammasome activation and IL-1β release in N/TERT-1 cells, but this was independent of NLRP1. Cell death after dsRNA and DNA transfection was also NLRP1-independent. When I transfected the cells in the presence of p38 and ZAKα inhibitors, I found that poly(I:C)-induced formation of ASC

specks and release of IL-1β was strongly decreased by all inhibitors (Fig. 3.8 D). In contrast, the NLRP1-independent inflammasome response to poly(dA:dT) was mostly unaffected by the inhibitors. This indicates that cytosolic dsRNA, accumulated during both

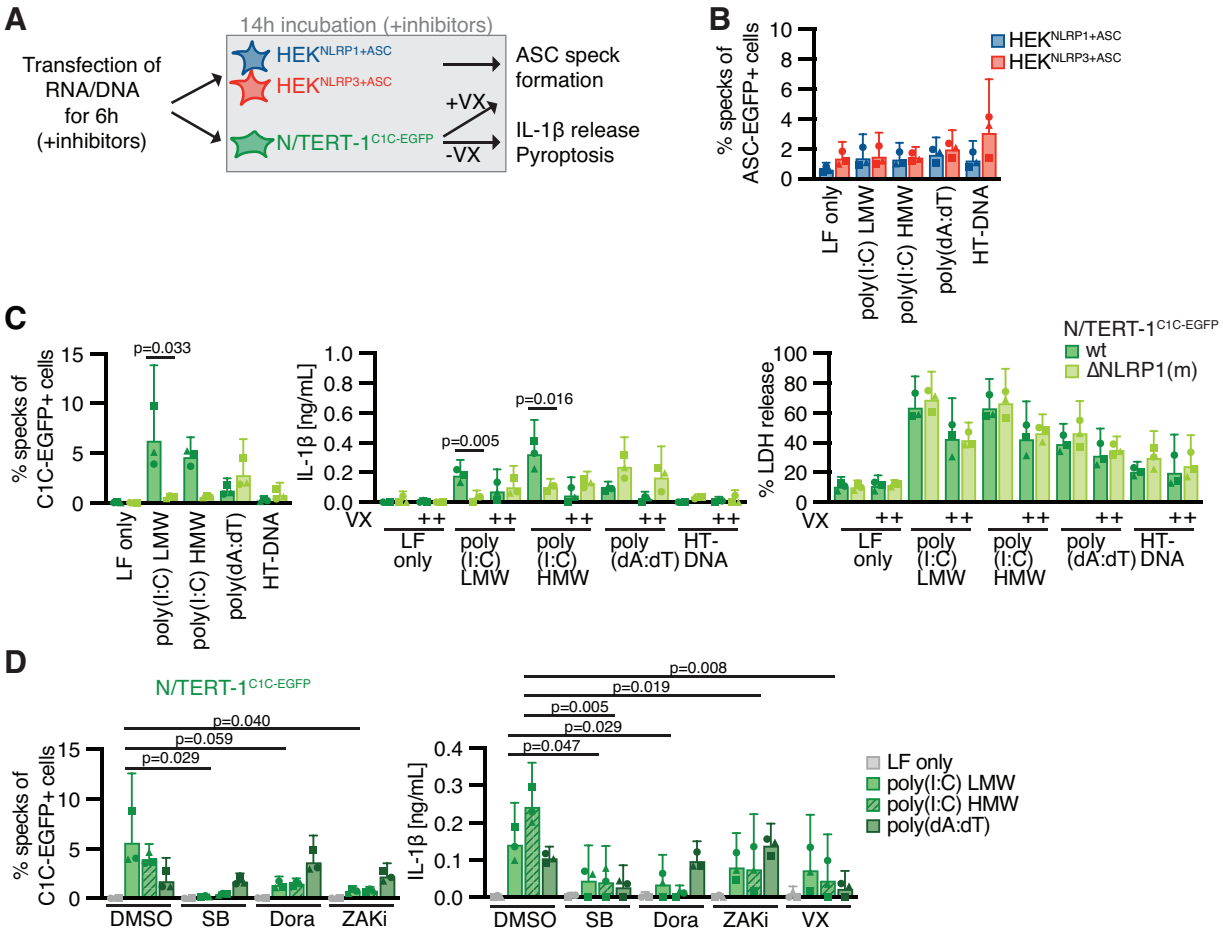

Figure 3.8: NLRP1 inflammasome activation by dsRNA is dependent on p38 and ZAKα activity. (**A**) Schematic overview of the experimental setup. HEK$^{NLRP1+ASC}$, HEK$^{NLRP3+ASC}$, or N/TERT-1$^{C1C-EGFP}$ cells were transfected with 1 µg/mL poly(I:C) low molecular weight (LMW), poly(I:C) high molecular weight (HMW), poly(dA:dT), or herring testis DNA (HT-DNA) for 6 h, where indicated in the presence of 20 µM SB, 10 µM Dora, 100 nM ZAKi, 100 µM VX, or DMSO. Lipofectamine (LF) only treated cells served as controls. Cells were further incubated for 14 h. ASC speck formation in N/TERT-1 cells was detected in the presence of caspase-1 inhibitor VX. (**B**) ASC speck formation in HEK$^{NLRP1+ASC}$ and HEK$^{NLRP3+ASC}$ cells was quantified by flow cytometry, as described in Fig. 2.1. (**C,D**) ASC speck formation in N/TERT-1$^{C1C-EGFP}$ cells and their monoclonal NLRP1 knockout derivatives was quantified by flow cytometry and supernatants from the same cells were collected. IL-1β release was quantified by HTRF. Cell death was quantified by detection of LDH release. Data represents average values (with individual data points) from three independent experiments ± 95 % CI, p-values were calculated using unpaired t-test.

alphavirus infection and poly(I:C) transfection, initiates NLRP1 activation through an RSR-like pathway involving ZAKα and p38 in the endogenous keratinocyte system, while only alphavirus infection is sufficient to activate NLRP1 in HEK 293T cells. Further experiments will be required to dissect if alphavirus infection induces genuine ribotoxic stress, or activates ZAKα differently.

I next tested whether NLRP1 is also important in the detection of alphaviruses that are clinically relevant as human pathogens. In collaboration with Anja vom Hemdt from the Institute of Virology in Bonn, we infected the HEK 293T and keratinocyte reporter cells with a panel of human pathogenic alphaviruses including EEEV, VEEV, MAYV, CHIKV, ONNV, BFV, and RRV, in the presence and absence of SB202190. All tested viruses were able to infect both $HEK^{NLRP1+ASC}$ and $HEK^{NLRP3+ASC}$ cells, as confirmed by staining of dsRNA (Fig. 3.9 A). In addition to the positive control SFV, we found that CHIKV and RRV activated NLRP1-dependent inflammasomes. ASC assembly in response to all three alphaviruses was inhibited by the p38α/β inhibitor SB202190. We were not able to infect the N/TERT-$1^{C1C-EGFP}$ cells with ONNV, BFV, and RRV (Fig. 3.9 B) and the fraction of infected cells was generally more variable for keratinocytes. However, analysis of inflammasome assembly in infected cells revealed clear ASC speck responses in keratinocytes infected with SFV, MAYV, and CHIKV. I cannot rule out that a weak NLRP1 activation in response to MAYV infection was not detected in $HEK^{NLRP1+ASC}$ cells due to the higher background caused by ectopically expressed ASC-EGFP. CHIKV-induced ASC speck assembly in the reporter keratinocytes was also dependent on p38 activity. Since SB202190 strongly decreased MAYV infection, we could not assess whether the weak inflammasome response depends on p38.

It is likely that related alphaviruses expose similar viral molecules in the cytosol and that they hijack similar cellular functions. Yet, only distinct alphaviruses triggered NLRP1 inflammasome assembly. I thus wondered if differential NLRP1 activation correlated to differences in p38 activation. I infected $HEK^{NLRP1+ASC}$ cells with two alphaviruses shown to trigger ASC specks (SFV and RRV) as well as two viruses that did not initiate inflammasome assembly (ONNV and BFV). I detected robust phosphorylation of p38 by flow cytometry in cells infected with SFV and RRV, which was comparable to p38 phosphorylation in anisomycin-treated cells (Fig. 3.9 C,D). However, cells infected with

ONNV and BFV did not trigger p38 phosphorylation. The ability to activate p38 thus correlated with NLRP1 activation, indicating that MAPK signaling is the critical determinant of NLRP1 activation by alphaviruses. Surprisingly, infection with the control virus VSV induced p38 phosphorylation as well, implying that either p38 activation by alphaviruses

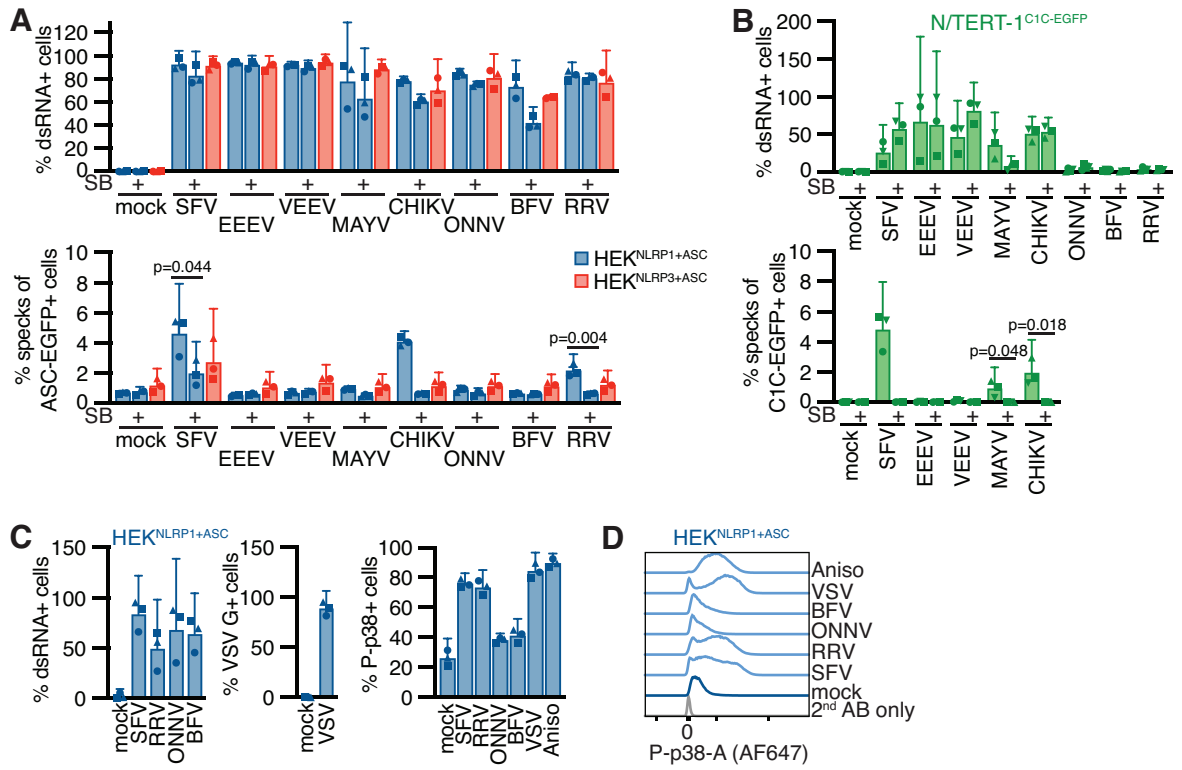

Figure 3.9: Alphavirus-induced p38 activity correlates with NLRP1 activation. (**A-C**) HEK$^{NLRP1+ASC}$, HEK$^{NLRP3+ASC}$, or N/TERT-1$^{C1C-EGFP}$ cells were infected with SFV (HEK: MOI 1/N/TERT-1: MOI 5), Eastern equine encephalitis virus (EEEV, MOI 1/5), Venezuelan equine encephalitis virus (VEEV, MOI 1/50), Chikungunya virus (CHIKV, MOI 1/50), Mayaro virus (MAYV, MOI 25/50), o'nyong nyong virus (ONNV, MOI 25/50), Barmah Forest Virus (BFV, MOI 25/50), or Ross River virus (RRV, MOI 25/50) for 1 h. Cells were further incubated for 19 h, where indicated in the presence of 20 µM SB. ASC speck formation in N/TERT-1 cells was detected in the presence of caspase-1 inhibitor VX. Infection was confirmed by staining of dsRNA. Quantification of specks was limited to infected cells, with exception of mock controls. Infection and ASC speck formation in HEK$^{NLRP1+ASC}$ and HEK$^{NLRP3+ASC}$ (A) or N/TERT-1$^{C1C-EGFP}$ cells (B) were quantified by flow cytometry, as described in Fig. 2.1. Fixed HEK$^{NLRP1+ASC}$ cells (C) were stained for phosphorylated p38 (P-p38), and infection and P-p38 were quantified by flow cytometry. Cells infected with VSV (MOI 1) or stimulated with 15 µM Aniso served as controls. (D) Representative histograms of P-p38 signal. Data represents average values (with individual data points) from three independent experiments ± 95 % CI, p-values were calculated using unpaired t-test.

differs from activation by VSV, or that VSV counteracts p38-dependent NLRP1 inflammasome stimulation.

Taken together, I confirmed NLRP1 activation by SFV infection in NLRP1 HEK 293T and keratinocyte reporter cells, but found that inflammasome activation is critically dependent on p38 and mostly dependent on ZAKα activation. It is thus unlikely that direct dsRNA binding to NLRP1 alone is sufficient for NLRP1 activation. We identified four additional alphaviruses, SINV, RRV, MAYV, and CHIKV, that activate NLRP1, supporting the relevance of NLRP1 as a sensor for the detection of alphavirus in the first organ that these viruses encounter after transmission by insect vectors.

3.2.4 Activation of NLRP1 by N-terminal ubiquitination is independent of p38 kinase activity

Up until here, I could show that NLRP1 inflammasome activation by both the RSR and alphavirus infection requires p38 activation. Both responses also require functional proteasomal degradation, suggesting that NLRP1 is N-terminally degraded, releasing the active $NLRP1^{UPA\text{-}CARD}$. Thus, I wanted to test whether the degradation of NLRP1 itself relies on p38 activity. Several viral proteases, like the HRV14 3C protease, cleave NLRP1 at the N-terminus, thereby inducing N-terminal degradation and inflammasome assembly (Planès et al., 2022; Robinson et al., 2020; Tsu et al., 2021). I transiently transfected a plasmid encoding FLAG-tagged HRV14 3C, or the catalytically inactive mutant C146A (Robinson et al., 2020), in $HEK^{NLRP1+ASC}$ and $HEK^{NLRP3+ASC}$ reporter cells (Fig. 3.10 A). Both proteases were sufficiently expressed, enabling the analysis of inflammasome assembly in successfully transfected FLAG+ cells. Only expression of catalytically active HRV14 3C induced ASC speck formation in more than 40 % of FLAG+ $HEK^{NLRP1+ASC}$ cells (Fig. 3.10 B), recapitulating the reports about NLRP1 activation by this viral protease. Yet, p38 inhibitors SB202190 and doramapimod did not affect inflammasome assembly (Fig. 3.10 C), suggesting that NLRP1 was still degraded after cleavage by the viral protease. The neddylation inhibitor MLN4924 reduced ASC speck formation but also affected the expression of HRV14 3C.

To further delineate the role of p38 kinase activity in N-terminal degradation of NLRP1, I made use of the VHL-VHH$_{PYD}$ system to induce targeted ubiquitination – and therefore direction activation – of NLRP1 (as established in chapter 2). Treatment with doramapimod had no effect on the activation of NLRP1 induced by the transient expression of VHL-VHH$_{PYD\ 1}$ and VHL-VHH$_{PYD\ 2}$ in HEK$^{NLRP1+ASC}$ cells (Fig. 3.10 D). Similar results were observed in N/TERT-1 cells, which still assembled ASC specks (Fig. 3.10 E), and released IL-1β and LDH (Fig. 3.10 F) following expression of VHL-VHH$_{PYD\ 1}$ or VHL-VHH$_{PYD\ 2}$ in the presence of the p38 inhibitor. Since VHL recruits CRL2 complexes to initiate ubiquitination, all observed responses were blocked by neddylation inhibitor MLN4924, as shown before.

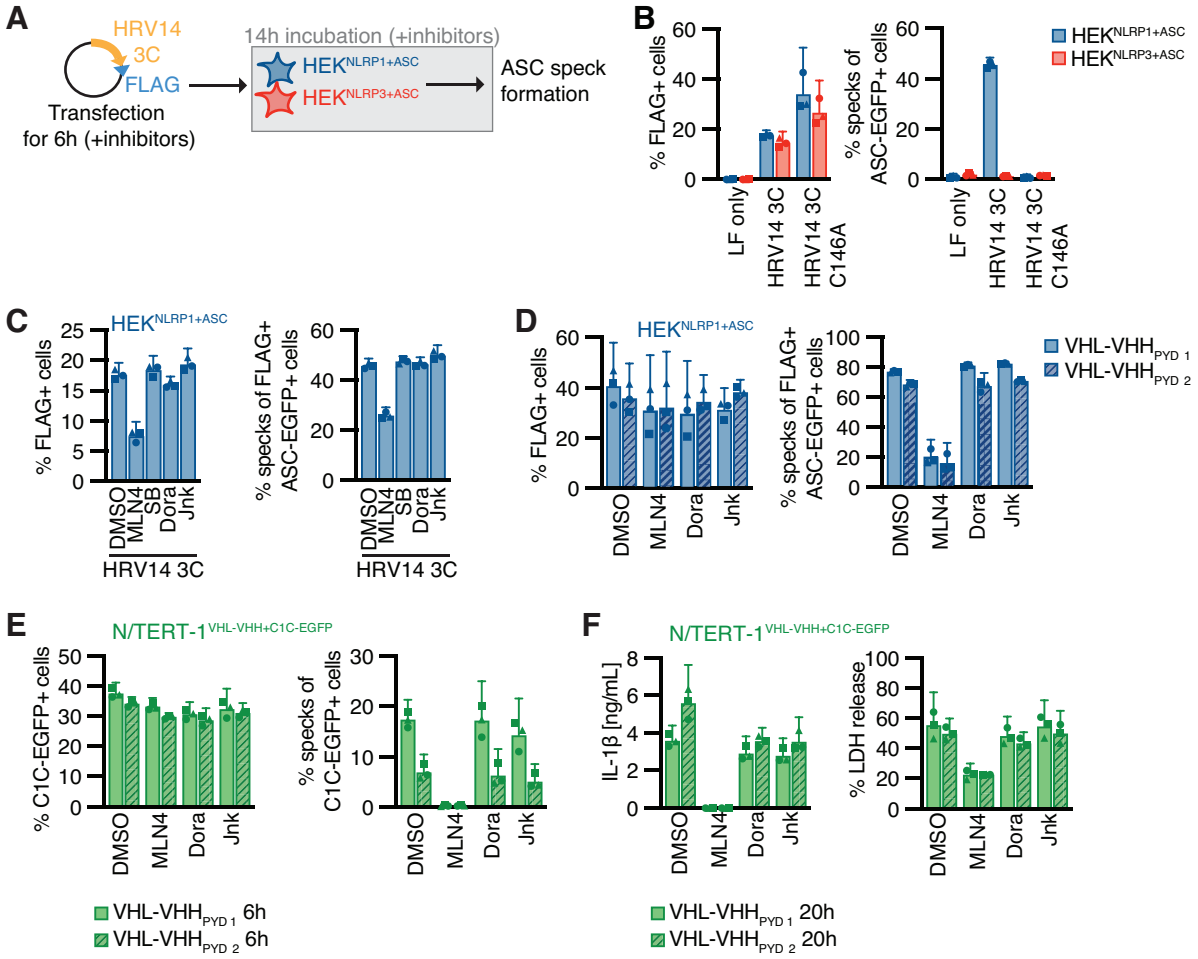

Figure 3.10: NLRP1 activation by N-terminal degradation is independent of p38 activity. (**A**) Schematic overview of the experimental setup. $HEK^{NLRP1+ASC}$ and $HEK^{NLRP3+ASC}$ cells were transiently transfected with expression vectors for FLAG-tagged human rhinovirus (HRV) 14 3C protease or its catalytically inactive mutant (C146A) for 6 h, where indicated in the presence of 1 µM MLN4, 20 µM SB, 10 µM Dora, 3 µM Jnk, or DMSO. Lipofectamine (LF) only treated cells served as controls. Cells were further incubated for 14 h. (**B,C**) FLAG-tagged HRV14 3C expression and ASC speck formation were quantified by flow cytometry, as described in Fig. 2.1. Quantification of specks was limited to FLAG-positive cells, except for untransfected controls. (**D**) $HEK^{NLRP1+ASC}$ cells were transiently transfected with expression vectors for FLAG-tagged VHL-VHH fusions, as described in Fig. 2.4, where indicated in the presence of 1 µM MLN4, 10 µM Dora, 3 µM Jnk, or DMSO. FLAG-tagged VHL-VHH expression and ASC speck formation were quantified by flow cytometry. Quantification of specks was limited to FLAG-positive cells. Values shown for DMSO and MLN4 are the same as in Fig. 2.4 C. (**E,F**) N/TERT-1 cells were transduced with lentiviral vectors encoding C1C-EGFP and VHL-VHH controlled by a bidirectional dox-inducible promoter, as described in Fig. 2.5. $N/TERT\text{-}1^{VHL\text{-}VHH+C1C\text{-}EGFP}$ cells were treated with 1 µg/mL dox for 6 or 20 h to induce expression, where indicated in the presence of 1 µM MLN4, 10 µM Dora, 3 µM Jnk, or DMSO. ASC speck formation was detected in the presence of caspase-1 inhibitor VX. (E) C1C-EGFP expression and ASC speck formation in C1C-EGFP+ cells were quantified after 6 h dox treatment by flow cytometry. Values shown for DMSO and MLN4 are the same as in Fig. 2.5 C. (F) Supernatants were collected after 20 h dox treatment. IL-1β release was quantified by HTRF. Cell death was quantified by detection of LDH release. Values shown for DMSO and MLN4 are the same as in Fig. 2.5 E. Data represents average values (with individual data points) from three independent experiments ± 95 % CI.

These experiments demonstrate that induction of NLRP1 degradation, by viral proteases or targeted ubiquitination, is sufficient for inflammasome activation. In contrast to NLRP1 activation by the RSR and alphaviruses, p38 activity is dispensable for this process. These findings suggest that activation of the MAP kinase is involved in a signaling step upstream of NLRP1 ubiquitination during p38-mediated inflammasome activation.

3.2.5 Strong p38 stimulation is sufficient for NLRP1 activation

So far, I could show that p38 activation, in the context of the RSR and alphavirus infection, is a critical part of a yet unknown signaling pathway upstream of NLRP1 ubiquitination and subsequent inflammasome activation. Importantly, p38 activation is not limited to the RSR, as it can be activated by diverse pathways like TLR (Han et al., 1994; C. Wang et al., 2001), tumor necrosis factor (TNF) (Kant et al., 2011), and EGF signaling (Kozyulina et al., 2013). To test whether other p38-stimulating pathways can induce NLRP1

activation, I treated N/TERT-1$^{C1C\text{-}EGFP}$ cells with the TLR ligands LPS and Pam3CSK4 (Pam3), as well as TNF-α or EGF, and analyzed p38 phosphorylation and ASC speck formation after 4 and 20 h. However, only stimulation with the positive control anisomycin induced a clear p38 phosphorylation signal, which was accompanied by ASC speck assembly in the reporter cells (Fig. 3.11 A,B). This indicates that either the N/TERT-1 cells do not express the relevant receptors to induce p38 activation, or the levels of activation are too low to exceed a threshold necessary for NLRP1 inflammasome formation.
Another way to stimulate p38 activation is the transient overexpression of relevant upstream kinases. I transiently transfected plasmids encoding the FLAG-tagged catalytic domain of TAOK2 (TAOK2 CD), a MAP3K that activates p38 via MKK3 or MKK6 (Canovas & Nebreda, 2021), in HEK$^{NLRP1+ASC}$ and HEK$^{NLRP3+ASC}$ reporter cells (Fig. 3.11 C). TAOK2 CD expression induced a clear phosphorylation of p38, similar to the direct upstream kinase MKK3 (Fig. 3.11 D). TAOK2 CD-induced p38 activity was accompanied by ASC speck assembly in HEK$^{NLRP1+ASC}$ cells (Fig. 3.11 E). The TAOK2 CD-induced inflammasome response was abrogated in the presence of p38 and neddylation inhibitors. However, ZAKα inhibitors had no such effect, indicating that p38 activation by other MAP3K than ZAKα can stimulate NLRP1 in the HEK 293T cell model (Fig. 3.11.F).

These data show that strong p38 activation is sufficient for NLRP1 inflammasome activation, at least in the reconstituted HEK 293T system. Further analyses are required to screen for additional stimuli that might trigger an adequate p38 activation and subsequent NLRP1 inflammasome response in more physiological cell models like keratinocytes.

3.2.6 P38 directly phosphorylates NLRP1 in the N-terminal linker region

All previously described experiments were performed using cells expressing human NLRP1. The human inflammasome sensor substantially differs from murine Nlrp1b alleles which lack the N-terminal PYD and the subsequent linker (Sastalla et al., 2013). To test if the RSR activates both human and murine NLRP1b, I generated polyclonal cell lines expressing HA-tagged human NLRP1 or the different murine Nlrp1b alleles in the

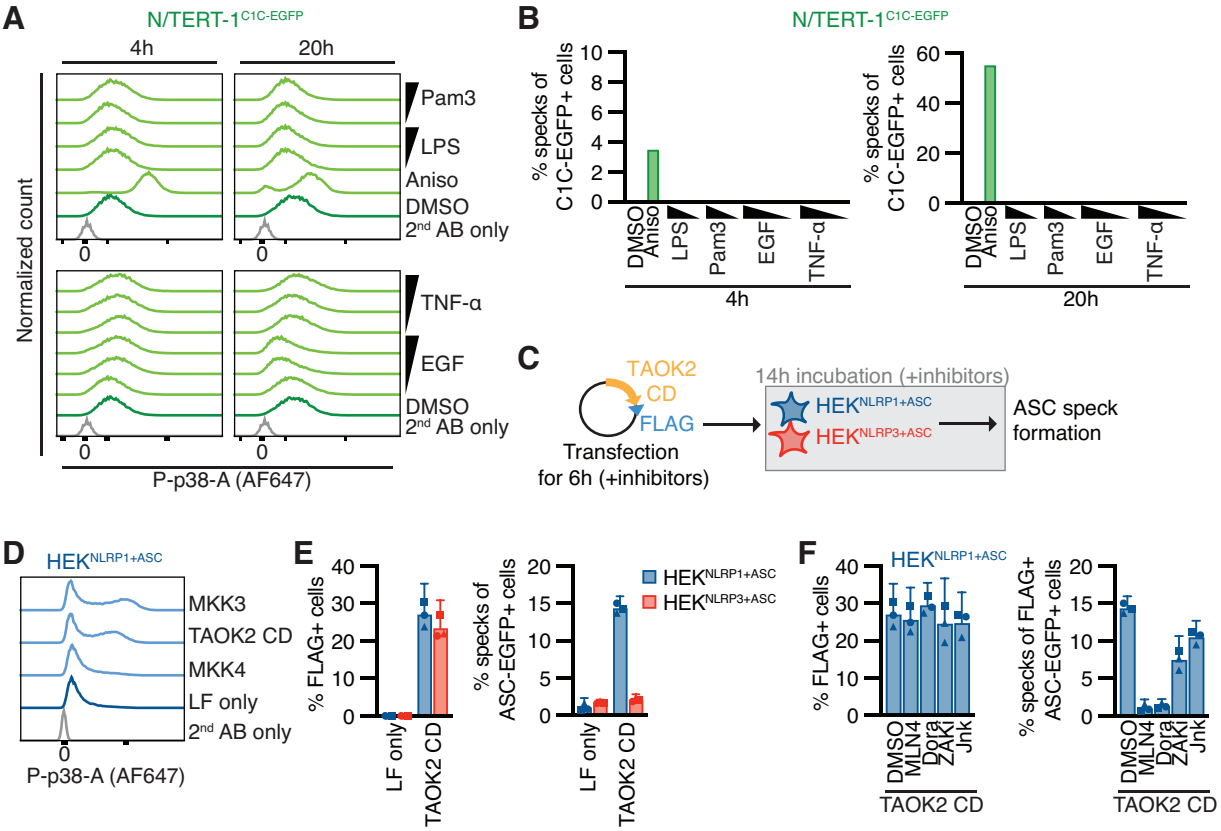

Figure 3.11: Strong P38 activation is sufficient for NLRP1 activation. (**A,B**) N/TERT-1$^{C1C\text{-}EGFP}$ cells were stimulated with 15 µM Aniso, 0.2/1 µg/mL LPS, 0.1/1 µg/mL Pam3CSK4 (Pam3), 10/50/100 ng/mL TNF-α, 0.01/0.1/1 µg/mL EGF, or DMSO for 4/20 h, all in the presence of caspase-1 inhibitor VX. (A) Fixed cells were stained for phosphorylated p38 (P-p38) and analyzed by flow cytometry. (B) ASC speck formation was quantified by flow cytometry, as described in Fig. 2.1. Data represents values from one experiment. (**C**) Schematic overview of the experimental setup. HEK$^{NLRP1+ASC}$ and HEK$^{NLRP3+ASC}$ cells were transiently transfected with expression vectors for FLAG-tagged catalytic domain of TAO kinase 2 (TAOK2 CD) for 6 h, where indicated in the presence of 1 µM MLN4, 10 µM Dora, 1 µM ZAKi, 3 µM Jnk, or DMSO. Lipofectamine (LF) only treated cells served as controls. Cells were further incubated for 14 h. (**D**) Fixed HEK$^{NLRP1+ASC}$ cells were stained for P-p38 and analyzed by flow cytometry, as shown in the representative histograms. Cell transfected with MKK3 and MKK4 served as controls. (**E,F**) FLAG-tagged TAOK2 expression and ASC speck formation were quantified by flow cytometry. Quantification of specks was limited to FLAG-positive cells, except for untransfected controls. Data represents average values (with individual data points) from three independent experiments ± 95 % CI.

background of HEK 293T cells expressing ASC-EGFP (HEK^{ASC}), exploiting that all variants can interact with human ASC (Fig. 3.12 A). Expression of all murine Nlrp1b alleles was verified by immunoblot (Fig. 3.12 B) and functionality was confirmed by treatment with talabostat (Fig. 3.12 C), a common activator of human NLRP1 and murine Nlrp1b. All

variants except for Nlrp1b3 were activated by talabostat treatment and stable expression of Nlrp1b2 led to substantial background activation, as described before (Chavarría-Smith et al., 2016; Gai et al., 2019). Cells expressing human NLRP1 assembled ASC specks in response to anisomycin treatment, while none of the murine alleles initiated ASC specks beyond background levels. Thus, murine Nlrp1b is not activated by the RSR, indicating that the N-terminal PYD and linker of human NLRP1 may determine responsiveness to this mode of activation.

Human NLRP1 activation by targeted ubiquitination of $NLRP1^{PYD}$ did not require p38 activity, and neither did the activation of NLRP1 by talabostat. This indicates that p38 is not required for NLRP1 function per se, but that p38 contributes to an upstream signaling cascade that integrates information from different stress signaling cascades to activate NLRP1. To test whether p38 can directly phosphorylate NLRP1, we performed radiometric *in vitro* kinase assays in collaboration with Ines Kaltheuner and Jonas Moecking from the Institute of Structural Biology in Bonn. The assays were based on recombinant activated p38α and purified full-length NLRP1 expressed in insect cells. We found that active p38α readily phosphorylates NLRP1, as detected by the transfer of radioactive phosphate from [32P]-γ-ATP to purified NLRP1 protein (Fig. 3.12 D). Importantly, a truncated NLRP1 protein lacking the N-terminal PYD and part of the linker, as well as the C-terminal FIIND-CARD, could no longer be phosphorylated by p38α. Combined with the results from the murine Nlrp1b stimulation experiments, it is tempting to speculate that p38 phosphorylates human NLRP1 at the N-terminus, which is why murine Nlrp1b is not responsive to anisomycin.

To evaluate the role of NLRP1 phosphorylation and ubiquitination for activation, I generated polyclonal cell lines expressing HA-tagged wild type or mutant NLRP1 in the background of HEK^{ASC} cells. As anisomycin-responsive human NLRP1 differs from unresponsive murine Nlrp1b primarily in the N-terminal PYD and linker region, I mutated serines, threonines, and lysines in the N-terminus of NLRP1 (Fig. 3.12 E). The preferred amino acid motifs recognized by p38 are SP and TP (J. L. Johnson et al., 2023). Hence, to study the potential direct phosphorylation of NLRP1 by p38, I designed constructs where every serine and threonine followed by proline in the PYD (aa 1-92) and linker region (aa 93-327) of NLRP1 is mutated to alanine (NLRP1 SP-AP TP-AP [PYD + linker]).

In a more unspecific approach, I designed constructs where all serines and threonines in

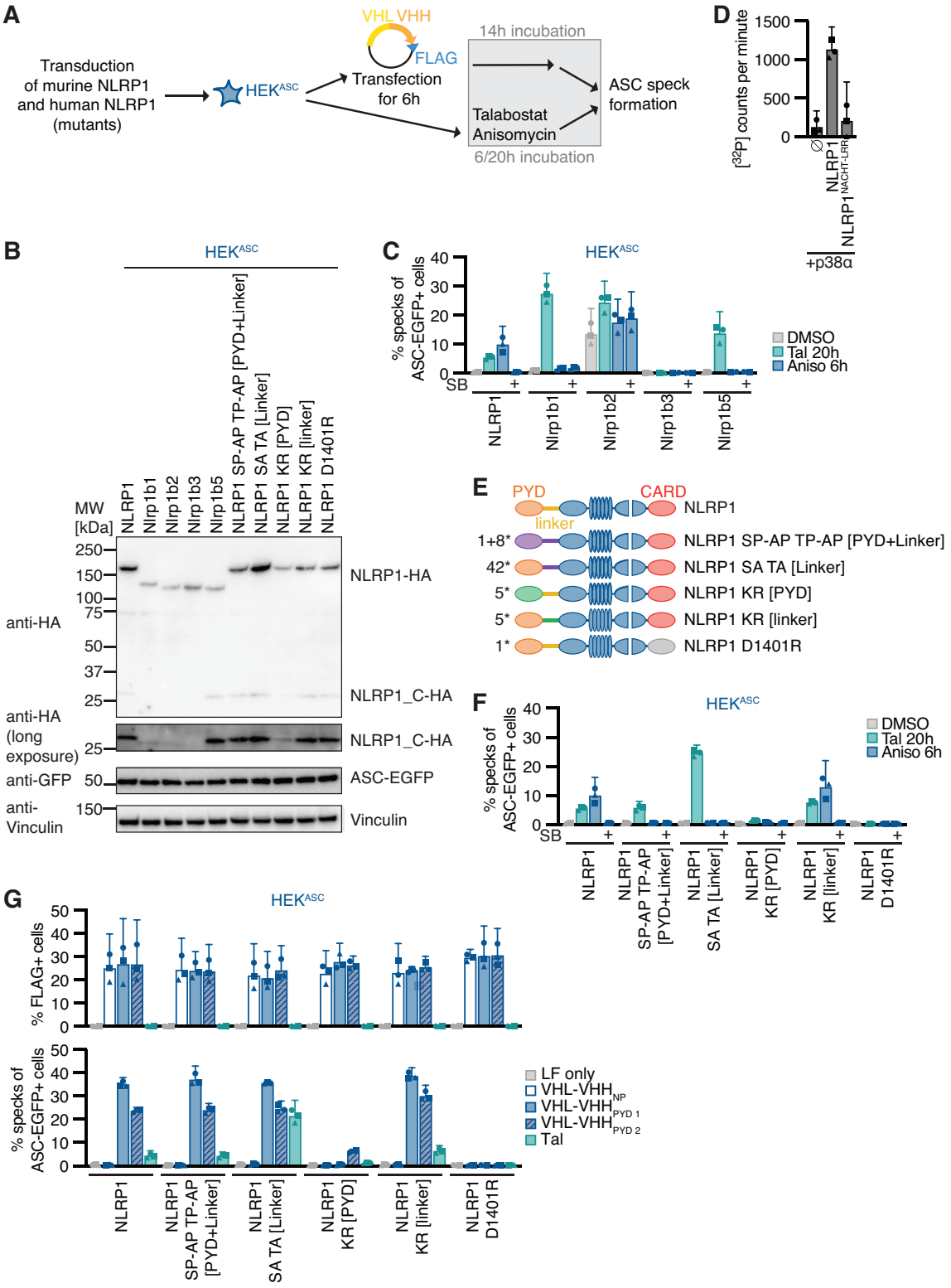

Figure 3.12: Direct phosphorylation of the human NLRP1 linker region by p38 is critical for activation by the ribotoxic stress response. (**A**) Schematic overview of the experimental setup. HEK cells expressing ASC-EGFP (HEK^{ASC}) were transduced with lentiviral vectors encoding murine NLRP1b alleles, human NLRP1 wild type, or human NLRP1 mutants, controlled by a constitutive promoter. Cells were either stimulated with 15 µM Aniso for 6 h, 30 µM Tal, or DMSO for 20 h, where indicated in the presence of 20 µM SB, or transiently transfected with expression vectors for FLAG-tagged VHL-VHH fusions, as described in Fig. 2.4. (**B**) Lysates of generated HEK^{ASC} cell lines expressing the depicted forms of NLRP1 were analyzed by immunoblot with the indicated antibodies to confirm expression of NLRP1-HA and ASC-EGFP. (**C**) ASC speck formation in HEK^{ASC} cells expressing human NLRP1 or murine NLRP1b alleles was quantified by flow cytometry, as described in Fig. 2.1. (**D**) 0.2 µM activated p38α was incubated with 7 µM MBP-NLRP1, MBP-$NLRP1^{NACHT\text{-}LRR}$ (aa 230-990), or no substrate (⃠) at 30 °C for 30 min in kinase buffer containing [^{32}P]-γ-ATP. Protein-associated ^{32}P was quantified by liquid scintillation counting. (**E**) Scheme of generated HEK^{ASC} cell lines expressing human NLRP1 mutants. The number of mutated amino acids in the PYD or linker is indicated to the left of the molecule. (**F,G**) FLAG-tagged VHL-VHH expression and ASC speck formation in HEK^{ASC} cells expressing human NLRP1 wild type or human NLRP1 mutants were quantified by flow cytometry. Quantification of specks was limited to FLAG-positive cells in VHL-VHH-transfected samples. The values for wild type NLRP1 in (F) are the same as in (C) as the experiments were performed in parallel. Data represents average values (with individual data points) from three independent experiments ± 95 % CI. Immunoblot in (B) displays experiment representatives of two independent experiments.

the linker are mutated to alanine (NLRP1 SA TA [linker]). Robust expression of NLRP1 variants was verified by immunoblot (Fig. 3.12 B). Expression of wild type NLRP1 allowed inflammasome activation by talabostat, anisomycin, and transient expression of $VHL\text{-}VHH_{PYD}$ as before (Fig. 3.12 F,G). As a negative control, the oligomerization-incompetent NLRP1 D1401R mutant (Hollingsworth, David, et al., 2021) was not activated by any of these stimuli. HEK^{ASC} cells expressing NLRP1 SP-AP TP-AP [PYD + linker] responded normally to talabostat and ectopic $VHL\text{-}VHH_{PYD}$, but were not activated by anisomycin treatment (Fig. 3.12 F,G). Of note, NLRP1 SA TA [linker] showed greater activation than the other NLRP1 constructs by talabostat, which may be explained by its higher expression (Fig. 3.12 B). Nevertheless, cells expressing NLRP1 SA TA [linker] were not activated by anisomycin either. This suggests that phosphorylation of canonical p38 substrate motifs in the NLRP1 linker is critical for p38-mediated activation of NLRP1, but not for p38-independent activation.

The prior inhibitor experiments indicate that most triggers of NLRP1 inflammasome activation rely on proteasome activity, NEDD8, and the E1 enzyme. I thus generated HEK^{ASC} cell lines expressing NLRP1 with all five lysines in the PYD (NLRP1 KR [PYD]), or all five lysines in the linker region (NLRP1 KR [linker]), mutated to arginine to prevent ubiquitination. I found that mutation of lysines in the PYD abrogated responses to talabostat, anisomycin, and VHL-$VHH_{PYD\ 1}$ transfection (Fig. 3.12 F,G). Of note, NLRP1 KR [PYD] was expressed at a weaker level than the other mutants (Fig. 3.12 B). Yet, the strong VHL-$VHH_{PYD\ 1}$-induced response was completely abolished in these cells, which is unlikely due to weak expression alone. Interestingly, transient expression of VHL-$VHH_{PYD\ 2}$ in NLRP1 KR [PYD] cells still induced a weak inflammasome response. It is possible that binding of VHL-$VHH_{PYD\ 2}$ enables the ubiquitination of lysines in the linker region of NLRP1 KR [PYD]. However, mutation of lysines in the linker did not affect responses at all, indicating that $NLRP1^{PYD}$ is the preferred domain for ubiquitination This suggests that ubiquitination of lysines in the PYD of NLRP1 is crucial for activation by p38-dependent and p38-independent stimuli.

I next set out to identify phosphorylation sites on NLRP1 during activation. $HEK^{NLRP1+ASC}$ cells were treated with anisomycin for 1 h or left untreated, followed by immunoprecipitation of NLRP1-HA with anti-HA antibodies bound to magnetic beads. Captured proteins were directly subjected to digestion with proteases to generate peptides for analysis by mass spectrometry. As the resulting peptides after trypsin cleavage did not represent the linker region of NLRP1 well, we also used chymotrypsin as an alternative protease. In collaboration with Stefan Ebner from the Institute of Innate Immunity in Bonn, we identified at least two amino acids in the linker region that were phosphorylated after anisomycin treatment: serine 107 and threonine 240. Notably, both phosphorylation sites were followed by prolines, suggesting they could be canonical p38 substrates. As the coverage of the linker was incomplete, it is possible that our efforts did not identify all phosphorylation sites in the linker region. We further identified anisomycin-induced phosphorylation sites in the C-terminal regions of NLRP1, including serines 1017, 1022, and 1371, as well as threonine 993. Threonine 993 and serine 1371 were followed by prolines and thus were part of canonical p38 motifs.

To analyze the functional role of identified p38 phosphorylation sites in the NLRP1 linker region, I next generated cell lines expressing HA-tagged NLRP1 S107A and T240A mutants. As controls, I also included NLRP1 mutants altered in the previously identified canonical p38 phosphorylation site T41 in the PYD (Casado et al., 2013), or S1371 in the UPA domain (Fig. 3.13 A). All NLRP1 mutants were expressed to comparable levels (Fig. 3.13 B). All phosphorylation mutants responded normally to talabostat and anisomycin, except NLRP1 S107A. This mutant was unresponsive to anisomycin stimulation and thus resembled the NLRP1 SP-AP TP-AP [PYD + linker] mutant (Fig. 3.13 C). As expected, the S107A mutation did not affect the p38-independent activation of NLRP1 by talabostat or transient expression of VHL-VHH$_{PYD}$ (Fig. 3.13 C,D).

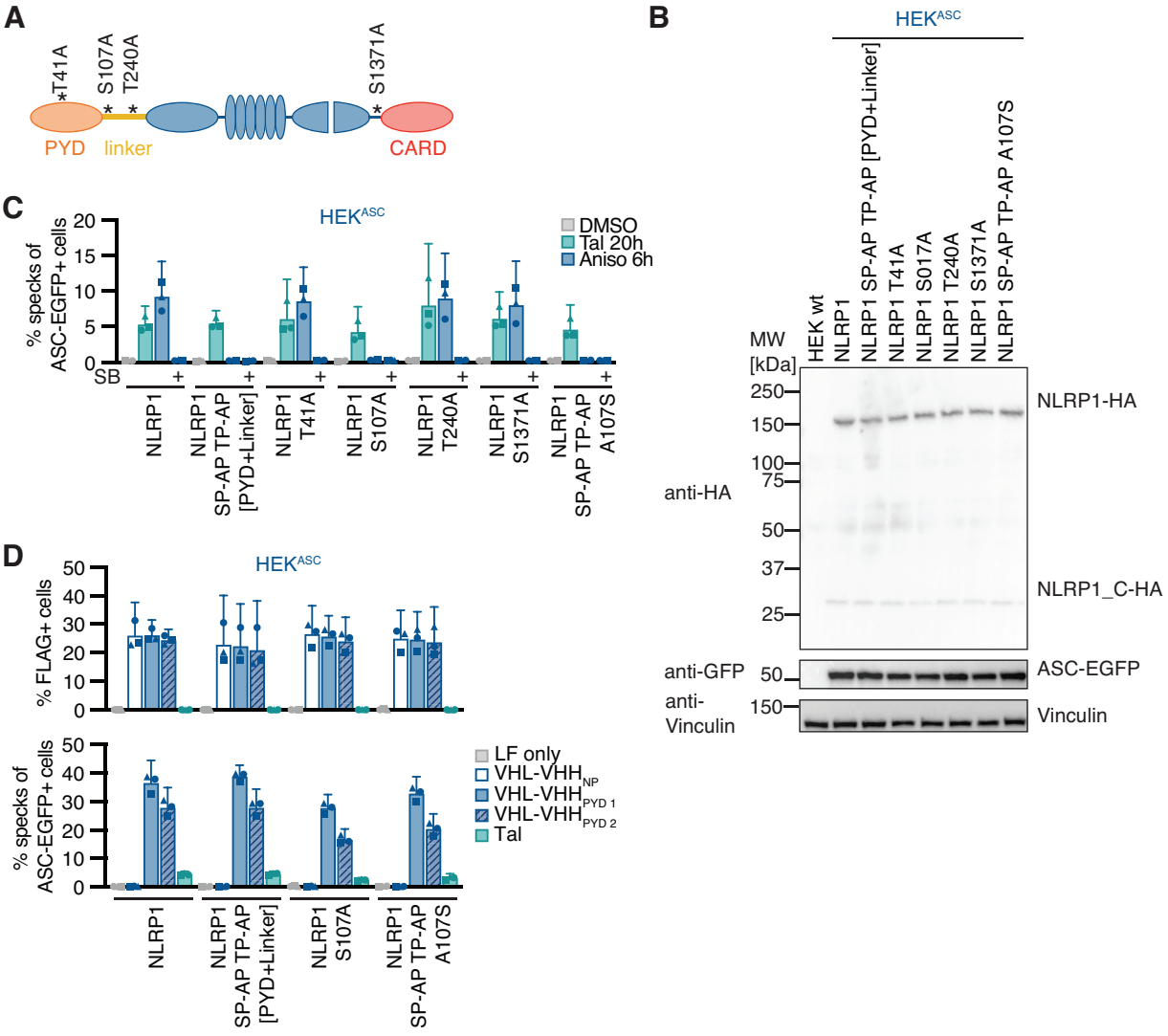

Figure 3.13: Serine 107 in the linker region is critical for p38-dependent NLRP1 activation by the ribotoxic stress response. (**A**) Scheme of NLRP1 phosphorylation sites detected in immunoprecipitated NLRP1-HA after stimulation with 15 μM Aniso for 1 h. (**B**) HEK cells expressing ASC-EGFP (HEK^{ASC}) were transduced with lentiviral vectors encoding human NLRP1 wild type or human NLRP1 phosphorylation mutants controlled by a constitutive promoter. Lysates of generated HEK^{ASC} cell lines expressing the depicted forms of NLRP1 were analyzed by immunoblot with the indicated antibodies to confirm expression of NLRP1-HA and ASC-EGFP. (**C**) HEK^{ASC} cells expressing NLRP1 phosphorylation mutants were stimulated with 15 μM Aniso for 6 h, 30 μM Tal, or DMSO for 20 h, where indicated in the presence of 20 μM SB. ASC speck formation was quantified by flow cytometry, as described in Fig. 2.1. (**D**) HEK^{ASC} cells expressing NLRP1 phosphorylation mutants were transiently transfected with expression vectors for FLAG-tagged VHL-VHH fusions, as described in Fig. 2.4. FLAG-tagged VHL-VHH expression and ASC speck formation were quantified by flow cytometry. Quantification of specks was limited to FLAG-positive cells, except for untransfected controls. Data represents average values (with individual data points) from three independent experiments ± 95 % CI. Immunoblot in (B) displays experiment representatives of two independent experiments.

Thus, phosphorylation of the SP motif at S107 is critical for anisomycin-induced NLRP1 activation.

Next, I tested the rescue mutant NLRP1 SP-AP TP-AP [PYD + linker] A107S, in which only the SP motif containing S107 was restored to wild type. This NLRP1 variant remained inactive following anisomycin stimulation (Fig. 3.13 C), suggesting that S107 is not the only important serine/threonine in the N-terminal linker region. Other serine or threonine residues may either be substrates of p38, or may be required for other functions of NLRP1, such as binding to p38 or ubiquitin ligases.

Due to the lower response rates in the polyclonal NLRP1 HEK cells, I could not determine the role of the SP motif at S107 in SFV-induced NLRP1 activation with this setup. Thus, I reconstituted NLRP1 knockout $N/TERT\text{-}1^{C1C\text{-}EGFP}$ cells with doxycycline-inducible HA-tagged NLRP1, NLRP1 S107A, and NLRP1 KR [PYD], selected polyclonal cell lines (Fig. 3.14 A), and confirmed robust inducible expression of the NLRP1 mutants (Fig. 3.14 B). I stimulated these cells with talabostat, anisomycin, and SFV, in the absence or presence of doxycycline. N/TERT-1 cells reconstituted with wild type NLRP1 responded to all stimuli, and all mutants responded to talabostat treatment with similar levels of inflammasome assembly, despite the somewhat varying expression levels of NLRP1 (Fig. 3.14 C). Cells expressing NLRP1 S107A did not respond to anisomycin and SFV,

confirming that phosphorylation of the SP motif at S107 is critical for the p38-dependent activation of NLRP1 by the RSR and SFV. In line with the universal role of proteasome-dependent N-terminal degradation of NLRP1, cells reconstituted with the lysine mutant

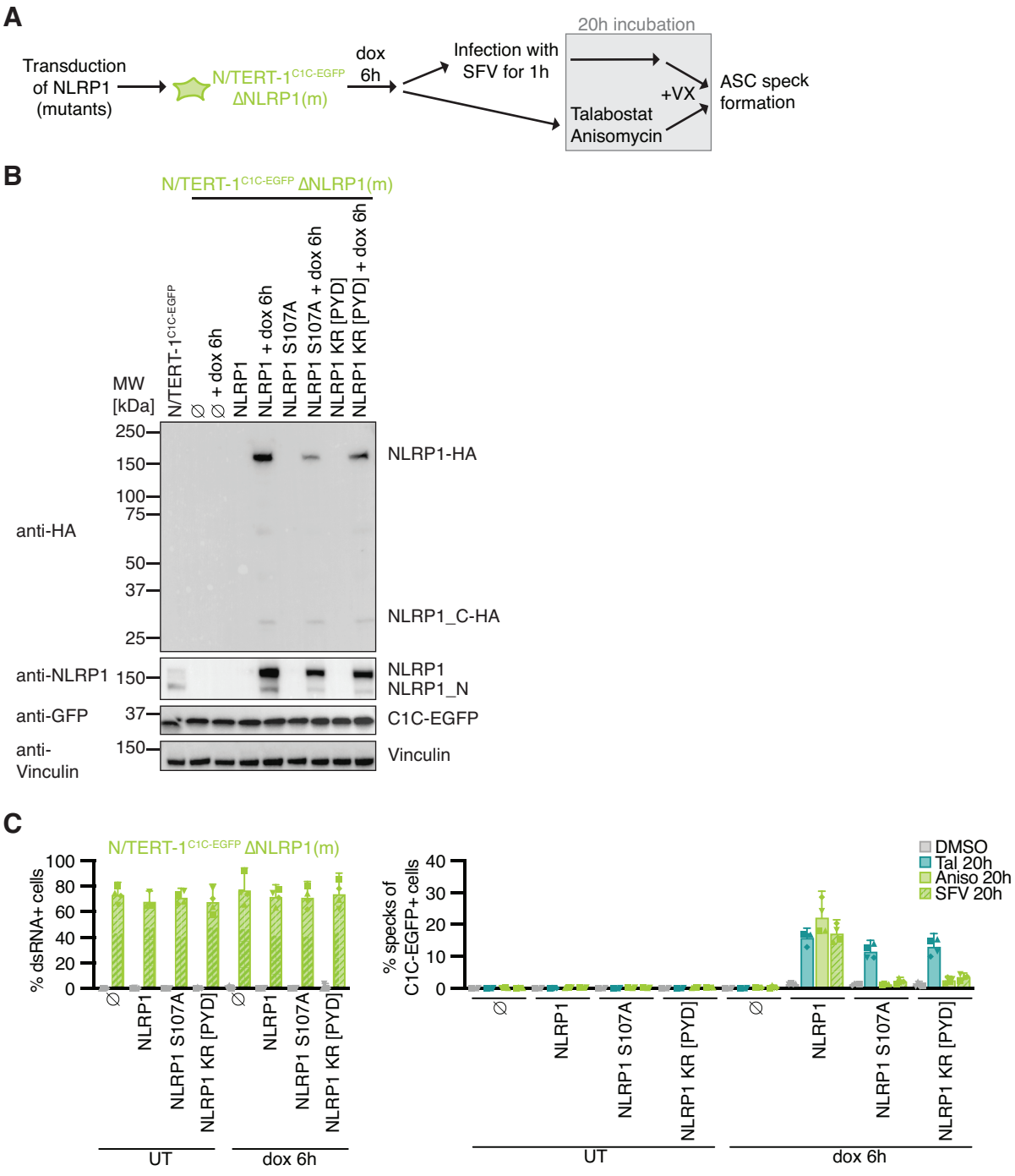

Figure 3.14: Serine 107 in the linker region is critical for p38-dependent NLRP1 activation by alphaviruses. (**A**) Schematic overview of the experimental setup. Monoclonal NLRP1 knockout derivatives of N/TERT$^{C1C\text{-}EGFP}$ cells were reconstituted with lentiviral vectors encoding human wild type NLRP1 or human NLRP1 mutants controlled by a doxycycline (dox)-inducible promoter. Cells were treated with 1 µg/mL dox for 6 h to induce expression. Untreated cells (UT) served as a control. Cells were then either stimulated with 15 µM Aniso, 30 µM Tal, or DMSO for 20 h or were infected with SFV at MOI 5 for 1 h, followed by incubation for 19 h. ASC speck formation was detected in the presence of caspase-1 inhibitor VX. Infection was confirmed by staining of dsRNA. (**B**) Lysates of N/TERT-1$^{C1C\text{-}EGFP}$ ΔNLRP1(m) cell lines reconstituted with NLRP1 mutants were analyzed by immunoblot with the indicated antibodies to confirm dox-inducible expression of NLRP1-HA. (**C**) Infection and ASC speck formation were quantified by flow cytometry, as described in Fig. 2.1. Quantification of specks was limited to infected cells in the SFV samples. Data represents average values (with individual data points) from four independent experiments ± 95 % CI. Immunoblot in (B) displays experiment representatives of two independent experiments.

NLRP1 KR [PYD] were unresponsive to anisomycin and SFV. Interestingly, in N/TERT keratinocytes, NLRP1 lacking lysine residues in the PYD was activated normally by talabostat, in contrast to HEK NLRP1 reporter cells.

In summary, in this section, I show that p38 can directly phosphorylate NLRP1 *in vitro*. Moreover, serine and threonine residues in canonical p38 motifs in the NLRP1 linker region are required for anisomycin-induced NLRP1 activation, with one critical SP motif at S107. This indicates that these residues are phosphorylated by p38 in the course of p38-mediated NLRP1 activation. Moreover, ubiquitination of NLRP1^{PYD} is required for activation of NLRP1 by both anisomycin and SFV. It is well possible that phosphorylation of the NLRP1 linker marks NLRP1 for ubiquitination by yet to be identified E3 ligases.

3.3 Discussion

The ribotoxic stress response activates human NLRP1 inflammasomes

UVB irradiation leads to NLRP1 inflammasome formation in human primary keratinocytes. However, the exact mechanism of NLRP1 activation was not explored (Fenini, Grossi, Contassot, et al., 2018; Sand et al., 2018). Here, I show that UVB-mediated NLRP1 activation depends on the induction of the RSR and the subsequent activation of the MAPK p38. The important role of p38 was also reported by Fenini et al. but they did not

further elucidate this mode of activation (Fenini, Grossi, Gehrke, et al., 2018). I demonstrated that additional stimuli of the RSR, like the antibiotics anisomycin and lactimidomycin, induce a strong NLRP1 inflammasome response in the HEK 293T and N/TERT-1 reporter cells. HEK 293T cells expressing murine Nlrp1b alleles revealed that activation by the RSR is specific for human NLRP1. Robinson et al. reported RSR-dependent human NLRP1 activation as well, confirming my observations of NLRP1 inflammasome formation in N/TERT keratinocytes after UVB and anisomycin stimulation (Robinson et al., 2022).

I used a set of inhibitors to prove the p38 dependency of RSR-mediated NLRP1 activation. In these experiments, inhibition of the MAPK JNK also reduced NLRP1 activation, mostly to a higher degree in N/TERT-1 keratinocytes than in the HEK 293T cells. Fenini et al. observed a reduction of UVB-mediated IL-1β release in JNK-inhibited keratinocytes as well (Fenini, Grossi, Gehrke, et al., 2018). Both MAP kinases are activated during the RSR and both preferentially phosphorylate SP/TP motifs, implying possible redundant activities (J. L. Johnson et al., 2023; Vind, Genzor, et al., 2020). However, JNK inhibition did not impair NLRP1 activation as clearly as p38 inhibition, especially in the HEK$^{NLRP1+ASC}$ reporter cells. Furthermore, NLRP1 responses were blocked to a similar degree in ASC and p38α knockout N/TERT-1 keratinocytes. It was reported that p38 negatively regulates JNK activity (Batlle et al., 2019; Miura et al., 2018; Staples et al., 2010), which implies that JNK might be more active in the presence of p38 inhibitors. These should thus boost any JNK-mediated NLRP1 activation. However, p38 inhibitors completely abrogated NLRP1 inflammasome activation. On the other hand, inhibition of JNK in cancer cell lines reduces p38 phosphorylation, in line with described positive feedback loops between the two MAP kinases (Ozfiliz Kilbas et al., 2020; Yue & López, 2020). Therefore, I conclude that NLRP1 activation depends on RSR-mediated p38 activation, which might be promoted by JNK in our reporter cells. Immunoblot analyses of phosphorylated p38 and JNK in the presence of the different inhibitors and after RSR stimulations, would help to delineate the interplay between the two MAP kinases in the context of NLRP1 activation.

NLRP1 activation by alphavirus infection is also dependent on p38 kinase activity

Bauernfried et al. reported that infection with the alphavirus SFV and transfection of dsRNA longer than 500 bp leads to NLRP1 inflammasome formation in N/TERT

keratinocytes (Bauernfried et al., 2021). I confirmed NLRP1 activation by SFV and dsRNA transfection, and further identified four additional alphaviruses that lead to NLRP1 inflammasome activation, namely SINV, RRV, MAYV, and CHIKV. Surprisingly, alphavirus- and dsRNA-induced NLRP1 activation was also critically dependent on p38 and mostly dependent on ZAKα activation, suggesting that both stimuli cause an RSR-like response. How alphavirus infection and intracellular dsRNA induce this RSR-like response is not clear yet. Infection with SINV (Nakatsue et al., 1998) and CHIKV (Nayak et al., 2019; Varghese et al., 2016) leads to p38 and JNK activation, and p38 activity is further required for successful replication of some viruses including MAYV (Cheng et al., 2020; Sugasti-Salazar et al., 2021). In accordance, MAYV replication was impaired by p38 inhibition in my N/TERT-1 keratinocyte infection assays. How alphaviruses activate p38 and whether this activation requires ZAKα was not explored. In a murine CHIKV infection model, the viral nsP2 protein interacted with phosphorylated p38 and JNK (Nayak et al., 2019). However, direct p38 activation by the virus would not explain why ZAKα inhibitors impair alphavirus-induced NLRP1 activation. The RSR is induced by ZAKα after the detection of ribosome stalling (Vind, Snieckute, et al., 2020) or ribosome collision (Wu et al., 2020). So how could alphavirus infections cause ZAKα activation by ribosome interference?

Alphavirus infection induces the ISR by PKR-mediated detection of dsRNA (Ventoso et al., 2006; White et al., 2011) and PERK-mediated detection of glycoprotein folding in the ER (Fros & Pijlman, 2016). This leads to eIF2α phosphorylation and host translational shutoff. Nevertheless, the viruses are still able to translate their structural proteins encoded by the subgenomic 26S mRNA. Indeed, this mRNA contains a downstream hairpin loop (DHL) close to the start codon and it was speculated that this DHL enables translation initiation in the absence of eIF2α by stalling the ribosome at the site of the start codon (Toribio et al., 2016; Ventoso et al., 2006). DHL-induced ribosome stalling could explain the RSR-like response during alphavirus infection, but I observed no p38 phosphorylation after expression of SFV 26S mRNA in HEK cells in preliminary experiments (data not shown). In line with that, others were not able to confirm DHL-induced translation initiation using artificial loops and start codons (Garcia-Moreno et al., 2015), or *in vitro*-transcribed 26S mRNA, suggesting that eIF2α-independent translation

of structural proteins requires transcription by the viral machinery (Sanz et al., 2007). Moreover, viruses like CHIKV exhibit no DHL at all (Toribio et al., 2016) but I still observe p38-dependent NLRP1 activation.

Additionally to inducing a strong PKR-dependent ISR, alphaviruses cause PKR-independent host translational shutdown via yet unknown mechanisms (White et al., 2011). The nonstructural proteins nsP2 (Gorchakov et al., 2005) and nsP3 (Akhrymuk et al., 2018), as well as excess viral RNA (Patel et al., 2013; Sanz et al., 2015), are proposed mediators of this alternative shutdown of translation. Furthermore, alphavirus mRNA binds to host proteins, causing their redistribution between nucleus and cytosol, and interfering with translation (Barnhart et al., 2013; Carrasco et al., 2018). It is worth speculating that this ISR-independent inhibition of host translation induces interferences in ribosome function, thereby stimulating ZAKα. This could also explain why only old-world alphaviruses stimulated NLRP1 in my experiments. Old- and new-world alphavirus host-modulatory proteins differ in their function during infection. For example, the old-world alphaviruses SFV, SINV, and CHIKV inhibit host transcription by nsP2-mediated degradation of RNA polymerase II subunits (Akhrymuk et al., 2012), whereas the new-world alphavirus VEEV blocks nuclear important using the capsid protein (Atasheva et al., 2010). Thus, differences in the mechanism of host translation inhibition between the two virus groups could explain the difference in NLRP1 stimulation. I tested the possible role of SINV nsP2 in NLRP1 activation by transient overexpression of the viral protein in $HEK^{NLRP1+ASC}$ reporter cells (data not shown). The nsP2 protein is also the viral protease that cleaves the polyprotein after initial translation. It is thus also possible that NLRP1 is activated by nsP2-mediated N-terminal cleavage. Transient expression of SINV nsP2 did not activate NLRP1 in the reporter cells, in line with my observations that p38 activity is not required for NLRP1 activation in the context of targeted or N-degron pathway-mediated degradation. Nevertheless, this overexpression experiment does not exclude the possibility that nsP2 (or another viral protein) interferes with ribosomes and stimulates ZAKα in the presence of additional viral factors that are only present during infection, such as dsRNA.

Another possible factor in alphavirus-induced NLRP1 activation is PKR. As already mentioned, alphavirus infections lead to strong PKR phosphorylation. PKR is required for dsRNA-induced p38 activation in the mouse (Goh et al., 2000). This is not the case for

RSR stimuli like UV irradiation and anisomycin. Goh et al. did not analyze how PKR initiates p38 activity, but PKR is not a MAP3K. I also already mentioned that ZAKα seems to interact with the ISR kinase GCN2 after stimulation with UV or anisomycin. Both kinases bind to ribosomes to detect their respective stimuli (Wu et al., 2020). As PKR binds ribosomes as well, it is tempting to speculate that active PKR stimulates ZAKα at the ribosome (H.-R. Zhou et al., 2014; Zhu et al., 1997). This mechanism would unify alphavirus- and dsRNA-mediated NLRP1 activation downstream of PKR stimulation. It could also explain why alphavirus infection, but not transfection of dsRNA, activates NLRP1 in $HEK^{NLRP1+ASC}$ reporter cells. HEK 293T cells might have impaired PKR signaling, enabling ZAKα activation after alphavirus-mediated PKR phosphorylation, but not after detection of dsRNA alone. One argument against a direct involvement of PKR in NLRP1 activation is the fact that Bauernfried et al. detected no difference in the NLRP1 inflammasome response after dsRNA transfection and SFV infection in PKR knockout keratinocytes (Bauernfried et al., 2021). We further found that some alphaviruses did not induce p38 phosphorylation and NLRP1 activation, even though their dsRNA should always be detected by PKR. However, most alphavirus studies are actually based on old-world alphaviruses, especially SFV and SINV as model viruses, which is why it is difficult to just extrapolate the findings to all other alphaviruses. Detailed analyses of PKR, ZAKα, and p38 phosphorylation for all tested alphaviruses would be necessary to make a clear statement about the role of PKR in alphavirus and dsRNA-induced p38 and NLRP1 activation. The experiments in PKR knockout keratinocytes should be reproduced as well.

Importantly, NLRP1 activation by alphaviruses and dsRNA was mostly but not completely dependent on ZAKα. Both drug-based inhibition and knockout of the MAP3K in N/TERT-1 cells were sufficient to abolish NLRP1 inflammasome formation after ZAKα stimulation with anisomycin, but not after SFV infection and dsRNA transfection. Zhou et al. confirmed ZAKα-independent NLRP1 activation by dsRNA and showed that p38 is still phosphorylated in dsRNA-transfected ZAKα knockout keratinocytes (J. Y. Zhou et al., 2023). Thus, alphavirus infection and intracellular dsRNA induce some form of cellular stress which can be detected by an alternative MAP3K to stimulate p38. CRISPR screens would be a great tool to identify the responsible MAP3K as well as other relevant factors

(like PKR), which may be involved in p38-dependent NLRP1 activation after alphavirus infection or dsRNA transfection.

Binding of (alphavirus) dsRNA to NLRP1^{LRR} was proposed to induce conformational changes of NLRP1, ATP hydrolysis at the NLRP1^{NACHT}, and subsequent inflammasome activation by degradation (Bauernfried et al., 2021). In my experiments, alphavirus-induced NLRP1 activation was indeed inhibited by neddylation inhibitors, implying that NLRP1 is ubiquitinated by CRLs. However, my observations that alphavirus- and dsRNA-induced NLRP1 activation was dependent on p38 activity suggest that direct dsRNA binding to NLRP1 alone is not sufficient for NLRP1 activation. This is also supported by the fact that transfection of dsRNA is not sufficient to activate NLRP1 in HEK 293T reporter cells.

NLRP1^{LRR} seems to negatively regulate NLRP1 activation, as NLRP1ΔLRR mutants are autoactive in reconstituted cell systems (Chavarría-Smith et al., 2016; Liao & Mogridge, 2009) and mutations in NLRP1^{LRR} lead to NLRP1-associated inflammatory diseases (Drutman et al., 2019; M. Li et al., 2023; Zhong et al., 2016). The same is true for the ATPase motifs within NLRP1^{NACHT}, the Walker A/B motifs. Reconstitution of cells with NLRP1 exhibiting inactive Walker A or B motifs leads to autoactivation (Ball et al., 2022; Neiman-Zenevich et al., 2014). Thus, it can be speculated that NLRP1$^{NACHT-LRR}$ keeps NLRP1 in an inhibited state, in a process that requires ATP hydrolysis. Binding of dsRNA to NLRP1^{LRR} might induce conformational changes that facilitate subsequent activation by additional signals. In line with this model, it was reported that oxidized TRX1 negatively regulates NLRP1 by binding to its NACHT-LRR domains. Reductive stress impairs the binding of TRX1, again potentially inducing conformational changes of the inflammasome sensor and causing higher responsiveness to subsequent talabostat stimulation (Ball et al., 2022). Binding of dsRNA to NLRP1^{LRR} did not interfere with TRX1 binding to NLRP1$^{NACHT-LRR}$, suggesting that the two mechanisms are independent. This model raises the question whether RSR-induced NLRP1 activation induces similar conformational changes in NLRP1$^{NACHT-LRR}$ and, if this is the case, how this is accomplished. It is also possible that the observed binding of dsRNA to NLRP1 is just an artifact and not required for inflammasome activation. In fact, dsRNA also binds NLRP6$^{NACHT-LRR}$, implying that this property is not restricted to NLRP1 (Shen et al., 2021).

I showed NLRP1 activation by five different alphaviruses, implying that NLRP1 plays an important role in the detection of alphaviruses. In line with this, CHIKV- and MAYV-infected patients show increased serum IL-1β levels (W. Chen et al., 2017; de Castro-Jorge et al., 2019; Ng et al., 2009) suggesting underlying inflammasome activity. However, in addition to NLRP1, alphaviruses were also reported to activate NLRP3 in infected mice (W. Chen et al., 2017; de Castro-Jorge et al., 2019) and AIM2 in human skin fibroblasts (Ekchariyawat et al., 2015). In addition, since alphaviruses are cytotoxic, inflammasome activation could be due to the release of DAMPs by dying cells, rather than the infection itself. So is there a relevance of NLRP1 as a sensor for the detection of alphaviruses?

Alphaviruses infect humans through mosquito bites. Keratinocytes are thus indeed one of the first cells these viruses encounter upon infection. It was shown that primary and immortalized HaCaT keratinocytes allow no productive infection with CHIKV because of impaired viral RNA synthesis (Bernard et al., 2015). In contrast, in my experiments, CHIKV-infected N/TERT-1 keratinocytes were positive for dsRNA, indicating viral RNA production. Puiprom et al. found productive CHIKV infection of HaCaT keratinocytes as well (Puiprom et al., 2013). MAYV replicated preferentially in skin fibroblasts, but not keratinocytes, in a skin explant infection model, but replication was confirmed by protein and not dsRNA staining (Esterly et al., 2022). I did not detect dsRNA in N/TERT-1 reporter cells infected with ONNV, RRV, and BFV, suggesting that either these viruses use different receptors for cell entry or that viral replication is restricted by the cells. Independent of the different host cell tropism, I detected inflammasome formation after infection with SFV, CHIKV, and MAYV, suggesting that NLRP1 in keratinocytes can help to induce an early immune response after infection. In line with this, patients infected with CHIKV and other old-world alphaviruses are prone to develop skin rashes (Hochedez et al., 2006; Ng et al., 2009; Skidmore & Bradfute, 2023).

As mentioned, alphavirus infections are cytotoxic and alphavirus-infected cells were described to undergo apoptosis at later stages (Levine et al., 1993; Sheahan et al., 1998). This was also reported for CHIKV-infected keratinocytes (Bernard et al., 2015). In line with other reports (Bauernfried et al., 2021) and the low percentage of NLRP1-responsive N/TERT-1 cells after SFV infection, I observed that virus-induced cell death was largely independent of NLRP1 in my experiments. This was similar to the tested RSR stimuli, UVB irradiation and anisomycin, which in the majority of cells triggered apoptosis but not

NLRP1-dependent pyroptosis, as it was previously reported (Y. Liu et al., 2012; X. Wang et al., 2005; Wu et al., 2020). Even if NLRP1 activation does not determine the cell fate, it promotes inflammation through the processing and release of IL-1β, thereby influencing the host response to the pathogen or danger signal.

Strong p38 stimulation is sufficient for NLRP1 activation

In addition to transfection of dsRNA, NLRP1 was in a later study also reported to be activated by transfection of the DNA analog poly(dA:dT) in N/TERT keratinocytes. Interestingly, NLRP1 inflammasome activation was dependent on p38/ZAKα activity and proteasomal degradation, suggesting a similar mechanism to alphavirus infection and dsRNA transfection (J. Y. Zhou et al., 2023). I also observed weak inflammasome activity after poly(dA:dT) transfection in the N/TERT-1 reporter cells but these responses were not inhibited in NLRP1 knockout cells, suggesting activation of a different sensor. The DNA analog poly(dA:dT) is a widely used stimulus of the AIM2 inflammasome (Fernandes-Alnemri et al., 2009; Hornung et al., 2009) and keratinocytes increase expression of this inflammasome sensor after IFN-γ stimulation (Dombrowski et al., 2011; J. Y. Zhou et al., 2023). Hence, the weak inflammasome response in my assays may be based on low baseline expression of AIM2 in the N/TERT-1 cells. In line with this, poly(dA:dT)-induced inflammasome formation was p38- and ZAKα-independent in my experiments. The contradicting observations could be explained by the fact that Zhou et al. used N/TERT-2G cells for their study, which substantially differ from N/TERT-1 cells (Smits et al., 2017). The fact that NLRP1 activation was specific to poly(dA:dT), and not DNA in general, implies that the DNA analog induces particular cellular stress that leads to p38-dependent NLRP1 activation. Zhou et al. propose that poly(dA:dT) induces oxidative nucleic acid damage that activates p38, which is in line with reported p38 stimulation by oxidative stress (Canovas & Nebreda, 2021).

Activation of p38 lies downstream of various cellular stress and inflammatory signals. It is thus tempting to speculate that NLRP1 detects multiple stress stimuli mediated by p38. I did not detect clear p38 phosphorylation in N/TERT-1 cells after stimulation of TLRs, TNF, or EGF receptors, even though these are reported to trigger downstream p38 activation (Goh et al., 2000; Han et al., 1994; Kant et al., 2011; Kozyulina et al., 2013; C. Wang et

al., 2001). Primary keratinocytes express the relevant TLRs, TLR2 and TLR4, and secrete CXCL8 and TNF-α after LPS stimulation (Lebre et al., 2007; Nestle et al., 2009). Human keratinocytes express TNF receptor 1 (Trefzer et al., 1993) and respond to TNF-α stimulation (Smits et al., 2017). N/TERT cells also require EGF to grow (Dickson et al., 2000). This implies that keratinocytes express all relevant receptors. In my experiments, TLR-, TNF-α-, and EGF-induced p38 activation was possibly too weak to be detected by flow cytometry, or the tested time points were suboptimal. As I did not observe NLRP1 activation for any of the tested stimuli, p38 activation was either not strong enough to activate NLRP1 inflammasomes or p38 activation alone is not sufficient. In line with the first hypothesis, p38 activity after TNF-α stimulation was reported to be less pronounced and shorter than after anisomycin or UV stimulation (Miura et al., 2018). Moreover, many studies showed that strong and sustained p38/JNK activation is necessary to induce apoptosis (Staples et al., 2010; Tobiume et al., 2001; Yue & López, 2020). Thus, it is possible that a similar threshold of MAPK activity exists for NLRP1 activation. The fact that p38 activation by transient overexpression of the MAP3K TAOK2 was sufficient to activate NLRP1 in $HEK^{NLRP1+ASC}$ cells, supports the idea that strong p38 activity alone induces inflammasome formation, independent of the upstream stress signals. It would be important to confirm this theory in the endogenous N/TERT-1 keratinocyte system. For this, additional p38 stimuli like IL-1β, osmotic shock, arsenite, and heat shock could be tested (Goh et al., 2000). Alternatively, primary keratinocytes could be used, as they might show stronger stimulation of p38 than N/TERT-1 cells.

On the other hand, VSV infection induced strong p38 phosphorylation, but no inflammasome formation in the HEK 293T system, arguing against the hypothesis that strong p38 activity alone induces NLRP1 activation. It is tempting to speculate that the virus counteracts NLRP1 inflammasome stimulation downstream of p38. To test this, one could analyze whether infection with VSV impairs NLRP1 responses induced by different NLRP1 stimuli in HEK 293T and N/TERT-1 keratinocyte reporter cells.

Another interesting p38 stimulus to be tested is muramyl-dipeptide (MDP). MDP was initially reported to activate NLRP1 (Faustin et al., 2007; L.-C. Hsu et al., 2008) but was then proven to stimulate the NLR sensor NOD2. MDP-mediated NOD2 activation leads to p38 phosphorylation as well (Girardin et al., 2003; Windheim et al., 2007). In addition, mutations in $NOD2^{NBD}$ cause the Blau syndrome which is associated with inflammation of

the skin and eyes (Sfriso et al., 2012), similar to NLRP1-associated inflammatory diseases. Thus, it is tempting to speculate that MDP-mediated NOD2 activation can cause subsequent p38-dependent NLRP1 inflammasome formation.

P38 directly phosphorylates NLRP1 in the N-terminal linker region

I showed that p38-dependent NLRP1 activation by RSR stimuli and alphavirus infection requires direct phosphorylation of NLRP1 by p38. NLRP1 was phosphorylated by p38α *in vitro* and canonical p38 SP/TP motifs in the N-terminal linker region determined the responsiveness of the inflammasome sensor. I identified a critical phosphorylation site at serine 107, which was necessary for SFV- and anisomycin-induced NLRP1 activation. Robinson et al. reported phosphorylation of the N-terminal linker of NLRP1 after RSR stimulation as well, but they proposed that direct phosphorylation by ZAKα was involved as well (Robinson et al., 2022). In contrast to my findings, in their experiments, knockout and inhibition of p38 did not completely abolish RSR-mediated NLRP1 activation. They also identified a critical ZAKα motif (TST, 178-180) in the linker region, which was necessary for NLRP1 activation by anisomycin. I showed that ZAKα is still active in the presence of p38 inhibitors. Thus, in these conditions, ZAKα-mediated NLRP1 phosphorylation should still be possible. However, p38 inhibition completely abrogated NLRP1 activation in my experiments, suggesting that ZAKα alone cannot activate the sensor by phosphorylation. Furthermore, HEK cells expressing the p38 motif mutant NLRP1 SP-AP TP-AP [PYD + linker], which still includes the ZAKα motif, did not respond to anisomycin stimulation. Moreover, alphavirus infection or intracellular dsRNA delivery induced ZAKα-independent and p38-dependent inflammasome assembly. The activation of p38 by transient overexpression of MAP3K TAOK2 was also sufficient to activate NLRP1 in $HEK^{NLRP1+ASC}$ cells. Thus, my observations strongly suggest that direct phosphorylation by p38 is the relevant stimulus for NLRP1 inflammasome activation. The p38 motif mutant of NLRP1, rescued with the critical phosphorylation site at serine 107, was not able to respond to anisomycin. This implies that either the other seven serines and threonines in the linker are involved in phosphorylation-independent functions or additional phosphorylations in the linker region may be important to activate NLRP1. The latter hypothesis is in line with the reported hyperphosphorylation of the NLRP1 N-terminal

linker after RSR stimulation (Robinson et al., 2022). It is also possible that both p38 and ZAKα phosphorylate NLRP1. It will be interesting to test the reported ZAKα motif mutant in my experimental setup, including stimulation with SFV.

I found that phosphorylation sites in the linker were not the only critical residues for NLRP1 activation. Lysine residues in NLRP1^{PYD} were important for anisomycin- and SFV-induced NLRP1 activation. This is in line with abolished NLRP1 inflammasome responses in the presence of neddylation and proteasomal degradation inhibitors. Thus, phosphorylation of the N-terminal linker region leads to ubiquitination of NLRP1^{PYD}, N-terminal degradation, and release of the active NLRP1$^{UPA\text{-}CARD}$ fragment. The N-terminal linker region of NLRP1 shows signs of positive selection in primate genomes and represents a largely unstructured coil (Chavarría-Smith et al., 2016). Phosphorylation modifications are often found in degron sequences. Specific CRL substrate receptors recognize these phospho-degrons and initiate degradation (Bulatov & Ciulli, 2015). In addition, degron sequences are mostly found within disordered regions of proteins, as these are critical initiation sites for proteasomal degradation (Prakash et al., 2004; Timms & Koren, 2020). It can thus be speculated that p38 phosphorylates NLRP1 in the N-terminal linker, creating a phospho-degron that is recognized by certain CRL substrate receptors, as indicated by the neddylation inhibitor experiments. CRLs then induce the ubiquitination of NLRP1^{PYD}, leading to efficient proteasomal degradation in combination with the unstructured linker region. Interestingly, similar regulatory phosphorylation sites were reported for NLRP3 and pyrin inflammasomes (McKee et al., 2021). Another possibility is that phosphorylation of the N-terminal linker interferes with the proposed inter- or intramolecular interaction of the linker region and the UPA-like domain of the FIIND (X. Yang et al., 2022). The ubiquitination of NLRP1^{PYD} could be enabled by the disruption of this interaction and subsequent conformational changes of the sensor. Regardless of the exact mechanism, it is remarkable that lysines in NLRP1^{PYD} but not the linker region are necessary for NLRP1 activation. It was shown that the N-terminal linker alone sensitizes CARD8 to RSR stimuli, without the need for PYD as a potential ubiquitination site (Robinson et al., 2022). However, it was also reported that one lysine in the N-terminal region or the ZU5-like domain of CARD8 is sufficient for talabostat-induced CARD8 activation, indicating that CARD8 can be ubiquitinated at multiple sites and is probably less restricted than NLRP1

(Chui et al., 2020). Hence, NLRP1^{PYD} and the linker might form a regulated system that allows N-terminal degradation of NLRP1 after p38-dependent phosphorylation. Identification of the CRL ligase complex that ubiquitinates NLRP1 after RSR stimulation and alphavirus infection will help to elucidate such a potential regulatory system. Ubiquitination could also be mediated by different substrate receptors and CRLs. CRISPR screens will be helpful tools to find the responsible factors. As already discussed in chapter 2, mass spectrometry would further help identify the exact positions of ubiquitination sites within NLRP1^{PYD} (Akimov et al., 2018).

N-terminal degradation of NLRP1 after inhibition of DPP8/9

When NLRP1$^{UPA\text{-}CARD}$ and CARD8$^{UPA\text{-}CARD}$ were shown to be sequestered by DPP8/9, it was assumed that both inflammasome sensors undergo spontaneous degradation during cell homeostasis to release free UPA-CARD fragments (Hollingsworth, Sharif, et al., 2021). It was later reported that talabostat not only interferes with DPP8/9 complexes but also induces further N-terminal degradation of both sensors (Orth-He et al., 2023; Q. Wang et al., 2023). This is in line with observations that activation of CARD8 (D. C. Johnson et al., 2018) and Nlrp1b (Okondo et al., 2018) by talabostat still required functional proteasomal degradation. Importantly, both observations were based on experiments with cells that endogenously express the respective sensors. Similarly, I found that talabostat-induced NLRP1 activation in N/TERT-1 cells was inhibited in the presence of neddylation inhibitors, which was also reported by others (Robinson et al., 2022). In contrast, neddylation inhibitors did not interfere with talabostat-induced NLRP1 activation in the HEK 293T reporter cells. This suggests that CRLs are responsible for the release of active NLRP1$^{UPA\text{-}CARD}$ fragments in keratinocytes, which then accumulate upon DPP8/9 inhibition. As HEK$^{NLRP1+ASC}$ cells exhibit a higher and probably less controlled NLRP1 expression, they might already generate higher levels of NLRP1$^{UPA\text{-}CARD}$ fragments during cell homeostasis. Following talabostat treatment, this would induce NLRP1 inflammasome activation without the need for further NLRP1 degradation. Furthermore, the HEK$^{NLRP1+ASC}$ cells were selected for a high NLRP1 response to talabostat which may further minimize the requirement for degradation.

Together these observations raise the following questions:

1) Which CRL components induce degradation of NLRP1 during cell homeostasis and after inhibition of DPP8/9? For CARD8, it was proposed that talabostat treatment leads to the degradation of proteins that present N-terminal disordered regions, including CARD8 (Chui et al., 2020). A follow-up study reported that CARD8 is degraded by 20S proteasomes independent of ubiquitination after talabostat stimulation (Hsiao et al., 2022), contradicting an earlier observation that one lysine is necessary for talabostat-induced CARD8 activation (Chui et al., 2020). Talabostat might indeed induce increased degradation of NLRP1 via a mechanism that differs from degradation during homeostasis. CRISPR screens and knockout experiments could answer this question. Experiments should be performed in endogenous systems, as overexpression of the sensor apparently alters homeostatic regulations.

2) Where is NLRP1 ubiquitinated in these processes? I could show that lysines in $NLRP1^{PYD}$ are necessary for activation after RSR stimuli and alphavirus infection. However, overexpression of NLRP1 KR [PYD] mutants in N/TERT-1 cells allowed unchanged stimulation by talabostat. This would mean that ubiquitination of other lysines of NLRP1 is sufficient for talabostat-induced degradation. Another option would be non-canonical ubiquitination of $NLRP1^{PYD}$ at cysteines, serines, threonines, or the N-terminus (Kelsall, 2022). This option is rather unlikely since canonical ubiquitination of lysines was critical for p38-dependent NLRP1 activation and linear ubiquitinations of N-termini are mostly associated with non-proteolytic processes (Tracz & Bialek, 2021). Similar to the reports about CARD8, NLRP1 KR [PYD] could be degraded by 20S proteasomes without the requirement of ubiquitination. The N-terminal linker region could provide the necessary disordered region (Ben-Nissan & Sharon, 2014). The NLRP1 KR [PYD] mutant in HEK 293T cells did not respond to talabostat, but this NLRP1 mutant showed impaired processing which was reported to directly correlate with talabostat responses (Chui et al., 2020). After all, reconstitution of NLRP1 knockout keratinocytes with NLRP1 KR [PYD] may disrupt endogenous regulations. Hence, lysines in $NLRP1^{PYD}$ expressed at endogenous levels might still get ubiquitinated in wild type cells after talabostat treatment. Mass spectrometry is a sensitive method that would allow to analyze ubiquitination of endogenous NLRP1 during cell homeostasis and talabostat treatment.

In summary, I showed that different stimuli of the RSR activate human NLRP1 in a p38-dependent manner. Similarly, SFV infection and transfection of dsRNA induced RSR-like responses that led to NLRP1 inflammasome formation. Thus, I defined the mechanism upstream of dsRNA-mediated NLRP1 stimulation, even though the involved components causing (ZAKα-dependent) p38 activation still await identification. I also determined four additional alphaviruses, namely SINV, CHIKV, MAYV, and RRV, which activate NLRP1 in a p38-dependent manner. Furthermore, p38 directly phosphorylates the N-terminal linker region of NLRP1, causing ubiquitination of $NLRP1^{PYD}$, N-terminal degradation, and inflammasome assembly. Serine 107 represents a critical phosphorylation site but additional phosphorylations of canonical p38 motifs may be required for activation of the inflammasome. The potential contribution of ZAKα in linker phosphorylation requires further analyses. It is also unclear under which circumstances p38 activates NLRP1 and where and how NLRP1 is ubiquitinated before and during stimulation.

3.4 Material and Methods

Cells

Cell culture

HEK 293T and N/TERT-1 keratinocytes were cultivated as described in chapter 2. Syrian baby hamster kidney (BHK)-21 cell clone BSR-T7/5 (*Mesocricetus auratus*, a kind gift of SeanWhelan, Harvard Medical School) were cultivated in DMEM containing 10 % FBS and GlutaMax. BHK-21/J cells (*Mesocricetus auratus*, a kind gift of Charles M. Rice, Rockefeller University) were cultivated in Minimum Essential medium (MEM) containing 7.5 % FBS, 1 % nonessential amino acids, and 1 % L-glutamine (all Thermo Fisher Scientific).

Generation of genetically modified cell lines

All genetically modified cell lines were generated as described in chapter 2. Generation and cultivation of $HEK^{NLRP1+ASC}$, $HEK^{NLRP3+ASC}$, $N/TERT\text{-}1^{C1C\text{-}EGFP}$, $N/TERT\text{-}1^{C1C\text{-}EGFP}$ ΔNLRP1 (m), $N/TERT\text{-}1^{C1C\text{-}EGFP}$ ΔASC (m), and $N/TERT\text{-}1^{(VHL\text{-})VHH+C1C\text{-}EGFP}$, were already described in chapter 2. Similarly, derivatives of HEK^{ASC} expressing wild type (cell line H151) and mutant human NLRP1 (cells lines H156-H160, H162-H164, H166, H172), as

well as murine Nlrp1b alleles (H152-H155), under the control of pUbC were generated by lentiviral transduction with virus MOIs that permit multiple insertions and selection in the presence of 1 µg/mL puromycin and 50 µg/mL hygromycin B. Lentiviral vectors for knockout generation were constructed as described in chapter 2 (see Table 3 for sgRNA target sequences). ASC (cell line K17), p38α (cell lines K23, K24), p38β (cell lines K27, K28), ZAKα (cell lines K63-K65), and TAOK2 (cell lines K66-K68) knockout derivatives of N/TERT-1$^{C1C\text{-}EGFP}$ cells were generated by lentiviral transduction with virus MOIs that permit multiple insertions and selection with 5 µg/mL blasticidin S (ASC, p38) or 500 µg/mL geneticin (ZAKα, TAOK2). All knockouts were verified by immunoblot. Reconstitution of monoclonal NLRP1 knockout N/TERT-1 keratinocytes with wild type (cell line K100) or mutant NLRP1 (cell lines K101, K102) was achieved by transduction with lentiviral vectors based on pInducer20 (Meerbrey et al., 2011), with virus MOIs that permit multiple insertions and selection with 500 µg/mL geneticin.

Target gene	sgRNA name	Target sequence
ASC	ASC sg5	GCTGGATGCTCTGTACGGGA
P38α	P38α sg1 (KO 1)	TGATGAAATGACAGGCTACG
P38α	P38α sg2 (KO 2)	CACAAAAACGGGGTTACGTG
P38β	P38β sg2 (KO 1)	GCTTCTGGACGTCTTCACGC
P38β	P38β sg3 (KO 2)	GGTGGATGATCCCGGCCGAG
ZAKα	ZAKα sg1	TGTATGGTTATGGAACCGAG
ZAKα	ZAKα sg2	GTGACAATGCCATAGTTGGG
ZAKα	ZAKα sg3	TCCTACACAACAAGGCGGAG
TAOK2	TAOK2 sg1	TCAAGACAGACCAACCTCAG
TAOK2	TAOK2 sg2	CCCAACACCATTCAGTACCG
TAOK2	TAOK2 sg3	GCACTGAGTGGCTACTCTCG

Table 3: sgRNA target sequences used for the generation of polyclonal ASC, p38, ZAKα, and TAOK2 knockout N/TERT-1 cell lines.

Viruses

Lentivirus production

Lentiviruses were produced as described in chapter 2.

Virus production for infection assays

All experiments involving viruses were conducted in respective Biosafety Level 2 or 3 laboratories. SFV 4 (a kind gift of Giuseppe Balistreri and Ari Helenius, ETH Zurich), SINV strain Toto 1101 (recovered from *in vitro* transcribed RNA (Rice et al., 1987)), and VSV strain Indiana (recovered from plasmid as described in (Whelan et al., 1995)) were amplified in BSR-T7 cells. EEEV, VEEV, MAYV, ONNV, BFV, and RRV (kindly provided by Klaus Grywna (Grywna et al., 2010)) were amplified in BHK-J cells. CHIKV was derived from an infectious cDNA clone as described earlier (Kümmerer et al., 2012). Virus-containing supernatants clarified from cell debris were aliquoted and frozen at -80 °C. Viral titers of SFV, SINV, and VSV were determined in BSR-T7 cells by flow cytometry using anti-dsRNA antibody J2 (Schonborn et al., 1991) or anti-VSV G I14 (clone 1E9F9, (Lefrancois & Lyles, 1982)) combined with fluorescent secondary antibodies. Viral titers of EEEV, VEEV, MAYV, ONNV, BFV, RRV, and CHIKV were determined by plaque assay using BHK-J cells (Karliuk et al., 2021).

Proteins

Expression and purification of active p38α

Human p38α-His, as well as untagged constitutively active human MKK3 S218E S222E, were cloned into pET-Duet by Gibson cloning. Proteins were expressed in *E. coli* LOBSTR (Andersen et al., 2013) cells in Terrific Broth induced with 0.2 mM IPTG at an OD600 of 0.6. Cells were cultivated for 24 h at 18 °C, and lysed by French Press. MKK3-activated p38α-His was purified by Ni-NTA affinity chromatography and gel filtration with a HiLoad 16/600 Superdex 75 pg column in buffers containing 50 mM HEPES pH 7.5, 150 mM NaCl, 0.5 mM Tris(2-carboxyethyl)phosphine (TCEP).

Expression and purification of MBP-NLRP1

Full-length human NLRP1 (aa 1-1473) and NLRP1$^{NACHT\text{-}LRR}$ (aa 230-990) constructs were expressed as N-terminal maltose-binding protein (MBP) fusion proteins in baculovirus-infected *Spodoptera frugiperda* (Sf9) insect cells. For expression, 0.5 L of Sf9 cells at a density of $2.0 \cdot 10^6$ cells/mL were infected with 5 % P2 virus and incubated at 28 °C for 48 h. Cells were lysed by sonication in buffer A (50 mM HEPES pH 7.5, 150 mM NaCl, 0.5 mM TCEP), freshly supplemented with 1 mM phenylmethylsulfonyl fluoride. Proteins

in the clarified lysate were affinity purified using an MBPTrap HP (GE Healthcare) affinity column and eluted in buffer A supplemented with 10 mM maltose.

Antibodies

The following antibodies were used: rabbit polyclonal anti-ASC (AdipoGen Cat# AG-25B-0006, RRID:AB_2490440), mouse anti-Caspase-1 clone Bally-1 (Apidogen Cat# AG-20B-0048, RRID:AB_2490257), rabbit anti-caspase-3 clone D3R6Y (Cell Signaling Technology Cat# 14220, RRID:AB_2798429), rabbit anti-FLAG clone D6W5B (Cell Signaling Technology Cat# 14793, RRID:AB_2572291), mouse anti-GAPDH clone 0411 (Santa Cruz, Cat# sc-47724, RRID:AB_627678), mouse anti-GFP clone JL-8 (Takara Bio Cat# 632380, RRID:AB_10013427), mouse anti-HA-HRP clone 6E2 (Cell Signaling Technology Cat# 2999S, RRID:AB_1264166), mouse anti-IL-1β clone 3A6 (Cell Signaling Technology Cat# 12242, RRID:AB_2715503), rabbit polyclonal anti-MKK3b (Cell Signaling Technology Cat# 9238, RRID:AB_2140797), rabbit anti-phospho-MKK3 (Ser189)/ MKK6 (Ser207) clone 22A8 (Cell Signaling Technology Cat# 9236, RRID:AB_491009), mouse anti-NLRP1 clone 9F9B12 (BioLegend Cat# 679802, RRID:AB_2566263), rabbit polyclonal anti-p38 (Cell Signaling Technology Cat# 9212, RRID:AB_330713), rabbit anti-phospho-p38 (T180/Y182) clone D3F9 (Cell Signaling Technology Cat# 4511, RRID:AB_2139682), rabbit anti-PARP clone 46D11 (Cell Signaling Technology Cat# 9532, RRID:AB_659884), mouse anti-dsRNA clone J2 (SCICONS Cat# 10010200, RRID:AB_2651015), mouse anti-vinculin clone hVIN-1 (Sigma-Aldrich Cat# V9131, RRID:AB_477629), mouse anti-VSV G I14 clone 1E9F9 (from D.S. Lyles, kindly provided by Ari Helenius), rabbit polyclonal anti-ZAK (Bethyl laboratories Cat# A301-993A, RRID:AB_1576612), goat polyclonal anti-rabbit IgG (H+L)-Alexa Flour™ Plus 647 (Invitrogen Cat#A32733, RRID:AB_2633282), goat polyclonal anti-mouse IgG (H+L)-Alexa Flour™ Plus 647 (Invitrogen Cat#A32728, RRID:AB_2633277), goat polyclonal anti-mouse IgG (H+L)-DyLight™ 405 (Invitrogen Cat#35500BID, RRID:AB_2533208), goat polyclonal anti-rabbit IgG (H+L)-HRP (Invitrogen Cat#31460, RRID:AB_228341), goat polyclonal anti-mouse IgG (H+L)-HRP (Invitrogen Cat#31430, RRID:AB_228307)

Small compound inhibitors and reagents

The following small compound inhibitors and reagents were used: anisomycin (Sigma-Aldrich), bafilomycin A1 (Sigma-Aldrich), bestatin methyl ester (Abcam), bortezomib (Selleckchem), deoxyribonucleic acid sodium salt from herring testes (Sigma-Aldrich), doramapimod (Cayman), doxycycline (Thermo Fisher Scientific), EGF (Thermo Fisher Scientific), ISRIB (Selleckchem), JNK-IN-8 (Selleckchem), lactimidomycin (Sigma-Aldrich), LPS-EK Ultrapure (Invivogen), MG-132 (Selleckchem), MLN4924 (MedChem Express), MLN7243 (ChemieTek), Nigericin sodium salt (Biomol), Pam3CSK4 (Invivogen), PF-3644022 (Sigma-Aldrich), poly(dA:dT) (Invivogen), poly(I:C) LMW and HMW (Invivogen), SB202190 (Sigma-Aldrich), talabostat mesylate (MedChemExpress), TNF-α (Immunotools), Vx-765 (Selleckchem), Z-VAD(Ome)-FMK (MedChemExpress), and ZAKα inhibitor 6p (J. Yang et al., 2020), was kindly provided by IFM Therapeutics.

Flow cytometry-based quantification of inflammasome assembly

The experimental procedures to quantify the assembly of ASC-EGFP or C1C-EGFP specks by flow cytometry were already described in chapter 2. Similarly, $2.5 \cdot 10^5$ (24 well-plate)/$1.25 \cdot 10^5$ (48 well-plate) $HEK^{NLRP1+ASC}$ (or other derivatives of HEK 293T), or $1 \cdot 10^5$ (24 well-plate)/$0.5\text{-}1 \cdot 10^5$ (48 well-plate) N/TERT-$1^{C1C\text{-}EGFP}$ (or other derivatives of N/TERT-1) cells were seeded per well and cultivated overnight in the absence of antibiotics. For UVB stimulation experiments cells were partially seeded in 12 well-plates ($5 \cdot 10^5$ HEK 293T cells or $2 \cdot 10^5$ N/TERT-1 cells per well) to increase the coverage of UVB irradiation.

For drug-induced inflammasome stimulation, cells were generally treated with 15 µM anisomycin, 2 µM lactimidomycin, 200 ng/mL LPS followed by 10 µM nigericin, or 30 µM talabostat. Cells treated with the solvent DMSO only served as controls.

For UVB-induced inflammasome stimulation, cells were irradiated in tissue culture plates (without lid) in a Bio-Link UVB irradiation system equipped with 5x 8 Watt T-8.M tubes emitting UVB at 312 nm for 3 min, followed by cultivation for 20 h.

For nucleic acid-induced inflammasome stimulation, cells were transfected with 1 µg/mL poly(I:C), poly(dA:dT), or HT-DNA using Lipofectamine 2000 (Thermo Fisher Scientific). Medium was replaced with full medium after 6 h, and cells were cultivated for another 14 h. Cells treated with Lipofectamine 2000 only served as controls.

For virus-induced inflammasome stimulation, cells were infected for 1 h in serum-free medium (0.2 % BSA, 20 mM HEPES in DMEM) at the indicated MOI, ranging from 1-50. Medium was subsequently replaced with full medium and cells were cultivated for another 19 h. Cells treated with infection medium only served as mock controls.

For inflammasome stimulation by transient overexpression of FLAG-tagged HRV14 3C protease, VHL-VHH fusions, MAP2K MKK3/4, or the catalytic domain of MAP3K TAOK2 in HEK-based reporter cells, cells in 24-wells were transfected with 500 ng total of expression vectors based on pCAGGS (Hitoshi et al., 1991) (HRV14 3C and VHL-VHH fusions) or Gateway-compatible derivatives of pcDNA3.1 (kinases) using Lipofectamine 2000. Medium was replaced with full medium after 6 h and cells were cultivated for another 14 h. Cells treated with Lipofectamine 2000 only served as controls.

For induction of doxycycline-inducible expression in lentivirus-generated cell lines, cells were cultivated in medium containing 1 µg/mL doxycycline for 6 or 20 h. For p38 stimulation, cells were treated with 0.2/1 µg/mL LPS, 0.1/1 µg/mL Pam3CSK4, 10/50/100 ng/mL TNF-α, or 0.01/0.1/1 µg/mL EGF for 4 or 20 h.

In case of additional inhibitor treatments, small compound inhibitors were added 30 min before and during the stimulation, with the following concentrations: 100 nM bafilomycin A1, 20 µM bestatin methyl ester, 1 µM bortezomib, 10 µM doramapimod, 200 nM ISRIB, 3 µM Jnk-In-8, 1 µM MG-132, 1 µM MLN4924, 1 µM MLN7243, 1 µM PF3644022, 20 µM SB202190, 100 µM Vx-765, 50 µM Z-VAD(Ome)-FMK or 100 nM (N/TERT-1 cells)/ 1 µM (HEK 293T cells) ZAKα inhibitor 6p. In the case of virus infection experiments, inhibitors were only added after 1 h infection, except for Bafilomycin A1 which was added before, during, and after infection. In the case of stimulation by transient overexpression of FLAG-tagged VHL-VHH fusions, inhibitors were only added with the medium change after 6 h transfection.

Stimulated cells were harvested and analyzed by flow cytometry as described in chapter 2. Where indicated, fixed and permeabilized cells were stained with anti-FLAG (1:300), anti-phospho-p38 (1:500), anti-dsRNA (1:500), or anti-VSV G (1:1,000) in Intracellular Staining Permeabilization Wash Buffer (Biolegend) combined with DyLight™ 405- or Alexa Flour™ Plus 647-coupled, highly cross-absorbed secondary antibodies (1:500). For the quantification of specks after virus infection or transient

transfection, only cells positive for dsRNA/VSV G, or FLAG were included in the analysis (with the exception of mock-infected or untreated controls).

Cytokine quantification by HTRF

To quantify IL-1β release, N/TERT-1-derived cells were seeded (10^5 cells in 300 µL per 48 well-plate) and stimulated as described for flow cytometry experiments in the absence and presence of Vx-765. Supernatants for the quantification of IL-1β levels after inducible expression of VHL-VHH fusions were collected from $5 \cdot 10^4$ cells in 200 µL per well in 96 well-plates. Supernatants for the quantification of IL-1β levels after infection with SFV, SINV, and VSV were collected from $5 \cdot 10^4$ cells in 250 µL per well in 48 well-plates. IL-1β was quantified as described in chapter 2.

Cell death quantification by LDH release

The same cell supernatants as for the IL-1β quantification were used to quantify cell death by pyroptosis. Release of lactate dehydrogenase (LDH) was quantified as described in chapter 2.

Cell death quantification by DRAQ7 uptake

To quantify cell death over time, the uptake of the non-cell permeable DNA dye DRAQ7 was analyzed as described in chapter 2.

Microscopy

Microscopy samples were generated as described in chapter 2.

Immunoblot

To confirm expression or knockout of proteins in cell lines, 10^6 cells were lysed in 200 µL 1x SDS-PAGE buffer (50 mM Tris pH 6.8; 0.01 % Bromophenol blue, 10 % glycerol, 2 % SDS, 100 mM DTT) to generate immunoblot samples. To confirm the doxycycline-inducible reconstitution of NLRP1 in N/TERT-$1^{C1C\text{-}EGFP}$ ΔNLRP1 (m) cells, $8 \cdot 10^5$ cells per well were seeded in 6 well-plates, followed by doxycycline stimulation for 6 h and lysis in 150 µL 1x SDS-PAGE buffer the next day. The same setup was used to analyze the phosphorylation of p38 and MKK3 in N/TERT-$1^{C1C\text{-}EGFP}$ cells after 0.5 h anisomycin or 20 h

talabostat stimulation in the presence of ZAKα and p38 inhibitors. To analyze p38 phosphorylation in HEK 293T and keratinocyte reporter cells after UVB and anisomycin stimulation, $1.5 \cdot 10^6$ HEK cells and $6 \cdot 10^5$ N/TERT-1 cells per well were seeded in 6 well-plates, followed by stimulation and lysis in 500 µL 1x SDS-PAGE buffer the next day. To analyze the processing of caspase-1, caspase-3, PARP, and IL-1β, N/TERT-1$^{C1C\text{-}EGFP}$ cells were seeded into 10 cm dishes and grown until they were around 70 % confluent. The inflammasome stimulations were performed in 6 mL medium. After stimulation, the cells were lysed in 400 µL 1x SDS-PAGE buffer to generate lysate immunoblot samples. The supernatant was harvested, clarified by centrifugation, and released proteins were precipitated using methanol and chloroform (Jakobs et al., 2013). Precipitated protein was resuspended in 50 µL 2x SDS-PAGE buffer to generate supernatant immunoblot samples. Immunoblots were performed as described in chapter 2, except for immunoblots of MKK3 and P-MKK3 which were detected on nitrocellulose membranes (0.45 µm, GVS). Membranes were probed with the following primary antibody dilutions: anti-ASC 1:1000, anti-caspase-1 1:1000, anti-caspase-3 1:500, anti-GAPDH 1:2000, anti-GFP 1:1000, anti-HA-HRP 1:1000, anti-IL-1β 1:1000, anti-MKK3 1:1000, anti-P-MKK3 1:1000, anti-NLRP1 1:1000, anti-p38 1:1000, anti-P-p38 1:1000, anti-PARP 1:500, anti-vinculin 1:1000, and anti-ZAK 1:1000. All primary antibodies were added in 5 % NFDM solution, except anti-IL-1β, anti-MKK3, anti-P-MKK3, anti-p38, and anti-P-p38 which were added in TBS-T (TBS with 0.05 % Tween-20) containing 3 % BSA. Chemiluminescent signal was induced by Western Lightning Plus-ECL (Perkin Elmer), except for immunoblots of ASC, Caspase-1, Caspase-3, IL-1β, MKK3, P-MKK3, NLRP1, PARP and ZAKα which required Western Lightning Ultra-ECL (Perkin Elmer).

In vitro kinase assay

For *in vitro* kinase assays, 0.2 µM kinase was incubated with 7 µM substrate and 0.2 mM ATP containing 0.45 mCi [32P]-γ-ATP/mL (Perkin Elmer) in kinase buffer (50 mM HEPES pH 7.6, 34 mM KCl, 7 mM MgCl2, 2.5 mM DTT, 5 mM β-glycerol phosphate). Reactions were incubated for 30 min at 30 °C and 300 rpm, and stopped by addition of EDTA to a final concentration of 50 mM. Samples were spotted onto Amersham Protran nitrocellulose membrane (GE Healthcare), followed by three washing steps for 5 min each

with PBS. Counts per minute were determined in a Beckman Liquid Scintillation Counter (Beckman-Coulter) for 1 min.

Identification of phosphorylation sites by mass spectrometry

To reveal phosphorylation sites on NLRP1, HEK$^{NLRP1+ASC}$ cells in 15 cm dishes (3 dishes per IP) were stimulated with or without 15 µM anisomycin for 1 h. Cells were lysed in low salt lysis buffer (1 % IGEPAL CA-630, 50 mM Tris pH 7.5, 150 mM NaCl, 1 mM EDTA) supplemented with HALT protease and phosphatase inhibitor cocktail (Thermo Fisher Scientific). After sedimentation of nuclei and debris, lysates were supplemented with NaCl to reach a final concentration of 500 mM. 50 µL Pierce magnetic anti-HA beads (Thermo Fisher Scientific) were subsequently incubated with the lysates to immunoprecipitate NLRP1-HA. Beads were washed 5 times with high salt lysis buffer (1 % IGEPAL CA-630, 50 mM Tris pH 7.5, 500 mM NaCl, 1 mM EDTA), once with detergent-free wash buffer (50 mM Tris pH 7.5, 500 mM NaCl, 1 mM EDTA), and twice with 50 mM Tris. Proteins were then denatured in 6 M Urea, 50 mM Tris pH 8.0 for 20 min on ice. Samples were reduced with 10 mM TCEP, alkylated with 40 mM chloroacetamide, and digested on beads with 1 µg trypsin and Lys-C (Promega) or chymotrypsin (Sigma-Aldrich) overnight. Peptides were desalted with SDB-RPS stage tips and resolubilized in buffer A (0.1 % formic acid) before loading onto 50-cm columns packed in-house with C18 1.9 µm ReproSil particles (Dr. Maisch GmbH), with an EASY-nLC 1200 system (Thermo Fisher Scientific) coupled to the Orbitrap Exploris 480 (Thermo Fisher Scientific). Temperature was maintained at 50 °C and peptides were eluted with a 70-min gradient starting at 5 % buffer B (80 % ACN, 0.1 % formic acid), followed by a stepwise increase to 30 % in 55 min, 65 % in 5 min, 95 % in 5 min, and maintained at 95 % for 5 min, at a flow rate of 300 nL/min. A data-dependent (TopN) acquisition MS method was used for proteome analysis in which one full scan (300–1650 m/z, R = 60000, ACG target 300 %) was first performed, followed by 10 data-dependent MS/MS scans with higher-energy collisional dissociation (ACG target 100 %, maximum injection time at 28 ms, isolation window 1.4 m/z, HCD collision energy 30 %, R=15000). Dynamic exclusion of 30 s was enabled. Data was acquired with the Xcalibur software (Thermo Fisher Scientific) and MS raw files were processed with MaxQuant version 2.0.3. Fragment lists were searched against the human UniProt FASTA database (November 2021) with cysteine carbamidomethylation

as a fixed modification and N-terminal acetylation, and serine/threonine/tyrosine phosphorylation and methionine oxidations as variable modifications. False-discovery rate was set to less than 1 % at the peptide and protein levels and a minimum ratio count of 1 was required for valid quantification events using MaxQuant's LFQ algorithm (MaxLFQ). All bioinformatics analyses were done with Perseus (version 1.6.15.0). Data were filtered for common contaminants and hits to the reverse data database. For phosphosite analysis, the localization probability cutoff was set to 0.75.

Statistical analyses

Statistical analyses were performed as described in chapter 2.

4. Simian rotavirus activates the human NLRP1 inflammasome by NSP1-induced degradation

4.1 Introduction

In this chapter, I will use the HEK 293T NLRP1 reporter cells to identify rotaviruses as another group of viruses that activate NLRP1 inflammasomes with a novel mechanism.
Rotaviruses (RV) belong to the family of Reoviridae and form triple-layered virions with a viral genome consisting of 11 dsRNA segments. Rotaviruses cause acute and often severe gastroenteritis, leading to life-threatening diseases in children younger than five years. These viruses are transmitted by the fecal-oral route and other mammals, including livestock, cats, dogs, and rodents, can be infected as well. Rotaviruses are classified into species (currently RVA-RVJ) based on the antigenicity of the middle layer protein VP6. Out of these species, RVA is responsible for most human infections (Caddy et al., 2021; Desselberger, 2014; Omatola & Olaniran, 2022; Sadiq et al., 2018). Furthermore, the genotypes of all 11 segments are defined based on distinct sequence identity cutoffs and by now specified for established and newly discovered virus strains (Matthijnssens, Ciarlet, Heiman, et al., 2008; Matthijnssens, Ciarlet, Rahman, et al., 2008).
Triple-layered rotavirus particles (TLPs) infect enterocytes at the top of small intestine villi and enteroendocrine cells. The outer layer contains trimers of VP7 and the spike protein VP4. VP4 is processed by trypsin-like proteases in the intestine into VP5 and VP8. Rotaviruses bind sialoglycans or histo-blood antigens to enter host cells by endocytosis. Low Ca^{2+} levels induce the removal of the outer layer and the release of double-layered particles (DLPs) into the cytosol. In addition to the genome segments, the inner VP2 layer contains the viral RNA-polymerase VP1 and the capping enzyme VP3. These two proteins form transcription complexes inside the DLPs that release capped mRNA through channels in the particles. Released mRNAs are translated by the host machinery and serve as templates for new genome segments later during infection (Arias & López, 2021; Desselberger, 2014; Omatola & Olaniran, 2022). Production of viral protein and RNA leads to the formation of protein-RNA condensates, the so-called viroplasm, in which replication of viral RNA and packaging of new DLPs takes place. Importantly, new dsRNA genomes are only synthesized in intermediate capsid assemblies (Geiger et al., 2021; Papa et al., 2021). Newly formed DLPs are transiently enveloped in the ER, enabling the

formation of VP4- and VP7-containing TLPs. The envelope is lost after TLP formation and the new virions are released by cell lysis or non-classical transport mechanisms (Caddy et al., 2021).

Rotaviruses antagonize host immune responses with the help of the non-structural protein NSP1. NSP1 has the highest sequence variability of all rotavirus proteins and is classified into at least 15 genotypes (A1-A15) based on a 79 % sequence identity cutoff (M. M. Arnold & Patton, 2011; Matthijnssens, Ciarlet, Heiman, et al., 2008; Matthijnssens et al., 2011). NSP1 induces the degradation of interferon regulatory factor (IRF) 3/5/7 or NF-κB regulator β-transducin repeats-containing protein (β-TrCP), thereby inhibiting expression of IFN or NF-κB -induced genes in infected cells (M. M. Arnold & Patton, 2011; Barro & Patton, 2007; Graff et al., 2009). β-TrCP is an F-box protein serving as a substrate receptor for CRL1 complexes and mediates the degradation of NF-κB inhibitor IκB after its phosphorylation by IκB kinases (Bulatov & Ciulli, 2015; Graff et al., 2009). NSP1 exhibits an N-terminal zinc-binding domain that is similar to the RING domain of E3 ligases, although a potential ubiquitin ligase activity of NSP1 has not been demonstrated so far (M. M. Arnold, 2016; Graff et al., 2007, 2009). Instead, NSP1 proteins seem to recruit CRL1/2/3 complexes to induce degradation of target proteins which are bound with the C-terminal target-binding domain (M. M. Arnold, 2016; S. Ding et al., 2016; Lutz et al., 2016). In the case of β-TrCP, NSP1 seems to mimic the phospho-degron of IκB to recruit the NF-κB regulator (K. A. Davis et al., 2017).

4.2 Results

Contributions

The experiments to quantify ASC speck formation in Fig. 4.1 C/D were performed by rotation student Laura Klein under my supervision. Part of the rotavirus SA11-4F stocks, as well as Alexa Flour™ 647-coupled anti-VP6 nanobodies, were generated by Florian Gohr. Both were members of the Institute of Innate Immunity (Florian Schmidt Lab) in Bonn when the experiments were performed. The recombinant rotavirus SA11-4F strains were generated by Lee Sherry, then member of the Department of Biochemistry (Alex Borodavka lab) in Cambridge. All other experiments and further analyses of the provided data were performed by myself.

4.2.1 Simian rotaviruses activate NLRP1 inflammasomes in a p38-independent manner

In the course of my experiments to analyze alphavirus-induced NLRP1 activation, I also screened other relevant viruses for potential NLRP1 inflammasome activation. One of the candidates was the simian RVA strain SA11-4F. As rotaviruses encode a segmented dsRNA-genome, accumulation of these segments in the cytosol might stimulate NLRP1, even though the genome is mostly concealed in viral particles (Papa et al., 2021). Accordingly, staining of infected cells with dsRNA antibodies yielded no signal beyond the background. Therefore, infection was quantified by staining VP6 proteins, which coat virus DLPs in the cell, using a fluorescently labeled nanobody (Garaicoechea et al., 2008). I was able to infect HEK 293T inflammasome reporter cells with RVA SA11-4F, but not N/TERT-1 cells (Fig. 4.1 A). Adequate infection levels in $HEK^{NLRP1+ASC}$ and $HEK^{NLRP3+ASC}$ cells also required MOIs up to 100, based on titration of virus stocks on MA-104 cells which are commonly used to produce and titer rotavirus stocks (Fig. 4.1 B). Interestingly, I observed a strong inflammasome response in infected $HEK^{NLRP1+ASC}$ cells with nearly 80 % of infected cells forming ASC specks 20 h post-infection. This response rate was therefore as high as after transient expression of VHL-VHH_{PYD} constructs, which was the strongest NLRP1 stimulus in $HEK^{NLRP1+ASC}$ cells observed so far (see chapter 2). Moreover, ASC speck formation was unchanged in the presence of p38α/β inhibitor SB202190 (SB), indicating a different mode of NLRP1 activation by rotaviruses compared to infection with alphaviruses.

To further define the cellular activities required for NLRP1 activation after rotavirus infection, I quantified inflammasome responses in $HEK^{NLRP1+ASC}$ cells in the presence of p38 inhibitors SB202190 and doramapimod (Dora), neddylation inhibitor MLN4924 (MLN4) and JNK kinases inhibitor (Jnk), which all inhibited NLRP1 activation by the RSR and alphaviruses to some extend (see chapter 3). As RVA SA11-4F induced a robust inflammasome formation already 6 h post-infection, I could analyze the role of proteasomal degradation using the more toxic E1 enzyme inhibitor MLN7243 (MLN7), as well as proteasome inhibitors MG-132 and bortezomib (Borte) (Fig. 4.1 C). NLRP1 activation by rotavirus infection was consistently shut down by all inhibitors of the ubiquitin-

proteasome pathway, whereas inhibition of p38 and JNK kinases had no influence (Fig. 4.1 C,D). In the previous chapter, I described HEK^{ASC} cells expressing NLRP1

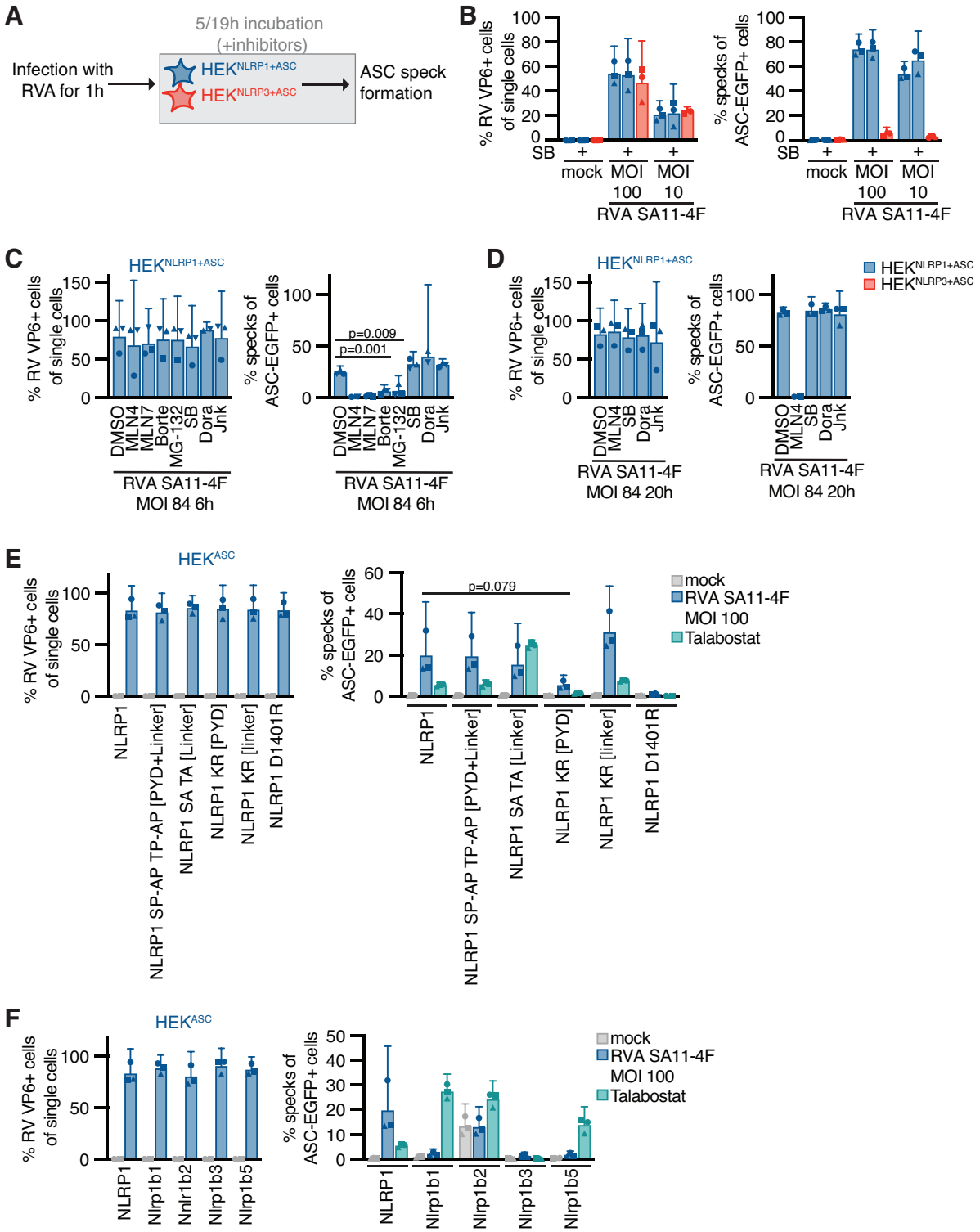

Figure 4.1: Simian rotavirus SA11-4F activates human NLRP1 in a p38-independent manner. (**A**) Schematic overview of the experimental setup. $HEK^{NLRP1+ASC}$ and $HEK^{NLRP3+ASC}$ cells were infected with rotavirus species A (RVA) SA11-4F at MOI 10-100 for 1 h. Cells were further incubated for 5 or 19 h, where indicated in the presence of 20 µM SB, 1 µM MLN4, 1 µM MLN7, 1 µM Borte, 1 µM MG-132, 10 µM Dora, 3 µM Jnk, or DMSO. Infection was confirmed by staining of RVA VP6 protein. Quantification of specks was limited to infected cells, with exception of uninfected controls. (**B-D**) Infection and ASC speck formation in $HEK^{NLRP1+ASC}$ and $HEK^{NLRP3+ASC}$ cells were quantified by flow cytometry, as described in Fig. 2.1. (**E,F**) Infection and ASC speck formation in HEK^{ASC} cells expressing human NLRP1, human NLRP1 mutants, or murine NLRP1b alleles, as described in Fig. 3.12, were quantified by flow cytometry. Cell stimulated with 30 µM Tal served as controls. Values shown for Tal are the same as in Fig. 3.12 C,F. The values for wild type NLRP1 in (E) are the same as in (F) as the experiments were performed in parallel. Data represents average values (with individual data points) from two (Dora in C) or three independent experiments ± 95 % CI, p-values were calculated using unpaired t-test.

mutants that cannot be phosphorylated by p38 in SP/TP motifs of the linker region (NLRP1 SP-AP TP-AP [PYD + linker] and NLRP1 SA TA [linker]), as well as NLRP1 mutants that cannot be ubiquitinated at lysines in the PYD (NLRP1 KR [PYD]) or the linker region (NLRP1 KR [linker]). RVA SA11-4F-infected HEK^{ASC} cells expressing NLRP1 SP-AP TP-AP [PYD + linker] and NLRP1 SA TA [linker] responded similarly to HEK^{ASC} cells expressing wild type NLRP1, confirming that phosphorylation by p38 is not necessary for inflammasome assembly (Fig. 4.1 E). In line with the proteasomal degradation inhibitor experiments, HEK^{ASC} cells expressing NLRP1 KR [PYD], but not NLRP1 KR [linker], showed reduced inflammasome assembly after rotavirus infection, even though NLRP1 activation was not completely blocked. As a control, expression of the NLRP1 D1401R mutant, which cannot oligomerize $NLRP1^{CARD}$, fully abrogated the response. Overall, the NLRP1 activation by RVA SA11-4F resembled either activation by DPP8/9 inhibitor talabostat or by VHL-VHH_{PYD}-mediated degradation, which were also independent of p38 phosphorylation but required ubiquitination of $NLRP1^{PYD}$ in the HEK cell system. If rotavirus infection releases DPP9-sequestered $NLRP1^{UPA\text{-}CARD}$ similarly to talabostat, the virus should also be able to activate murine Nlrp1b alleles expressed in the HEK^{ASC} system. I have already shown that murine Nlrp1b alleles 1,2, and 5 assembled inflammasomes in HEK^{ASC} cells after talabostat treatment (Fig. 4.1 F). When infected with RVA SA11-4F, HEK^{ASC} cells expressing murine Nlrp1b allele 1,2, and 5 showed no increased ASC speck formation compared to mock-infected cells. This shows that murine

Nlrp1b is not activated by rotaviruses, indicating that the mechanism of activation is different from talabostat-mediated release of DPP9-sequestered NLRP1$^{UPA-CARD}$, but rather requires properties that are specific for human NLRP1.

Next, I infected HEK 293T inflammasome reporter cells with RVA RRV, another simian RVA strain obtained from Sarah Londrigan (University of Melbourne). In a preliminary experiment, HEK$^{NLRP1+ASC}$ cells were similarly infected by RVA SA11-4F and RVA RRV (Fig. 4.2 A). Likewise, both viruses induced strong ASC speck assembly in more than 70 % of the infected cells (Fig. 4.2 B). To further characterize the NLRP1 response after

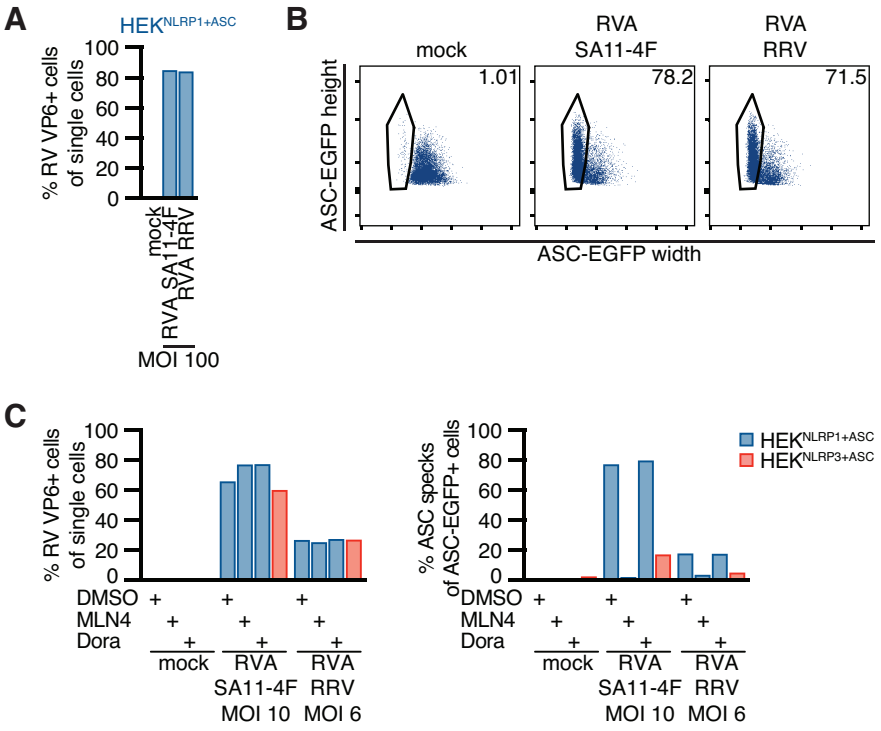

Figure 4.2: Rhesus rotavirus RRV activates NLRP1 in a p38-independent manner. HEK$^{NLRP1+ASC}$ cells were infected with RVA SA11-4F or RVA RRV at MOI 100 for 1 h. Cells were further incubated for 19 h. (**A**) Infection was confirmed by staining of RVA VP6 protein and quantified by flow cytometry. (**B**) ASC speck formation was quantified by flow cytometry, as shown in the dot plots. Quantification of specks was limited to infected cells, with exception of uninfected controls. (**C**) HEK$^{NLRP1+ASC}$ and HEK$^{NLRP3+ASC}$ cells were infected with RVA SA11-4F at MOI 10 or RVA RRV at MOI 6 for 1 h, where indicated in the presence of 1 µM MLN4, 10 µM Dora, or DMSO. Cells were further incubated for 19 h. Infection and ASC speck formation were quantified by flow cytometry. Quantification of specks was limited to infected cells, with exception of uninfected controls. Data represents values from one experiment

RVA RRV infection, I needed to amplify this rotavirus strain to perform more experiments. Unfortunately, I only achieved RVA RRV stocks with a low titer in preliminary attempts, allowing a maximal MOI of 6 in the HEK reporter cells. This new stock infected around 20 % of $HEK^{NLRP1+ASC}$ and $HEK^{NLRP3+ASC}$ cells, while infection rates with RVA SA11-4F, using only a slightly higher MOI, were three times higher (Fig. 4.2 C). The poor quality of the RVA RRV stock probably interfered with successful infection and replication of the virus in the HEK reporter cells. Nevertheless, I still observed a clearly detectable formation of ASC specks in $HEK^{NLRP1+ASC}$ cells, but not $HEK^{NLRP3+ASC}$ cells, after infection with RVA RRV, confirming that the response is NLRP1-specific. The neddylation inhibitor MLN4924, but not p38 inhibitor doramapimod, blocked RVA RRV-induced inflammasome activation, indicating that RVA RRV stimulates NLRP1 in a similar manner to RVA SA11-4F. The RVA RRV-induced inflammasome response was weak compared to the experiment using the original stock, suggesting that successful infection and virus replication are necessary for NLRP1 activation by rotaviruses.

In summary, I show that two simian RVA strains activate human NLRP1 in a p38-independent manner. Instead, activation by RVA SA11-4F requires ubiquitination of $NLRP1^{PYD}$ and proteasomal degradation, and it is specific for human NLRP1. Since human and mouse sensors mostly differ at the N-terminus, and rotavirus-induced activation of NLRP1 resembles that of VHL-VHH_{PYD}, it is tempting to speculate that rotavirus infection is specifically recognized by the N-terminus of human NLRP1, followed by subsequent degradation and inflammasome activation.

4.2.2 Rotavirus SA11-4F NSP1 is necessary and sufficient to activate NLRP1 inflammasomes

Since NLRP1 activation by rotaviruses resembled activation by VHL-VHH_{PYD}-mediated targeted ubiquitination, I wondered how the virus could induce the N-terminal degradation of the inflammasome sensor. I was especially intrigued by RVA non-structural protein NSP1, a known interferon antagonist that mediates the degradation of interferon pathway-relevant molecules like IRF3 (Barro & Patton, 2007), and the NF-κB regulator β-TrCP (Graff et al., 2009). More importantly, NSP1 was reported to act as a substrate adaptor for CRLs (S. Ding et al., 2016; Lutz et al., 2016) and NLRP1 activation by rotaviruses was

sensitive to inhibitors of neddylation, suggesting that CRLs are critical for inflammasome assembly. Therefore, I speculated that RVA NSP1 might bind NLRP1, thereby causing its degradation and activation. To test this, I generated expression vectors for FLAG-tagged RVA NSP1 and transiently transfected these constructs in $HEK^{NLRP1+ASC}$ and $HEK^{NLRP3+ASC}$ reporter cells (Fig. 4.3 A). I decided to test NSP1 proteins from SA11-4F and RRV, as well as from RVA strains that represent the different NSP1 genotypes, as NSP1 exhibits the highest sequence variability amongst all rotavirus proteins (M. M. Arnold & Patton, 2011)(Fig. 4.3 B). I also included NSP1 from RVA SA11-5S which represents a truncated form of RVA SA11-4F NSP1, lacking 17 amino acids at the C-terminal target-binding domain, and which is no longer able to induce degradation of IRF3 (M. M. Arnold & Patton, 2011; Barro & Patton, 2007). As positive controls, I transiently transfected plasmids encoding FLAG-tagged HRV14 3C protease, which activates NLRP1 by N-terminal cleavage, as well as the catalytic domain of TAOK2 (TAOK2 CD), which activates the inflammasome by stimulating p38, as established in chapter 3.

All RVA NSP1 proteins were expressed in varying levels in the HEK 293T inflammasome reporter cells (Fig. 4.3 C,D). Expression of RVA SA11-4F and RVA SA11-5S NSP1 was indeed sufficient to induce inflammasome assembly in $HEK^{NLRP1+ASC}$ cells, but not $HEK^{NLRP3+ASC}$ cells. Thus, NLRP1 activation by RVA SA11-4F might be solely dependent on the expression of the viral host antagonist NSP1. Activation by the truncated form of NSP1 was only slightly diminished compared to the full-length form, suggesting that the deletion of 17 amino acids is not sufficient to interfere with NPS1-mediated NLRP1 stimulation. None of the other tested RVA NSP1 proteins induced NLRP1 inflammasome assembly, including RVA RRV NSP1. Either the rhesus rotavirus NSP1 requires additional factors only present during infection, or it activates NLRP1 in an NSP1-independent manner. As the modes of NLRP1 activation were very similar for the two simian rotaviruses, the first hypothesis is more likely, but further experiments have to be performed to decipher NLRP1 activation by RVA RRV.

Around 60 % of all cells expressing RVA SA11-4F NSP1 responded with inflammasome formation, similar to cells overexpressing HRV14 3C. The difference in activation levels between RVA SA11-4F infection and NSP1 expression might be due to higher abundance of viral proteins or the presence of supporting factors during infection. In line with the prior infection experiments and the fact that NSP1 acts as a substrate receptor for CRLs, RVA

SA11 NSP1-induced ASC speck assembly was blocked in the presence of neddylation inhibitor MLN4924, but not p38 inhibitor doramapimod (Fig. 4.3 E). In contrast, TAOK2 CD-induced activation was completely abolished in the presence of both inhibitors, as shown before.

To confirm the functionality of the transiently expressed NSP1 proteins, I analyzed the reported degradation of IRF3 and β-TrCP using immunoblots (Fig. 4.3 F). As a control, cells were treated with MLN4924 to block NSP1-mediated degradation of host proteins.

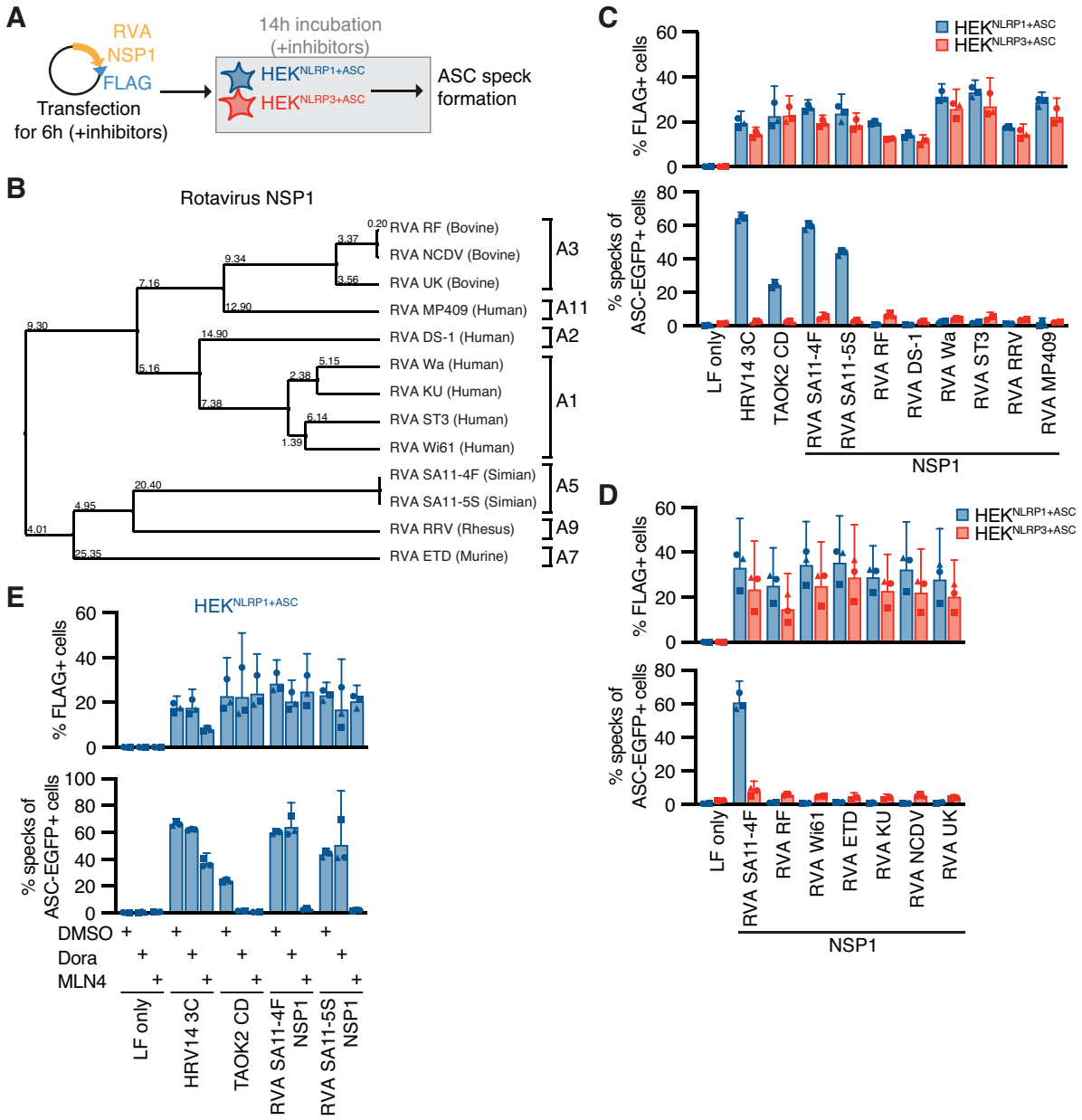

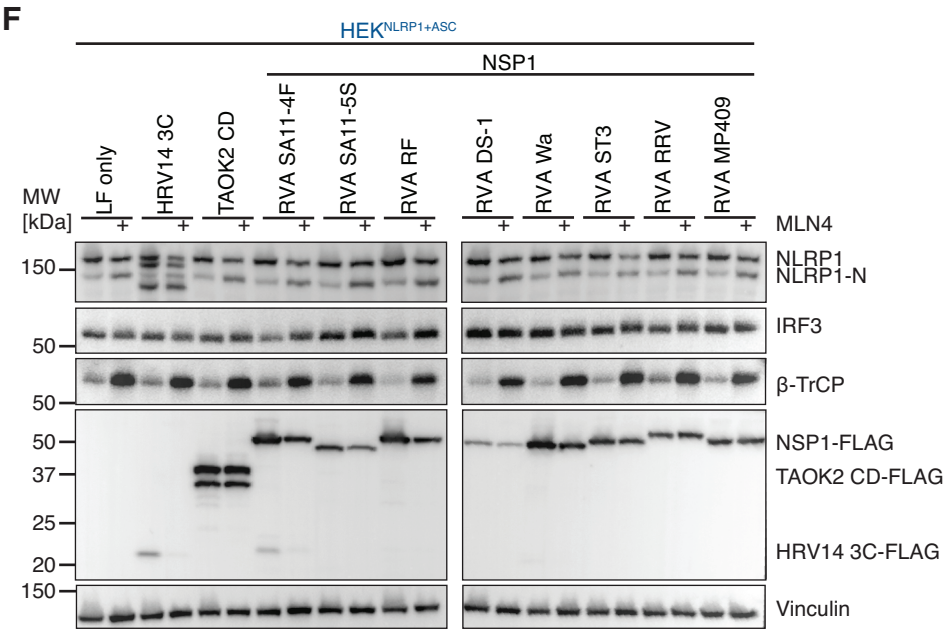

Figure 4.3: Expression of simian rotavirus SA11-4F NSP1 protein is sufficient for NLRP1 activation. (**A**) Schematic overview of the experimental setup. HEK$^{NLRP1+ASC}$ and HEK$^{NLRP3+ASC}$ cells were transiently transfected with expression vectors for FLAG-tagged RVA NSP1 proteins for 6 h, where indicated in the presence of 1 µM MLN4, 10 µM Dora, or DMSO. Transfection of FLAG-tagged HRV14 3C protease and TAOK2, as well as Lipofectamine (LF) only treated cells served as controls. Cells were further incubated for 14 h. (**B**) Average Distance Tree for all tested RVA NSP1 proteins with genotype classification according to (Matthijnssens, Ciarlet, Heiman, et al., 2008). (**C-E**) FLAG-tagged NSP1, HRV14 3C, and TAOK2 expression and ASC speck formation were quantified by flow cytometry, as described in Fig. 2.1. Quantification of specks was limited to FLAG-positive cells, except for untransfected controls. (**F**) Lysates of HEK$^{NLRP1+ASC}$ cells were analyzed by immunoblot with the indicated antibodies to confirm IRF3 and β-TrCP degradation. Data represents average values (with individual data points) from three independent experiments ± 95 % CI. Immunoblot in (F) displays experiment representatives of two independent experiments.

Unfortunately, I could not detect reproducible CRL-dependent degradation of either IRF3 or β-TrCP. β-TrCP levels were strongly increased in all cells treated with the neddylation inhibitor, highlighting its constant turnover as CRL substrate receptor during cell homeostasis. Considering that maximal 40 % of the cells successfully expressed NSP1, immunoblot analyses were probably not sensitive enough to detect differences in protein levels. Since I could not confirm NSP1-mediated degradation, I cannot exclude that some of the tested NSP1 proteins are not functional during transient overexpression. Similarly to β-TrCP, the levels of N-terminal fragments of NLRP1 were slightly increased in all cells treated with the neddylation inhibitor, indicating constant degradation of the

inflammasome sensor by CRLs even in unstimulated cells. The immunoblot confirmed the cleavage of NLRP1 by HRV14 3C protease, but the protease- as well as RVA SA11 NSP1-induced NLRP1 degradation was not obvious.

I hypothesized that RVA SA11-4F NSP1 may bind directly to NLRP1, acting as a substrate receptor for CRLs, and leading to inflammasome activation by ubiquitination and N-terminal degradation of the sensor. To test whether the viral NSP1 protein and NLRP1 interact, I performed co-immunoprecipitation analyses using HEK$^{NLRP1+ASC}$ and

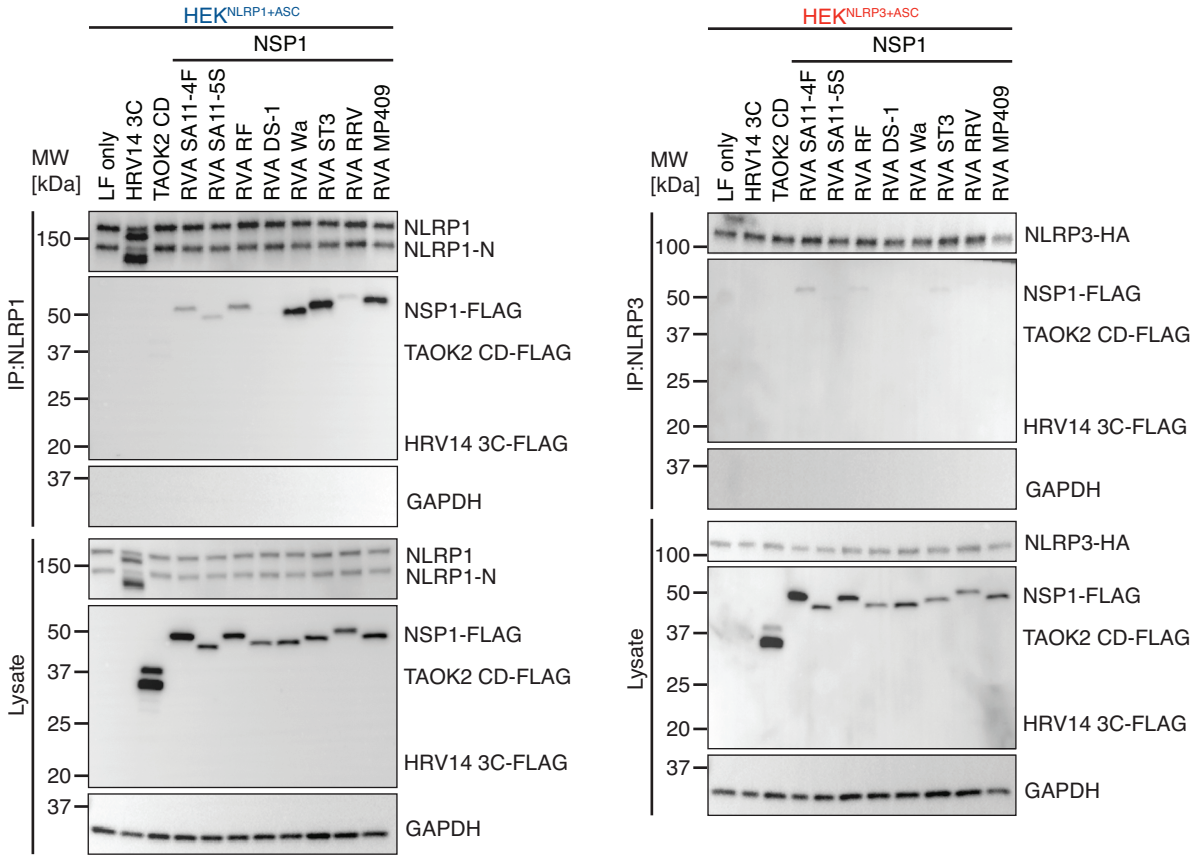

Figure 4.4: Rotavirus NSP1 proteins interact with NLRP1. (A) HEK$^{NLRP1+ASC}$ and HEK$^{NLRP3+ASC}$ cells were transiently transfected with expression vectors for FLAG-tagged RVA NSP1 proteins for 6 h, all in the presence of 1 µM MLN4 to prevent NLRP1 degradation. Transfection of FLAG-tagged HRV14 3C protease and TAOK2, as well as Lipofectamine (LF) only treated cells served as controls. Cells were further incubated for 14 h. HA-tagged NLRP1 and NLRP3 in cell lysates were immunoprecipitated and both lysates and IP fractions were analyzed by immunoblot with the indicated antibodies. Immunoblots display experiment representatives of two independent experiments.

HEK$^{NLRP3+ASC}$ cells transiently overexpressing a set of FLAG-tagged RVA NSP1 proteins, as described before (Fig. 4.4). The experiments were performed in the presence of MLN4924 to prevent the potential NSP1-mediated NLRP1 degradation. Unexpectedly, immunoprecipitation of HA-tagged NLRP1 from HEK$^{NLRP1+ASC}$ cell lysates led to co-immunoprecipitation of most RVA NSP1 forms, including RVA SA11 and RVA RRV. There were also weak bands for some NSP1 proteins, including RVA SA11, after immunoprecipitation of HA-tagged NLRP3 from HEK$^{NLRP3+ASC}$ cell lysates. Importantly, and as expected, TAOK2 did not interact with NLRP1 in these co-immunoprecipitation experiments. Thus, NSP1 proteins from a variety of RVA strains can interact with human NLRP1. However, expression of RVA SA11 NSP1 alone was sufficient for NLRP1 inflammasome activation in the HEK 293T reporter cells. If my hypothesis about additional necessary factors only present during viral infection holds true, it is tempting to speculate that more rotavirus strains can activate NLRP1 in the context of infection.

I could show that expression of RVA SA11-4F NSP1 in HEK$^{NLRP1+ASC}$ cells is sufficient for inflammasome assembly. In a reciprocal approach, I wanted to test whether NSP1 is necessary for NLRP1 activation during RVA SA11-4F infection. I tested recombinant RVA SA11-4F viruses, encoding C-terminally truncated forms of NSP1 (NSP1 Δ42 and NSP1 Δ103). Importantly, these truncations were larger than the one from RVA SA11-5S, which still induced NLRP1 activation in the previous experiments. In addition, I tested recombinant RVA SA11-4F viruses, encoding NSP1 proteins from different RVA strains (NSP1 RF and NSP1 DS-1) whose expression alone did not activate NLRP1 in transient overexpression assays (Fig. 4.5 A). All recombinant RVA SA11-4F viruses successfully infected HEK$^{NLRP1+ASC}$ reporter cells (Fig. 4.5 B). This is in line with reports that NSP1 is not essential for virus replication *in vitro* but influences *in vivo* infections, as shown in murine rotavirus infection models (G. Hou et al., 2021). Analysis of ASC speck formation in infected cells revealed that only cells infected with rotavirus encoding wild type NSP1 induced a strong inflammasome response, whereas all recombinant viruses failed to stimulate the inflammasome (Fig. 4.5 C). Thus, RVA SA11-4F NSP1 is necessary and sufficient to activate the human NLRP1 inflammasome in HEK 293T reporter cells. The abolished activation by viruses expressing NSP1 Δ42 truncations suggests that the C-

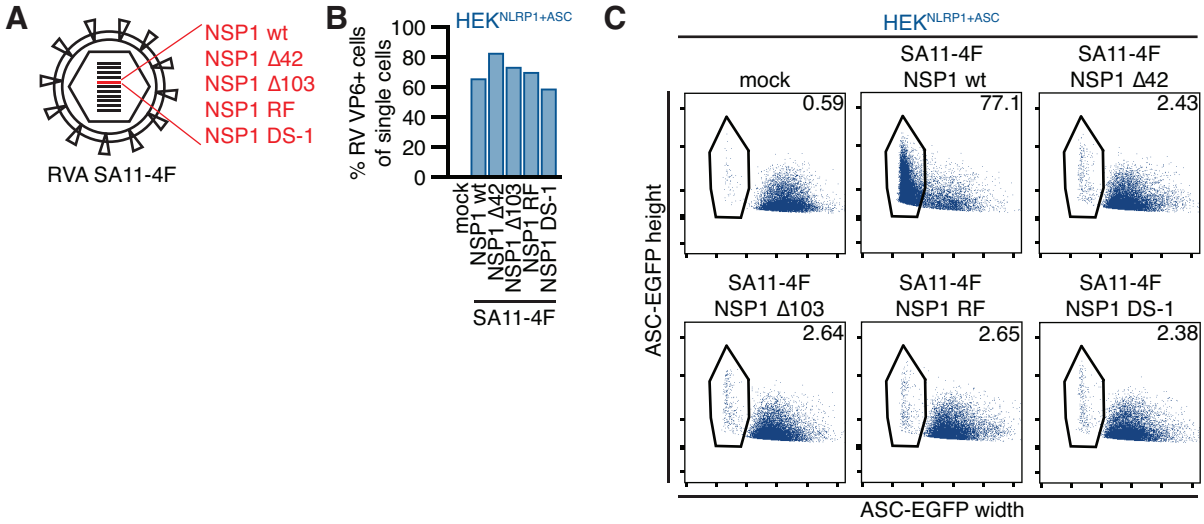

Figure 4.5: Expression of simian rotavirus SA11-4F NSP1 is necessary for NLRP1 activation. (**A**) HEK$^{NLRP1+ASC}$ cells were infected with RVA SA11-4F or recombinant virus, encoding truncated forms of NSP1 or NSP1 from different RVA strains, for 1 h. Cells were further incubated for 19 h. (**B**) Infection was confirmed by staining of RVA VP6 protein and quantified by flow cytometry. (**C**) ASC speck formation was quantified by flow cytometry, as shown in the dot plots. Quantification of specks was limited to infected cells, with exception of uninfected controls. Data represents values from one experiment

terminal target binding domain is important to bind NLRP1, but this has to be validated in further co-immunoprecipitation experiments.

Together, these data show that the RVA SA11-4F host antagonist NSP1 is necessary and sufficient to activate the human NLRP1 inflammasome. The viral protein binds NLRP1, probably leading to the recruitment of CRL complexes and subsequent degradation of the sensor. RVA RRV infection, but not RVA RRV NSP1 expression, induced NLRP1 inflammasome assembly, raising the question whether this activation is still NSP1-dependent. The next experiments should focus on possible additional factors that are only present during infection and that are necessary for RVA RRV NSP1-induced NLRP1 activation.

4.3 Discussion

Rotavirus SA11-4F NSP1 is necessary and sufficient to activate the NLRP1 inflammasome

As rotavirus genomes are composed of 11 dsRNA segments and as dsRNA is a described NLRP1 stimulus, I tested the simian RVA strain SA11-4F for potential NLRP1 inflammasome activation. The virus indeed stimulated NLRP1 in the HEK 293T reporter cells and the response was much stronger than after alphavirus infection. In contrast to alphavirus-mediated NLRP1 activation, inflammasome formation was also independent of p38 MAPK activity. As the viral dsRNA genome is permanently concealed inside viral particles (Papa et al., 2021), it is consistent that NLRP1 is not activated in a dsRNA-dependent manner, as discussed for alphaviruses. It was reported that RVA SA11 and RRV induce p38 activation in Caco-2 and MA-104 cells, but not in murine macrophages, suggesting that rotavirus-induced p38 activation is cell type-specific (Di Fiore et al., 2015; Holloway & Coulson, 2006). Even if p38 is activated in infected HEK 293T reporter cells, p38-mediated phosphorylation of the N-terminal linker was not required for inflammasome formation, as shown for the reporter cells expressing p38 motif mutants of NLRP1. Instead, I showed that the transient expression of RVA SA11-4F nonstructural protein NSP1 is sufficient to activate NLRP1 inflammasomes and that expression of full-length NSP1 is necessary for RVA SA11-4F-induced NLRP1 activation. I thus speculate that the simian RVA NSP1 protein binds NLRP1 at the N-terminus, recruiting CRL complexes, and thereby inducing N-terminal degradation and inflammasome activation. Although I confirmed the interaction of full-length NLRP1 and RVA SA11-4F NSP1 in co-immunoprecipitation experiments, it still has to be proven that NSP1 binds the sensor at the N-terminus. Additional co-immunoprecipitation experiments in HEK 293T cells expressing truncated forms of NLRP1 or NSP1 would help to identify the interacting domains of both proteins. The fact that recombinant RVA SA11-4F expressing NSP1 Δ42 truncations cannot activate NLRP1 inflammasomes already suggests that the C-terminal target-binding domain is important to bind NLRP1. It would be relevant to show that transiently expressed NSP1 Δ42 is inactive as well, as the 17 amino acid truncation of SA11-5S NSP1 was still able to stimulate the inflammasome sensor. Different observations suggest that rotavirus NSP1 binds NLRP1 at the N-terminus: First, murine

Nlrp1b, which differs mostly at the N-terminus, is not activated by RVA SA11-4F infection. Second, NLRP1 KR [PYD] mutants show diminished activation in the HEK 293T system, indicating that NLRP1^{PYD} is ubiquitinated during rotavirus infection. Third, the response rates after infection with RVA SA11-4F in HEK$^{NLRP1+ASC}$ cells are as high as after overexpression of VHL-VHH$_{PYD}$ constructs which also cause ubiquitination of NLRP1^{PYD} and N-terminal degradation. Detection of NLRP1 in immunoblots after transient expression of NSP1 showed no clear degradation of the N-terminal sensor fragment but this was also the case for cells expressing HRV14 3C proteases which cause N-degron pathway-mediated NLRP1 degradation. Since only a fraction of the cells was successfully transfected and small amounts of NLRP1$^{UPA-CARD}$ are already sufficient for inflammasome formation (Hollingsworth, Sharif, et al., 2021; Sandstrom et al., 2019), this method is probably not sensitive enough to detect the loss of the N-terminal fragment. Nevertheless, both RVA SA11-4F infection and NSP1 expression required functional CRL complexes and proteasomal degradation to induce NLRP1 activation, suggesting that the sensor is finally degraded in a cullin-dependent manner. This is in line with the reported recruitment of CRL 1/2/3 complexes by NSP1. Knockdown experiments suggest that rotavirus NSP1 proteins recruit no specific CRL to degrade host proteins (S. Ding et al., 2016; Lutz et al., 2016), but further analyses will be necessary to identify the involved factors. As already discussed in chapters 2 and 3, mass spectrometry would be the method of choice to analyze and confirm NSP1-mediated ubiquitination of NLRP1 (Akimov et al., 2018).

To my knowledge, this is the first report of rotavirus NSP1-mediated activation of human NLRP1 inflammasomes. There are reports about activation of Nlrp6 and Nlrp9b inflammasomes in murine rotavirus infection models and both sensors are described to detect the viral dsRNA (Shen et al., 2021; Zhu et al., 2017). However, this was not confirmed for humans and we and others observed no NLRP9-mediated inflammasome formation in HEK cells, questioning the function of human NLRP9 as an inflammasome sensor (Marleaux et al., 2020, unpublished observations). The NSP1 protein of RVA SA11-4F was reported to degrade IRF3/5/7 (M. M. Arnold & Patton, 2011), RNaseL (Dai et al., 2022), and p53 to delay host apoptosis (Bhowmick et al., 2013), indicating a broad range of antagonistic functions. It is tempting to speculate that some rotavirus NSP1 proteins actually target PYD-containing inflammasome sensors like NLRP3 or NLRP6 to

interfere with inflammasome formation and that NLRP1 counteracts this by functional degradation. Indeed, the concept of NLRP1 as a decoy sensor for PYD-modifying pathogens was proposed before (Chavarría-Smith et al., 2016). The rotavirus protein NSP4 acts as an enterotoxin/viroporin, causing increased intracellular Ca^{2+} levels, which is important for the generation of new viral particles (Chang-Graham et al., 2019; Desselberger, 2014). As alterations of intracellular ion levels are associated with NLRP3 activation (Kelley et al., 2019), it would be conclusive if rotaviruses induce and antagonize such an inflammasome response. To test this, one could analyze whether $HEK^{NLRP3+ASC}$ cells show impaired NLRP3 activation after transient expression of rotavirus NSP1 proteins. I observed weak interaction of RVA SA11-4F NSP1 with NLRP3 in co-immunoprecipitation experiments and it would be interesting to test other PYD-containing inflammasome sensors. Of particular interest would be NLRP6 as an abundantly expressed sensor in intestinal cells, which are the main target of rotavirus infection (Venuprasad & Theiss, 2021). Regardless of whether NLRP1 acts as a decoy sensor or not, RVA SA11-4F NSP1 represents the first pathogenic protein that induces targeted degradation of human NLRP1. It was shown that the IpaH7.8 E3 ligase of *Shigella flexneri* degrades and activates murine Nlrp1b, but this was not the case for human NLRP1 (Sandstrom et al., 2019).

Rotavirus RRV infection but not NSP1 expression activates NLRP1 inflammasomes

I observed NLRP1 inflammasome activation after RVA RRV infection. Similar to RVA SA11-4F infection, the response rates were high and activation was dependent on neddylation, but not p38 activity. However, in contrast to RVA SA11-4F, transient expression of RVA RRV NSP1 was not sufficient to stimulate NLRP1. As the modes of NLRP1 activation were so similar for the two simian rotaviruses, I speculate that RVA RRV NSP1 requires additional factors that are only present during infection to activate the inflammasome sensor. On the other hand, I have no proof that the individual NSP1 proteins are functional after transient expression in the HEK 293T cells, leaving the additional possibility that RVA RRV NSP1 was just not functional. It was reported that Halo-tagged NSP1 proteins show impaired degradation of host proteins in a comparable HEK cell system (Lutz et al., 2016). As I used FLAG-tagged NSP1 proteins, it would be important to confirm their functionality. According to different reports, I should be able to

observe IRF3 degradation by NSP1 of RVA SA11, RVA ETD, RVA RRV, RVA UK, RVA NCDV, and RVA Wi61, as well as β-TrCP degradation by NSP1 of RVA UK, RVA NCDV, RVA Wi61, RVA DS-1, RVA Wa, RVA ST3, and RVA KU, even though some of the reports are inconsistent (M. M. Arnold & Patton, 2011; Barro & Patton, 2007; K. A. Davis et al., 2017; Di Fiore et al., 2015; S. Ding et al., 2016; Graff et al., 2009). As RVA RF NSP1 is of the same genotype as RVA UK and RVA NCDV, similar degradation patterns can be expected (Matthijnssens, Ciarlet, Heiman, et al., 2008). As already mentioned, the fraction of successfully transfected cells was less than 50 % in my assays, impeding the detection of host protein degradation in whole-cell lysate analyses like immunoblots. Many analyses of NSP1-mediated host protein degradation were performed in HEK cells which additionally overexpressed the relevant targets (M. M. Arnold & Patton, 2011; Barro & Patton, 2007; Graff et al., 2009), which might help to detect the loss of protein. It would be best to detect the relevant proteins on a single-cell level using flow cytometry, allowing the comparison of IRF3 or β-TrCP levels in cells that express and do not express the viral NSP1 proteins.

It would be interesting to test a recombinant RVA RRV virus that lacks a functional NSP1 protein. If this virus still induces NLRP1 inflammasome formation, the mode of activation would be different from RVA SA11-4F. Other viral proteins could potentially be involved in inflammasome activation. It was for example reported that RVA RRV VP3, but not NSP1, leads to the degradation of MAVS. VP3 was described to induce the phosphorylation of MAVS, thereby causing its degradation (S. Ding et al., 2018). However, this degradation was insensitive to neddylation inhibitors, which contradicts my observations of RVA RRV-mediated NLRP1 activation. On the other hand, VP3 could initiate p38-independent phosphorylation of NLRP1, but the identified phosphorylation motif is not present in the inflammasome sensor. The rotavirus protein NSP3 enhances the translation of viral mRNAs by interacting with host translation initiation factors to overcome limitations caused by the missing polyA-tail (Gratia et al., 2015). NLRP1 could be activated by interference with ribosomal function similar to alphaviruses, but the inflammasome response would then be p38-dependent. Moreover, there is no report of direct inhibition of host translation by rotaviruses, instead the virus rather relies on a high abundance of viral mRNA to promote viral translation (Gratia et al., 2015). If a recombinant RVA RRV virus that lacks a functional NSP1 failed to induce NLRP1 activation, this would prove that

the inflammasome response is still NSP1-dependent. To confirm that RVA RRV NSP1 requires additional factors only present during infection to activate NLRP1, one could generate a recombinant RVA SA11-4F rotavirus that expresses the NSP1 protein of RVA RRV.

The NSP1 proteins of RVA SA11-4F and RVA RRV show only 57 % sequence similarity and are therefore classified into different genotypes. NSP1 proteins exhibit the highest sequence variability of all rotavirus proteins and the differences are mostly found in the C-terminus which defines the binding of potential host targets. However, NSP1 proteins of viruses that infect the same species are usually more similar because the viruses evolved to antagonize the same host proteins (M. M. Arnold, 2016; M. M. Arnold & Patton, 2011; Dunn et al., 1994). Thus, it would be plausible if the two simian rotavirus NSP1 proteins target the same inflammasome sensor. In contrast, only RVA SA11 NSP1 but not RVA RRV NSP1 was shown to degrade RNaseL (Dai et al., 2022).

Is there a physiological relevance for rotavirus-mediated NLRP1 activation?

So far, I have shown that two simian rotavirus strains activate the human NLRP1 inflammasome in a reconstituted HEK 293T cell model. This raises two important questions:

1) Do human rotavirus strains activate NLRP1? I could show that none of the transiently expressed human rotavirus NSP1 proteins activates NLRP1. Nevertheless, the same holds true for RVA RRV NSP1 which still activates the inflammasome in the context of infection. Moreover, most of the tested human NSP1 proteins interacted with NLRP1 in co-immunoprecipitation experiments, suggesting that human rotaviruses might still be able to stimulate NLRP1 in an NSP1-dependent manner. However, NSP1 proteins can bind target proteins in immunoprecipitation assays without induction of degradation (Graff et al., 2007). Interestingly, the NSP1 genotypes of human rotavirus strains are associated with degradation of β-TrCP, but not IRF proteins. This is in contrast to RVA SA11-4F and RVA RRV NSP1, indicating that human rotaviruses evolved NSP1 proteins with different properties (M. M. Arnold & Patton, 2011). It could be speculated that they adapted their NSP1 proteins to specifically avoid NLRP1 degradation but are still able to degrade other PYD-containing inflammasome sensors. It would be interesting to test whether human rotavirus NSP1 proteins can interfere with the activation of different inflammasome

sensors. Of course, it is also still possible that RVA RRV and human rotavirus strains activate NLRP1 in an NSP1-independent manner. It will be important to screen the respective human rotavirus strains in proper infection experiments, to see whether they can activate NLRP1 or not.

Even if only NSP1 proteins from non-human rotavirus strains activate human NLRP1, it is still possible that these proteins find their way into human hosts. On the one hand, simian rotaviruses could cause zoonotic infections in humans, in line with a report of an infant infected with an SA11-like rotavirus strain (Ghosh et al., 2011). On the other hand, as rotaviruses exhibit a segmented genome, parallel infections with different virus strains can cause recombination but also complete reassortments of individual segments. Zoonotic reassortments are also common, as for example the human AU-1-like strains show feline and canine rotavirus characteristics, whereas the human DS-1-like strains exhibit bovine rotavirus elements (Matthijnssens, Ciarlet, Heiman, et al., 2008; Matthijnssens et al., 2011). Today, newly isolated rotavirus strains are often completely sequenced, revealing the great variability of genotypes and putative zoonotic strains (Phan et al., 2016). Thus, NLRP1-activating NSP1 proteins could end up in human rotavirus strains after recombination or reassortment events. In line with this, a new rotavirus strain that exhibits a recombination of the human A1 and the porcine A8 NSP1 genotype was recently reported (Esona et al., 2017). Nevertheless, as already mentioned, it is rather unlikely that rotaviruses with complete NSP1 reassortments are established, as the NSP1 proteins are strongly adapted to the respective host species. Based on this, one could speculate that the presence of NLRP1-activating NSP1 proteins prevents successful zoonotic rotavirus infections in the first place. If this was true, NLRP1 activation by zoonotic rotaviruses would help to detect and suppress the viral infection, which brings me to the second question:

2) Do rotaviruses infect cells that have functional NLRP1 inflammasomes? Rotaviruses infect primarily villous epithelium and enteroendocrine cells in the small intestine (Omatola & Olaniran, 2022). There are reports about the involvement of Nlrp1a/b in intestinal inflammation in the mouse (Costa et al., 2021; Tye et al., 2018) but so far there is no description of functional NLRP1 inflammasomes in human intestinal epithelial cells. CaCo-2 cells are immortalized human colon cells that are often used to study rotavirus infections (Barro & Patton, 2007; Holloway & Coulson, 2006), but these cells do not express NLRP1. It would be important to find a physiologically relevant cell model that has

functional NLRP1 inflammasomes, similar to the N/TERT-1 cells in the context of alphavirus infection. Apart from intestinal epithelial cells, rotaviruses may also infect tissue-resident immune cells such as intestinal macrophages. As human monocytes can form NLRP1 inflammasomes (see chapter 5), monocyte-derived intestinal macrophages might be an NLRP1-expressing physiologically relevant cell type. It was shown that RVA RRV can infect murine macrophages (Di Fiore et al., 2015), but similar infection experiments have to be performed with primary human macrophages. In some cases, especially in immunocompromised patients, rotavirus infections can also cause extra-intestinal symptoms such as neurological dysfunction and hepatitis. Therefore, it can be argued that extra-intestinal replication could cause NLRP1 inflammasome activation in other cell types. However, as extra-intestinal rotavirus replication is mostly studied in animal models, the relevance in human patients is mostly unknown (Dian et al., 2021; Omatola & Olaniran, 2022).

In summary, I showed that the simian rotavirus strain RVA SA11-4F activates human NLRP1 in an NSP1-dependent manner. NSP1 probably binds to the N-terminus of the sensor to recruit CRL complexes and induce N-terminal degradation, even though the exact binding domains and ubiquitination sites require further analyses. It is tempting to speculate that rotavirus NSP1 proteins target PYD-containing inflammasome sensors and that NLRP1 acts as a decoy sensor. The rhesus rotavirus strain RVA RRV stimulates NLRP1 as well but the role of NSP1 in this process is still in question. It will be important to focus further studies on human rotavirus strains as well as physiologically relevant cell models.

4.4 Material and Methods

Cells

Cell culture

HEK 293T cells were cultivated as described in chapter 2. African green monkey epithelial kidney cells (MA-104) (*Cercopithecus aethiops*, a kind gift of Anna Eis-Hübinger, University Bonn) were cultivated in MEM containing 10 % FBS (all Thermo Fisher Scientific).

Generation of genetically modified cell lines

Generation of $HEK^{NLRP1+ASC}$ and $HEK^{NLRP3+ASC}$ cell lines was already described in chapter 2. Generation of HEK^{ASC} expressing wild type human NLRP1, mutant human NLRP1, or murine Nlrp1b alleles was already described in chapter 3.

Viruses

All experiments involving rotaviruses were conducted in respective Biosafety Level 2 laboratories. RVA strain SA11-4F (a kind gift of Alexander Falkenhagen and Reimar Johne, Bundesinsitut für Risikobewertung Berlin) and RRV (a kind gift of Sandra Londrigan, Peter Doherty Institute) were amplified in MA-104 cells as described before (M. Arnold et al., 2009). Briefly, rotaviruses were activated by incubation with 10 µg/mL trypsin at 37 °C for 1 h. MA-104 cells were infected at an MOI of 0.05 for 1 h and incubated in MEM supplemented with 0.5 µg/mL trypsin and 20 mM HEPES until most cells detached. Remaining cells and supernatant were harvested and cells were ruptured by three consecutive freeze-thaw cycles at -80 °C and room temperature. Viruses in the clarified supernatant were further purified by sedimentation (29,000 rpm (SW 32 Ti), 4 °C, 1.5 h) through 35 % sucrose in TNC buffer (20 mM Tris pH 8.0, 100 mM NaCl, 1 mM $CaCl_2$). Virus pellets were resuspended in TNC buffer, aliquoted, and frozen at -80 °C. Viral titers were determined in MA-104 cells by flow cytometry using Alexa Flour™ 647-coupled anti-VP6 nanobody 2KD1 (Garaicoechea et al., 2008). Rotaviruses were always activated by incubation with 10 µg/mL trypsin at 37 °C for 1 h before titration.

Recombinant SA11-4F rotaviruses were kindly provided by Alex Borodavka (University of Cambridge). Recombinant viruses were rescued from BHK-T7 cells which were co-transfected with pT_7 rescue plasmids, encoding all 11 rotavirus segments, as well as NSP2-, NSP5-, and T7-encoding helper plasmids. MA-104 cells were added 24 h post-transfection to enable virus propagation. Cells were co-cultured for 3 days in presence of 0.5 µg/mL trypsin and then lysed by freeze-thawing. Recombinant rotaviruses were again amplified in MA-104 cells and confirmed by sequencing. Viral titers were determined by plaque assay using MA-104 cells.

Proteins

Expression and purification of anti-VP6 nanobody 2KD1

The nanobody-coding sequence (Garaicoechea et al., 2008) was cloned into pHEN6-based bacterial, periplasmic expression vectors with C-terminal LPETG-His tags using Gibson cloning. Nanobodies were expressed in *E. coli* WK6 cells in Terrific Broth induced with 1 mM IPTG at an OD600 of 0.6. Cells were cultivated for 16 h at 30 °C. Bacterial pellets were resuspended in TES buffer (200 mM Tris-HCl pH 8.0, 0.65 mM EDTA, 0.5 M sucrose) and periplasmic extracts were generated by osmotic shock in 0.25x TES. Clarified lysates were further purified by affinity chromatography using Ni-NTA and gel filtration with a HiLoad 16/600 Superdex 75 pg column in buffer containing 20 mM HEPES pH 7.4, 150 mM NaCl, and 10 % glycerol.

Sortase labeling of anti-VP6 nanobody 2KD1

0.67 mg purified LPETG-His-tagged nanobodies were incubated with 500 µM GGGC-Alexa Flour™ 647 (custom-synthesized peptides from Thermo Fisher Scientific) and 20 µM sortase A 7m in HEPES buffer (20 mM HEPES pH 7.4, 150 mM NaCl). His-tagged sortase A 7m was recombinantly expressed as described before (Guimaraes et al., 2013). Sortase A-mediated coupling of Alexa Flour™ 647 to LPETG-encoding nanobodies was performed for 16 h at 4 °C. His-tagged sortase A and unreacted nanobodies were removed by Ni-NTA purification. Alexa Flour™ 647-coupled nanobodies were further purified by gel filtration using a Superdex 75 Increase 10/300 GL column in PBS.

Antibodies

The following antibodies were used: rabbit anti-β-TrCP clone D13F10 (Cell Signaling Technology Cat# 4394, RRID:AB_10545763), rabbit anti-FLAG clone D6W5B (Cell Signaling Technology Cat# 14793, RRID:AB_2572291), mouse anti-GAPDH clone 0411 (Santa Cruz, Cat# sc-47724, RRID:AB_627678), mouse anti-HA-HRP clone 6E2 (Cell Signaling Technology Cat# 2999S, RRID:AB_1264166), rabbit anti-IRF3 clone D83B9 (Cell Signaling Technology Cat# 4302, RRID:AB_190403), mouse anti-NLRP1 clone 9F9B12 (BioLegend Cat# 679802, RRID:AB_2566263), mouse anti-vinculin clone hVIN-1 (Sigma-Aldrich Cat# V9131, RRID:AB_477629), goat polyclonal anti-rabbit IgG (H+L)-Alexa FlourTM Plus 647 (Invitrogen Cat#A32733, RRID:AB_2633282), goat polyclonal

anti-rabbit IgG (H+L)-HRP (Invitrogen Cat#31460, RRID:AB_228341), goat polyclonal anti-mouse IgG (H+L)-HRP (Invitrogen Cat#31430, RRID:AB_228307)

Small compound inhibitors and reagents

The following small compound inhibitors and reagents were used: bortezomib (Selleckchem), doramapimod (Cayman), JNK-IN-8 (Selleckchem), MG-132 (Selleckchem), MLN4924 (MedChem Express), MLN7243 (ChemieTek), SB202190 (Sigma-Aldrich), and talabostat mesylate (MedChemExpress).

Flow cytometry-based quantification of inflammasome assembly

The experimental procedures to quantify the assembly of ASC-EGFP specks by flow cytometry were already described in chapter 2. Similarly, $2.5 \cdot 10^5$ (24 well-plate)/$1.25 \cdot 10^5$ (48 well-plate) $HEK^{NLRP1+ASC}$ (or other derivatives of HEK 293T) were seeded per well and cultivated overnight in the absence of antibiotics.

For drug-induced inflammasome stimulation, cells were treated with 30 µM talabostat.

For rotavirus-induced inflammasome stimulation, cells were infected for 1 h in serum-free medium (0.2 % BSA, 20 mM HEPES in DMEM) at the indicated MOI, ranging from 6-100. In the beginning, rotaviruses were activated by incubation with 10 µg/mL trypsin at 37 °C for 30 min prior to infection. As it turned out that the incubation with trypsin did not affect the infection of HEK 293T reporter cells, rotaviruses were used without prior trypsin activation in the later experiments. Inocolum was replaced with full medium after infection and cells were cultivated for another 5 or 19 h. Cells treated with infection medium only served as mock controls.

For inflammasome stimulation by transient overexpression of FLAG-tagged HRV14 3C protease, catalytic domain of TAOK2, or RVA NSP1, cells in 24 well-plates were transfected with 500 ng total of expression vectors based on pCAGGS (Hitoshi et al., 1991) (HRV14 3C and NSP1) or Gateway-compatible derivatives of pcDNA3.1 (TAOK2 CD) using Lipofectamine 2000. Medium was replaced with full medium after 6 h and cells were cultivated for another 14 h. Cells treated with Lipofectamine 2000 only served as controls. Plasmids to construct expression constructs for RVA NSP1 were kindly provided by John T. Patton (Indiana University).

In case of additional inhibitor treatments, small compound inhibitors were added 30 min before and during the stimulation, with the following concentrations: 1 µM bortezomib, 10 µM doramapimod, 3 µM Jnk-In-8, 1 µM MG-132, 1 µM MLN4924, 1 µM MLN7243, or 20 µM SB202190. In the case of rotavirus infection experiments, inhibitors were only added after 1 h infection.

Stimulated cells were harvested and analyzed by flow cytometry as described in chapter 2. Where indicated, fixed and permeabilized cells were stained with anti-FLAG (1:300) combined with Alexa Flour™ Plus 647-coupled, highly cross-absorbed secondary antibodies (1:500) or Alexa Flour™ 647-coupled anti-VP6 nanobody 2KD1 (1.2 µg/mL) in Intracellular Staining Permeabilization Wash Buffer (Biolegend). For the quantification of specks after virus infection or transient transfection, only cells positive for VP6 or FLAG were included in the analysis (except for mock-infected or untreated controls).

Co-Immunoprecipitation

To analyze the interaction of RVA NSP1 with human NLRP1 and NLRP3, $1 \cdot 10^6$ $HEK^{NLRP1+ASC}$ or $HEK^{NLRP3+ASC}$ cells per well were seeded in 6 well-plates, followed by transfection of 2 µg total of expression vectors as described for the flow cytometry experiments. Cells were treated with 1 µM MLN4924 during and after transfection. 20 h post-transfection, cells were harvested by scraping and lysed in 200 µL low salt lysis buffer (1 % NP-40, 50 mM Tris pH 7.5, 150 mM NaCl, 1 mM EDTA) supplemented with protease inhibitor (Roche). Clarified lysates were incubated with 10 µL Pierce magnetic anti-HA beads (Thermo Fisher Scientific) at 4 °C for 3 h. Immunoprecipitated protein was eluted by boiling the beads in 40 µL 2x SDS-PAGE buffer without DTT. Supernatants were harvested, DTT was added to reach a concentration of 100 mM and samples were analyzed by immunoblot.

Immunoblot

To analyze NSP1-induced IRF3 and β-TrCP degradation, $2.5 \cdot 10^5$ $HEK^{NLRP1+ASC}$ cells per well were seeded in 24 well-plates, followed by transfection of expression vectors as described for the flow cytometry experiments. Cells were lysed in 100 µL 1x SDS-PAGE buffer (50 mM Tris pH 6.8; 0.01 % Bromophenol blue, 10 % glycerol, 2 % SDS, 100 mM DTT) 20 h post-transfection.

Immunoblots were performed as described in chapter 2. Membranes were probed with the following primary antibody dilutions: anti-β-TrCP 1:1000, anti-GAPDH 1:2000, anti-HA-HRP 1:1000, anti-IRF3 1:1000, anti-NLRP1 1:1000, and anti-vinculin 1:1000. All primary antibodies were added in 5 % NFDM solution. Chemiluminescent signal was induced by Western Lightning Plus-ECL (Perkin Elmer), except for immunoblots of NLRP1 which required Western Lightning Ultra-ECL (Perkin Elmer).

NSP1 sequence analysis

NSP1 sequences were collected from GenBank (National Center for Biotechnology Information) and analyzed using Jalview 2.11.2.6 software (Waterhouse et al., 2009). Sequences were aligned using Clustal algorithm and Average distance trees (Percentage Identity) were generated. Genotype classifications were based on (Matthijnssens, Ciarlet, Heiman, et al., 2008).

Statistical analyses

Statistical analyses were performed as described in chapter 2.

5. Human T cells assemble NLRP1 inflammasomes and undergo NLRP1-induced pyroptosis

5.1 Introduction

In this chapter, I will screen human blood cells for the ability to assemble functional NLRP1 inflammasomes. I will establish lymphocytes, especially T cells, as NLRP1 inflammasome-competent cells. Moreover, I will use the VHL-VHH_{PYD} system to prove that T cells undergo NLRP1-dependent pyroptosis.

As discussed in chapter 2, most NLRP1 studies are performed in reconstituted HEK cell systems or epithelial cells like keratinocytes. There are only a few reports about NLRP1 inflammasomes in human blood cells. Treatment of peripheral blood mononuclear cells (PBMCs) with talabostat leads to cell death and IL-1β release, but the role of NLRP1 versus CARD8 or the responsive cell type(s) were not determined (Okondo et al., 2017; Zhong et al., 2018). Several studies analyzed inflammasome responses in PBMCs on a single-cell level using flow cytometry, but all only focused on monocytes and NLRP3 activation (Lage et al., 2019; Nagar et al., 2019; Sester et al., 2015; Tran et al., 2019). Monocytes/macrophages are well-established cell models to study inflammasomes. In contrast, lymphocytes are mostly analyzed in interaction with myeloid inflammasome-forming cells (Donado et al., 2020; Guarda et al., 2009) or in the context of inflammasome-mediated inflammation. Indeed, IL-1β stimulates T helper (Th)17 differentiation and cytotoxic T cell responses and IL-18 induces INF-γ production by cytotoxic T cells (Chung et al., 2009; H. Zhang et al., 2023). Lymphocytes as potential inflammasome-competent cells only start to get attention. Stimulation of primary human T cells with talabostat leads to CARD8-dependent pyroptosis, which was restricted to T cell receptor (TCR)-unstimulated lymphocytes (D. C. Johnson et al., 2020; Linder et al., 2020). In addition, CARD8 is cleaved and activated by HIV-1 proteases in productively or latently infected T cells (Moore et al., 2022; Q. Wang et al., 2021). HIV-1-induced NLRP3 activation in human T cells was described as well (C. Zhang et al., 2021). Regarding B cells, there are reports about AIM2 (Svensson et al., 2017), Nlrc4 (Perez-Lopez et al., 2013), and NLRP3/Nlrp3 (Ali et al., 2017; M. L. Hsu & Zouali, 2023; Lim et al., 2020; Schoenlaub et al., 2016) inflammasomes in these cells, causing pyroptosis and IL-1β release but also influencing IgM release and B cell homing.

5.2 Results

Contributions

RNA extractions and transcriptome data generation of sorted T cells shown in Fig. 5.9 were performed by Susanne Schmidt and her team, who were part of the Institute of Innate Immunity in Bonn at that time. The microscopy pictures in Fig. 5.11 E were taken with the help of Lisa Schiffelers, who was a member of the Institute of Innate Immunity (Florian Schmidt lab) in Bonn at that time. All other experiments and further analyses of the data were performed by myself.

5.2.1 Lymphocytes assemble NLRP1 inflammasomes after inhibition of DPP8/9

Using the HEK 293T and N/TERT-1 inflammasome reporter cells, I studied NLRP1 activation in the context of targeted ubiquitination, the RSR, and alphavirus or rotavirus infection. Although these cell lines are a valuable tool to screen NLRP1 stimuli and to analyze the detailed mechanisms of inflammasome activation, I next wanted to apply the gained knowledge to study NLRP1 in primary cells.

I started by analyzing NLRP1 inflammasome responses in PBMCs after stimulation with the DPP8/9 inhibitor talabostat (Tal) (Fig. 5.1 A). Similar to the experiments using inflammasome reporter cells, I stained endogenous ASC and used ASC speck formation as the main readout for inflammasome activation. This is especially important since talabostat also activates the CARD8 inflammasome (D. C. Johnson et al., 2018). The subsequent CARD8-induced pyroptosis can lead to NLRP3 activation by potassium efflux, similar to non-canonical inflammasomes (Rühl & Broz, 2015; Schmid-Burgk et al., 2015). Therefore, I cannot distinguish between talabostat-induced NLRP1 and CARD8/NLRP3 activation by analyzing downstream effects of inflammasome formation, like pyroptosis and IL-1β release. Only analysis of ASC speck formation in the presence of caspase-1 inhibitor Vx-765 (VX) allows to specifically study NLRP1 activation, as CARD8 alone cannot form ASC specks (Ball et al., 2020; Gong et al., 2021) and inhibition of caspase-1 blocks pyroptosis-induced NLRP3 activation. To still rule out any influence of NLRP3, I used the NLRP3 inhibitor Crid3, also called MCC950, which stabilizes the inactive state of NLRP3 cages (Coll et al., 2015; Hochheiser et al., 2022). I also included NLRP3 stimulation with LPS and nigericin (LPS+N) to compare the activation of the two

inflammasomes. In addition to PBMCs, I also analyzed PBMCs that were depleted of CD14+ monocytes (CD14- PBMCs) (Fig. 5.1 B). As monocytes are one of the main cell types to respond to NLRP3 inflammasome stimulation (Lage et al., 2019; Sester et al., 2015), their depletion helped to focus on other cell types whose response might otherwise be overshadowed by the dominant monocyte activation.

After inflammasome stimulation of PBMCs and CD14- PBMCs in the presence of Vx-765, I stained endogenous ASC and analyzed ASC speck assembly in all ASC-expressing cells by flow cytometry (Fig. 5.1 C), as described for the inflammasome reporter cells before. The used antibody (clone HASC-71) was chosen based on a clear signal and high

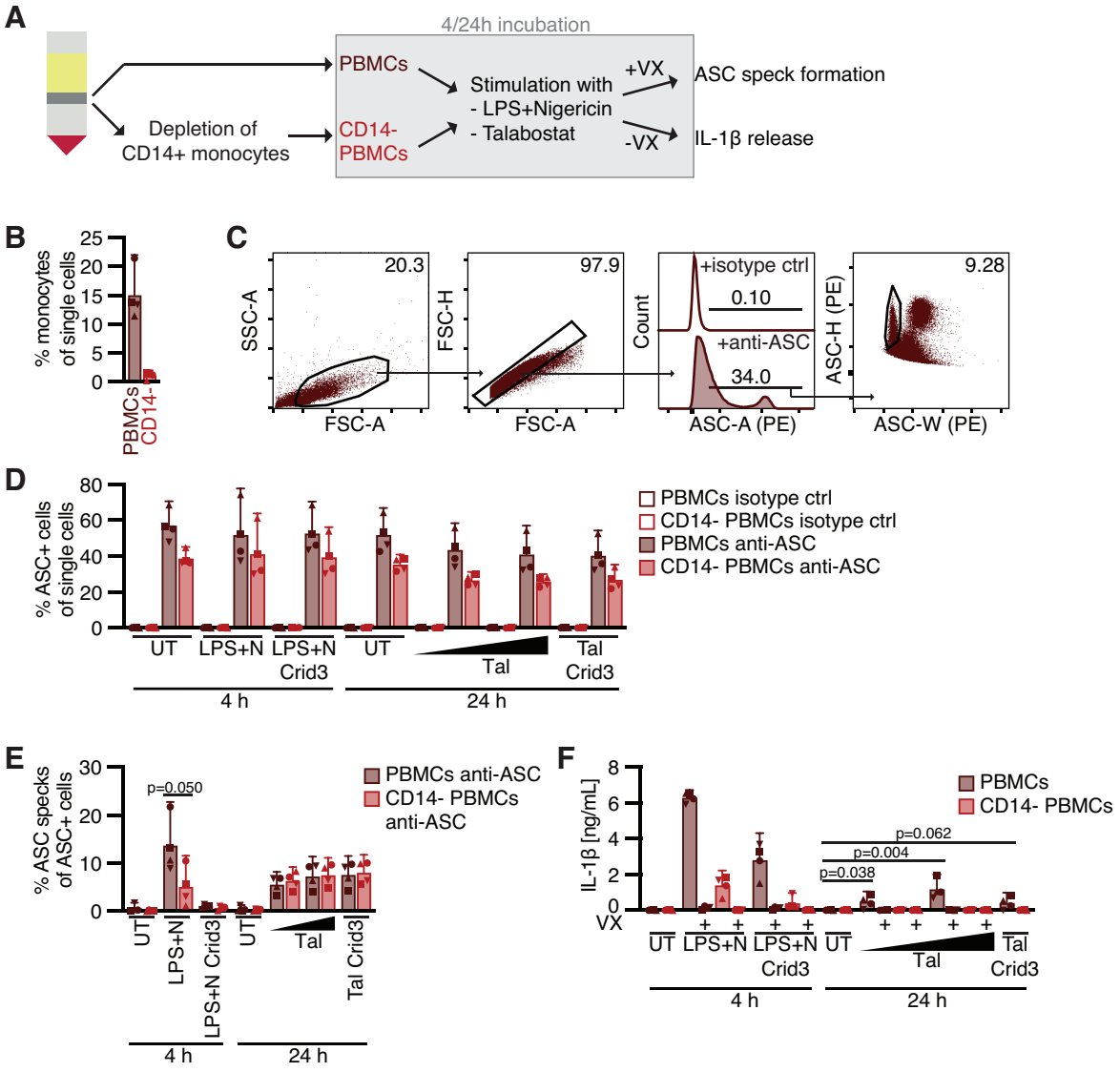

Figure 5.1: CD14- PBMCs show ASC speck assembly after inhibition of DPP8/9. (**A**) Schematic overview of the experimental setup. Human PBMCs were isolated from fresh blood and part of the cells was depleted of CD14+ monocytes. PBMCs and CD14- PBMCs were stimulated with either 200 ng/mL LPS for 3 h and 10 µM Nig for 1 h, or 3/30 µM Tal for 24 h, or left untreated (UT), where indicated in the presence of 2.5 µM Crid3 or 100 µM VX. ASC speck formation was detected in the presence of caspase-1 inhibitor VX. (**B**) Expression of CD14 in freshly isolated PBMCs and CD14- PBMCs was quantified by flow cytometry to confirm successful depletion of monocytes. (**C**) PBMCs and CD14- PBMCs were stained for ASC (or with an isotype control (ctrl)) and ASC speck formation was analyzed by flow cytometry, as shown in the representative dot plots. The plots show PBMCs stimulated with 30 µM Tal for 24 h. (**D,E**) ASC expression and ASC speck formation in ASC+ cells were quantified by flow cytometry, as described in (C). (**F**) Supernatants from stimulated PBMCs and CD14- PBMCs were collected. IL-1β release was quantified by HTRF. Data represents average values (with individual data points) from four independent experiments with cells from four different donors ± 95 % CI, p-values were calculated using unpaired t-test.

specificity in experiments comparing wild type and ASC knockout THP-1 cells (data not shown), in line with data from others (Beilharz et al., 2016). To ensure specificity of the ASC speck staining, I further included an isotype control staining. Analyzing single cells (see Fig. 5.1 C), I detected ASC expression in around 50 % of all PBMCs (Fig. 5.1 D). Depletion of monocytes decreased the percentage of ASC-expressing cells by 20-40 %, indicating that monocytes show a high expression of the inflammasome adaptor. ASC expression was unchanged by LPS priming, showing robust expression throughout all stimulations. When I analyzed ASC speck assembly in ASC-expressing cells, around 15 % of PBMCs responded to NLRP3 stimulation (Fig. 5.1 E). The response was clearly diminished in CD14- PBMCs, demonstrating that monocytes are indeed the main cell type to form inflammasomes after stimulation with LPS and nigericin. ASC speck assembly in both PBMCs and CD14- PBMCs was completely blocked by NLRP3 inhibitor Crid3. In contrast, stimulation with talabostat induced slightly lower inflammasome responses which were similar in PBMCs and CD14- PBMCs, indicating that monocytes are not the main cell type to form inflammasomes after stimulation of NLRP1. ASC speck assembly following stimulation with talabostat was independent of NLRP3, as it was unchanged by Crid3.

ASC speck assembly in NLRP3-stimulated PBMCs was accompanied by caspase-1-dependent IL-1β release (Fig. 5.1 F). CD14- PBMCs released substantially less IL-1β, demonstrating that monocytes are not only the main PBMC cell type to form NLRP3

inflammasomes but also the main producers of the proinflammatory cytokine. This was also true following talabostat stimulation, which induced low levels of IL-1β release from PBMCs but not from CD14- PBMCs. Moreover, the talabostat-induced release of IL-1β was nearly abolished by Crid3, suggesting that it may indeed be dependent on CARD8-induced NLRP3 activation, rather than NLRP1 activation. Thus, although I detected monocyte- and NLRP3-independent ASC speck assembly after talabostat stimulation, this did not result in caspase-1-dependent IL-1β release.

To follow up on the monocyte-independent inflammasome formation after talabostat stimulation, I stained different PBMC subpopulations and analyzed inflammasome responses in specific cell types (Fig. 5.2 A). I focused my analyses on CD14+ monocytes, CD3+ T cells, CD19+ B cells, and CD14- HLA-DR+ cells, the latter representing mostly DCs (Carenza et al., 2021)(Fig. 5.2 B). Frequencies of T cells and B cells were mostly unchanged throughout NLRP3 and NLRP1 stimulation (Fig. 5.2 C). In contrast, most of the monocytes were lost after stimulation with LPS and nigericin. Instead, there was an increase in CD14- HLA-DR+ cells, suggesting that this stimulation leads to loss of CD14 expression in monocytes. As the same drop in CD14+ monocytes occurred in samples that were treated with the NLRP3 inhibitor, it can be excluded that the loss is due to insufficient inhibition of pyroptosis by Vx-765. A similar increase in CD14- HLA-DR+ cells was observed after talabostat stimulation, even though the frequencies of monocytes were unchanged.

First, I analyzed the expression of ASC in the different PBMC subpopulations. Nearly all monocytes and CD14- HLA-DR+ cells expressed high levels of the inflammasome adaptor, even in unstimulated conditions (Fig. 5.3 A,B). This demonstrates that these cells are equipped to initiate a robust inflammasome response whenever necessary. Interestingly, while LPS and nigericin stimulation induced a decrease of CD14+ monocytes, the remaining CD14+ monocytes exhibited diminished ASC expression. Both CD14+ monocytes and CD14- HLA-DR+ cells showed slightly decreased ASC expression after talabostat treatment. In contrast, T and B lymphocytes expressed only low to moderate levels of ASC, in only a fraction of the cells. While around 50 % of untreated T cells were positive for ASC, only around 30 % of untreated B cells expressed the

inflammasome adaptor. Thus, lymphocytes already have less potential to stimulate ASC-dependent inflammasome responses than monocytes and DCs.

Next, I quantified inflammasome assembly in the ASC-expressing PBMC subpopulations. While the high ASC expression in CD14+ monocytes and CD14- HLA-DR+ cells enabled a clear separation of cells with and without ASC specks, the differentiation was more difficult for lymphocytes with low ASC expression (Fig. 5.4 A). Nevertheless, I was able to quantify inflammasome responses after NLRP3 and NLRP1 stimulation for the four cell types (Fig. 5.4 B). Around 80 % of ASC-positive CD14+ monocytes formed

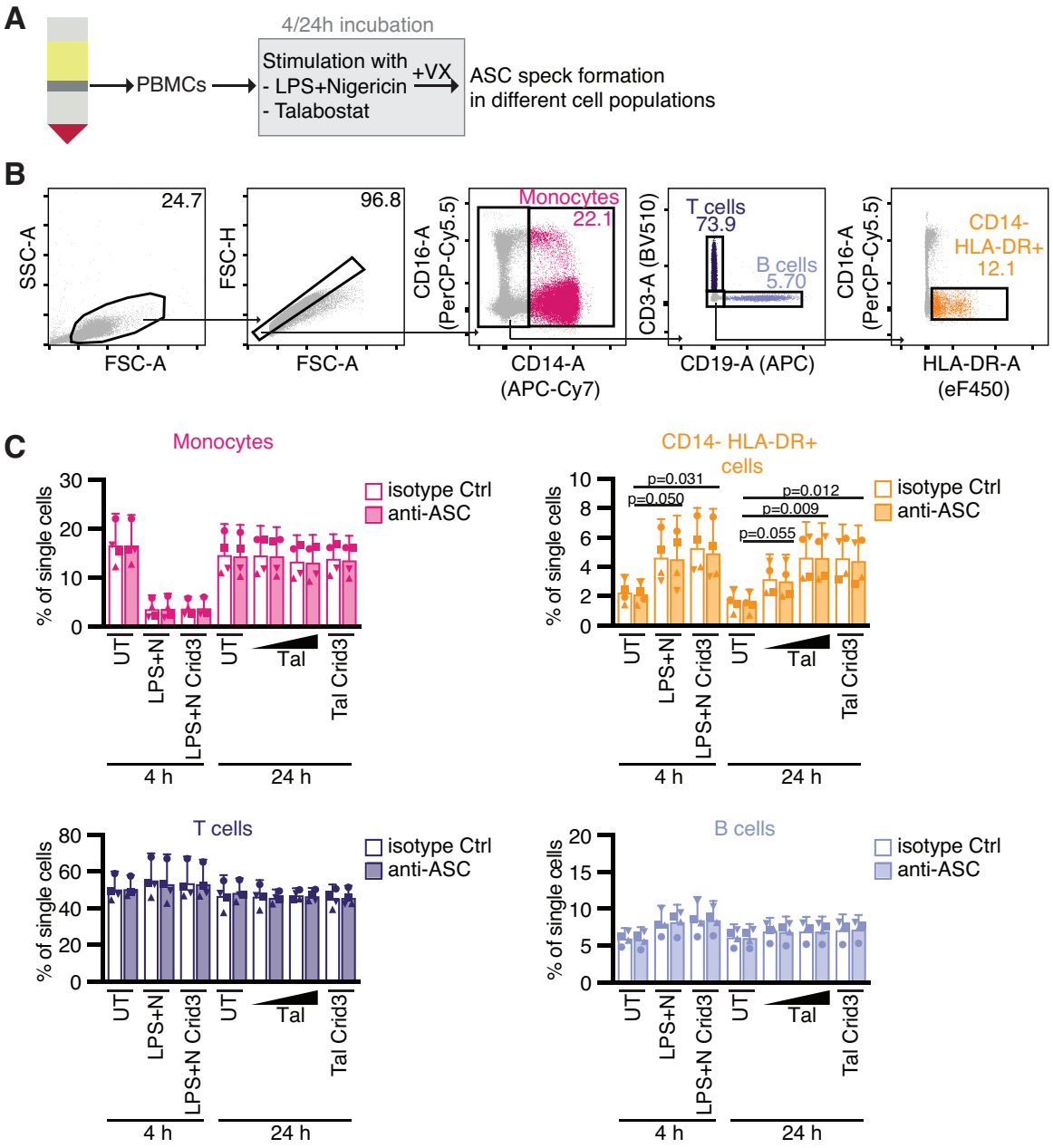

Figure 5.2: Characterization of different PBMC subpopulations after inflammasome stimulation. (**A**) Schematic overview of the experimental setup. Human PBMCs were isolated from fresh blood and stimulated with either 200 ng/mL LPS for 3 h and 10 µM Nig for 1 h, or 3/30 µM Tal for 24 h, or left untreated (UT), where indicated in the presence of 2.5 µM Crid3. All stimulations were performed in the presence of caspase-1 inhibitor VX. (**B**) PBMCs were stained for CD14+ monocytes, CD14- CD3+ T cells, CD14- CD19+ B cells, and CD14- CD3- C19- HLA-DR+ cells. PBMC subpopulations were analyzed by flow cytometry, as shown in the representative dot plots. The plots show 4 h untreated PBMCs. (**C**) PBMC subpopulations were quantified by flow cytometry, as described in (B). Each sample was additionally stained for ASC or with the corresponding isotype control (Ctrl) to analyze ASC speck formation in the different subpopulations. Data represents average values (with individual data points) from four independent experiments with cells from four different donors ± 95 % CI, p-values were calculated using unpaired t-test.

inflammasomes after stimulation with LPS and nigericin. In contrast, their response to talabostat was rather weak with only around 10 % responsive cells, highlighting that

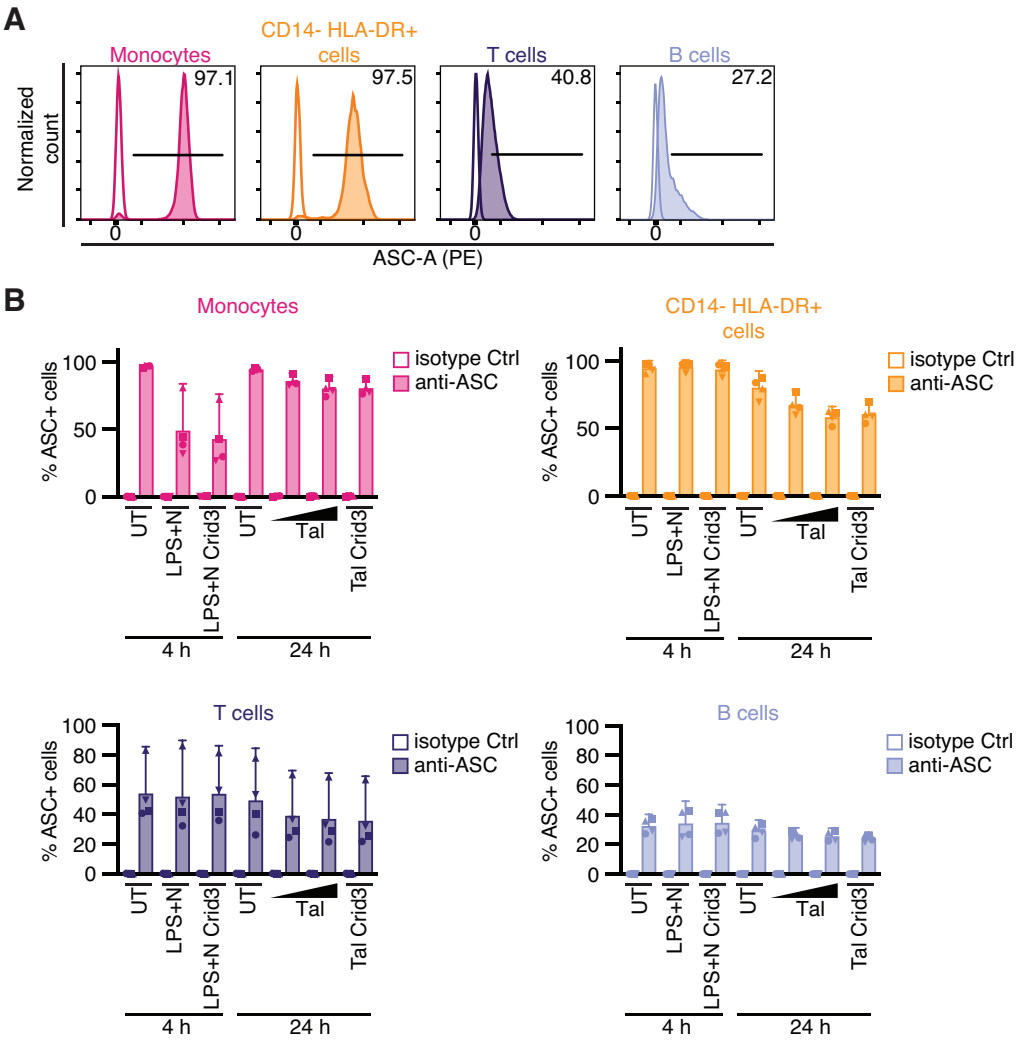

Figure 5.3: Lymphocytes show only moderate ASC expression compared to myeloid cells. Human PBMCs were isolated from fresh blood and stimulated with either 200 ng/mL LPS for 3 h and 10 µM Nig for 1 h, or 3/30 µM Tal for 24 h, or left untreated (UT), where indicated in the presence of 2.5 µM Crid3. All stimulations were performed in the presence of caspase-1 inhibitor VX. (**A**) PBMCs were stained for monocytes, T cells, B cells, and CD14- HLA-DR+ cells, as described in Fig. 5.2. Each sample was additionally stained for ASC (filled histograms) or with the corresponding isotype control (Ctrl, unfilled histograms) to analyze ASC expression in the different subpopulations by flow cytometry, as shown in the representative histograms. The plots show 4 h untreated PBMCs. (**B**) ASC expression of PBMC subpopulations was quantified by flow cytometry, as described in (A). Data represents average values (with individual data points) from four independent experiments with cells from four different donors ± 95 % CI.

monocytes are rather destined to activate NLRP3 than NLRP1 inflammasomes. On the other hand, inhibition of DPP8/9 was also a weak NLRP1 stimulus in the N/TERT-1 keratinocytes, so other triggers might induce a stronger activation of NLRP1 in monocytes. ASC-positive CD14- HLA-DR+ cells showed a similar trend in NLRP3 and NLRP1 inflammasome formation, but around 30 % of the cells reacted to talabostat. Surprisingly, when I checked ASC speck assembly in lymphocytes, I detected a weak but clear talabostat-induced inflammasome response in both T and B cells. Around 3 % of ASC-positive T cells and 2 % of ASC-positive B cells assembled NLRP1 inflammasomes, but neither cell type responded to LPS and nigericin at all. As T cells are the dominant subpopulation of PBMCs, even the low frequencies of responding cells represented 15 % of all cells with ASC specks after inhibition of DPP8/9 (Fig. 5.4 C). B cells represented only around 1 % and are therefore not visible in the graph. It is not surprising that both NLRP3 and NLRP1 inflammasome responses were dominated by CD14+ monocytes and CD14- HLA-DR+ cells, as their high ASC expression prepares them for inflammasome formation.

Since the weak ASC expression in lymphocytes complicated the quantification of ASC specks by flow cytometry, I wanted to confirm that the detected signals derive from proper ASC specks and not staining artifacts. Therefore, I analyzed the same cell populations by imaging flow cytometry, allowing the examination of the distribution of ASC by recording fluorescence images for every detected cell. The images confirmed the difference in ASC expression levels between CD14+ monocytes and lymphocytes (Fig. 5.5). Moreover, CD14+ monocytes, T cells, and B cells showed a clear accumulation of ASC in a single

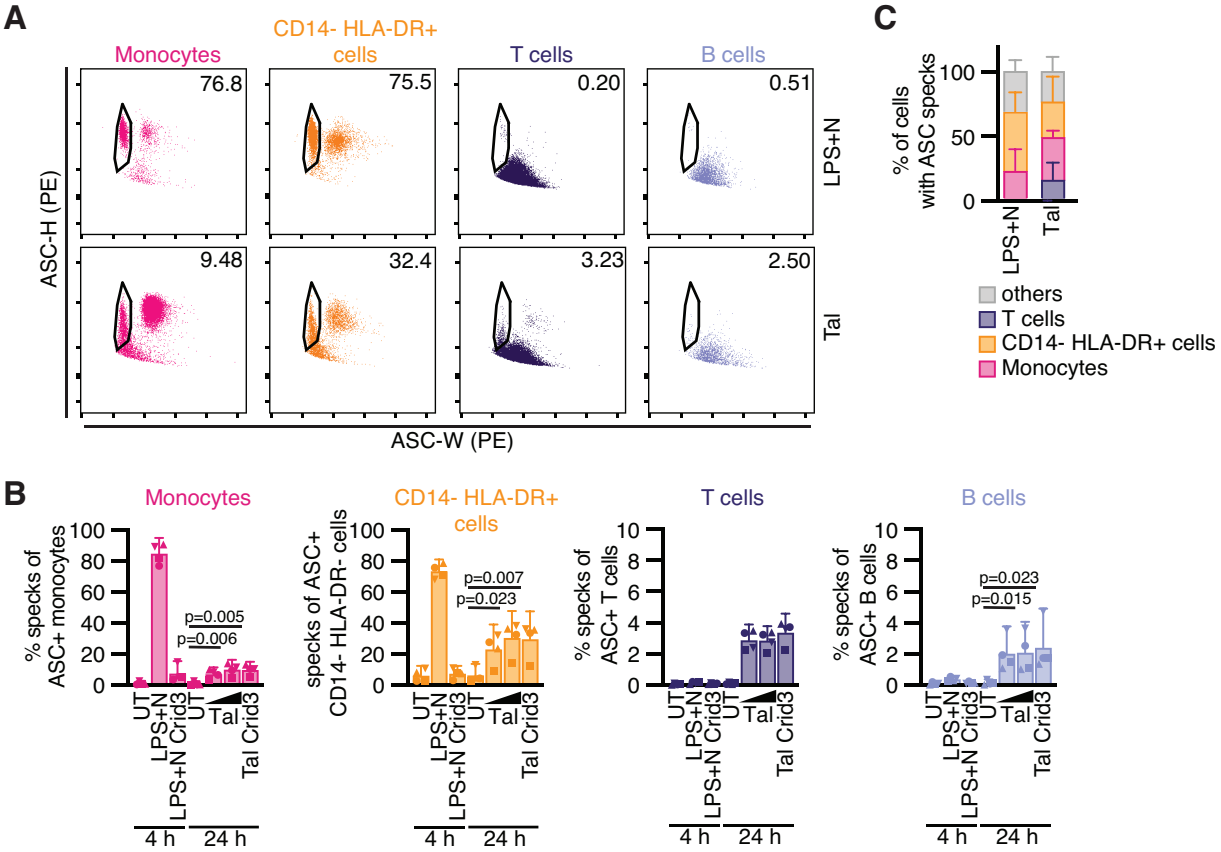

Figure 5.4: Lymphocytes show ASC speck assembly after inhibition of DPP8/9. Human PBMCs were isolated from fresh blood and stimulated with either 200 ng/mL LPS for 3 h and 10 µM Nig for 1 h, or 3/30 µM Tal for 24 h, or left untreated (UT), where indicated in the presence of 2.5 µM Crid3. All stimulations were performed in the presence of caspase-1 inhibitor VX. (**A**) PBMCs were stained for monocytes, T cells, B cells, and CD14- HLA-DR+ cells, as described in Fig. 5.2. Each sample was additionally stained for ASC to analyze ASC speck formation in the different subpopulations by flow cytometry, as shown in the representative dot plots. (**B**) ASC speck formation of ASC+ PBMC subpopulations was quantified by flow cytometry, as described in (A). (**C**) Contribution of PBMC subpopulations to ASC speck response after inflammasome stimulation. Data represents average values (with individual data points) from four independent experiments with cells from four different donors ± 95 % CI, p-values were calculated using unpaired t-test.

speck per cell after treatment with talabostat, as shown in the representative images in Fig. 5.5 (please note that the figure shows ASC specks where available and is not reflecting the response rates of the individual cell populations). In line with the flow cytometry analysis, lymphocytes did not assemble ASC specks after NLRP3 stimulation. Thus, I am confident that lymphocytes can form NLRP1 inflammasomes after inhibition of DPP8/9, even though these responses are limited by the low expression of ASC.

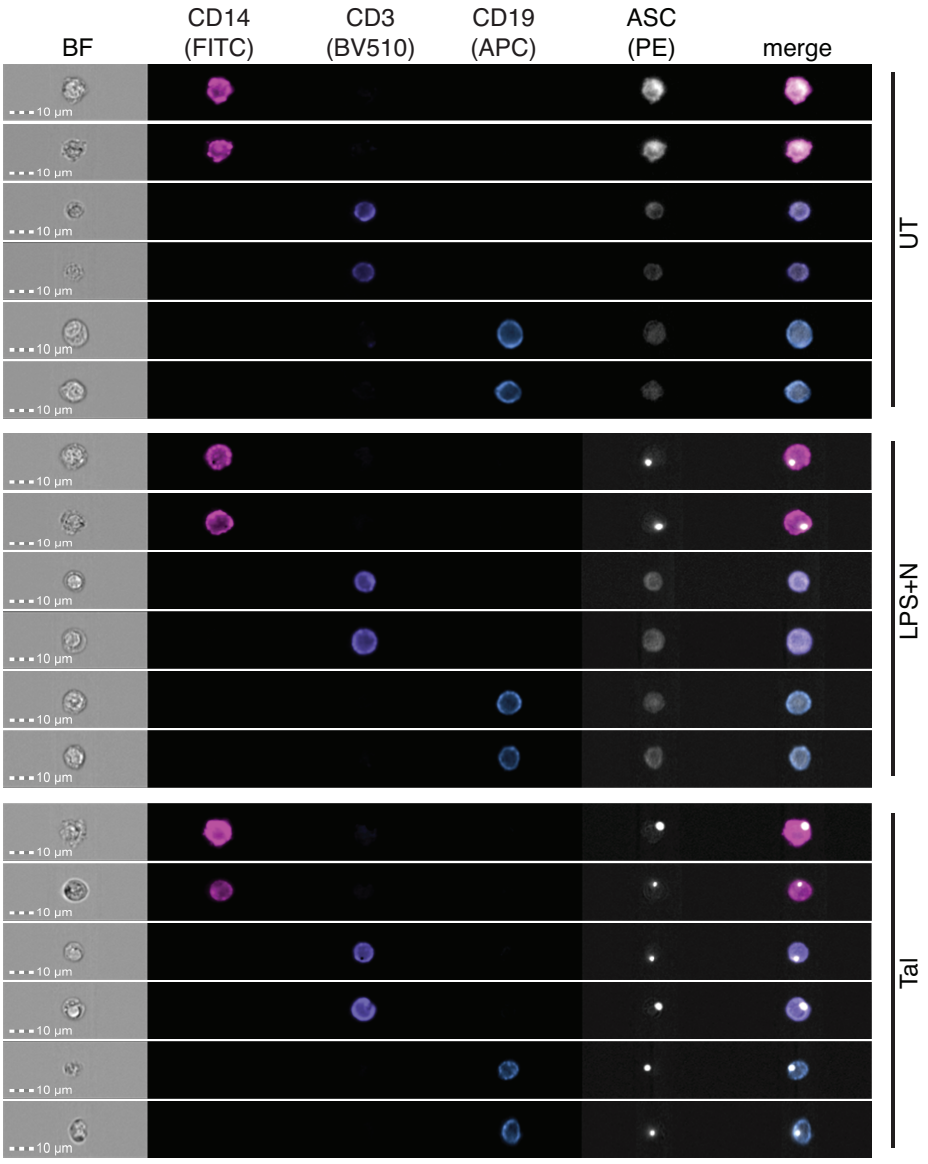

Figure 5.5: Validation of ASC speck assembly in lymphocytes after inhibition of DPP8/9 by imaging flow cytometry. Human PBMCs were isolated from fresh blood and stimulated with either 200 ng/mL LPS for 3 h and 10 µM Nig for 1 h, or 30 µM Tal for 24 h, or left untreated (UT). All stimulations were performed in the presence of caspase-1 inhibitor VX. PBMCs were stained for CD14+ monocytes, CD3+ T cells, or CD19+ B cells. Each sample was additionally stained for ASC to analyze ASC speck formation in the different subpopulations by imaging flow cytometry, as shown in the representative images. Images display experiment representatives of two independent experiments with cells from two different donors.

In summary, the analysis of ASC speck formation by staining endogenous ASC enabled me to study talabostat-induced NLRP1 inflammasome responses in PBMCs. I discovered

that lymphocytes can assemble NLRP1 inflammasomes, although their responses were limited by low ASC expression and did not induce notable IL-1β release.

5.2.2 Isolated T cells assemble NLRP1 inflammasomes after inhibition of DPP8/9

After the detection of NLRP1 inflammasome formation in lymphocytes, I focused my analyses on T cells, as they showed a more robust response after talabostat treatment than B cells, and because the functions of inflammasome assembly in T cells were still elusive. To test whether T cells need to be in contact with other PBMC subpopulations to initiate an inflammasome response, I isolated CD3+ T cells by negative selection and compared ASC speck formation in isolated T cells and PBMCs from the same donor (Fig. 5.6 A). For this, I compared different kits for T cell isolation and found that kits from StemCell provided consistent purities >98 % (Fig. 5.6 B,C). The kit retained the original T cell composition, except for NKT cells which were removed (data not shown).
T cells, either isolated or within the heterogeneous PBMC population, showed around 3 % ASC speck assembly following stimulation with talabostat (Fig. 5.6 D). Here again, nigericin failed to induce the formation of ASC specks in these cells. Thus, T cells do not need to be in contact with other cells to activate NLRP1 inflammasomes. Alongside, I analyzed the supernatants for IL-1β release (Fig. 5.6 E). As before, I detected robust IL-1β levels after NLRP3 stimulation and only weak IL-1β release after inhibition of DPP8/9 in PBMCs. Importantly, isolated T cells showed no signs of IL-1β release. Either the inflammasome responses after talabostat were too weak to induce the release of detectable amounts or (unprimed) T cells simply do not express pro-IL-1β.
Next, I stained the T cell markers CD4 and CD8 to test whether only CD4+ or CD8+ T cells assemble inflammasomes. I compared the distribution of CD4 and CD8 expression in all T cells with the distribution in ASC speck-forming T cells only (Fig. 5.6 F). Both CD4+ T cells and CD8+ T cells exhibited specks. Thus, the ability to activate NLRP1 inflammasomes is not restricted to CD4+ T helper cells.

All my analyses so far were based on lymphocytes isolated from blood. In addition, I was able to isolate lymphocytes from tonsils that had been removed from patients by surgery, allowing me to study cells from secondary lymphoid organs (Fig. 5.7 A). All analyzed

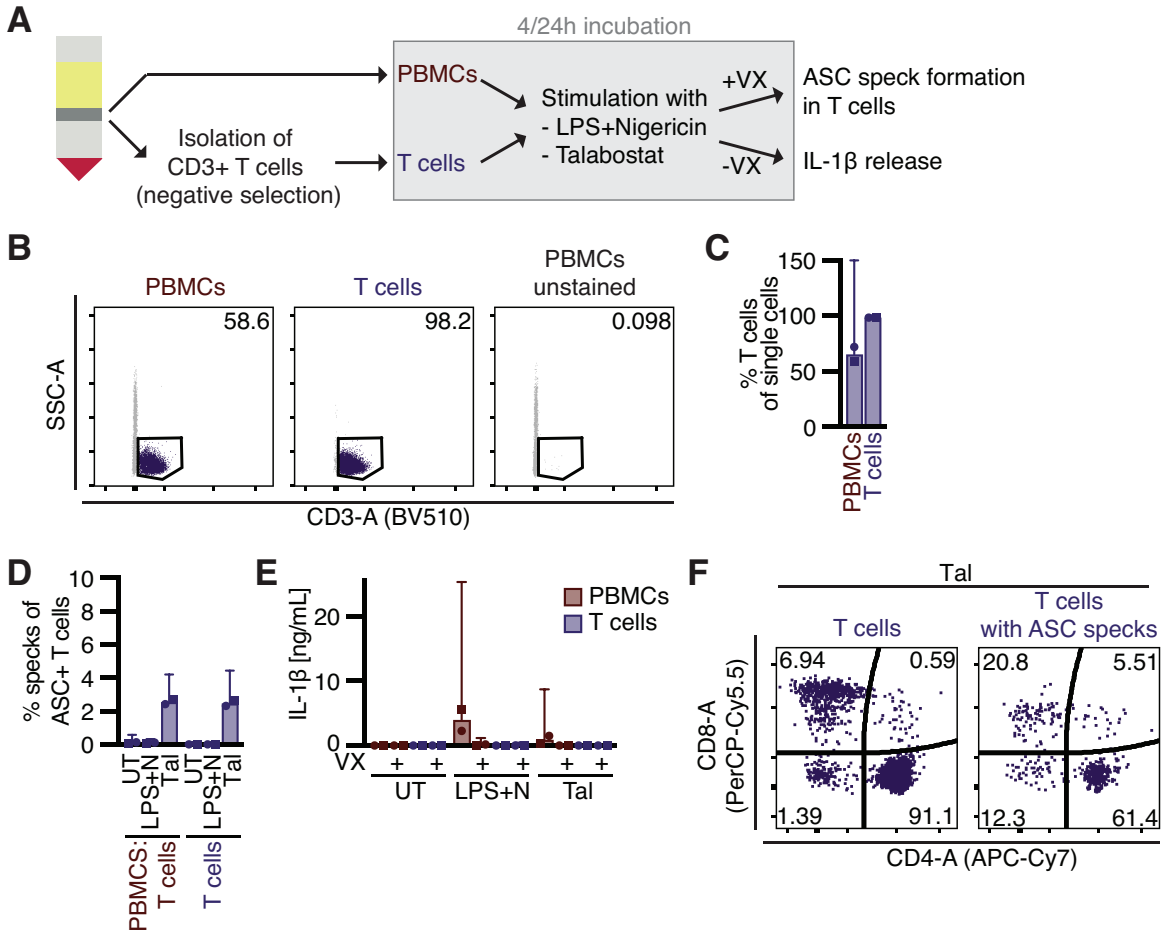

Figure 5.6: Isolated CD4+ and CD8+ T cells show ASC speck assembly after inhibition of DPP8/9. (**A**) Schematic overview of the experimental setup. Human PBMCs were isolated from fresh blood and CD3+ T cells were isolated from part of the cells. PBMCs and T cells were stimulated with either 200 ng/mL LPS for 3 h and 10 µM Nig for 1 h, or 30 µM Tal for 24 h, or left untreated (UT), where indicated in the presence of 100 µM VX. ASC speck formation was detected in the presence of caspase-1 inhibitor VX. (**B,C**) Expression of CD3 in freshly isolated PBMCs and T cells was quantified by flow cytometry to confirm successful isolation of T cells, as shown in the representative dot plots. (**D**) Stimulated PBMCs and T cells were stained for ASC and ASC speck formation in ASC+ T cells was quantified by flow cytometry, as shown in Fig. 5.4. (**E**) Supernatants from stimulated PBMCs and T cells were collected. IL-1β release was quantified by HTRF. (**F**) Representative dot plots show the expression of CD4 and CD8 in Tal-stimulated isolated T cells (all T cells or T cells with ASC specks only). Data represents average values (with individual data points) from two independent experiments with cells from two different donors ± 95 % CI.

tonsils contained around 70 % B cells and 30 % T cells, and the B cell/T cell ratios were stable throughout LPS/nigericin and talabostat stimulation (Fig. 5.7 B,C). Similar to the PBMC experiments, I stained endogenous ASC and analyzed ASC speck formation in

response to NLRP3 and NLRP1 stimulation. As before, I detected ASC speck assembly in talabostat-stimulated B and T cells, but no response in LPS/nigericin-stimulated lymphocytes (Fig. 5.7 E). The levels of ASC specks were as low as in lymphocytes isolated from blood, except for one donor. The cells from one tonsil preparation showed a remarkably high inflammasome response after talabostat stimulation, with 13 % of ASC-positive T cells and 8 % of ASC-positive B cells forming ASC specks (Fig. 5.7 D). It has

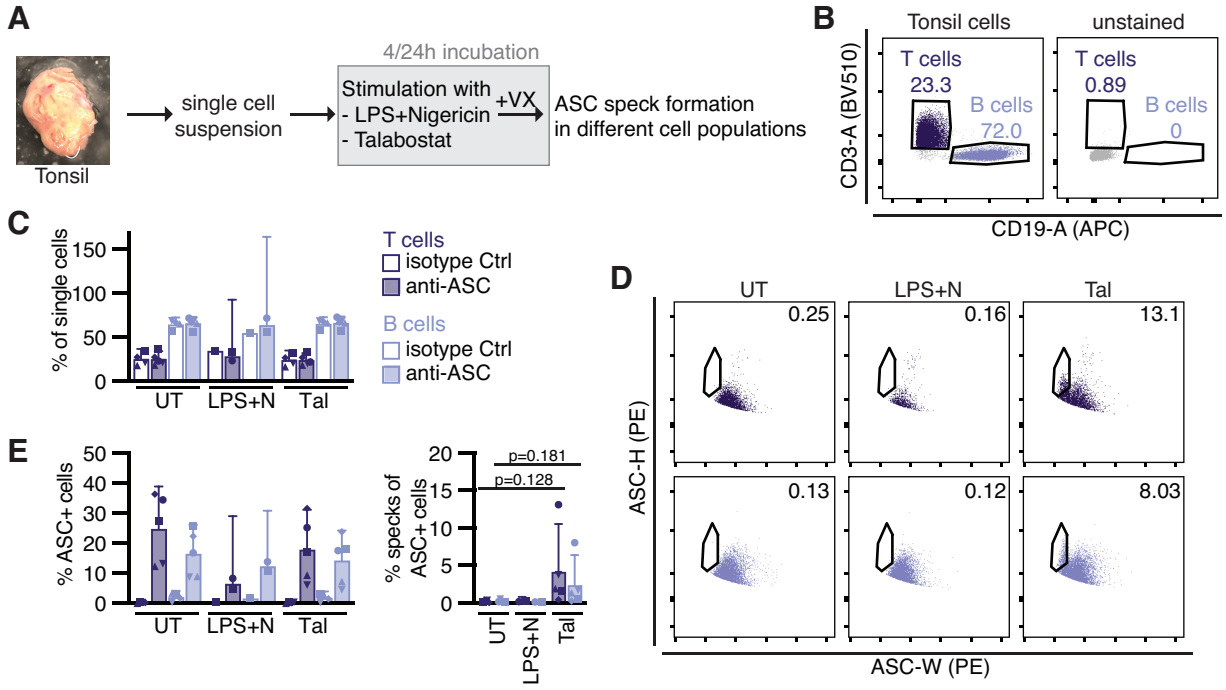

Figure 5.7: Tonsil-derived lymphocytes show ASC speck assembly after inhibition of DPP8/9. (**A**) Schematic overview of the experimental setup. Tonsil cells were isolated from surgically removed tonsils and stimulated with either 200 ng/mL LPS for 3 h and 10 µM Nig for 1 h, or 30 µM Tal for 24 h, or left untreated (UT). ASC speck formation was detected in the presence of caspase-1 inhibitor VX. (**B**) Tonsil cells were stained for CD3+ T cells and CD19+ B cells. Lymphocyte subpopulations were analyzed by flow cytometry, as shown in the representative dot plots. The plots show 24 h untreated cells. (**C**) T and B cells were quantified by flow cytometry, as described in (B). Each sample was additionally stained for ASC or with the corresponding isotype control (Ctrl) to analyze ASC speck formation in the different subpopulations. (**D**) ASC speck formation in ASC+ cells was analyzed by flow cytometry, as shown in the representative dot plots. (**E**) ASC expression and ASC speck formation in ASC+ cells were quantified by flow cytometry. Data represents average values (with individual data points) from one (LPS+Nig isotype control data in C,E), two (LPS+Nig anti-ASC data in C,E), or five independent experiments with cells from one, two, or five different donors ± 95 % CI, p-values were calculated using unpaired t-test.

to be mentioned that the ASC signals in tonsil-derived cells were partially compromised by strong autofluorescence, causing lower and more variable levels of ASC-expressing cells. Nevertheless, I confirmed that lymphocytes from secondary lymphoid organs can form inflammasomes after NLRP1 stimulation. The strong response in cells from one donor indicates that factors like the activation status or donor-specific mutations may boost NLRP1 inflammasome activation in these cells.

Thus, I could show that isolated T cells from both blood and secondary lymphoid organs form NLRP1 inflammasomes after inhibition of DPP8/9. Both CD4+ and CD8+ T cells are responsive, but they do not release detectable amounts of IL-1β.

5.2.3 Inflammasome reporter T cells enable further analyses of NLRP1 activation in T cells

So far, my analyses of inflammasome formation in lymphocytes were based on staining of endogenous ASC to detect ASC speck assembly. The staining revealed that these cells have a limited ASC expression, which complicated the analysis of ASC specks by flow cytometry. Thus, I decided to generate inflammasome reporter T cells that express the caspase-1^{CARD} (C1C)-EGFP reporter, as already used in N/TERT-1 keratinocytes (see chapters 2 and 3).

I isolated T cells by negative selection as described before, and stimulated them in plates coated with anti-CD3/anti-CD28 antibodies. After one day of stimulation, cells were lentivirally transduced to constitutively express C1C-EGFP. T cells were further cultivated in the presence of anti-CD3/anti-CD28 antibodies until robust C1C-EGFP expression was detected (Fig. 5.8 A). To validate these inflammasome reporter T cells, I additionally stained ASC as before and compared ASC staining specks and C1C-EGFP specks following talabostat treatment. I immediately noticed that the C1C-EGFP signal was a lot stronger than the endogenous ASC signal, offering a clearer separation between cells with and without specks (Fig. 5.8 B). This enabled the detection of higher frequencies of ASC speck-forming cells using the C1C-EGFP reporter (Fig. 5.8 C). Around 10 % of C1C-EGFP-positive T cells but only around 5 % of stained ASC-positive T cells assembled ASC specks after talabostat treatment. As the different levels of specks were detected in the same cells, this demonstrates the higher sensitivity of the C1C-EGFP reporter

compared to the weak ASC staining. As C1C-EGFP forms homotypic filaments nucleated by ASC^{CARD}, the number of C1C-EGFP molecules recruited to ASC specks is not limited by the absolute number of ASC molecules. This explains why a better signal-to-noise ratio could be achieved.

It is worth mentioning that stimulation of T cells with anti-CD3/anti-CD28 antibodies did not inhibit NLRP1 inflammasome activation, as shown for CARD8 inflammasomes (D. C. Johnson et al., 2020; Linder et al., 2020). Preliminary data even suggests that stimulation slightly increased NLRP1 inflammasome responses, but a clean comparison of unstimulated and stimulated T cells from the same donor will have to validate this observation.

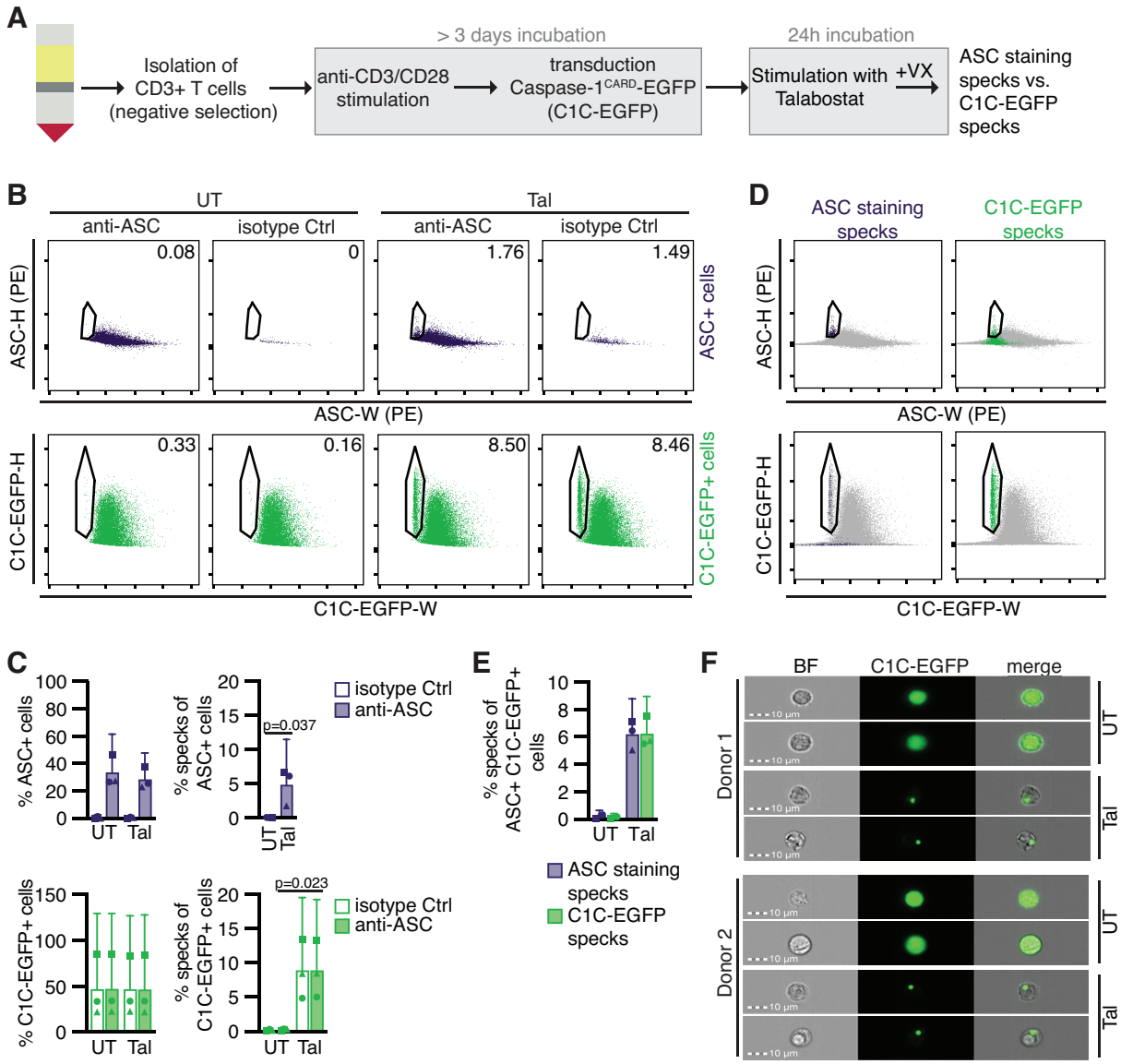

Figure 5.8: Inflammasome reporter T cells enable robust analysis of ASC speck assembly. (**A**) Schematic overview of the experimental setup. CD3+ T cells were isolated from fresh blood and stimulated with anti-CD3/CD28 antibodies. The next day, T cells were transduced with lentiviral vectors encoding the inflammasome reporter C1C-EGFP controlled by a constitutive promoter. After at least 48 h, reporter T cells were stimulated with 30 µM Tal for 24 h, or left untreated (UT). ASC speck formation was detected in the presence of caspase-1 inhibitor VX. (**B**) Reporter T cells were additionally stained for ASC, or with the corresponding isotype control (Ctrl), to compare ASC speck formation detected by staining and C1C-EGFP reporter. ASC speck formation in ASC+/C1C-EGFP+ cells was analyzed by flow cytometry, as shown in the representative dot plots. (**C**) ASC/C1C-EGFP expression and corresponding speck formation were quantified by flow cytometry. (**D**) Representative dot plots of comparison of ASC staining and C1C-EGFP specks in the contrary channels. (**E**) ASC speck formation in ASC+ C1C-EGFP+ cells was quantified by flow cytometry. (**F**) Representative images of reporter T cells analyzed by imaging flow cytometry. Data represents average values (with individual data points) from three independent experiments with cells from three different donors ± 95 % CI, p-values were calculated using unpaired t-test. Imaging flow cytometry images display representatives of one experiment with cells from two different donors.

The higher sensitivity of the C1C-EGFP reporter became even more apparent when I overlaid the stained ASC specks with C1C-EGFP specks and vice versa (Fig. 5.8 D). All cells with stained ASC specks that successfully expressed the inflammasome reporter coincided with the C1C-EGFP speck gate, confirming that reporter and staining detected the same ASC specks. In contrast, most of the cells with C1C-EGFP specks were found outside of the stained ASC speck gate, illustrating that the staining is not sensitive enough to detect all inflammasome-forming cells with my flow cytometry detection strategy. When I only analyzed cells that expressed the reporter and showed sufficient signal in ASC staining, the response rates were similar (Fig. 5.8 E), proving once again that the reporter indeed detects cells with ASC specks. Thus, C1C-EGFP reporter T cells enable a more sensitive analysis of inflammasome formation by overcoming the limitations of endogenous ASC staining. I also confirmed the characteristic ASC speck morphology in talabostat-treated C1C-EGFP-expressing T cells by imaging flow cytometry (Fig. 5.8 F).

After establishing the inflammasome reporter T cells, I aimed to identify additional properties that are characteristic of the inflammasome-forming cells. This would help to understand whether inflammasome activation is restricted to a certain T cell subpopulation and whether inflammasome formation is linked to other (inflammatory) pathways in these

cells. Therefore, I generated C1C-EGFP reporter T cells as described before. After stimulation with talabostat, C1C-EGFP-positive cells with and without ASC specks were sorted and their transcriptome was analyzed by bulk 3'-RNA sequencing (Fig. 5.9 A). Untreated reporter cells without ASC specks were similarly sorted and analyzed as a control. T cells from all donors assembled inflammasomes after inhibition of DPP8/9 (Fig. 5.9 B). The lower frequencies of ASC speck-forming cells are based on the stricter gating strategy used for sorting, which should ensure the clean sorting of responding cells only. Inflammasome-forming T cells indeed clustered completely separately in the transcriptome analysis (Fig. 5.9 C). ASC speck-forming T cells showed upregulation of 221 genes and downregulation of 60 genes in comparison to talabostat-treated cells without ASC specks. The latter group exhibited no difference to untreated reporter cells, highlighting that talabostat treatment has no transcriptomic effects on T cells that do not activate inflammasomes. The transcriptome analysis revealed that T cells indeed express NLRP1, ASC (PYCARD), and DPP8/9, demonstrating that the talabostat-induced inflammasome response can be based on NLRP1 activation (Fig. 5.9 D). Nevertheless, neither of these inflammasome components was unique to T cells with ASC specks, ruling out that ASC or NLRP1 expression determines the responsiveness of T cells. Other inflammasome sensors expressed in T cells were AIM2 and CARD8, but not NLRP3, in line with the undetectable inflammasome response after LPS and nigericin treatment. T cells also expressed caspase-1 (CASP1) and GSDMD, indicating that they can undergo pyroptosis downstream of inflammasome activation. Interestingly, T cells with ASC specks showed an increase in pyroptosis mediator NINJ1 transcripts.

When I analyzed the transcriptome data of cytokines and chemokines, I was surprised to see that T cells with ASC specks had increased expression levels of proinflammatory cytokines like IFN-γ (IFNG), TNF-α (TNF), and LT-α (LTA) (Fig. 5.9 E). This was not the case for all cytokines, as for example IL-16 transcript levels were similar in all sorted T cell subsets. In line with the undetectable IL-1β release from T cells, transcriptional expression of this cytokine was also undetectable. Next to increased cytokine expression, chemokines like CCL3-5 were also upregulated in T cells with ASC specks on a transcriptional level.

Next, I checked the transcriptome data of different T cell markers to see whether NLRP1 inflammasome activation is restricted to a certain T cell subpopulation (Mousset et al.,

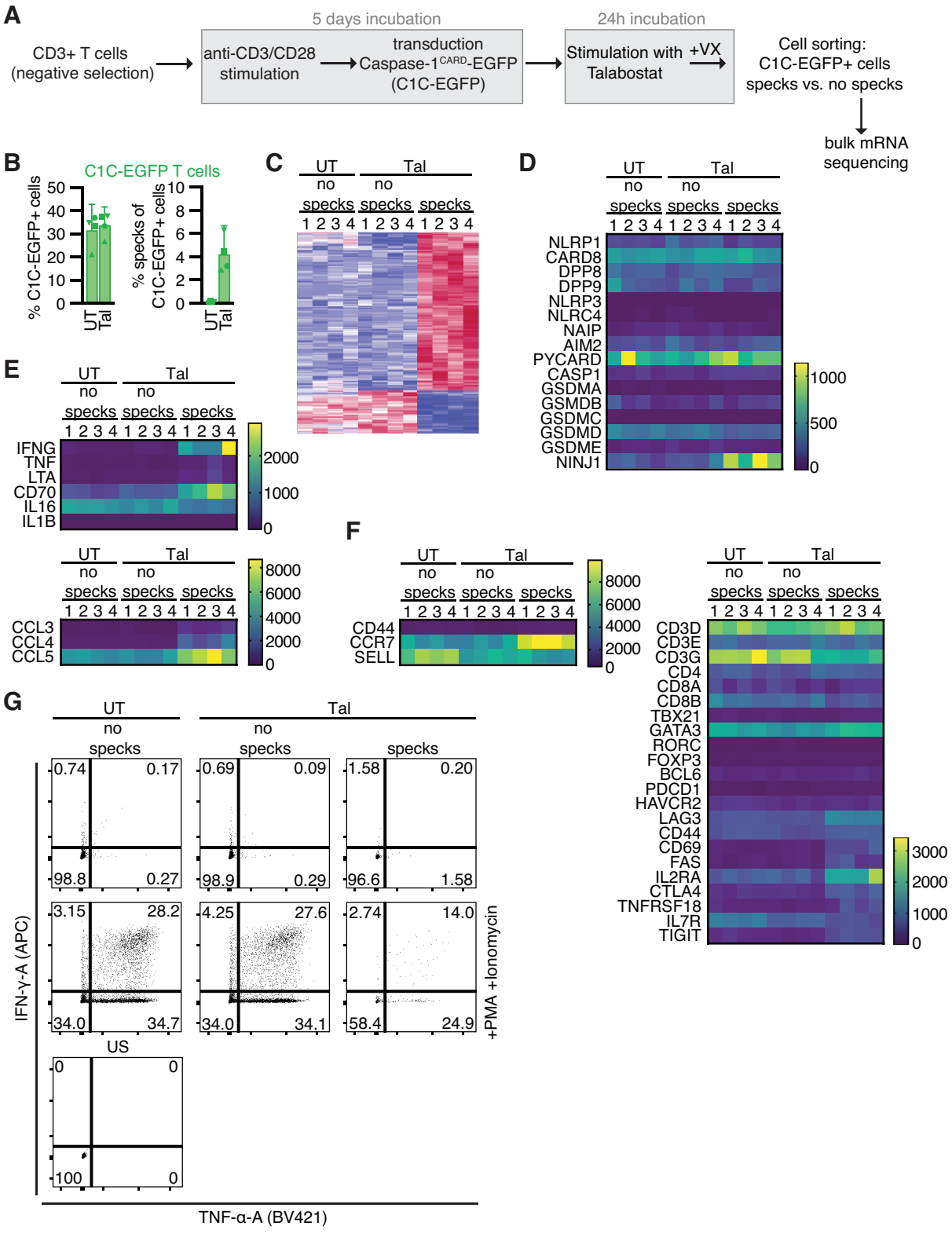

Figure 5.9: Inflammasome-forming reporter T cells show no clear phenotype in transcriptome analysis. (**A**) Schematic overview of the experimental setup. CD3+ T cells were isolated from fresh blood, stimulated with anti-CD3/CD28 antibodies, and transduced with lentiviral vectors encoding the inflammasome reporter C1C-EGFP controlled by a constitutive promoter. After 5 days, reporter T cells were stimulated with 30 µM Tal for 24 h, or left untreated (UT), all in the presence of caspase-1 inhibitor VX. C1C-EGFP+ cells with and without specks were sorted and analyzed by bulk 3'-RNA sequencing. (**B**) C1C-EGFP expression and ASC speck formation in C1C-EGFP+ T cells for all sorted donors. (**C**) Heatmap overview of upregulated and downregulated genes in the sorted T cell fractions (**D-F**) Heatmap of expression levels of selected inflammasome-related genes (D), cytokines and chemokines (E), and T cell-related genes (F) in the sorted T cell fractions of all donors. (**G**) Reporter T cells were stimulated with 30 µM Tal for 24 h and/or 50 ng/mL PMA + 1 µg/mL ionomycin for 5 h. Cells were stained for IFN-γ and TNF-α, and cytokine expression in cells with and without ASC specks was analyzed by flow cytometry, as shown in the dot plots. Sequencing data represents average values with individual data points ± 95 % CI (B) or single values for each donor (C-F) from two independent experiments with cells from four different donors. Flow cytometry dot plots in (G) display values from one experiment.

2019). In line with my flow cytometry data, T cells with ASC specks expressed both CD4 or CD8 markers in the transcriptome analysis (Fig. 5.9 F). The most strongly expressed T helper subset transcription factor was GATA-3 and expression levels were similar for all sorted groups. T cells with ASC specks had increased transcript levels of LAG3, but other T cell exhaustion markers like PD-1 (PDCD1) and Tim3 (HAVCR2) were unchanged. All T cells showed high levels of CCR7 and CD62L (SELL), and low levels of CD44 transcripts, demonstrating that the anti-CD3/anti-CD28 stimulation did not lead to a full effector T cell phenotype. Nevertheless, T cells with ASC specks presented slightly upregulated CD69 and CD95 (FAS) levels, indicating a more effector-like phenotype. Interestingly, I observed a transcriptomic profile that is reminiscent of regulatory T (T_{reg}) cells in ASC speck-forming T cells, showing upregulation of CD25 (IL2RA), CTLA-4, GITR (TNFRSF18), and TIGIT, as well as downregulation of CD127 (IL7R) (Trzupek et al., 2020).

As I observed upregulation of different cytokine and chemokine transcripts in T cells with ASC specks, I tried to confirm the transcriptome data by detecting the cytokines IFN-γ and TNF-α on protein level using flow cytometry. As the IFN-γ transcripts were strongly upregulated in inflammasome-forming T cells, this increase should be detectable on protein level as well. I stimulated inflammasome reporter T cells with talabostat in the

presence of a Golgi protein transport inhibitor for the last 5 h of stimulation to accumulate intracellular cytokines. As a positive control, T cells were additionally stimulated with phorbol myristate acetate (PMA) and ionomycin. Analysis of cytokine levels by flow cytometry revealed that T cells with ASC specks showed no intracellular IFN-γ or TNF-α (Fig. 5.9 G). Additional stimulation with PMA and ionomycin induced IFN-γ and/or TNF-α expression in all T cells, but the response was unchanged in inflammasome-forming cells. I also analyzed the expression of surface markers like CD25 and CTLA-4, which were upregulated on the transcriptional level, but I did not detect differences between T cells with and without ASC specks (data not shown). Thus, the upregulation of certain cytokines, chemokines, and surface markers on only transcriptional levels represents probably just an artifact caused by prolonged inflammasome activation in the presence of caspase-1 inhibitor and thereby inhibited pyroptosis. The inflammasome-forming T cells probably initiated apoptosis, as it was reported that caspase-8 is activated on ASC specks in cells unable to undergo pyroptosis (Mascarenhas et al., 2017; Sagulenko et al., 2013). This effect made it difficult to distinguish, if transcriptional profiles of inflammasome-forming cells define the NLRP1-responsive T cell subpopulation or whether they are a consequence of inflammasome formation in the presence of caspase-1 inhibitor itself.

Although the transcriptome analysis did not provide the anticipated characteristics of inflammasome-forming T cells, I still wanted to explore potential biological functions of inflammasomes in T cells. For this, I screened additional NLRP1 as well as T cell-specific stimuli using the C1C-EGFP-expressing reporter T cells (Fig. 5.10). I first tested NLRP1 activation by the RSR following treatment with anisomycin and lactimidomycin, but this failed to induce inflammasome activation in the reporter cells. Furthermore, the T cells were not infected by SFV or RVA SA11-4F, excluding NLRP1 activation by these viruses. Next, I stimulated the T cells with PMA and ionomycin (Iono), as well as increasing concentrations of anti-CD3/anti-CD28 antibodies. None of these stimulations induced inflammasome formation, suggesting that the tested T cell stimulations are not associated with inflammasome activation.

Altogether, the generation of C1C-EGFP-expressing reporter T cells enabled the more sensitive detection of ASC specks compared to staining endogenous ASC. Moreover,

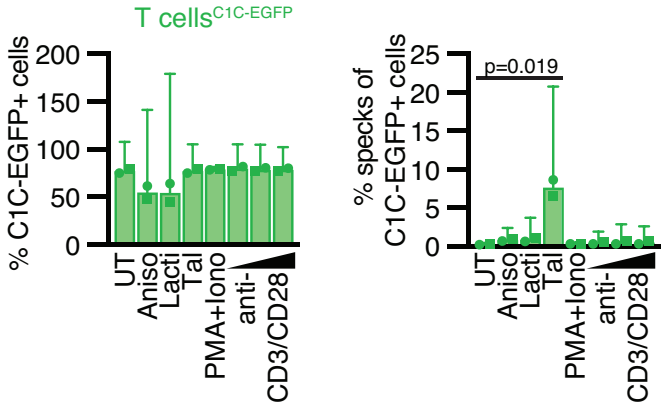

Figure 5.10: Inflammasome reporter T cells show no inflammasome assembly after induction of the ribotoxic stress reponse. CD3+ T cells were isolated from fresh blood, stimulated with anti-CD3/CD28 antibodies, and transduced with lentiviral vectors encoding the inflammasome reporter C1C-EGFP controlled by a constitutive promoter. Reporter T cells were stimulated with 15 µM Aniso, 2.5 µM Lacti, 30 µM Tal, 50 ng/mL PMA + 1 µg/mL ionomycin (Iono), or left untreated (UT) for 20 h. Cells were also stimulated with 2/4, 10/20, or 20/40 µg/mL anti-CD3/CD28 antibodies for 48-90 h. All stimulations were performed in the presence of caspase-1 inhibitor VX. C1C-EGFP expression and ASC speck formation in C1C-EGFP+ T cells were quantified by flow cytometry, as shown in Fig. 5.8. Data represents average values (with individual data points) from two independent experiments with cells from the same donor ± 95 % CI, p-values were calculated using unpaired t-test.

inflammasome reporter T cells allowed easy screening of potential inflammasome stimuli, revealing no NLRP1 activation by RSR and T cell stimulation. I was able to specifically sort inflammasome-forming reporter cells and the transcriptome analysis revealed altered expression of 281 genes in these cells. T cells with ASC specks showed upregulation of different cytokines, chemokines, and surface markers but protein stainings for some of the hits did not confirm increased expression on protein level. The transcriptional changes are probably caused by prolonged inflammasome activation in cells that cannot undergo pyroptosis, leading to the activation of caspase-8 and the initiation of apoptosis.

5.2.4 Targeted ubiquitination of NLRP1^{PYD} by VHL-VHH$_{PYD}$ induces inflammasome formation and pyroptosis in T cells

The only way to stimulate NLRP1 inflammasomes in T cells so far was treatment with talabostat, which still leaves some doubts about the specificity of the response, as inhibition of DPP8/9 stimulates CARD8 as well. T cells did not respond to anisomycin and

lactimidomycin, and could not be infected by NLRP1-activating viruses. Therefore, I decided to use the VHL-VHH$_{PYD}$ system again, which is the cleanest way to specifically stimulate NLRP1. As before, I transduced anti-CD3/anti-CD28-stimulated T cells with constructs expressing C1C-EGFP as well as VHHs or VHL-VHH fusions under the control of a bidirectional doxycycline-inducible promoter, the same constructs that were already successfully used for the generation of N/TERT-1 cell lines (see chapter 2). Expression of (VHL-)VHH was induced and ASC speck formation was analyzed in the presence or absence of caspase-1 inhibitor Vx-765 by flow cytometry (Fig. 5.11 A). With these experiments, I also aimed to test whether T cells undergo caspase-1-dependent pyroptosis after inflammasome activation. In fact, the transcriptome analysis indicated that T cells express caspase-1 and GSDMD and therefore all the necessary components for pyroptosis.

Already 4 h after doxycycline induction, I detected C1C-EGFP expression in T cells co-expressing VHL-VHH$_{NP-1}$ and VHL-VHH$_{PYD\ 1}$, and expression levels increased similarly for both nanobody fusions over time (Fig. 5.11 B). When I checked ASC speck formation in these cells, only T cells expressing VHL-VHH$_{PYD\ 1}$ showed robust ASC speck assembly starting already 4 h post-induction (Fig. 5.11 C). The inflammasome response was significantly stronger than after talabostat treatment with nearly 30 % of the C1C-EGFP-expressing T cells forming ASC specks 14 h post-induction. Analysis of ASC speck formation after 8 h doxycycline induction revealed NLRP1 activation by VHL-VHH$_{PYD\ 2}$ as well, even though the response was lower compared to VHL-VHH$_{PYD\ 1}$, in line with observations in N/TERT-1 keratinocytes (Fig. 5.11 D). Neither of the VHL-VHH$_{PYD}$ fusions yielded detectable inflammasome-forming cells in the absence of Vx-765. Likewise, when T cells were transduced with lentiviral vectors expressing VHL-VHH$_{PYD\ 1}$, a smaller fraction of C1C-EGFP-positive cells was detected when caspase-1 was not inhibited. Both findings indicate that the NLRP1-activating T cells indeed undergo caspase-1-dependent pyroptotic cell death, causing their loss during the sample preparation process. Importantly, expression of VHL-VHH$_{NP-1}$ and VHH$_{PYD}$ alone did not stimulate inflammasome activation. Independent of the co-expressed (VHL-)VHH, all T cells showed ASC speck formation after stimulation with talabostat, confirming the functionality of the C1C-EGFP reporter. Expression of both VHL-VHH$_{PYD}$ increased the weak

talabostat-induced inflammasome response to more than 20 % ASC speck assembly in C1C-EGFP-positive T cells.

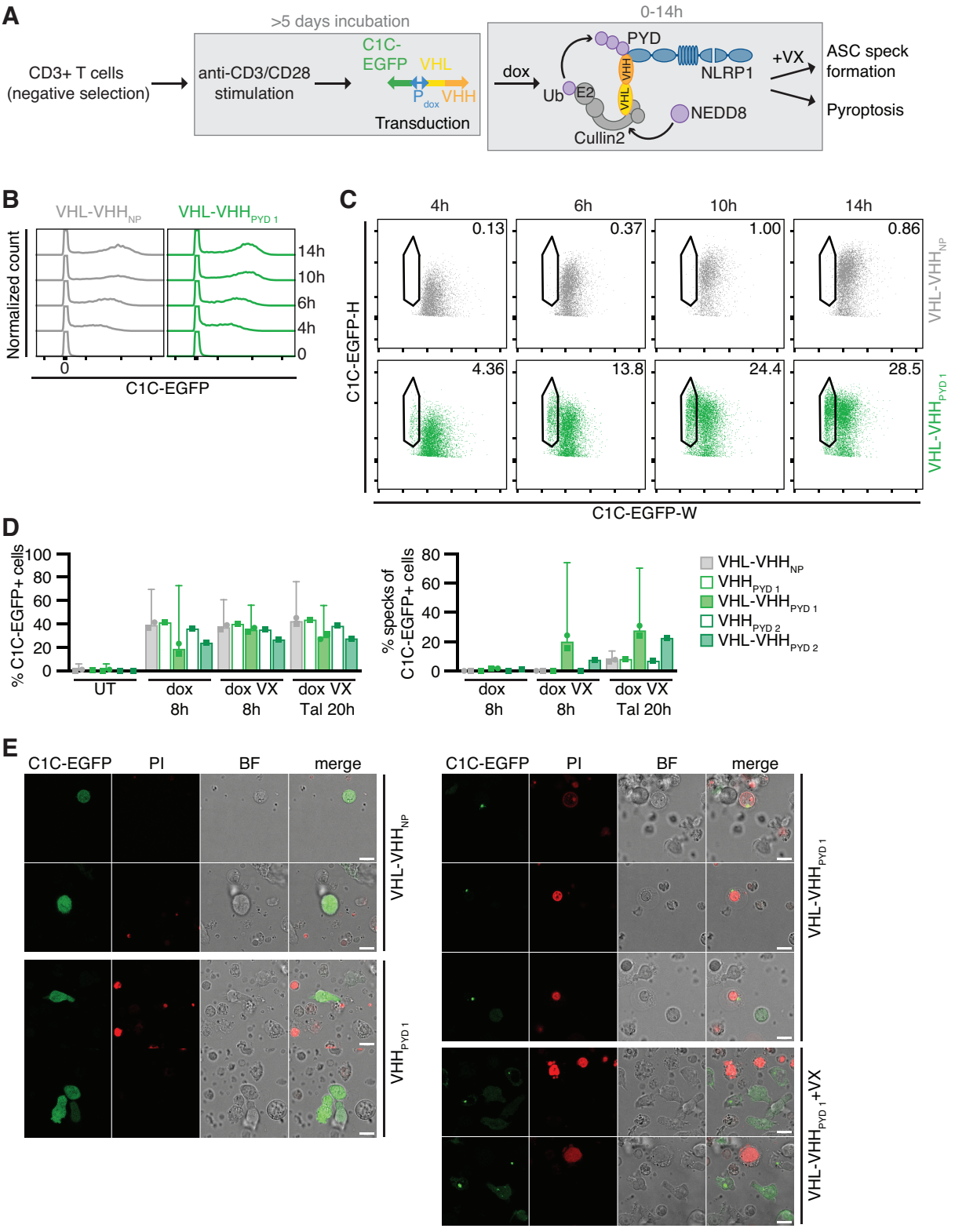

Figure 5.11: Targeted ubiquitination of NLRP1^{PYD} by VHL-VHH$_{PYD}$ induces inflammasome assembly and pyroptosis in T cells. (**A**) Schematic overview of the experimental setup. CD3+ T cells were isolated from fresh blood, stimulated with anti-CD3/CD28 antibodies, and transduced with lentiviral vectors encoding C1C-EGFP and (VHL)-VHH controlled by a bidirectional dox-inducible promoter, as described in Fig. 2.5. Cells were treated with 1 µg/mL dox to induce expression. ASC speck formation was detected in the presence of caspase-1 inhibitor VX. (**B,C**) T cells, encoding the indicated VHL-VHH fusions, were treated with dox for 0-14 h. C1C-EGFP expression (B) and ASC speck formation in C1C-EGFP+ cells (C) were quantified over time by flow cytometry, as shown in the histograms and dot plots. (**D**) T cells, encoding the indicated VHL-VHH fusions or VHHs alone, were treated with dox, or left untreated (UT) for 8 h, where indicated in the presence of 100 µM VX. Cells stimulated with dox, 30 µM Tal and VX for 24 h served as control. C1C-EGFP expression and ASC speck formation in C1C-EGFP+ cells were quantified by flow cytometry, as shown in (B,C). (**E**) T cells, encoding the indicated VHL-VHH fusions or VHHs alone, were treated with dox for 6 h, where indicated in the presence of VX. ASC speck formation and pyroptosis were analyzed by live-cell confocal fluorescence microscopy. The medium contained non-cell permeable DNA dye propidium iodide (PI). Scale bars represent 10 µm. Data represents (average) values with individual data points (± 95 % CI) from one (VHH$_{PYD\ 1}$, VHH$_{PYD\ 2}$, VHL-VHH$_{PYD\ 2}$ data in D) or two (VHL-VHH$_{NP}$, VHL-VHH$_{PYD\ 1}$ data in D) independent experiments with cells from one or two donors. Flow cytometry dot plots in (B,C) display values from one experiment. Microscopy images originate from one experiment.

To confirm that VHL-VHH$_{PYD}$-expressing T cells indeed undergo pyroptosis, I analyzed the cells by microscopy in the presence or absence of caspase-1 inhibitor. T cells expressing VHL-VHH$_{NP-1}$ and VHH$_{PYD\ 1}$ showed evenly distributed C1C-EGFP expression and regular morphology (Fig. 5.11 E). In contrast, T cells expressing VHL-VHH$_{PYD\ 1}$ not only formed ASC specks but also had the characteristic ballooning phenotype of pyroptotic cells. Pyroptosis was completely inhibited in the presence of Vx-765.

Thus, targeted ubiquitination of NLRP1^{PYD} by VHL-VHH$_{PYD}$ induces inflammasome formation in T cells. The NLRP1 response is a lot stronger than after inhibition of DPP8/9, suggesting that a large fraction of T cells can actually form inflammasomes and that responsiveness is not limited to a small subpopulation of T cells. NLRP1 activation in T cells induces caspase-1-dependent pyroptosis, highlighting that NLRP1 inflammasome formation can have relevant consequences in a physiological setting.

5.3 Discussion

I detected inflammasome responses in primary human blood cells by staining endogenous ASC and analyzing inflammasome formation in different PBMC cell subsets by flow cytometry. I focused on the analysis of NLRP1 inflammasomes but I also stimulated NLRP3 as a control. I will first discuss the observed NLRP1 and NLRP3 responses in different cell types, before I specifically discuss the formation of NLRP1 inflammasomes in T cells.

Monocytes are the major NLRP3-competent PBMC subpopulation

Inflammasome responses in primary human blood cells were already analyzed by flow cytometry, but with a focus on NLRP3 inflammasomes in monocytes (Lage et al., 2019; Nagar et al., 2019; Sester et al., 2015). In line with these studies, I found that mostly monocytes form NLRP3 inflammasomes and release IL-1β after stimulation with LPS and nigericin. Depletion of CD14+ monocytes strongly reduced both inflammasome readouts, confirming that monocytes form the major NLRP3-competent PBMC subpopulation. However, stimulation of PBMCs with LPS and nigericin led to a loss of CD14+ monocytes, an observation that was also reported after LPS and ATP stimulation (Sester et al., 2015). Moreover, the remaining CD14+ monocytes showed reduced ASC expression. Thus, although most residual ASC-positive monocytes formed NLRP3 inflammasomes, this cannot explain the dominant monocyte-dependent response seen in the depletion experiments. It was shown that LPS-induced stimulation of CD14 leads to TLR4 internalization, thus CD14 might be internalized after LPS treatment as well (Kim & Kim, 2014; Zanoni et al., 2011). In line with the concomitant increase in CD14- HLA-DR+ cells, some of the CD14- monocytes are probably found in this population after LPS/nigericin stimulation, as they also showed a strong NLRP3 inflammasome response. A similar loss of CD14 expression and differentiation of monocytes into a more DC-like phenotype was reported after different viral infections (W. Hou et al., 2012). The remaining CD14- monocytes are probably found in ungated cell populations like non-classical monocytes which feature low CD14 but high CD16 expression levels (Zawada et al., 2012; Ziegler-Heitbrock, 2015). Monocyte- and DC-specific stainings could help to distinguish different

monocyte and DC subsets to understand the relation and differentiation of these populations after NLRP3 stimulation (Carenza et al., 2021; Thomas et al., 2017).

Lymphocytes assemble NLRP1 inflammasomes after inhibition of DPP8/9

I stimulated PBMCs with talabostat to induce NLRP1 activation by inhibition of DPP8/9. This mode of activation is well described and the treatment itself was not toxic in the N/TERT-1 experiments. In contrast, all of the RSR stimuli induced apoptosis at some point, which would complicate the analysis of NLRP1 activation. The cleanest way to specifically stimulate NLRP1 would be the VHL-VHH_{PYD} system, but cells would have to be transfected or transduced to achieve expression of the constructs in the cytosol. As these processes probably would have to be optimized for every analyzed cell type, the VHL-VHH_{PYD} system is not suitable for a screening of a mixture of cells like PBMCs.

Talabostat causes activation of CARD8 as well (D. C. Johnson et al., 2018) but detection of ASC specks allows to distinguish between the two inflammasome sensors, as active CARD8 cannot nucleate ASC specks (Ball et al., 2020; Gong et al., 2021). I observed robust inflammasome assembly in PBMCs after stimulation with talabostat. Inflammasome responses were lower than after NLRP3 stimulation, but the levels of ASC speck-forming cells were unchanged in monocyte-depleted PBMCs. This already implied that monocytes are not the main cell type to form inflammasomes after stimulation of NLRP1. Surprisingly, the analysis of inflammasome-forming cell subsets revealed that talabostat causes weak but robust ASC speck assembly in lymphocytes. Around 2 % of ASC-positive B cells and 3 % of ASC-positive T cells showed inflammasome formation. As T cells are the dominant subpopulation of PBMCs, they represented 15 % of all cells with ASC specks after inhibition of DPP8/9. Compared to monocytes and DCs, lymphocytes expressed only low levels of ASC in only a fraction of the cells and they did not respond to NLRP3 stimulation at all. I confirmed my observations in lymphocytes from secondary lymphoid tonsil tissue, which also formed inflammasomes after NLRP1 but not NLRP3 stimulation, similar to PBMC-derived lymphocytes. Tonsil-derived lymphocytes from one donor even showed increased inflammasome assembly after talabostat stimulation.

Stimulation of primary human T cells with talabostat causes CARD8-dependent pyroptosis (D. C. Johnson et al., 2020; Linder et al., 2020) which can induce NLRP3 activation by

following potassium efflux from the pyroptotic cell (Rühl & Broz, 2015; Schmid-Burgk et al., 2015). However, in my assays, the cells cannot undergo CARD8-mediated pyroptosis, as they were stimulated in the presence of caspase-1 inhibitors to prevent the loss of fragile pyroptotic cells during the harvesting process. Moreover, the observed inflammasome response was unchanged in the presence of NLRP3 inhibitors, excluding the possibility of CARD8-mediated NLRP3 activation. Most importantly, I confirmed NLRP1 inflammasome assembly in human T cells by specifically activating NLRP1 in isolated T cells using the VHL-VHH_{PYD} system. Targeted ubiquitination of NLRP1 by VHL-VHH_{PYD} revealed that human T cells can assemble functional NLRP1 inflammasomes, causing caspase-1-dependent pyroptotic cell death. Similar to the experiments in HEK 293T and N/TERT-1 cells, expression of VHL-VHH_{PYD} induced a much stronger NLRP1 response than talabostat, revealing that a large fraction of stimulated T cells can form functional NLRP1 inflammasomes. To my knowledge, this is the first report about NLRP1 inflammasomes in human T and B cells. The only record of NLRP1 in T cells describes murine Nlrp1 as a negative regulator of Th17 differentiation in the context of type 1 diabetes, independent of its functions as an inflammasome sensor (Costa et al., 2021). Johnson et al. observed talabostat-induced pyroptosis in primary human B cells, but they did not further analyze this phenomenon (D. C. Johnson et al., 2020). Therefore, it is impossible to tell whether pyroptosis was CARD8- or NLRP1-dependent. Expression of the proposed NLRP1 stimulus KSHV ORF45 in the BJAB B cell line induced pyroptosis as well (X. Yang et al., 2022). Yang et al. confirmed NLRP1 expression in this cell line, but there was no validation of functional NLRP1 inflammasomes.

I observed talabostat-induced NLRP1 but not LPS/nigericin-induced NLRP3 activation in blood- and tonsil-derived lymphocytes. Similarly, Sester et al. reported a lack of NLRP3 inflammasome activation after LPS and ATP stimulation in CD14- PBMCs (Sester et al., 2015). In line with my observations, it was reported that human T and B cells express NLRP1, but no or only low levels of NLRP3 (K. W. Chen et al., 2014; Kummer et al., 2007; Lech et al., 2010). Petterson et al. showed NLRP3 in immunohistochemical stainings of tonsillar T cells but they did not validate the used antibody (Petterson et al., 2011). However, there are some reports about functional NLRP3 inflammasomes in both B cells

and T cells. Human blood memory B cells release IL-1β and IgM in an NLRP3-dependent manner after stimulation with fungal β-glucan (Ali et al., 2017). Lim et al. found that B cell-activating factor signaling induces NLRP3 inflammasome formation in primary human B cells (Lim et al., 2020). And murine peritoneal B1a cells undergo Nlrp3-dependent pyroptosis after *Coxiella burnetii* infection (Schoenlaub et al., 2016). Thus, NLRP3 activation in B cells might require a different stimulation than LPS/nigericin. Certain B cell subsets may further not be (abundantly) present in the cell preparations that I analyzed. Regarding NLRP3 inflammasomes in T cells, it was reported that a distinct Th17 subset forms NLRP3 inflammasomes without additional stimulation to release IL-1α in a caspase-1- and GSDMD-independent manner (Chao et al., 2023). Arbore et al. described autocrine NLRP3-dependent IL-1β as a critical factor in Th1 differentiation, but their ASC stainings show no ASC speck formation and they prove IL-1β processing by intracellular cytokine staining only (Arbore et al., 2016). And, as suggested by other studies, NLRP3 might influence T cell differentiation independent of inflammasome formation (Bruchard et al., 2015; Javanmard Khameneh et al., 2019; S.-H. Park et al., 2019). In a murine experimental autoimmune encephalomyelitis model, autocrine Nlrp3- and caspase-8-dependent IL-1β stimulation was similarly reported as a critical factor in Th17 differentiation, and Nlrp3-deficient Th17 cells showed inhibited IL-1β release after ATP stimulation (Martin et al., 2016). Knockout and inhibition of Nlrp3 also impaired humoral responses in mice, and Zhao et al. propose that this is due to the inhibition of autocrine Nlrp3-dependent IL-1β release by T follicular helper cells (Z. Zhao et al., 2022). However, human and murine T cells might not be that comparable, as LPS leads to upregulation of Nlrp3 in murine T cells which was not observed for human T cells (Lech et al., 2010). Thus, at least for human T cells, there is no convincing proof of functional canonical NLRP3 inflammasomes.

Even though I detected robust and partially lymphocyte-based inflammasome assembly in monocyte-depleted PBMCs after stimulation with talabostat, concomitant IL-1β release was critically dependent on monocytes. Thus, lymphocytes and other non-monocyte cells that activate NLRP1 after talabostat treatment probably do not express pro-IL-1β under the conditions of my assay. This is in line with reports that monocytes are the primary

source of IL-1β after inflammasome activation in blood cells (Dinarello, 2009; Tran et al., 2019). The IL-1β levels after talabostat treatment were also low compared to LPS/nigericin stimulation, highlighting the importance of priming to upregulate pro-IL-1β. Unprimed PBMCs show low levels of pro-IL-1β (Puren et al., 1999), and therefore Zhong et al. were able to increase talabostat-induced IL-1β release by LPS pretreatment (Zhong et al., 2018). Thus, lymphocytes and other non-monocyte cells that activate NLRP1 might be able to release IL-1β after certain priming treatments.

Competition of NLRP1 and CARD8 inflammasomes

Although talabostat-induced inflammasome assembly in PBMCs was independent of NLRP3, talabostat-induced IL-1β release was strongly suppressed in the presence of NLRP3 inhibitors. Thus, inhibition of DPP8/9 causes not NLRP1- but NLRP3-dependent IL-1β release by monocytes. This suggests that talabostat causes CARD8-dependent pyroptosis of monocytes, inducing subsequent NLRP3 activation by potassium efflux (Rühl & Broz, 2015; Schmid-Burgk et al., 2015). Zhong et al. reported NLRP1-mediated IL-1β release by talabostat-treated PBMCs but they did not control for NLRP3 with a specific inhibitor (Zhong et al., 2018). Moreover, PBMCs undergo pyroptosis after talabostat stimulation, justifying pyroptosis-mediated NLRP3 activation (Okondo et al., 2017).

Talabostat treatment induced NLRP1 inflammasome assembly in around 10 % of ASC-positive monocytes, raising the question why most of the IL-1β release depends on CARD8-mediated NLRP3 activation. To analyze ASC speck formation by flow cytometry, the cells have to be stimulated in the presence of caspase-1 inhibitors to prevent the loss of pyroptotic cells. As this prevents CARD8-mediated pyroptosis, the observed NLRP1-mediated inflammasome response might be outperformed by CARD8-induced pyroptosis under regular conditions. This would also explain why others observed no role of NLRP1-mediated pyroptosis in talabostat-treated human T cells (D. C. Johnson et al., 2020; Linder et al., 2020), whereas I showed NLRP1 inflammasome assembly in talabostat-treated and caspase-1-inhibited T cells. These observations imply that CARD8 may dominate NLRP1 in cells that express and activate both inflammasomes. This is in line with reports about the monocytic THP-1 cell line, which also undergoes primarily CARD8-dependent

pyroptosis after talabostat stimulation, even though they express some NLRP1 (D. C. Johnson et al., 2018; X. Yang et al., 2022). Similar observations were made in primary human aortic endothelial cells which also express both inflammasome sensors. Infection of these cells with Coxsackie virus B3 induced CARD8-dependent pyroptosis, although the viral 3C protease induces N-terminal cleavage and degradation of NLRP1 (Nadkarni et al., 2022). One explanation for all these observations would be that CARD8 directly suppresses NLRP1 activation, whenever both sensors are activated in parallel. In line with this hypothesis, it was described that the CARD8 T60 isoform binds to NLRP1, which leads to the inhibition of NLRP1 activation in HEK 293T cells (Z. Xu et al., 2022). Before CARD8 was described as an inflammasome sensor, different studies suggested that CARD8 binds and regulates NLRP3 (Agostini et al., 2004; Ito et al., 2014; Mao et al., 2018), thus it is possible that CARD8 has regulatory functions as well. Another explanation would be that NLRP1 has a higher threshold of activation compared to CARD8, which was proposed by others as well (Q. Wang et al., 2023). It sounds logical to regulate NLRP1 activity more strictly, as ASC-dependent NLRP1 inflammasomes cause not only pyroptosis but also the release of proinflammatory cytokines. Interestingly, TCR-stimulated T cells do not activate CARD8 after talabostat stimulation but I still observe NLRP1 inflammasome formation in these cells. Johnson et al. hypothesize that T cell stimulation leads to less CARD8 autoproteolysis, which is why talabostat-induced pyroptosis is inhibited. Moreover, the immunoblots of stimulated T cells show increased levels of NLRP1 (D. C. Johnson et al., 2020). Thus, it is tempting to speculate that activated T cells overcome the higher NLRP1 threshold by reduced CARD8 processing and increased NLRP1 expression. This would align with my preliminary observations that stimulation of T cells even increased talabostat-mediated NLRP1 activation, although this finding has to be validated by comparing unstimulated and stimulated T cells from the same donor. Even though stimulated T cells do not activate CARD8 after inhibition of DPP8/9, CARD8 can still be functional in stimulated T cells after N-terminal cleavage by HIV-1 proteases, implying that CARD8 responses in activated T cells depend on the stimulus (Q. Wang et al., 2021).

Stimulated T cells activate NLRP1 after inhibition of DPP8/9 but not after induction of the ribotoxic stress response

Following up on the observed NLRP1 inflammasome response in PBMC- and tonsil-derived T cells, I found that isolated T cells show the same NLRP1 inflammasome formation as PBMC-derived T cells after stimulation with talabostat. Thus, I generated C1C-EGFP-expressing reporter T cells, which enabled a more sensitive analysis of inflammasome formation by overcoming the limitations of endogenous ASC expression and staining. The transduction protocol included stimulation of the primary T cells with anti-CD3/CD28 antibodies for at least 3 days. TCR stimulation of T cells did not inhibit NLRP1 inflammasome formation after talabostat stimulation. This is in contrast to CARD8-mediated pyroptosis which was only observed in naïve unstimulated T cells (D. C. Johnson et al., 2020; Linder et al., 2020). Neither Johnson et al. nor Linder et al. detected pyroptosis after talabostat treatment of stimulated T cells, whereas I observed NLRP1 inflammasome formation in stimulated T cells after inhibition of DPP8/9. Then why did they not detect NLRP1-mediated pyroptosis? I showed that NLRP1 activation by VHL-VHH_{PYD}-mediated targeted ubiquitination induces pyroptosis in T cells, suggesting that NLRP1 activation in T cells is in principle able to drive pyroptosis. Similar to the experiments in N/TERT-1 cells, the NLRP1 response in T cells after inhibition of DPP8/9 was rather weak, which is why supernatant-based analyses of cell death might just not be sensitive enough to detect the death of a few pyroptotic T cells. Microscopy analyses in the presence of a non-cell permeable DNA dye would show whether talabostat-treated stimulated T cells undergo pyroptosis, similar to VHL-VHH_{PYD}-expressing cells.

The C1C-EGFP reporter T cells enabled a straightforward screening of NLRP1 stimuli like the RSR-inducing antibiotics anisomycin and lactimidomycin. Surprisingly, in contrast to HEK 293T and N/TERT-1 reporter cells, T cells did not show inflammasome activation after stimulation with either of the drugs. Murine T cells revealed MAPK2-dependent p38 phosphorylation after UV irradiation (Alam et al., 2014) and Jurkat T cells showed p38 and JNK phosphorylation after stimulation with anisomycin (Shifrin & Anderson, 1999), suggesting that T cells can mount a functional RSR. However, it was reported that TCR stimulation causes alternative p38 phosphorylation at tyrosine 323 by the TCR-proximal tyrosine kinase Zap70, which then leads to autophosphorylation of the canonical p38

phosphorylation sites (Salvador et al., 2005). TCR-mediated mono-phosphorylation of p38, which caused altered substrate specificity of the MAP kinase, was also described (Mittelstadt et al., 2009). In addition, p38 seems to play a role in T cell differentiation (Gurusamy et al., 2020; Hayakawa et al., 2017) and IFN-γ expression by Th1 cells (Rincon et al., 1998). Thus, p38-mediated NLRP1 activation might be dysfunctional in T cells to prevent pyroptosis after TCR stimulation and differentiation. It will be important to stain phosphorylated p38 in TCR- and anisomycin/lactimidomycin-stimulated T cells to analyze the regulation of p38 activity. As all of the cited studies were performed in murine T cells or the human T cell line Jurkat, this will help to confirm the described pathways in primary human T cells. If the T cells have a functional RSR and show phosphorylation of p38, it would be important to study how the T cells inhibit p38-mediated NLRP1 activation. One could speculate that alternative modifications of the sensor block the N-terminal linker region, alternative locations in the cytosol impair interaction with p38, or that NLRP1 is immediately dephosphorylated.

NLRP1 activation is not limited to a specific T cell subpopulation

I found that both CD4+ and CD8+ T cells can form ASC specks after talabostat stimulation. Talabostat-induced activation of CARD8 was similarly observed in both naïve and memory CD4+ and CD8+ T cells, indicating that NLRP1 and CARD8 inflammasomes are not restricted to a specific T cell subpopulation (D. C. Johnson et al., 2020; Linder et al., 2020). To further define the NLRP1 inflammasome-forming cells, I sorted talabostat-treated C1C-EGFP reporter T cells and compared the transcriptome of cells with and without ASC specks. Stimulated T cells expressed NLRP1, CARD8, AIM2, ASC, caspase-1, and GSDMD, but not NLRP3 or NAIP/NLRC4, on a transcriptional level, in line with other reports (D. C. Johnson et al., 2020; Linder et al., 2020; Lozano-Ruiz et al., 2022). T cells with ASC specks showed more than 200 upregulated genes in comparison to talabostat-treated cells without ASC specks, but most inflammasome-related genes were unchanged in the two groups. This implies that the expression of NLRP1 and additional inflammasome proteins is not determining the responsiveness to talabostat. Some of the upregulated genes in T cells with ASC specks were cytokines and chemokines like IFN-γ, TNF-α and CCL3-5, but intracellular cytokine stainings of IFN-γ and TNF-α revealed no difference between T cells with and without inflammasomes. Transcriptional upregulation of surface

markers like CD25 and CTLA-4 could also not be confirmed on protein level by flow cytometry. The observed transcriptional changes are probably an artifact caused by prolonged inflammasome activation in the presence of caspase-1 inhibitor and thereby inhibited pyroptosis. There are reports about alternative caspase-8 activation in caspase-1-inhibited murine macrophages after Aim2, Nlrp3, and Nlrc4 stimulation, implying that caspase-8 is activated on ASC specks whenever caspase-1 is not inducing pyroptosis (Mascarenhas et al., 2017; Sagulenko et al., 2013). Since NLRP1 activation by talabostat requires incubation of up to 24 hours, the prolonged presence of ASC specks in caspase-1-inhibited T cells might induce similar alternative cell death pathways which then cause the detected transcriptional changes. Apart from the discussed dysregulated transcription of several genes, the transcriptome analyses gave no additional hints about the identity of the NLRP1 inflammasome-forming cells. T cells with ASC specks expressed both CD4 and CD8 and showed no clear T helper subset phenotype, which is not surprising as I did not add differentiation-inducing cytokines to the T cell culture. Some dysregulated genes in inflammasome-forming T cells were reminiscent of the transcriptomic profile of T_{reg} cells like high expression of CD25 and CTLA-4 and low expression of CD127 (Trzupek et al., 2020). However, as already mentioned, representative flow cytometry analyses of some of the surface markers showed unchanged expression between T cells with and without ASC specks. Moreover, when I stimulated the T cells with VHL-VHH_{PYD}, I observed NLRP1 inflammasome formation in up to 30 % of all T cells, excluding the possibility that only T_{reg} cells form NLRP1 inflammasomes. The strong response after VHL-VHH_{PYD} stimulation suggests that NLRP1 responsiveness is not limited to a small subpopulation of T cells, but rather that talabostat is a weak stimulus of NLRP1 in T cells, as observed in N/TERT-1 cells.

What is the physiological relevance of NLRP1 inflammasomes in T cells?

Using the VHL-VHH_{PYD} system, I showed that NLRP1 inflammasome formation in T cells is linked to subsequent pyroptotic cell death. Importantly, NLRP1 activation by targeted ubiquitination was much stronger than after inhibition of DPP8/9 by talabostat. Thus, the VHL-VHH_{PYD} system will be useful to further analyze the consequences of NLRP1 activation in T cells. Using the weak NLRP1 activator talabostat, I could not detect IL-1β release by isolated naïve T cells. The same was observed by others, although they even

primed the cells with LPS (D. C. Johnson et al., 2020; Linder et al., 2020). In contrast to human tonsillar B cells, T cells seem to express at least low levels of TLR4 and they show LPS-mediated upregulation of antiviral genes, suggesting that the lack of IL-1β release was not due to unsuccessful TLR4 stimulation (Kabelitz, 2007; Lech et al., 2010; Mansson et al., 2006). As already mentioned, there are some reports about autocrine IL-1β stimulation of T cells in the context of Th1, Th17, and follicular T helper cell differentiation. Others showed IL-1β release by Jurkat T cells (X. Li et al., 2020), primary CD4+ T cells (C. Zhao et al., 2018), or CCR5+ lymphoid T cells (Doitsh et al., 2014), implying that these lymphocytes can release the proinflammatory cytokine in the context of certain stimulations. Since the talabostat-induced NLRP1 response was rather weak and probably completely overshadowed by the faster CARD8 inflammasome, it will be important to analyze whether NLRP1 activation by VHL-VHH_{PYD} causes IL-1β release. However, the transcriptome analyses of stimulated T cells showed no expression of pro-IL-1β, so the T cells probably require additional stimulations to upregulate the cytokine. On the other hand, NLRP1 inflammasome-forming T cells might release other relevant cytokines in the course of pyroptosis. T cells with ASC specks showed transcriptional upregulation of the pyroptosis mediator NINJ1, which would promote bursting and subsequent passive release of cellular content. Thus, it would be relevant to analyze the supernatants of VHL-VHH_{PYD}-stimulated T cells for different cytokines using multiplex analyses.

It was reported that Nlrp1 influences murine Th17 differentiation (Costa et al., 2021) and similar studies, reporting a role of inflammasome components in T cell differentiation, exist for NLRP3/Nlrp3 (Bruchard et al., 2015; Javanmard Khameneh et al., 2019; S.-H. Park et al., 2019), Aim2 (Chou et al., 2021; Lozano-Ruiz et al., 2022), caspase-1 (Y. Gao et al., 2020), and ASC (Cheong et al., 2020; Javanmard Khameneh et al., 2019). Therefore, it would be interesting to differentiate Th1, Th2, and Th17 cells *in vitro* to test whether one of these groups is more or less responsive to NLRP1 activation. The differentiation will probably also influence the consequences of inflammasome formation, as these T cell subsets express different cytokines, which might be released by pyroptosis. In murine T cells, Nlrp1 seems to negatively regulate Th17 differentiation, and type I diabetes patients who exhibit a gain-of-function NLRP1 mutation (L155H) showed impaired Th17

development as well (Costa et al., 2021). The L155H mutation of NLRP1 is also associated with the autoimmune disease vitiligo, in which autoreactive Th17 cells contribute to the destruction of melanocytes in the skin. It was shown that PBMCs of vitiligo patients express increased levels of the Th17 transcription factor RORγT and NLRP1 (Bhardwaj et al., 2020), but since IL-1β stimulates Th17 differentiation, this does not have to be a T cell-intrinsic effect (Chung et al., 2009). FKCL patients who exhibit a different gain-of-function NLRP1 mutation also showed enhanced IL-17 levels in the skin (Li et al., 2023). As different NLRP1 mutations are associated with various autoimmune diseases, it is still possible that increased NLRP1 activation in T cells (and B cells) contributes to disease development (Tupik et al., 2020). One of the tonsil donors showed a strong inflammasome response in both lymphocyte subsets after talabostat stimulation, which could also be explained by NLRP1-activating mutations. To differentiate between lymphocyte- and IL-1β-mediated effects, it will be important to directly analyze lymphocytes from donors with confirmed NLRP1 mutations and compare their inflammasome responses to control cells.

So far, I have shown NLRP1 activation by talabostat and nanobody-mediated targeted ubiquitination in lymphocytes. This confirms that these cells can indeed assemble functional NLRP1 inflammasomes. However, in which physiological settings is NLRP1 activated? Talabostat is a widely used and accepted stimulus of NLRP1 (and CARD8), but it is still unknown whether inhibition of DPP8/9 represents a relevant danger signal, indicating for example intracellular pathogenic activity. I was not able to infect T cells with SFV and RVA SA11-4F, and T cells did not form inflammasomes after anisomycin- and lactimidomycin-induced ribotoxic stress. Other potential NLRP1 stimuli that can be tested are N-terminal cleavage by rhinovirus 3C proteases, as it was reported that T cells can be infected by rhinovirus 16, which caused subsequent cell death (Ilarraza et al., 2013). In addition, KSHV can infect T and B cells, potentially enabling ORF45-mediated NLRP1 activation (X. Yang et al., 2022). It is also possible that lymphocytes undergo NLRP1-mediated cell death after cell type-specific stimulation, for example during selection or differentiation. In line with that, it was described that Nlrp1a activation causes pyroptosis of hematopoietic progenitor stem cells in mutated mice (Masters et al., 2012). Murine T cells did not undergo pyroptosis after talabostat stimulation, but similar to my assays with

human T cells and N/TERT-1 keratinocytes, the response might have been too weak to be detectable (D. C. Johnson et al., 2020). Of course, murine Nlrp1 differs highly from the human sensor, and the role of inflammasomes in lymphocytes might also differ between mice and humans, as discussed before. Thus, it remains to be confirmed whether murine T and B cells exhibit functional NLRP1 inflammasomes as well.

In summary, I analyzed inflammasome formation in primary blood cells by staining endogenous ASC. I confirmed that monocytes form the major NLRP3-competent PBMC subpopulation and are the main producers of IL-1β. NLRP1 stimulation by inhibition of DPP8/9 revealed that lymphocytes can assemble inflammasomes, which was also observed in tonsil-derived cells. Targeted ubiquitination of NLRP1 by VHL-VHH_{PYD} in stimulated T cells caused strong NLRP1 inflammasome activation and pyroptosis, verifying that T cells have functional NLRP1 inflammasomes. The regulation of CARD8 and NLRP1 inflammasomes in naïve and stimulated T cells, as well as potential cytokine release by NLRP1-activated T cells, require further analyses. NLRP1 responsiveness does not seem to be limited to a certain T cell subpopulation, but the physiological settings in which lymphocytes activate NLRP1 remain to be discovered. It will be important to study the influence of NLRP1 in lymphocytes in the development of autoimmune diseases that are associated with NLRP1 gain-of-function mutations.

5.4 Material and Methods

Cells

Cell culture

HEK 293T cells were cultivated as described in chapter 2. PBMCs and primary T cells were cultivated in Roswell Park Memorial Institute (RPMI) medium supplemented with GlutaMax, 10 % FBS, 1x penicillin/streptomycin, 1 % nonessential amino acids, 1 % sodium pyruvate, and 50 µM β-mercaptoethanol. Tonsil-derived cells were cultivated in RPMI supplemented with GlutaMax, 15 % FBS, 1x penicillin/streptomycin, 1 % sodium pyruvate, and 0.5 % gentamicin (all Thermo Fisher Scientific).

Purification of PBMCs

Human PBMCs were purified from blood samples that were freshly taken in EDTA-containing blood collection tubes. Blood was mixed 1:2 with PBS and PBMCs were isolated by density gradient centrifugation using Ficoll-Paque (VWR) at 400 g for 20 min at 4 °C. All cells from the PBMC layer were collected, washed once with PBS, and resuspended in full medium.

Depletion of monocytes

Isolated PBMCs were resuspended in sterile-filtered MACS buffer (0.5 % BSA, 2 mM EDTA, PBS), incubated with human CD14 Microbeads (Miltenyi Biotec), and added to LS-columns with 30 µm pre-separation filters (Miltenyi Biotec), all according to manufacturer instructions. Columns were washed three times with 3 mL MACS buffer and the flow through, containing (CD14+) monocyte-depleted PBMCs, was collected. CD14- PBMCs were washed once with PBS and resuspended in full medium. 10^6 PBMCs and CD14-PBMCs were stained for CD14 and analyzed by flow cytometry to confirm successful depletion of CD14+ monocytes.

Isolation of T cells

Isolated PBMCs were resuspended in sterile-filtered EasySep buffer (2 % FBS, 1 mM EDTA, PBS) and incubated with isolation cocktail and RapidSpheres (EasySep human T cell isolation kit, StemCell) according to manufacturer instructions. The negatively-selected isolated T cells in the supernatant were collected using StemCell magnets, and T cells were resuspended in full medium. 10^6 PBMCs and T cells were stained for CD3 and analyzed by flow cytometry to confirm successful isolation of T cells.

Anti-CD3/Anti-CD28 stimulation of T cells

To stimulate isolated T cells, 96 well-plates (TPP) were coated with 50 µL PBS containing 2 µg/mL anti-CD3 and 4 µg/mL anti-CD28 (both Ultra-LEAF purified, Biolegend) for 2 h at 37 °C. Plates were washed three times with PBS before 10^5 isolated T cells were seeded in 200 µL medium per well. T cells stimulated with anti-CD3/anti-CD28 antibodies were additionally supplemented with 20 U/mL human recombinant IL-2 (Sigma-Aldrich).

Tonsil-derived single cell suspension

Intact or fragmented tonsils were provided by Alina Franzen (Klinik für Hals-/Nasen-/Ohrenheilkunde/Chirurgie, University Hospital Bonn) after surgical removal. Tonsils were placed in dishes containing Hanks' balanced salt solution (HBSS) buffer (1x HBSS, 5 % FSC, 0.5 % GlutaMax, 1x penicillin/streptomycin, 0.5 % gentamicin), and remaining connective tissue, fibrotic tissue, and fat were carefully removed using scissors and scalpels. Clean tonsils were cut into 3-10 mm fragments and fragments were further dispersed using 70 µm cell strainers. Obtained cells were washed three times with PBS, before incubation in sterile-filtered red blood cell lysis buffer (155 mM NH_4Cl, 10 mM $KHCO_3$, 0.1 mM EDTA, pH 7.4) for 10 min. Tonsil-derived cells were resuspended in full medium afterwards.

Generation of genetically modified T cells

T cells were genetically modified to constitutively express C1C-EGFP under the control of pUbC, or C1C-EGFP and VHHs/VHL-VHH fusions under a bidirectional doxycycline-inducible promoter. Construction of the lentiviral plasmids was described in chapter 2. Isolated T cells were seeded in anti-CD3/anti-CD28-coated wells as described before. The next day, T cells were transduced by addition of 200 µL undiluted lentivirus supplemented with 10 µg/mL polybrene (Sigma-Aldrich) for 7-8 h. In case the lentivirus suspensions did not contain β-mercaptoethanol, it was added for the transduction as well. Transduced T cells were cultivated in full medium without addition of antibiotics. Cells were cultivated for at least 2 days before experiments were performed.

Viruses

Lentivirus production

Lentiviruses for transduction of primary human T cells were produced as described in chapter 2, but with some adaptations to increase the virus yield and therefore the transduction efficiency. Confluent HEK 293T cells in 10 cm dishes were co-transfected with 9 µg lentiviral vector, 3.9 µg psPax2, and 2.1 µg pMD2.G using PEI Max (Polysciences). HEK 293T cells were transfected for 6-8 h, before addition of 10 mL T cell medium without β-mercaptoethanol and further cultivation for 48 h. Lentivirus-containing supernatants were harvested, filtered using 0.45 µm filter (Millipore), and directly used for

transduction or frozen at -80 °C. To achieve even higher virus titers, cells in 15 cm dishes were co-transfected with 20.25 µg lentiviral vector, 8.8 µg psPax2, and 4.7 µg pMD2.G, before addition of 30 mL medium (DMEM supplemented with 10 % FBS) and further cultivation for 48 h. Lentivirus-containing supernatants were harvested, filtered using 0.45 µm filter, and lentiviruses were additionally precipitated using Lenti-X™ Concentrator (Takara Bio). Pelleted lentiviruses were resuspended in T cell medium and directly used for transduction or frozen at -80 °C.

Antibodies

The following antibodies were used: mouse anti-human ASC PE clone HASC-71 (Biolegend Cat# 653903, RRID:AB_2564507), mouse anti-human CD14 APC-Cy7 clone HCD14 (Biolegend Cat# 325620, RRID:AB_830693), mouse anti-human CD14 FITC clone Tük4 (Miltenyi Biotec Cat# 5151221299, discontinued product), mouse anti-human CD16 PerCP/Cy5.5 clone 3G8 (Biolegend Cat# 302027, RRID:AB_893263), mouse anti-human CD19 APC clone HIB19 (Biolegend Cat# 302211, RRID:AB_314241), Ultra-LEAF purified mouse anti-human CD28 clone CD28.2 (Biolegend Cat# 302934, RRID:AB_11148949), Ultra-LEAF purified mouse anti-human CD3 clone UCHT1 (Biolegend Cat# 300438, RRID:AB_11146991), mouse anti-human CD3 BV510 clone OKT3 (Biolegend Cat# 317331, RRID:AB_2561376), mouse anti-human CD4 APC-Cy7 clone RPA-T4 (Biolegend Cat# 300517, RRID:AB_314085), mouse anti-human CD56 FITC clone HCD56 (Biolegend Cat# 318303, RRID:AB_604091), mouse anti-human CD8 PerCP/Cy5.5 clone SK1 (Biolegend Cat# 344709, RRID:AB_2044009), mouse anti-human HLA-DR eF450 clone LN3 (Thermo Fisher Scientific Cat# 48-9956-41, RRID:AB_10717673), mouse IgG1 κ isotype control PE clone MOPC-21 (Biolegend Cat# 400113, RRID:AB_326435), mouse anti-human IFN-γ APC clone 4S.B3 (Biolegend Cat# 502512, RRID:AB_315237), mouse anti-human TNF-α BV421 clone Mab11 (Biolegend Cat# 502931, RRID:AB_10898321)

Small compound inhibitors and reagents

The following small compound inhibitors and reagents were used: anisomycin (Sigma-Aldrich), Crid3 (Tocris), doxycycline (Thermo Fisher Scientific), ionomycin (Enzo), lactimidomycin (Sigma-Aldrich), LPS-EK Ultrapure (Invivogen), Nigericin sodium salt

(Biomol), PMA (Sigma-Aldrich), talabostat mesylate (MedChemExpress), Vx-765 (Selleckchem).

Flow cytometry-based quantification of inflammasome assembly

Seeding and stimulation of cells

To quantify the assembly of ASC specks by staining endogenous ASC, $3 \cdot 10^6$ (CD14-) PBMCs were seeded in 6 well-plates in a total volume of 1.5 mL. In experiments that compared inflammasome responses in PBMCs and isolated T cells, $5 \cdot 10^5$ PBMCs or T cells were seeded in 96 well-plates (TPP) in a total volume of 150 µL. Tonsil-derived cells were seeded in 96 well-plates as well but with $2 \cdot 10^6$ cells per well in 200 µL medium. To quantify the assembly of ASC specks in C1C-EGFP-expressing reporter T cells, $0.5\text{-}3.5 \cdot 10^5$ transduced T cells were seeded in 96 well-plates (TPP) in a total volume of 200 µL. Stimulation of reporter T cells was always performed in the absence of anti-CD3/anti-CD28 coating (except for antibody stimulation screen) and IL-2. All mentioned cells were stimulated in full medium in the presence of 100 µM Vx-765 for all flow cytometry experiments to prevent loss of responding cells by caspase-1-dependent pyroptosis.

For drug-induced stimulation, cells were treated with 200 ng/mL LPS for 3 h followed by 10 µM nigericin for 1 h, 3 or 30 µM talabostat for 20-24 h, 50 ng/mL PMA and 1 µg/mL ionomycin for 5-20 h, 15 µM anisomycin for 20 h, or 2.5 µM lactimidomycin for 20 h. Nigericin was directly added to the LPS-containing medium without additional medium change. For induction of doxycycline-inducible expression, cells were cultivated in medium containing 1 µg/mL doxycycline. For antibody-induced stimulation, cells were cultivated in 96 well-plates coated with the indicated concentrations of anti-CD3 and anti-CD28 antibodies for 48 and 90 h.

In case of additional inhibitor treatments, small compound inhibitors were added 30 min before and during the stimulation, with the following concentrations: 2.5 µM Crid3 or 100 µM Vx-765. For staining of intracellular cytokines, T cells were stimulated with PMA and ionomycin in the presence of GolgiPlug Protein Transport Inhibitor (1:1000, BD). The inhibitor was added to talabostat-stimulated cells for the last 5 h of incubation.

Flow cytometry staining and analysis

After stimulation, cells were harvested by resuspension (96 well-plate) or careful scraping (6 well-plate) and resuspended in FACS buffer (2 % FBS, 5 mM EDTA, PBS). Surface marker stainings were performed before fixation. Whenever cells were stained with anti-ASC PE and the corresponding isotype control, samples were split into two fractions which were stained in parallel. Small fractions from all samples were pooled for the unstained controls. Cells were stained for the indicated surface marker in FACS buffer containing 320 µg/mL human immunoglobin (CSL Behring) for 30 min at 4 °C. Cells were stained with the following antibody dilutions: anti-CD14 APC-Cy7 1:200, anti-CD16 PerCP/Cy5.5 1:200, anti-CD19 APC 1:200, anti-CD3 BV510 1:200, anti-CD4 APC-Cy7 1:200, anti-CD8 PerCP/Cy5.5 1:200, and anti-HLA-DR eF450 1:200. Afterwards, cells were fixed in 4 % methanol-free formaldehyde (Thermo Fisher Scientific) in PBS. If necessary, fixed cells were then permeabilized and stained for ASC or cytokines in Intracellular Staining Permeabilization Wash Buffer (Biolegend) containing 320 µg/mL human immunoglobin for 1 h at 4 °C. Cells were stained with the following antibody dilutions: anti-ASC PE 1:100, PE isotype control 1:160, anti-IFN-γ APC 1:100, and anti-TNF-α BV421 1:100. Samples were analyzed using BD FACSCanto flow cytometers, recording area, width, and height of the ASC-PE or C1C-EGFP signal of single cells. Flow cytometers were provided and serviced by the Flow Cytometry Core Facility (University Hospital, Bonn, Germany). Compensation was performed by recording single stain signals for all used fluorophores using OneComp compensation beads (Thermo Fisher Scientific). Flow Cytometry data was analyzed using FlowJo 10.8.1 software, based on the indicated gating strategies.

Imaging flow cytometry

To confirm ASC speck formation by imaging flow cytometry, PBMCs and inflammasome reporter T cells were stimulated and harvested as described for standard flow cytometry experiments. PBMCs were stained for surface markers and endogenous ASC as described above, but all surface marker antibodies were diluted 1:100 to achieve stronger fluorescence signals. Stained samples were filtered and concentrated in FACS buffer to reach a concentration of $2 \cdot 10^7$ cells/mL. Samples were analyzed using the ImageStream® X Mark II instrument (Luminex), provided by the Flow Cytometry Core Facility (University Hospital, Bonn, Germany). Cells were recorded using 40x magnification (0.5 µm per

pixel). If necessary, compensation was performed by recording single stain signals for all used fluorophores using additionally stained PBMCs. As the ASC signal of cells with specks is different from unstimulated cells, it was ensured that the ASC PE single stains, as well as the unstained controls, contained ASC speck-forming cells. Imaging Flow Cytometry data was analyzed using IDEAS® software (Luminex).

Cytokine quantification by HTRF

To quantify IL-1β release, (CD14-) PBMCs were seeded ($6 \cdot 10^5$ cells in 300 µL per 24 well-plate) and stimulated as described for flow cytometry experiments in the absence and presence of Vx-765. Supernatants for the quantification of IL-1β levels after T cell isolation were collected from $5 \cdot 10^5$ PBMCs or T cells in 150 µL per well in 96 well-plates. IL-1β was quantified as described in chapter 2.

Transcriptome analysis of inflammasome reporter T cells

To perform transcriptome analysis of C1C-EGFP-expressing T cells with and without ASC specks, reporter T cells were generated by transduction as described before. 3 days after transduction, half of the cells were transferred into a new anti-CD3/anti-CD28-coated 96 well-plates to expand cells as much as possible. 5 days after transduction all cells were harvested, pooled, and seeded into uncoated 96 well-plates to perform talabostat stimulation as described for flow cytometry experiments. Untreated T cells without ASC specks, as well as talabostat-treated T cells with and without ASC specks, were sorted using the BD FACSAria III instrument equipped with a 100 µm nozzle (see Table 4 for the number of sorted cells for each donor). The sorting was performed with the help of the Flow Cytometry Core Facility (University Hospital, Bonn, Germany). Sorted cells were lysed in 700 µL Trizol (Thermo Fisher Scientific) and frozen at -80 °C until RNA was extracted. Isolation of bulk RNA was performed with the RNeasy Micro Kit (Qiagen). Library production for 3'-mRNA sequencing was performed according to the manufacturer's protocol and sequenced on a HiSeq2500 (Illumina) at the NGS Core Facility (University Hospital, Bonn, Germany). Reads were aligned with STAR (v2.7.3a) against the human reference genome hg19. Transcripts were quantified with the Partek E/M algorithm and further DEseq2 normalized. Batch-corrected data were used to calculate the differentially expressed genes between specking T cells, non-specking T

cells, and respective controls by 2way ANOVA analysis (fold-change |1.5|, FDR-adjusted p-Value ≤0.05). Data visualization and biological interpretation were performed with the Partek Genomics Suite (v7.0) and R (v3.5.0).

Donor	Untreated cells	Talabostat-treated cells	
	Without ASC specks	Without ASC specks	With ASC specks
Donor 1	$2.61 \cdot 10^5$	$5 \cdot 10^5$	$7 \cdot 10^4$
Donor 2	$2 \cdot 10^5$	$5 \cdot 10^5$	$7 \cdot 10^4$
Donor 3	$1.74 \cdot 10^5$	$5 \cdot 10^5$	$6.34 \cdot 10^4$
Donor 4	$2 \cdot 10^5$	$5 \cdot 10^5$	$1.7 \cdot 10^5$

Table 4: Number of sorted inflammasome reporter T cells used for transcriptome analysis.

Microscopy

To analyze pyroptosis in T cells expressing (VHL-)VHH constructs by live cell microscopy, around $3 \cdot 10^4$ transduced T cells were seeded into 8 well glass bottom µ-slides (Ibidi). The next day, expression was induced by addition of 1 µg/mL doxycycline in the absence and presence of 100 µM Vx-765 and cells were analyzed by live cell confocal microscopy starting after 4 h. Shortly before imaging, 2.5 µg/mL propidium iodide (Biolegend) and 30 mM HEPES were added to the medium. Cells were cultivated at 37 °C and images were recorded using the HC PL APO CS2 63x1.20 water objective on a Leica SP8 Lightning confocal microscope, provided and serviced by the Microscopy Core Facility (University Hospital, Bonn, Germany). Images were processed using ImageJ 2.3.0 software.

Statistical analyses

Statistical analyses were performed as described in chapter 2.

6. Summary and outlook

Within the five years that I worked on this thesis, there has been remarkable progress in our understanding of the human NLRP1 inflammasome. Most importantly, it was shown that the sensor is activated by functional degradation and inhibition of NLRP1-DPP8/9 complex formation, both causing the release of active NLRP1$^{UPA\text{-}CARD}$ fragments which recruit ASC and assemble inflammasomes. With the work presented in this thesis, I extended the knowledge about human NLRP1 inflammasomes by delineating p38-mediated NLRP1 activation, identifying several alphavirus and rotavirus strains as novel NLRP1 stimuli, and establishing lymphocytes as NLRP1-competent cell types.

To study NLRP1 inflammasomes, I verified HEK 293T and N/TERT-1 keratinocyte inflammasome reporter cell lines, which enabled the complementary analysis of NLRP1 in the background of either a minimally defined inflammasome setting or an endogenously regulated cellular system. I also identified NLRP1^{PYD}-specific nanobodies which, combined with the VHL system, were able to stimulate endogenous NLRP1 by targeted ubiquitination and subsequent N-terminal degradation (Fig. 6.1). This VHL-VHH$_{PYD}$ system not only proves for the first time that targeted degradation of human NLRP1 is sufficient to activate the inflammasome sensor in an endogenous setting, but also represents a strong NLRP1-specific stimulus that allows the differentiation between NLRP1 and the highly similar inflammasome sensor CARD8. The system should be optimized to enable NLRP1 activation in primary cells/tissues without the need for lentiviral transduction or transfection.

Using the reporter cell lines, I complemented, refined, and unified the mechanisms of NLRP1 activation by the proposed NLRP1 stimuli UVB irradiation, SFV infection, and transfection of dsRNA (Fig. 6.1). All these stimuli, as well as various inducers of the RSR, caused NLRP1 activation in a p38-dependent manner. I also identified additional alphaviruses, namely SINV, CHIKV, MAYV, and RRV, which similarly activate NLRP1. The MAP kinase p38 phosphorylates the N-terminal linker region of the sensor, in which serine 107 represents a critical phosphorylation site but additional phosphorylations of canonical p38 motifs are likely required for activation of the inflammasome. I propose that phosphorylation of the N-terminal linker generates a phospho-degron which is recognized by CRL complexes, causing the ubiquitination of NLRP1^{PYD}, N-terminal degradation, and

inflammasome assembly. Thus, p38 activation acts as a signaling hub that integrates various stress signals to activate NLRP1 by direct phosphorylation. Further studies will have to delineate p38 activation by alphaviruses, define the required conditions of p38-mediated NLRP1 activation, and determine the exact events causing N-terminal ubiquitination and degradation.

Next to additional alphaviruses, I identified two simian rotavirus strains that activate NLRP1 in a p38-independent manner. For the RVA SA11-4F strain, I found that expression of the viral host antagonist NSP1 is necessary and sufficient for inflammasome activation, whereas the role of NSP1 in RVA RRV-mediated activation requires further analyses (Fig. 6.1). I hypothesize that rotavirus NSP1 binds the N-terminus of NLRP1, leading to the recruitment of CRL complexes and N-terminal degradation, but the exact mechanism of NSP1-mediated NLRP1 activation needs further studies. These studies should also focus on human rotavirus strains as well as physiologically relevant cell models to elucidate in which biological settings this mode of activation is relevant.

Finally, I analyzed NLRP1 inflammasome assembly in primary blood cells and determined T and B lymphocytes as NLRP1-competent cells. NLRP1-specific activation by VHL-VHH_{PYD} induced strong inflammasome formation and pyroptosis in stimulated primary T cells, confirming that T cells can assemble functional NLRP1 inflammasomes. The strong response, combined with a transcriptome analysis of inflammasome-forming cells, suggests that NLRP1 activation is not limited to a small subpopulation of T cells. It will be important to investigate whether NLRP1-activated T cells release relevant cytokines and in which physiological settings lymphocytes activate the inflammasome sensor.

Although the understanding of NLRP1 inflammasomes improved greatly within the last few years, many questions remain that have not been answered. One of the most important questions is probably: Does NLRP1 activation always require N-terminal degradation and what is the function of the N-terminal domains if they are degraded most of the time?

All NLRP1 stimuli that I tested in the N/TERT-1 keratinocytes, representing an endogenously regulated NLRP1 cell model, required functional neddylation, suggesting that CRL complexes cause the ubiquitination and subsequent degradation of the sensor

at some point of the stimulation. The activation by functional degradation enables NLRP1

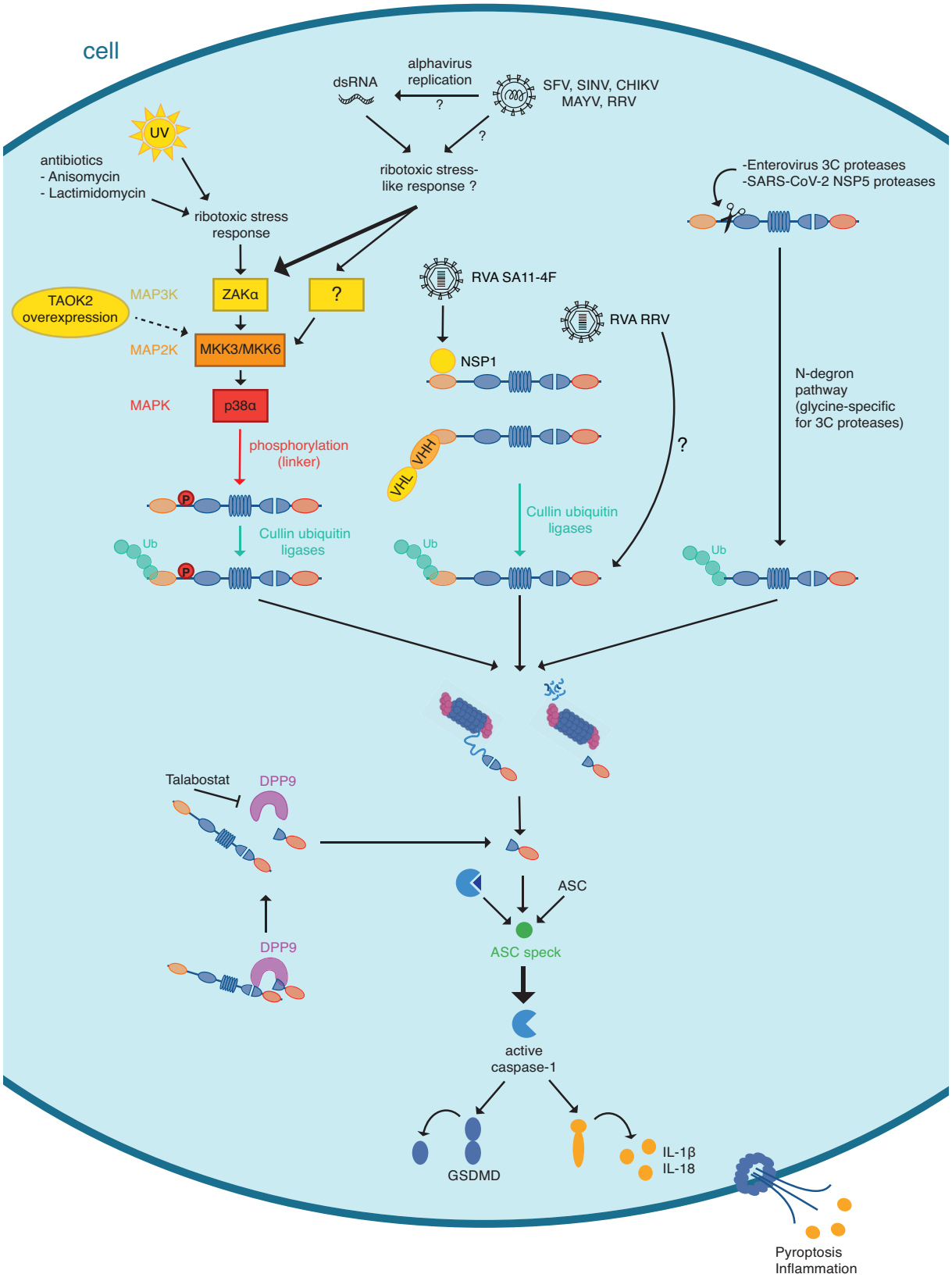

Figure 6.1: Graphical abstract of NLRP1 inflammasome activation by ribotoxic stress- and alphavirus-induced p38 phosphorylation, as well as nanobody- and rotavirus NSP1-mediated targeted ubiquitination.

to detect pathogenic proteases and interferences with DPP8/9 activity, but the same is true for the substantially less complex sensor CARD8. It was suggested that the N-terminal linker of NLRP1 forms a tripwire region, presenting conserved pathogen-encoded protease cleavage sites like Q130/G131 for enterovirus 3C proteases (Robinson et al., 2020; Tsu et al., 2021). However, the N-terminal unstructured region of CARD8 exhibits cleavage sites of Coxsackie virus B3 3C and 2A proteases, enabling the detection of viral protease activity without the need for PYD, NACHT, and LRR domains (Chui et al., 2020; Nadkarni et al., 2022). If the less complex CARD8 can detect the same danger signals as NLRP1, why do humans express both? First of all, NLRP1 activation has more severe consequences than CARD8, as the latter forms ASC-independent inflammasomes causing pyroptosis but no proinflammatory cytokine processing (D. C. Johnson et al., 2018; Okondo et al., 2017). It may therefore be important to ensure tighter regulation of NLRP1 activity, since even small amounts of IL-1β can strongly promote inflammation (Dinarello, 2009, 2018). This is probably why NLRP1 exhibits a higher threshold of activation than CARD8 (Q. Wang et al., 2023), causing the dominant CARD8 response in primary monocytes and unstimulated T cells after inhibition of DPP8/9. The tighter regulation of NLRP1 is presumably mediated by $NLRP1^{NACHT\text{-}LRR}$, as expression of NLRP1ΔLRR (Chavarría-Smith et al., 2016; Liao & Mogridge, 2009) and inactive NLRP1 Walker A/B mutants (within $NLRP1^{NACHT}$) in reconstituted cell systems leads to autoactivation (Ball et al., 2022; Neiman-Zenevich et al., 2014). I already speculated about $NLRP1^{NACHT\text{-}LRR}$ keeping NLRP1 in an inhibited state, in an ATP hydrolysis-dependent manner, potentially regulated by binding of dsRNA (Bauernfried et al., 2021) and oxidized TRX1 (Ball et al., 2022).

But what is the function of $NLRP1^{PYD}$? Expression of NLRP1ΔPYD displaying the fluorophore mScarlet at the N-terminus in N/TERT keratinocytes leads to increased NLRP1 activation after talabostat, SFV, and dsRNA stimulation (Bauernfried et al., 2021). And mutations in $NLRP1^{PYD}$ (Grandemange et al., 2017; Herlin et al., 2020; Zhong et al., 2016) cause increased NLRP1 activity and NLRP1-associated inflammatory diseases similar to mutations in $NLRP1^{LRR}$ (Drutman et al., 2019; M. Li et al., 2023; Zhong et al.,

2016). So is NLRP1^{PYD} just another domain that negatively regulates NLRP1? The N-termini of primate and human NLRP1 show evidence of evolutionary positive selection (Chavarría-Smith et al., 2016), suggesting an important function of the NLRP1^{PYD} and the linker region apart from regulation. The findings of my thesis allow further speculations on this function: On the one hand, in the context of NLRP1 activation by rotavirus NSP1, I discussed the possibility that NLRP1^{PYD} acts as a decoy domain for PYD-modifying pathogens, as suggested before (Chavarría-Smith et al., 2016). Human NLRP1 might exhibit the N-terminal PYD domain to detect cleavage or degradation of PYD-containing inflammasome sensors by pathogens. There is no evidence for this hypothesis yet, but the analysis of rotavirus NSP1-mediated NLRP1 degradation might provide new insights. On the other hand, p38 phosphorylates NLRP1 in the N-terminal linker and lysines in NLRP1^{PYD}, but not the linker, are necessary for activation, implying that NLRP1^{PYD} and the linker form a regulated system that allows N-terminal degradation of NLRP1 after p38-dependent phosphorylation. Such a system allows NLRP1 to detect multiple stress signals integrated by p38 activity. As it was shown that ZAKα can phosphorylate the N-terminal linker *in vitro* as well (Robinson et al., 2022), it is possible that linker modifications by different kinases or other enzymes lead to NLRP1 activation, potentially enabling an even wider range of danger signal detection. The increased NLRP1 response in N/TERT keratinocytes expressing NLRP1ΔPYD displaying the fluorophore mScarlet at the N-terminus could then be based on the higher number of lysines in mScarlet compared to NLRP1^{PYD}. Thus, the original function of the N-terminal linker could be the presentation of degron-forming modification sites, but also the provision of the necessary unstructured region for N-terminal degradation (Chui et al., 2020; Prakash et al., 2004). If this was the main function of the NLRP1 N-terminus, NLRP1 would show a different mode of activation than CARD8, and the presence of pathogenic protease cleavage sites could just be a coincidence. In line with this, some murine Nlrp1b alleles are activated by lethal factor-mediated cleavage but monocytes from cattle and bison, which are herbivores and therefore the most common hosts for *Bacillus anthracis*, show no cleavage and activation of NLRP1 by lethal factor (Vrentas et al., 2020). Moreover, the activation of Nlrp1b is not protecting mice from challenges with the Bacillus toxin (Greaney et al., 2020; Terra et al., 2010), questioning the directed evolution of lethal factor cleavage sites in rodents.

Continuative studies will have to determine whether NLRP1 and/or CARD8 really evolved to detect pathogenic protease activity.

My observations that murine Nlrp1b and NLRP1 in T cells did not respond to RSR stimulation argue against the hypothesis that the original function of the N-terminal linker is the presentation of degron-forming modification sites. The only known common stimulus of rodent and human NLRP1 is DPP8/9 inhibition, making the detection of DPP8/9 interferences a possible candidate for the original function of this sensor. Many NLRP1 reviews conclude that *Toxoplasma gondii* infection could present the common NLRP1 stimulus that interferes with DPP8/9-mediated sequestration. However, as already mentioned, there is no concrete proof of NLRP1 activation by the parasite in human (Gov et al., 2013; Witola et al., 2011) and murine (Ewald et al., 2014; Gorfu et al., 2014) cells. Therefore, additional studies have to prove whether *Toxoplasma gondii* or other intracellular pathogens cause NLRP1 activation by inhibition of DPP9 complex formation. However, such pathogens would be similarly detected by the less complex sensor CARD8, questioning again the function of the NLRP1 N-terminal domains. It is also possible that NLRP1 and CARD8 are not guarding DPP8/9 activity, but that the sequestration by these enzymes is just a safety mechanism to prevent activation of the FIIND-containing inflammasome sensors during normal cell homeostasis. This way, activation of NLRP1 and CARD8 by talabostat would present an artificial stimulus that is not reflecting physiologically relevant danger signals at all. This would explain why talabostat is such a weak activator of endogenous NLRP1 in N/TERT-1 keratinocytes and T cells. Thus, the common stimulus of rodent and human NLRP1 might be a danger signal that still needs to be discovered.

21 years ago, NLRP1 was the first inflammasome sensor to be described (Martinon et al., 2002), but it seems like we only recently started to comprehend the complexity of this unique protein. It took more than 15 years until the concepts of activation by functional degradation and inhibition of DPP8/9 complex formation were developed, which were complemented by me and others, reporting activation by viral proteases, p38 phosphorylation, and rotavirus IFN antagonist NSP1. It is astonishing that we did not have a clue about NLRP1 inflammasome activation for so long, whereas new modes of activation are now proposed every year. It feels like NLRP1 acts as a “Swiss Army knife”

that can detect multiple danger signals which all come down to N-terminal degradation of the sensor and the release of the active NLRP1$^{UPA\text{-}CARD}$ fragment. Continuative studies will have to find out whether the human NLRP1 N-terminus evolved to present pathogenic protease cleavage sites, degron-forming modification sites, and/or decoy inflammasome domains, why humans and primates express both NLRP1 and CARD8, and which common endogenous stimulus activates human and rodent NLRP1.

7. Abstract

The assembly of inflammasomes is linked to the detection of pathogens and other danger signals by intracellular pattern-recognition receptors of the mammalian innate immune system. The human inflammasome sensor NLRP1 exhibits a unique structure containing both an N-terminal PYD and a C-terminal CARD, the latter being part of a smaller NLRP1$^{UPA\text{-}CARD}$ fragment that is separated by autoproteolysis. NLRP1 is mainly expressed in epithelial cells, such as keratinocytes in the skin. The sensor is activated by N-terminal proteolytic cleavage and subsequent N-degron pathway-mediated degradation of the sensor, or after inhibition of DPP8/9 which sequester free NLRP1$^{UPA\text{-}CARD}$ fragments. The release of the C-terminal NLRP1$^{UPA\text{-}CARD}$ fragment causes the recruitment of the adaptor protein ASC and caspase-1, resulting in the assembly of ASC specks, processing of IL-1β/IL-18, and pyroptotic cell death.

To study NLRP1 inflammasomes, I characterized HEK 293T and N/TERT-1 keratinocyte inflammasome reporter cell lines, which enabled the complementary analysis of NLRP1 in the background of either a minimally defined inflammasome setting or an endogenously regulated cellular system. In addition, I identified two NLRP1^{PYD}-specific nanobodies which, combined with the E3 ligase receptor VHL, allowed the precise stimulation of endogenous NLRP1 by targeted NLRP1^{PYD} ubiquitination and subsequent N-terminal degradation. The nanobody-mediated activation represents a strong NLRP1-specific stimulus that allows the distinction between NLRP1 and the highly similar inflammasome sensor CARD8.

Using the reporter cell lines, I found that various stimuli of the ribotoxic stress response activate human NLRP1 in a p38-dependent manner. In addition, infection with alphaviruses, including Semliki Forrest virus and Chikungunya virus, as well as intracellular dsRNA caused p38-dependent NLRP1 activation. p38 kinases directly phosphorylate the N-terminal linker region of the inflammasome sensor, in which serine 107 represents a critical phosphorylation site. I propose that phosphorylation of the N-terminal linker generates a phospho-degron which is recognized by cullin RING E3 ligases, causing the ubiquitination of NLRP1^{PYD}, N-terminal degradation, and inflammasome assembly. This way, p38 activation acts as a signaling hub that integrates

various stress signals to activate NLRP1 by direct phosphorylation. This pathway represents an independent mode of activation, as p38 activity was not required for NLRP1 activation by nanobody-mediated N-terminal degradation or DPP8/9 inhibition.

Using the HEK 293T reporter cell lines, I further discovered two simian rotavirus strains that activate NLRP1 in a p38-independent manner. For the rotavirus A SA11-4F strain, I found that expression of the viral host antagonist NSP1 is necessary and sufficient for inflammasome activation, whereas rotavirus A RRV-mediated activation cannot be attributed to NSP1 expression alone. Since rotavirus NSP1 is known to induce host protein degradation, I hypothesize that NSP1 binds the N-terminus of NLRP1, leading to the recruitment of cullin RING E3 ligases and activation of the inflammasome by N-terminal degradation. This would make rotavirus NSP1 the first pathogen protein to cause targeted degradation of human NLRP1.

Finally, I analyzed NLRP1 inflammasome assembly in primary blood cells and found that T and B lymphocytes, isolated from blood and tonsils, can form NLRP1 inflammasomes after inhibition of DPP8/9. Moreover, NLRP1-specific activation by nanobody-mediated N-terminal degradation induced strong inflammasome formation and pyroptosis in stimulated primary T cells, confirming that T cells have functional NLRP1 inflammasomes. The strong response, combined with a transcriptome analysis of inflammasome-forming cells, suggests that NLRP1 activation is not limited to a small subpopulation of T cells. The identification of lymphocytes as NLRP1 inflammasome-forming cells might provide new insights into the development of autoimmune diseases that are associated with NLRP1 gain-of-function mutations.

Altogether, I extended the knowledge about human NLRP1 inflammasomes by delineating p38-mediated NLRP1 activation, identifying several novel viral NLRP1 stimuli, and establishing lymphocytes as NLRP1-competent cell types.

8. List of figures

9. List of tables

10. References

Acosta-Ampudia, Y., Monsalve, D. M., Rodríguez, Y., Pacheco, Y., Anaya, J.-M., & Ramírez-Santana, C. (2018). Mayaro: an emerging viral threat? *Emerging Microbes & Infections*, *7*(1), 1–11. https://doi.org/10.1038/s41426-018-0163-5

Agostini, L., Martinon, F., Burns, K., McDermott, M. F., Hawkins, P. N., & Tschopp, J. (2004). NALP3 forms an IL-1beta-processing inflammasome with increased activity in Muckle-Wells autoinflammatory disorder. *Immunity*, *20*(3), 319–325. https://doi.org/10.1016/s1074-7613(04)00046-9

Akbal, A., Dernst, A., Lovotti, M., Mangan, M. S. J., McManus, R. M., & Latz, E. (2022). How location and cellular signaling combine to activate the NLRP3 inflammasome. *Cellular & Molecular Immunology*, *19*(11), 1201–1214. https://doi.org/10.1038/s41423-022-00922-w

Akhrymuk, I., Frolov, I., & Frolova, E. I. (2018). Sindbis Virus Infection Causes Cell Death by nsP2-Induced Transcriptional Shutoff or by nsP3-Dependent Translational Shutoff. *Journal of Virology*, *92*(23). https://doi.org/10.1128/JVI.01388-18

Akhrymuk, I., Kulemzin, S. V., & Frolova, E. I. (2012). Evasion of the Innate Immune Response: the Old World Alphavirus nsP2 Protein Induces Rapid Degradation of Rpb1, a Catalytic Subunit of RNA Polymerase II. *Journal of Virology*, *86*(13), 7180–7191. https://doi.org/10.1128/JVI.00541-12

Akimov, V., Barrio-Hernandez, I., Hansen, S. V. F., Hallenborg, P., Pedersen, A.-K., Bekker-Jensen, D. B., Puglia, M., Christensen, S. D. K., Vanselow, J. T., Nielsen, M. M., Kratchmarova, I., Kelstrup, C. D., Olsen, J. V, & Blagoev, B. (2018). UbiSite approach for comprehensive mapping of lysine and N-terminal ubiquitination sites. *Nature Structural & Molecular Biology*, *25*(7), 631–640. https://doi.org/10.1038/s41594-018-0084-y

Alam, M. S., Gaida, M. M., Ogawa, Y., Kolios, A. G. A., Lasitschka, F., & Ashwell, J. D. (2014). Counter-regulation of T cell effector function by differentially activated p38. *Journal of Experimental Medicine*, *211*(6), 1257–1270. https://doi.org/10.1084/jem.20131917

Ali, M. F., Dasari, H., Van Keulen, V. P., & Carmona, E. M. (2017). Canonical Stimulation of the NLRP3 Inflammasome by Fungal Antigens Links Innate and Adaptive B-Lymphocyte Responses by Modulating IL-1β and IgM Production. *Frontiers in Immunology*, *8*. https://doi.org/10.3389/fimmu.2017.01504

Andersen, K. R., Leksa, N. C., & Schwartz, T. U. (2013). Optimized E. coli expression strain LOBSTR eliminates common contaminants from His-tag purification. *Proteins: Structure, Function, and Bioinformatics*, *81*(11), 1857–1861. https://doi.org/10.1002/prot.24364

Arbabi Ghahroudi, M., Desmyter, A., Wyns, L., Hamers, R., & Muyldermans, S. (1997). Selection and identification of single domain antibody fragments from camel heavy-chain antibodies. *FEBS Letters*, *414*(3), 521–526. https://doi.org/10.1016/s0014-5793(97)01062-4

Arbore, G., West, E. E., Spolski, R., Robertson, A. A. B., Klos, A., Rheinheimer, C., Dutow, P., Woodruff, T. M., Yu, Z. X., O'Neill, L. A., Coll, R. C., Sher, A., Leonard, W. J., Köhl, J., Monk, P., Cooper, M. A., Arno, M., Afzali, B., Lachmann, H. J., … Kemper, C. (2016). T helper 1 immunity requires complement-driven NLRP3 inflammasome activity in CD4+ T cells. *Science*, *352*(6292). https://doi.org/10.1126/science.aad1210

Arias, C. F., & López, S. (2021). Rotavirus cell entry: not so simple after all. *Current Opinion in Virology*, *48*, 42–48. https://doi.org/10.1016/j.coviro.2021.03.011

Arnold, M. M. (2016). The Rotavirus Interferon Antagonist NSP1: Many Targets, Many Questions. *Journal of Virology*, *90*(11), 5212–5215. https://doi.org/10.1128/JVI.03068-15

Arnold, M. M., & Patton, J. T. (2011). Diversity of Interferon Antagonist Activities Mediated by NSP1 Proteins of Different Rotavirus Strains. *Journal of Virology*, *85*(5), 1970–1979. https://doi.org/10.1128/JVI.01801-10

Arnold, M., Patton, J. T., & McDonald, S. M. (2009). Culturing, Storage, and Quantification of Rotaviruses. *Current Protocols in Microbiology*, *15*(1). https://doi.org/10.1002/9780471729259.mc15c03s15

Ashour, J., Schmidt, F. I., Hanke, L., Cragnolini, J., Cavallari, M., Altenburg, A., Brewer, R., Ingram, J., Shoemaker, C., & Ploegh, H. L. (2015). Intracellular Expression of Camelid Single-Domain Antibodies Specific for Influenza Virus Nucleoprotein Uncovers Distinct Features of Its Nuclear Localization. *Journal of Virology*, *89*(5), 2792–2800. https://doi.org/10.1128/JVI.02693-14

Atasheva, S., Fish, A., Fornerod, M., & Frolova, E. I. (2010). Venezuelan Equine Encephalitis Virus Capsid Protein Forms a Tetrameric Complex with CRM1 and Importin α/β That Obstructs Nuclear Pore Complex Function. *Journal of Virology*, *84*(9), 4158–4171. https://doi.org/10.1128/JVI.02554-09

Atkins, G. J., Sheahan, B. J., & Liljeström, P. (1999). The molecular pathogenesis of Semliki Forest virus: a model virus made useful? *Journal of General Virology*, *80*(9), 2287–2297. https://doi.org/10.1099/0022-1317-80-9-2287

Baek, K., Scott, D. C., & Schulman, B. A. (2021). NEDD8 and ubiquitin ligation by cullin-RING E3 ligases. *Current Opinion in Structural Biology*, *67*, 101–109. https://doi.org/10.1016/j.sbi.2020.10.007

Bagnall, R. D., Roberts, R. G., Mirza, M. M., Torigoe, T., Prescott, N. J., & Mathew, C. G. (2008). Novel isoforms of the CARD8 (TUCAN) gene evade a nonsense mutation. *European Journal of Human Genetics : EJHG*, *16*(5), 619–625. https://doi.org/10.1038/sj.ejhg.5201996

Ball, D. P., Taabazuing, C. Y., Griswold, A. R., Orth, E. L., Rao, S. D., Kotliar, I. B., Vostal, L. E., Johnson, D. C., & Bachovchin, D. A. (2020). Caspase-1 interdomain linker cleavage is required for pyroptosis. *Life Science Alliance*, *3*(3). https://doi.org/10.26508/lsa.202000664

Ball, D. P., Tsamouri, L. P., Wang, A. E., Huang, H.-C., Warren, C. D., Wang, Q., Edmondson, I. H., Griswold, A. R., Rao, S. D., Johnson, D. C., & Bachovchin, D. A. (2022). Oxidized thioredoxin-1 restrains the NLRP1 inflammasome. *Science Immunology*, *7*(77), eabm7200. https://doi.org/10.1126/sciimmunol.abm7200

Bard, J. A. M., Goodall, E. A., Greene, E. R., Jonsson, E., Dong, K. C., & Martin, A. (2018). Structure and Function of the 26S Proteasome. *Annual Review of Biochemistry*, *87*(1), 697–724. https://doi.org/10.1146/annurev-biochem-062917-011931

Barnhart, M. D., Moon, S. L., Emch, A. W., Wilusz, C. J., & Wilusz, J. (2013). Changes in Cellular mRNA Stability, Splicing, and Polyadenylation through HuR Protein Sequestration by a Cytoplasmic RNA Virus. *Cell Reports*, *5*(4), 909–917. https://doi.org/10.1016/j.celrep.2013.10.012

Barro, M., & Patton, J. T. (2007). Rotavirus NSP1 Inhibits Expression of Type I Interferon by Antagonizing the Function of Interferon Regulatory Factors IRF3, IRF5, and IRF7. *Journal of Virology*, *81*(9), 4473–4481. https://doi.org/10.1128/JVI.02498-06

Batlle, R., Andrés, E., Gonzalez, L., Llonch, E., Igea, A., Gutierrez-Prat, N., Berenguer-Llergo, A., & Nebreda, A. R. (2019). Regulation of tumor angiogenesis and mesenchymal–endothelial transition by p38α through TGF-β and JNK signaling. *Nature Communications*, *10*(1), 3071. https://doi.org/10.1038/s41467-019-10946-y

Bauernfeind, F. G., Horvath, G., Stutz, A., Alnemri, E. S., MacDonald, K., Speert, D., Fernandes-Alnemri, T., Wu, J., Monks, B. G., Fitzgerald, K. A., Hornung, V., & Latz, E. (2009). Cutting Edge: NF-κB Activating Pattern Recognition and Cytokine Receptors License NLRP3 Inflammasome Activation by Regulating NLRP3 Expression. *The Journal of Immunology*, *183*(2), 787–791. https://doi.org/10.4049/jimmunol.0901363

Bauernfried, S., Scherr, M. J., Pichlmair, A., Duderstadt, K. E., & Hornung, V. (2021). Human NLRP1 is a sensor for double-stranded RNA. *Science*, *371*(6528). https://doi.org/10.1126/science.abd0811

Beilharz, M., De Nardo, D., Latz, E., & Franklin, B. S. (2016). *Measuring NLR Oligomerization II: Detection of ASC Speck Formation by Confocal Microscopy and Immunofluorescence* (pp. 145–158). https://doi.org/10.1007/978-1-4939-3566-6_9

Ben-Nissan, G., & Sharon, M. (2014). Regulating the 20S Proteasome Ubiquitin-Independent Degradation Pathway. *Biomolecules*, *4*(3), 862–884. https://doi.org/10.3390/biom4030862

Bernard, E., Hamel, R., Neyret, A., Ekchariyawat, P., Molès, J.-P., Simmons, G., Chazal, N., Desprès, P., Missé, D., & Briant, L. (2015). Human keratinocytes restrict chikungunya virus replication at a post-fusion step. *Virology*, *476*, 1–10. https://doi.org/10.1016/j.virol.2014.11.013

Bertheloot, D., Wanderley, C. W., Schneider, A. H., Schiffelers, L. D., Wuerth, J. D., Tödtmann, J. M., Maasewerd, S., Hawwari, I., Duthie, F., Rohland, C., Ribeiro, L. S., Jenster, L., Rosero, N., Tesfamariam, Y. M., Cunha, F. Q., Schmidt, F. I., & Franklin, B. S. (2022). Nanobodies dismantle post-pyroptotic ASC specks and counteract inflammation in vivo. *EMBO Molecular Medicine*, *14*(6). https://doi.org/10.15252/emmm.202115415

Beutler, B. (2004). Innate immunity: an overview. *Molecular Immunology*, *40*(12), 845–859. https://doi.org/10.1016/j.molimm.2003.10.005

Bhardwaj, S., Rani, S., Kumaran, M. S., Bhatia, A., & Parsad, D. (2020). Expression of Th17- and Treg-specific transcription factors in vitiligo patients. *International Journal of Dermatology*, *59*(4), 474–481. https://doi.org/10.1111/ijd.14766

Bhowmick, R., Halder, U. C., Chattopadhyay, S., Nayak, M. K., & Chawla-Sarkar, M. (2013). Rotavirus-Encoded Nonstructural Protein 1 Modulates Cellular Apoptotic Machinery by Targeting Tumor Suppressor Protein p53. *Journal of Virology*, *87*(12), 6840–6850. https://doi.org/10.1128/JVI.00734-13

Boucher, D., Monteleone, M., Coll, R. C., Chen, K. W., Ross, C. M., Teo, J. L., Gomez, G. A., Holley, C. L., Bierschenk, D., Stacey, K. J., Yap, A. S., Bezbradica, J. S., & Schroder, K. (2018). Caspase-1 self-cleavage is an intrinsic mechanism to terminate inflammasome activity. *Journal of Experimental Medicine*, *215*(3), 827–840. https://doi.org/10.1084/jem.20172222

Boyden, E. D., & Dietrich, W. F. (2006). Nalp1b controls mouse macrophage susceptibility to anthrax lethal toxin. *Nature Genetics*, *38*(2), 240–244. https://doi.org/10.1038/ng1724

Broz, P., von Moltke, J., Jones, J. W., Vance, R. E., & Monack, D. M. (2010). Differential Requirement for Caspase-1 Autoproteolysis in Pathogen-Induced Cell Death and

Cytokine Processing. *Cell Host & Microbe*, *8*(6), 471–483. https://doi.org/10.1016/j.chom.2010.11.007

Brubaker, S. W., Bonham, K. S., Zanoni, I., & Kagan, J. C. (2015). Innate Immune Pattern Recognition: A Cell Biological Perspective. *Annual Review of Immunology*, *33*(1), 257–290. https://doi.org/10.1146/annurev-immunol-032414-112240

Bruchard, M., Rebé, C., Derangère, V., Togbé, D., Ryffel, B., Boidot, R., Humblin, E., Hamman, A., Chalmin, F., Berger, H., Chevriaux, A., Limagne, E., Apetoh, L., Végran, F., & Ghiringhelli, F. (2015). The receptor NLRP3 is a transcriptional regulator of TH2 differentiation. *Nature Immunology*, *16*(8), 859–870. https://doi.org/10.1038/ni.3202

Bulatov, E., & Ciulli, A. (2015). Targeting Cullin–RING E3 ubiquitin ligases for drug discovery: structure, assembly and small-molecule modulation. *Biochemical Journal*, *467*(3), 365–386. https://doi.org/10.1042/BJ20141450

Caddy, S., Papa, G., Borodavka, A., & Desselberger, U. (2021). Rotavirus research: 2014–2020. *Virus Research*, *304*, 198499. https://doi.org/10.1016/j.virusres.2021.198499

Canovas, B., & Nebreda, A. R. (2021). Diversity and versatility of p38 kinase signalling in health and disease. *Nature Reviews Molecular Cell Biology*, *22*(5), 346–366. https://doi.org/10.1038/s41580-020-00322-w

Carenza, C., Franzese, S., Calcaterra, F., Mavilio, D., & Della Bella, S. (2021). Comprehensive Phenotyping of Dendritic Cells in Cancer Patients by Flow Cytometry. *Cytometry Part A*, *99*(3), 218–230. https://doi.org/10.1002/cyto.a.24245

Cargnello, M., & Roux, P. P. (2011). Activation and Function of the MAPKs and Their Substrates, the MAPK-Activated Protein Kinases. *Microbiology and Molecular Biology Reviews*, *75*(1), 50–83. https://doi.org/10.1128/MMBR.00031-10

Carrasco, L., Sanz, M., & González-Almela, E. (2018). The Regulation of Translation in Alphavirus-Infected Cells. *Viruses*, *10*(2), 70. https://doi.org/10.3390/v10020070

Casado, P., Alcolea, M. P., Iorio, F., Rodríguez-Prados, J.-C., Vanhaesebroeck, B., Saez-Rodriguez, J., Joel, S., & Cutillas, P. R. (2013). Phosphoproteomics data classify hematological cancer cell lines according to tumor type and sensitivity to kinase inhibitors. *Genome Biology*, *14*(4), R37. https://doi.org/10.1186/gb-2013-14-4-r37

Casson, C. N., Yu, J., Reyes, V. M., Taschuk, F. O., Yadav, A., Copenhaver, A. M., Nguyen, H. T., Collman, R. G., & Shin, S. (2015). Human caspase-4 mediates noncanonical inflammasome activation against gram-negative bacterial pathogens. *Proceedings of the National Academy of Sciences of the United States of America*, *112*(21), 6688–6693. https://doi.org/10.1073/pnas.1421699112

Caussinus, E., Kanca, O., & Affolter, M. (2012). Fluorescent fusion protein knockout mediated by anti-GFP nanobody. *Nature Structural & Molecular Biology*, *19*(1), 117–121. https://doi.org/10.1038/nsmb.2180

Cavailles, P., Flori, P., Papapietro, O., Bisanz, C., Lagrange, D., Pilloux, L., Massera, C., Cristinelli, S., Jublot, D., Bastien, O., Loeuillet, C., Aldebert, D., Touquet, B., Fournié, G. J., & Cesbron-Delauw, M. F. (2014). A Highly Conserved Toxo1 Haplotype Directs Resistance to Toxoplasmosis and Its Associated Caspase-1 Dependent Killing of Parasite and Host Macrophage. *PLoS Pathogens*, *10*(4). https://doi.org/10.1371/journal.ppat.1004005

Chang-Graham, A. L., Perry, J. L., Strtak, A. C., Ramachandran, N. K., Criglar, J. M., Philip, A. A., Patton, J. T., Estes, M. K., & Hyser, J. M. (2019). Rotavirus Calcium Dysregulation Manifests as Dynamic Calcium Signaling in the Cytoplasm and

Endoplasmic Reticulum. *Scientific Reports*, *9*(1), 10822. https://doi.org/10.1038/s41598-019-46856-8

Chao, Y.-Y., Puhach, A., Frieser, D., Arunkumar, M., Lehner, L., Seeholzer, T., Garcia-Lopez, A., van der Wal, M., Fibi-Smetana, S., Dietschmann, A., Sommermann, T., Ćiković, T., Taher, L., Gresnigt, M. S., Vastert, S. J., van Wijk, F., Panagiotou, G., Krappmann, D., Groß, O., & Zielinski, C. E. (2023). Human TH17 cells engage gasdermin E pores to release IL-1α on NLRP3 inflammasome activation. *Nature Immunology*, *24*(2), 295–308. https://doi.org/10.1038/s41590-022-01386-w

Chavarría-Smith, J., Mitchell, P. S., Ho, A. M., Daugherty, M. D., & Vance, R. E. (2016). Functional and Evolutionary Analyses Identify Proteolysis as a General Mechanism for NLRP1 Inflammasome Activation. *PLoS Pathogens*, *12*(12). https://doi.org/10.1371/journal.ppat.1006052

Chavarría-Smith, J., & Vance, R. E. (2013). Direct Proteolytic Cleavage of NLRP1B Is Necessary and Sufficient for Inflammasome Activation by Anthrax Lethal Factor. *PLoS Pathogens*, *9*(6). https://doi.org/10.1371/journal.ppat.1003452

Chen, K. W., Groß, C. J., Sotomayor, F. V., Stacey, K. J., Tschopp, J., Sweet, M. J., & Schroder, K. (2014). The Neutrophil NLRC4 Inflammasome Selectively Promotes IL-1β Maturation without Pyroptosis during Acute Salmonella Challenge. *Cell Reports*, *8*(2), 570–582. https://doi.org/10.1016/j.celrep.2014.06.028

Chen, W., Foo, S.-S., Zaid, A., Teng, T.-S., Herrero, L. J., Wolf, S., Tharmarajah, K., Vu, L. D., van Vreden, C., Taylor, A., Freitas, J. R., Li, R. W., Woodruff, T. M., Gordon, R., Ojcius, D. M., Nakaya, H. I., Kanneganti, T.-D., O'Neill, L. A. J., Robertson, A. A. B., … Mahalingam, S. (2017). Specific inhibition of NLRP3 in chikungunya disease reveals a role for inflammasomes in alphavirus-induced inflammation. *Nature Microbiology*, *2*(10), 1435–1445. https://doi.org/10.1038/s41564-017-0015-4

Cheng, Y., Sun, F., Wang, L., Gao, M., Xie, Y., Sun, Y., Liu, H., Yuan, Y., Yi, W., Huang, Z., Yan, H., Peng, K., Wu, Y., & Cao, Z. (2020). Virus-induced p38 MAPK activation facilitates viral infection. *Theranostics*, *10*(26), 12223–12240. https://doi.org/10.7150/thno.50992

Cheong, M., Gartlan, K. H., Lee, J. S., Tey, S.-K., Zhang, P., Kuns, R. D., Andoniou, C. E., Martins, J. P., Chang, K., Sutton, V. R., Kelly, G., Varelias, A., Vuckovic, S., Markey, K. A., Boyle, G. M., Smyth, M. J., Engwerda, C. R., MacDonald, K. P. A., Trapani, J. A., … Hill, G. R. (2020). ASC Modulates CTL Cytotoxicity and Transplant Outcome Independent of the Inflammasome. *Cancer Immunology Research*, *8*(8), 1085–1098. https://doi.org/10.1158/2326-6066.CIR-19-0653

Chou, W.-C., Guo, Z., Guo, H., Chen, L., Zhang, G., Liang, K., Xie, L., Tan, X., Gibson, S. A., Rampanelli, E., Wang, Y., Montgomery, S. A., Brickey, W. J., Deng, M., Freeman, L., Zhang, S., Su, M. A., Chen, X., Wan, Y. Y., & Ting, J. P.-Y. (2021). AIM2 in regulatory T cells restrains autoimmune diseases. *Nature*, *591*(7849), 300–305. https://doi.org/10.1038/s41586-021-03231-w

Chu, Z. L., Pio, F., Xie, Z., Welsh, K., Krajewska, M., Krajewski, S., Godzik, A., & Reed, J. C. (2001). A Novel Enhancer of the Apaf1 Apoptosome Involved in Cytochrome c-dependent Caspase Activation and Apoptosis. *Journal of Biological Chemistry*, *276*(12), 9239–9245. https://doi.org/10.1074/jbc.M006309200

Chui, A. J., Griswold, A. R., Taabazuing, C. Y., Orth, E. L., Gai, K., Rao, S. D., Ball, D. P., Hsiao, J. C., & Bachovchin, D. A. (2020). Activation of the CARD8 Inflammasome Requires a Disordered Region. *Cell Reports*, *33*(2), 108264. https://doi.org/10.1016/j.celrep.2020.108264

Chui, A. J., Okondo, M. C., Rao, S. D., Gai, K., Griswold, A. R., Johnson, D. C., Ball, D. P., Taabazuing, C. Y., Orth, E. L., Vittimberga, B. A., & Bachovchin, D. A. (2019). N-terminal degradation activates the NLRP1B inflammasome. *Science*, *364*(6435), 82–85. https://doi.org/10.1126/science.aau1208

Chung, Y., Chang, S. H., Martinez, G. J., Yang, X. O., Nurieva, R., Kang, H. S., Ma, L., Watowich, S. S., Jetten, A. M., Tian, Q., & Dong, C. (2009). Critical Regulation of Early Th17 Cell Differentiation by Interleukin-1 Signaling. *Immunity*, *30*(4), 576–587. https://doi.org/10.1016/j.immuni.2009.02.007

Cirelli, K. M., Gorfu, G., Hassan, M. A., Printz, M., Crown, D., Leppla, S. H., Grigg, M. E., Saeij, J. P. J., & Moayeri, M. (2014). Inflammasome Sensor NLRP1 Controls Rat Macrophage Susceptibility to Toxoplasma gondii. *PLoS Pathogens*, *10*(3), e1003927. https://doi.org/10.1371/journal.ppat.1003927

Coll, R. C., Robertson, A. A. B., Chae, J. J., Higgins, S. C., Muñoz-Planillo, R., Inserra, M. C., Vetter, I., Dungan, L. S., Monks, B. G., Stutz, A., Croker, D. E., Butler, M. S., Haneklaus, M., Sutton, C. E., Núñez, G., Latz, E., Kastner, D. L., Mills, K. H. G., Masters, S. L., … O'Neill, L. A. J. (2015). A small-molecule inhibitor of the NLRP3 inflammasome for the treatment of inflammatory diseases. *Nature Medicine*, *21*(3), 248–255. https://doi.org/10.1038/nm.3806

Costa, F. R. C., Leite, J. A., Rassi, D. M., da Silva, J. F., Elias-Oliveira, J., Guimarães, J. B., Foss-Freitas, M. C., Câmara, N. O. S., Pontillo, A., Tostes, R. C., Silva, J. S., & Carlos, D. (2021). NLRP1 acts as a negative regulator of Th17 cell programming in mice and humans with autoimmune diabetes. *Cell Reports*, *35*(8), 109176. https://doi.org/10.1016/j.celrep.2021.109176

Dai, J., Yi, G., Philip, A. A., & Patton, J. T. (2022). Rotavirus NSP1 Subverts the Antiviral Oligoadenylate Synthetase-RNase L Pathway by Inducing RNase L Degradation. *MBio*, *13*(6). https://doi.org/10.1128/mbio.02995-22

Davis, K. A., Morelli, M., & Patton, J. T. (2017). Rotavirus NSP1 Requires Casein Kinase II-Mediated Phosphorylation for Hijacking of Cullin-RING Ligases. *MBio*, *8*(4). https://doi.org/10.1128/mBio.01213-17

Davis, M. A., Fairgrieve, M. R., Den Hartigh, A., Yakovenko, O., Duvvuri, B., Lood, C., Thomas, W. E., Fink, S. L., & Gale, M. (2019). Calpain drives pyroptotic vimentin cleavage, intermediate filament loss, and cell rupture that mediates immunostimulation. *Proceedings of the National Academy of Sciences*, *116*(11), 5061–5070. https://doi.org/10.1073/pnas.1818598116

de Castro-Jorge, L. A., de Carvalho, R. V. H., Klein, T. M., Hiroki, C. H., Lopes, A. H., Guimarães, R. M., Fumagalli, M. J., Floriano, V. G., Agostinho, M. R., Slhessarenko, R. D., Ramalho, F. S., Cunha, T. M., Cunha, F. Q., da Fonseca, B. A. L., & Zamboni, D. S. (2019). The NLRP3 inflammasome is involved with the pathogenesis of Mayaro virus. *PLOS Pathogens*, *15*(9), e1007934. https://doi.org/10.1371/journal.ppat.1007934

Desselberger, U. (2014). Rotaviruses. *Virus Research*, *190*, 75–96. https://doi.org/10.1016/j.virusres.2014.06.016

Di Fiore, I. J. M., Holloway, G., & Coulson, B. S. (2015). Innate immune responses to rotavirus infection in macrophages depend on MAVS but involve neither the NLRP3 inflammasome nor JNK and p38 signaling pathways. *Virus Research*, *208*, 89–97. https://doi.org/10.1016/j.virusres.2015.06.004

Dian, Z., Sun, Y., Zhang, G., Xu, Y., Fan, X., Yang, X., Pan, Q., Peppelenbosch, M., & Miao, Z. (2021). Rotavirus-related systemic diseases: clinical manifestation, evidence

and pathogenesis. *Critical Reviews in Microbiology*, *47*(5), 580–595. https://doi.org/10.1080/1040841X.2021.1907738

Dick, M. S., Sborgi, L., Rühl, S., Hiller, S., & Broz, P. (2016). ASC filament formation serves as a signal amplification mechanism for inflammasomes. *Nature Communications*, *7*(1), 11929. https://doi.org/10.1038/ncomms11929

Dickson, M. A., Hahn, W. C., Ino, Y., Ronfard, V., Wu, J. Y., Weinberg, R. A., Louis, D. N., Li, F. P., & Rheinwald, J. G. (2000). Human Keratinocytes That Express hTERT and Also Bypass a p16 INK4a-Enforced Mechanism That Limits Life Span Become Immortal yet Retain Normal Growth and Differentiation Characteristics. *Molecular and Cellular Biology*, *20*(4), 1436–1447. https://doi.org/10.1128/MCB.20.4.1436-1447.2000

Dinarello, C. A. (2009). Immunological and Inflammatory Functions of the Interleukin-1 Family. *Annual Review of Immunology*, *27*(1), 519–550. https://doi.org/10.1146/annurev.immunol.021908.132612

Dinarello, C. A. (2018). Overview of the IL-1 family in innate inflammation and acquired immunity. *Immunological Reviews*, *281*(1), 8–27. https://doi.org/10.1111/imr.12621

Ding, J., Wang, K., Liu, W., She, Y., Sun, Q., Shi, J., Sun, H., Wang, D.-C., & Shao, F. (2016). Pore-forming activity and structural autoinhibition of the gasdermin family. *Nature*, *535*(7610), 111–116. https://doi.org/10.1038/nature18590

Ding, S., Mooney, N., Li, B., Kelly, M. R., Feng, N., Loktev, A. V., Sen, A., Patton, J. T., Jackson, P. K., & Greenberg, H. B. (2016). Comparative Proteomics Reveals Strain-Specific β-TrCP Degradation via Rotavirus NSP1 Hijacking a Host Cullin-3-Rbx1 Complex. *PLOS Pathogens*, *12*(10), e1005929. https://doi.org/10.1371/journal.ppat.1005929

Ding, S., Zhu, S., Ren, L., Feng, N., Song, Y., Ge, X., Li, B., Flavell, R. A., & Greenberg, H. B. (2018). Rotavirus VP3 targets MAVS for degradation to inhibit type III interferon expression in intestinal epithelial cells. *ELife*, *7*. https://doi.org/10.7554/eLife.39494

Doitsh, G., Galloway, N. L. K., Geng, X., Yang, Z., Monroe, K. M., Zepeda, O., Hunt, P. W., Hatano, H., Sowinski, S., Muñoz-Arias, I., & Greene, W. C. (2014). Cell death by pyroptosis drives CD4 T-cell depletion in HIV-1 infection. *Nature*, *505*(7484), 509–514. https://doi.org/10.1038/nature12940

Dombrowski, Y., Peric, M., Koglin, S., Kammerbauer, C., Göß, C., Anz, D., Simanski, M., Gläser, R., Harder, J., Hornung, V., Gallo, R. L., Ruzicka, T., Besch, R., & Schauber, J. (2011). Cytosolic DNA Triggers Inflammasome Activation in Keratinocytes in Psoriatic Lesions. *Science Translational Medicine*, *3*(82). https://doi.org/10.1126/scitranslmed.3002001

Donado, C. A., Cao, A. B., Simmons, D. P., Croker, B. A., Brennan, P. J., & Brenner, M. B. (2020). A Two-Cell Model for IL-1β Release Mediated by Death-Receptor Signaling. *Cell Reports*, *31*(1), 107466. https://doi.org/10.1016/j.celrep.2020.03.030

D'Osualdo, A., Weichenberger, C. X., Wagner, R. N., Godzik, A., Wooley, J., & Reed, J. C. (2011). CARD8 and NLRP1 undergo autoproteolytic processing through a ZU5-like domain. *PLoS ONE*, *6*(11). https://doi.org/10.1371/journal.pone.0027396

Drutman, S. B., Haerynck, F., Zhong, F. L., Hum, D., Hernandez, N. J., Belkaya, S., Rapaport, F., de Jong, S. J., Creytens, D., Tavernier, S. J., Bonte, K., De Schepper, S., der Werff ten Bosch, J. van, Lorenzo-Diaz, L., Wullaert, A., Bossuyt, X., Orth, G., Bonagura, V. R., Béziat, V., … Laurent-Casanova, J. (2019). Homozygous NLRP1 gain-of-function mutation in siblings with a syndromic form of recurrent respiratory

papillomatosis. *Proceedings of the National Academy of Sciences of the United States of America*, *116*(38), 19055–19063. https://doi.org/10.1073/pnas.1906184116

Dunn, S. J., Cross, T. L., & Greenberg, H. B. (1994). Comparison of the Rotavirus Nonstructural Protein NSP1 (NS53) from Different Species by Sequence Analysis and Northern Blot Hybridization. *Virology*, *203*(1), 178–183. https://doi.org/10.1006/viro.1994.1471

Ekchariyawat, P., Hamel, R., Bernard, E., Wichit, S., Surasombatpattana, P., Talignani, L., Thomas, F., Choumet, V., Yssel, H., Desprès, P., Briant, L., & Missé, D. (2015). Inflammasome signaling pathways exert antiviral effect against Chikungunya virus in human dermal fibroblasts. *Infection, Genetics and Evolution : Journal of Molecular Epidemiology and Evolutionary Genetics in Infectious Diseases*, *32*, 401–408. https://doi.org/10.1016/j.meegid.2015.03.025

Enchev, R. I., Schulman, B. A., & Peter, M. (2015). Protein neddylation: beyond cullin–RING ligases. *Nature Reviews Molecular Cell Biology*, *16*(1), 30–44. https://doi.org/10.1038/nrm3919

Esona, M. D., Roy, S., Rungsrisuriyachai, K., Sanchez, J., Vasquez, L., Gomez, V., Rios, L. A., Bowen, M. D., & Vazquez, M. (2017). Characterization of a triple-recombinant, reassortant rotavirus strain from the Dominican Republic. *Journal of General Virology*, *98*(2), 134–142. https://doi.org/10.1099/jgv.0.000688

Esterly, A. T., Lloyd, M. G., Upadhyaya, P., Moffat, J. F., & Thangamani, S. (2022). A Human Skin Model for Assessing Arboviral Infections. *JID Innovations*, *2*(4), 100128. https://doi.org/10.1016/j.xjidi.2022.100128

Evavold, C. L., Ruan, J., Tan, Y., Xia, S., Wu, H., & Kagan, J. C. (2018). The Pore-Forming Protein Gasdermin D Regulates Interleukin-1 Secretion from Living Macrophages. *Immunity*, *48*(1), 35-44.e6. https://doi.org/10.1016/j.immuni.2017.11.013

Ewald, S. E., Chavarria-Smith, J., & Boothroyd, J. C. (2014). NLRP1 Is an Inflammasome Sensor for Toxoplasma gondii. *Infection and Immunity*, *82*(1), 460–468. https://doi.org/10.1128/IAI.01170-13

Faenza, I., & Blalock, W. L. (2022). Innate Immunity: A Balance between Disease and Adaption to Stress. *Biomolecules*, *12*(5), 737. https://doi.org/10.3390/biom12050737

Faustin, B., Lartigue, L., Bruey, J.-M., Luciano, F., Sergienko, E., Bailly-Maitre, B., Volkmann, N., Hanein, D., Rouiller, I., & Reed, J. C. (2007). Reconstituted NALP1 Inflammasome Reveals Two-Step Mechanism of Caspase-1 Activation. *Molecular Cell*, *25*(5), 713–724. https://doi.org/10.1016/j.molcel.2007.01.032

Feldmeyer, L., Keller, M., Niklaus, G., Hohl, D., Werner, S., & Beer, H. D. (2007). The Inflammasome Mediates UVB-Induced Activation and Secretion of Interleukin-1β by Keratinocytes. *Current Biology*, *17*(13), 1140–1145. https://doi.org/10.1016/j.cub.2007.05.074

Fenini, G., Grossi, S., Contassot, E., Biedermann, T., Reichmann, E., French, L. E., & Beer, H. D. (2018). Genome Editing of Human Primary Keratinocytes by CRISPR/Cas9 Reveals an Essential Role of the NLRP1 Inflammasome in UVB Sensing. *Journal of Investigative Dermatology*, *138*(12), 2644–2652. https://doi.org/10.1016/j.jid.2018.07.016

Fenini, G., Grossi, S., Gehrke, S., Beer, H.-D., Satoh, T. K., Contassot, E., & French, L. E. (2018). The p38 Mitogen-Activated Protein Kinase Critically Regulates Human Keratinocyte Inflammasome Activation. *Journal of Investigative Dermatology*, *138*(6), 1380–1390. https://doi.org/10.1016/j.jid.2017.10.037

Fernandes-Alnemri, T., Wu, J., Yu, J.-W., Datta, P., Miller, B., Jankowski, W., Rosenberg, S., Zhang, J., & Alnemri, E. S. (2007). The pyroptosome: a supramolecular assembly of ASC dimers mediating inflammatory cell death via caspase-1 activation. *Cell Death & Differentiation*, *14*(9), 1590–1604. https://doi.org/10.1038/sj.cdd.4402194

Fernandes-Alnemri, T., Yu, J.-W., Datta, P., Wu, J., & Alnemri, E. S. (2009). AIM2 activates the inflammasome and cell death in response to cytoplasmic DNA. *Nature*, *458*(7237), 509–513. https://doi.org/10.1038/nature07710

Finger, J. N., Lich, J. D., Dare, L. C., Cook, M. N., Brown, K. K., Duraiswamis, C., Bertin, J. J., & Gough, P. J. (2012). Autolytic proteolysis within the function to find domain (FIIND) is required for NLRP1 inflammasome activity. *Journal of Biological Chemistry*, *287*(30), 25030–25037. https://doi.org/10.1074/jbc.M112.378323

Fink, S. L., Bergsbaken, T., & Cookson, B. T. (2008). Anthrax lethal toxin and Salmonella elicit the common cell death pathway of caspase-1-dependent pyroptosis via distinct mechanisms. *Proceedings of the National Academy of Sciences*, *105*(11), 4312–4317. https://doi.org/10.1073/pnas.0707370105

Franklin, B. S., Bossaller, L., De Nardo, D., Ratter, J. M., Stutz, A., Engels, G., Brenker, C., Nordhoff, M., Mirandola, S. R., Al-Amoudi, A., Mangan, M. S., Zimmer, S., Monks, B. G., Fricke, M., Schmidt, R. E., Espevik, T., Jones, B., Jarnicki, A. G., Hansbro, P. M., … Latz, E. (2014). The adaptor ASC has extracellular and “prionoid” activities that propagate inflammation. *Nature Immunology*, *15*(8), 727–737. https://doi.org/10.1038/ni.2913

Frew, B. C., Joag, V. R., & Mogridge, J. (2012). Proteolytic processing of Nlrp1b is required for inflammasome activity. *PLoS Pathogens*, *8*(4). https://doi.org/10.1371/journal.ppat.1002659

Fros, J., & Pijlman, G. (2016). Alphavirus Infection: Host Cell Shut-Off and Inhibition of Antiviral Responses. *Viruses*, *8*(6), 166. https://doi.org/10.3390/v8060166

Fu, J., & Wu, H. (2023). Structural Mechanisms of NLRP3 Inflammasome Assembly and Activation. *Annual Review of Immunology*, *41*, 301–316. https://doi.org/10.1146/annurev-immunol-081022-021207

Fulcher, L. J., Hutchinson, L. D., Macartney, T. J., Turnbull, C., & Sapkota, G. P. (2017). Targeting endogenous proteins for degradation through the affinity-directed protein missile system. *Open Biology*, *7*(5), 170066. https://doi.org/10.1098/rsob.170066

Fulcher, L. J., Macartney, T., Bozatzi, P., Hornberger, A., Rojas-Fernandez, A., & Sapkota, G. P. (2016). An affinity-directed protein missile system for targeted proteolysis. *Open Biology*, *6*(10). https://doi.org/10.1098/rsob.160255

Gaestel, M. (2006). MAPKAP kinases — MKs — two’s company, three’s a crowd. *Nature Reviews Molecular Cell Biology*, *7*(2), 120–130. https://doi.org/10.1038/nrm1834

Gai, K., Okondo, M. C., Rao, S. D., Chui, A. J., Ball, D. P., Johnson, D. C., & Bachovchin, D. A. (2019). DPP8/9 inhibitors are universal activators of functional NLRP1 alleles. *Cell Death and Disease*, *10*(8). https://doi.org/10.1038/s41419-019-1817-5

Galluzzi, L., Vitale, I., Aaronson, S. A., Abrams, J. M., Adam, D., Agostinis, P., Alnemri, E. S., Altucci, L., Amelio, I., Andrews, D. W., Annicchiarico-Petruzzelli, M., Antonov, A. V., Arama, E., Baehrecke, E. H., Barlev, N. A., Bazan, N. G., Bernassola, F., Bertrand, M. J. M., Bianchi, K., … Kroemer, G. (2018). Molecular mechanisms of cell death: recommendations of the Nomenclature Committee on Cell Death 2018. *Cell Death & Differentiation*, *25*(3), 486–541. https://doi.org/10.1038/s41418-017-0012-4

Gao, W., Yang, J., Liu, W., Wang, Y., & Shao, F. (2016). Site-specific phosphorylation and microtubule dynamics control Pyrin inflammasome activation. *Proceedings of the National Academy of Sciences*, *113*(33). https://doi.org/10.1073/pnas.1601700113

Gao, Y., Deason, K., Jain, A., Irizarry-Caro, R. A., Dozmorov, I., Coughlin, L. A., Rauch, I., Evers, B. M., Koh, A. Y., Wakeland, E. K., & Pasare, C. (2020). Transcriptional profiling identifies caspase-1 as a T cell–intrinsic regulator of Th17 differentiation. *Journal of Experimental Medicine*, *217*(4). https://doi.org/10.1084/jem.20190476

Garaicoechea, L., Olichon, A., Marcoppido, G., Wigdorovitz, A., Mozgovoj, M., Saif, L., Surrey, T., & Parreño, V. (2008). Llama-Derived Single-Chain Antibody Fragments Directed to Rotavirus VP6 Protein Possess Broad Neutralizing Activity In Vitro and Confer Protection against Diarrhea in Mice. *Journal of Virology*, *82*(19), 9753–9764. https://doi.org/10.1128/JVI.00436-08

Garcia-Moreno, M., Sanz, M. A., & Carrasco, L. (2015). Initiation codon selection is accomplished by a scanning mechanism without crucial initiation factors in Sindbis virus subgenomic mRNA. *RNA*, *21*(1), 93–112. https://doi.org/10.1261/rna.047084.114

Garreau de Loubresse, N., Prokhorova, I., Holtkamp, W., Rodnina, M. V., Yusupova, G., & Yusupov, M. (2014). Structural basis for the inhibition of the eukaryotic ribosome. *Nature*, *513*(7519), 517–522. https://doi.org/10.1038/nature13737

Geiger, F., Acker, J., Papa, G., Wang, X., Arter, W. E., Saar, K. L., Erkamp, N. A., Qi, R., Bravo, J. P., Strauss, S., Krainer, G., Burrone, O. R., Jungmann, R., Knowles, T. P., Engelke, H., & Borodavka, A. (2021). Liquid–liquid phase separation underpins the formation of replication factories in rotaviruses. *The EMBO Journal*, *40*(21). https://doi.org/10.15252/embj.2021107711

Ghosh, S., Gatheru, Z., Nyangao, J., Adachi, N., Urushibara, N., & Kobayashi, N. (2011). Full genomic analysis of a simian SA11-like G3P[2] rotavirus strain isolated from an asymptomatic infant: Identification of novel VP1, VP6 and NSP4 genotypes. *Infection, Genetics and Evolution*, *11*(1), 57–63. https://doi.org/10.1016/j.meegid.2010.10.010

Girardin, S. E., Boneca, I. G., Viala, J., Chamaillard, M., Labigne, A., Thomas, G., Philpott, D. J., & Sansonetti, P. J. (2003). Nod2 Is a General Sensor of Peptidoglycan through Muramyl Dipeptide (MDP) Detection. *Journal of Biological Chemistry*, *278*(11), 8869–8872. https://doi.org/10.1074/jbc.C200651200

Goh, K. C., deVeer, M. J., & Williams, B. R. G. (2000). The protein kinase PKR is required for p38 MAPK activation and the innate immune response to bacterial endotoxin. *The EMBO Journal*, *19*(16), 4292–4297. https://doi.org/10.1093/emboj/19.16.4292

Gong, Q., Robinson, K., Xu, C., Huynh, P. T., Chong, K. H. C., Tan, E. Y. J., Zhang, J., Boo, Z. Z., Teo, D. E. T., Lay, K., Zhang, Y., Lim, J. S. Y., Goh, W. I., Wright, G., Zhong, F. L., Reversade, B., & Wu, B. (2021). Structural basis for distinct inflammasome complex assembly by human NLRP1 and CARD8. *Nature Communications*, *12*(1). https://doi.org/10.1038/s41467-020-20319-5

Gorchakov, R., Frolova, E., & Frolov, I. (2005). Inhibition of Transcription and Translation in Sindbis Virus-Infected Cells. *Journal of Virology*, *79*(15), 9397–9409. https://doi.org/10.1128/JVI.79.15.9397-9409.2005

Gorfu, G., Cirelli, K. M., Melo, M. B., Mayer-Barber, K., Crown, D., Koller, B. H., Masters, S., Sher, A., Leppla, S. H., Moayeri, M., Saeij, J. P. J., & Grigg, M. E. (2014). Dual role for inflammasome sensors NLRP1 and NLRP3 in murine resistance to Toxoplasma gondii. *MBio*, *5*(1). https://doi.org/10.1128/mBio.01117-13

Gov, L., Karimzadeh, A., Ueno, N., & Lodoen, M. B. (2013). Human innate immunity to Toxoplasma gondii is mediated by host caspase-1 and ASC and parasite GRA15. *MBio*, *4*(4). https://doi.org/10.1128/mBio.00255-13

Graff, J. W., Ettayebi, K., & Hardy, M. E. (2009). Rotavirus NSP1 Inhibits NFκB Activation by Inducing Proteasome-Dependent Degradation of β-TrCP: A Novel Mechanism of IFN Antagonism. *PLoS Pathogens*, *5*(1), e1000280. https://doi.org/10.1371/journal.ppat.1000280

Graff, J. W., Ewen, J., Ettayebi, K., & Hardy, M. E. (2007). Zinc-binding domain of rotavirus NSP1 is required for proteasome-dependent degradation of IRF3 and autoregulatory NSP1 stability. *Journal of General Virology*, *88*(2), 613–620. https://doi.org/10.1099/vir.0.82255-0

Grandemange, S., Sanchez, E., Louis-Plence, P., Tran Mau-Them, F., Bessis, D., Coubes, C., Frouin, E., Seyger, M., Girard, M., Puechberty, J., Costes, V., Rodière, M., Carbasse, A., Jeziorski, E., Portales, P., Sarrabay, G., Mondain, M., Jorgensen, C., Apparailly, F., … Geneviève, D. (2017). A new autoinflammatory and autoimmune syndrome associated with NLRP1 mutations: NAIAD (NLRP1-associated autoinflammation with arthritis and dyskeratosis). *Annals of the Rheumatic Diseases*, *76*(7), 1191–1198. https://doi.org/10.1136/annrheumdis-2016-210021

Gratia, M., Sarot, E., Vende, P., Charpilienne, A., Baron, C. H., Duarte, M., Pyronnet, S., & Poncet, D. (2015). Rotavirus NSP3 Is a Translational Surrogate of the Poly(A) Binding Protein-Poly(A) Complex. *Journal of Virology*, *89*(17), 8773–8782. https://doi.org/10.1128/JVI.01402-15

Greaney, A. J., Portley, M. K., O'Mard, D., Crown, D., Maier, N. K., Mendenhall, M. A., Mayer-Barber, K. D., Leppla, S. H., & Moayeri, M. (2020). Frontline Science: Anthrax lethal toxin-induced, NLRP1-mediated IL-1β release is a neutrophil and PAD4-dependent event. *Journal of Leukocyte Biology*, *108*(3), 773–786. https://doi.org/10.1002/JLB.4HI0320-028R

Griswold, A. R., Ball, D. P., Bhattacharjee, A., Chui, A. J., Rao, S. D., Taabazuing, C. Y., & Bachovchin, D. A. (2019). DPP9's Enzymatic Activity and Not Its Binding to CARD8 Inhibits Inflammasome Activation. *ACS Chemical Biology*, *14*(11), 2424–2429. https://doi.org/10.1021/acschembio.9b00462

Griswold, A. R., Cifani, P., Rao, S. D., Axelrod, A. J., Miele, M. M., Hendrickson, R. C., Kentsis, A., & Bachovchin, D. A. (2019). A Chemical Strategy for Protease Substrate Profiling. *Cell Chemical Biology*, *26*(6), 901-907.e6. https://doi.org/10.1016/j.chembiol.2019.03.007

Griswold, A. R., Huang, H. C., & Bachovchin, D. A. (2022). The NLRP1 Inflammasome Induces Pyroptosis in Human Corneal Epithelial Cells. *Investigative Ophthalmology and Visual Science*, *63*(3). https://doi.org/10.1167/iovs.63.3.2

Groß, C. J., Mishra, R., Schneider, K. S., Médard, G., Wettmarshausen, J., Dittlein, D. C., Shi, H., Gorka, O., Koenig, P.-A., Fromm, S., Magnani, G., Ćiković, T., Hartjes, L., Smollich, J., Robertson, A. A. B., Cooper, M. A., Schmidt-Supprian, M., Schuster, M., Schroder, K., … Groß, O. (2016). K + Efflux-Independent NLRP3 Inflammasome Activation by Small Molecules Targeting Mitochondria. *Immunity*, *45*(4), 761–773. https://doi.org/10.1016/j.immuni.2016.08.010

Grywna, K., Kupfer, B., Panning, M., Drexler, J. F., Emmerich, P., Drosten, C., & Kümmerer, B. M. (2010). Detection of All Species of the Genus Alphavirus by Reverse Transcription-PCR with Diagnostic Sensitivity. *Journal of Clinical Microbiology*, *48*(9), 3386–3387. https://doi.org/10.1128/JCM.00317-10

Guarda, G., Dostert, C., Staehli, F., Cabalzar, K., Castillo, R., Tardivel, A., Schneider, P., & Tschopp, J. (2009). T cells dampen innate immune responses through inhibition of NLRP1 and NLRP3 inflammasomes. *Nature*, *460*(7252), 269–273. https://doi.org/10.1038/nature08100

Guey, B., Bodnar, M., Manié, S. N., Tardivel, A., & Petrilli, V. (2014). Caspase-1 autoproteolysis is differentially required for NLRP1b and NLRP3 inflammasome function. *Proceedings of the National Academy of Sciences of the United States of America*, *111*(48), 17254–17259. https://doi.org/10.1073/pnas.1415756111

Guimaraes, C. P., Witte, M. D., Theile, C. S., Bozkurt, G., Kundrat, L., Blom, A. E. M., & Ploegh, H. L. (2013). Site-specific C-terminal and internal loop labeling of proteins using sortase-mediated reactions. *Nature Protocols*, *8*(9), 1787–1799. https://doi.org/10.1038/nprot.2013.101

Gurusamy, D., Henning, A. N., Yamamoto, T. N., Yu, Z., Zacharakis, N., Krishna, S., Kishton, R. J., Vodnala, S. K., Eidizadeh, A., Jia, L., Kariya, C. M., Black, M. A., Eil, R., Palmer, D. C., Pan, J. H., Sukumar, M., Patel, S. J., & Restifo, N. P. (2020). Multi-phenotype CRISPR-Cas9 Screen Identifies p38 Kinase as a Target for Adoptive Immunotherapies. *Cancer Cell*, *37*(6), 818-833.e9. https://doi.org/10.1016/j.ccell.2020.05.004

Hamers-Casterman, C., Atarhouch, T., Muyldermans, S., Robinson, G., Hamers, C., Songa, E. B., Bendahman, N., & Hamers, R. (1993). Naturally occurring antibodies devoid of light chains. *Nature*, *363*(6428), 446–448. https://doi.org/10.1038/363446a0

Han, J., Lee, J.-D., Bibbs, L., & Ulevitch, R. J. (1994). A MAP Kinase Targeted by Endotoxin and Hyperosmolarity in Mammalian Cells. *Science*, *265*(5173), 808–811. https://doi.org/10.1126/science.7914033

Harapas, C. R., Robinson, K. S., Lay, K., Wong, J., Moreno Traspas, R., Nabavizadeh, N., Rass-Rothschild, A., Boisson, B., Drutman, S. B., Laohamonthonkul, P., Bonner, D., Xiong, J. R., Gorrell, M. D., Davidson, S., Yu, C.-H., Fleming, M. D., Gudera, J., Stein, J., Ben-Harosh, M., … Reversade, B. (2022). DPP9 deficiency: An inflammasomopathy that can be rescued by lowering NLRP1/IL-1 signaling. *Science Immunology*, *7*(75), eabi4611. https://doi.org/10.1126/sciimmunol.abi4611

Harper, J. W., & Schulman, B. A. (2021). Cullin-RING Ubiquitin Ligase Regulatory Circuits: A Quarter Century Beyond the F-Box Hypothesis. *Annual Review of Biochemistry*, *90*(1), 403–429. https://doi.org/10.1146/annurev-biochem-090120-013613

Hayakawa, M., Hayakawa, H., Petrova, T., Ritprajak, P., Sutavani, R. V., Jiménez-Andrade, G. Y., Sano, Y., Choo, M.-K., Seavitt, J., Venigalla, R. K. C., Otsu, K., Georgopoulos, K., Arthur, J. S. C., & Park, J. M. (2017). Loss of Functionally Redundant p38 Isoforms in T Cells Enhances Regulatory T Cell Induction. *Journal of Biological Chemistry*, *292*(5), 1762–1772. https://doi.org/10.1074/jbc.M116.764548

Heilig, R., Dick, M. S., Sborgi, L., Meunier, E., Hiller, S., & Broz, P. (2018). The Gasdermin-D pore acts as a conduit for IL-1β secretion in mice. *European Journal of Immunology*, *48*(4), 584–592. https://doi.org/10.1002/eji.201747404

Hellmich, K. A., Levinsohn, J. L., Fattah, R., Newman, Z. L., Maier, N., Sastalla, I., Liu, S., Leppla, S. H., & Moayeri, M. (2012). Anthrax Lethal Factor Cleaves Mouse Nlrp1b in Both Toxin-Sensitive and Toxin-Resistant Macrophages. *PLoS ONE*, *7*(11). https://doi.org/10.1371/journal.pone.0049741

Herce, H. D., Schumacher, D., Schneider, A. F. L., Ludwig, A. K., Mann, F. A., Fillies, M., Kasper, M.-A., Reinke, S., Krause, E., Leonhardt, H., Cardoso, M. C., & Hackenberger, C. P. R. (2017). Cell-permeable nanobodies for targeted

immunolabelling and antigen manipulation in living cells. *Nature Chemistry*, *9*(8), 762–771. https://doi.org/10.1038/nchem.2811

Herlin, T., Jørgensen, S. E., Høst, C., Mitchell, P. S., Christensen, M. H., Laustsen, M., Larsen, D. A., Schmidt, F. I., Christiansen, M., & Mogensen, T. H. (2020). Autoinflammatory disease with corneal and mucosal dyskeratosis caused by a novel NLRP1 variant. *Rheumatology*, *59*(9), 2334–2339. https://doi.org/10.1093/rheumatology/kez612

Hitoshi, N., Ken-ichi, Y., & Jun-ichi, M. (1991). Efficient selection for high-expression transfectants with a novel eukaryotic vector. *Gene*, *108*(2), 193–199. https://doi.org/10.1016/0378-1119(91)90434-D

Hochedez, P., Jaureguiberry, S., Debruyne, M., Bossi, P., Hausfater, P., Brucker, G., Bricaire, F., & Caumes, E. (2006). Chikungunya Infection in Travelers. *Emerging Infectious Diseases*, *12*(10), 1565–1567. https://doi.org/10.3201/eid1210.060495

Hochheiser, I. V., Pilsl, M., Hagelueken, G., Moecking, J., Marleaux, M., Brinkschulte, R., Latz, E., Engel, C., & Geyer, M. (2022). Structure of the NLRP3 decamer bound to the cytokine release inhibitor CRID3. *Nature*, *604*(7904), 184–189. https://doi.org/10.1038/s41586-022-04467-w

Hollingsworth, L. R., David, L., Li, Y., Griswold, A. R., Ruan, J., Sharif, H., Fontana, P., Orth-He, E. L., Fu, T. M., Bachovchin, D. A., & Wu, H. (2021). Mechanism of filament formation in UPA-promoted CARD8 and NLRP1 inflammasomes. *Nature Communications*, *12*(1). https://doi.org/10.1038/s41467-020-20320-y

Hollingsworth, L. R., Sharif, H., Griswold, A. R., Fontana, P., Mintseris, J., Dagbay, K. B., Paulo, J. A., Gygi, S. P., Bachovchin, D. A., & Wu, H. (2021). DPP9 sequesters the C terminus of NLRP1 to repress inflammasome activation. *Nature*, *592*(7856), 778–783. https://doi.org/10.1038/s41586-021-03350-4

Holloway, G., & Coulson, B. S. (2006). Rotavirus Activates JNK and p38 Signaling Pathways in Intestinal Cells, Leading to AP-1-Driven Transcriptional Responses and Enhanced Virus Replication. *Journal of Virology*, *80*(21), 10624–10633. https://doi.org/10.1128/JVI.00390-06

Hornung, V., Ablasser, A., Charrel-Dennis, M., Bauernfeind, F., Horvath, G., Caffrey, Daniel. R., Latz, E., & Fitzgerald, K. A. (2009). AIM2 recognizes cytosolic dsDNA and forms a caspase-1-activating inflammasome with ASC. *Nature*, *458*(7237), 514–518. https://doi.org/10.1038/nature07725

Hou, G., Zeng, Q., Matthijnssens, J., Greenberg, H. B., & Ding, S. (2021). Rotavirus NSP1 Contributes to Intestinal Viral Replication, Pathogenesis, and Transmission. *MBio*, *12*(6). https://doi.org/10.1128/mBio.03208-21

Hou, W., Gibbs, J. S., Lu, X., Brooke, C. B., Roy, D., Modlin, R. L., Bennink, J. R., & Yewdell, J. W. (2012). Viral infection triggers rapid differentiation of human blood monocytes into dendritic cells. *Blood*, *119*(13), 3128–3131. https://doi.org/10.1182/blood-2011-09-379479

Hsiao, J. C., Neugroschl, A. R., Chui, A. J., Taabazuing, C. Y., Griswold, A. R., Wang, Q., Huang, H.-C., Orth-He, E. L., Ball, D. P., Hiotis, G., & Bachovchin, D. A. (2022). A ubiquitin-independent proteasome pathway controls activation of the CARD8 inflammasome. *Journal of Biological Chemistry*, *298*(7), 102032. https://doi.org/10.1016/j.jbc.2022.102032

Hsu, L.-C., Ali, S. R., McGillivray, S., Tseng, P.-H., Mariathasan, S., Humke, E. W., Eckmann, L., Powell, J. J., Nizet, V., Dixit, V. M., & Karin, M. (2008). A NOD2–NALP1 complex mediates caspase-1-dependent IL-1β secretion in response to *Bacillus*

anthracis infection and muramyl dipeptide. *Proceedings of the National Academy of Sciences*, *105*(22), 7803–7808. https://doi.org/10.1073/pnas.0802726105

Hsu, M. L., & Zouali, M. (2023). Inflammasome is a central player in B cell development and homing. *Life Science Alliance*, *6*(2), e202201700. https://doi.org/10.26508/lsa.202201700

Huang, M., Zhang, X., Toh, G. A., Gong, Q., Wang, J., Han, Z., Wu, B., Zhong, F., & Chai, J. (2021). Structural and biochemical mechanisms of NLRP1 inhibition by DPP9. *Nature*, *592*(7856), 773–777. https://doi.org/10.1038/s41586-021-03320-w

Ilarraza, R., Wu, Y., Skappak, C. D., Ajamian, F., Proud, D., & Adamko, D. J. (2013). Rhinovirus has the unique ability to directly activate human T cells in vitro. *Journal of Allergy and Clinical Immunology*, *131*(2), 395–404. https://doi.org/10.1016/j.jaci.2012.11.041

Iordanov, M. S., Pribnow, D., Magun, J. L., Dinh, T. H., Pearson, J. A., Chen, S. L., & Magun, B. E. (1997). Ribotoxic stress response: activation of the stress-activated protein kinase JNK1 by inhibitors of the peptidyl transferase reaction and by sequence-specific RNA damage to the alpha-sarcin/ricin loop in the 28S rRNA. *Molecular and Cellular Biology*, *17*(6), 3373–3381. https://doi.org/10.1128/MCB.17.6.3373

Iordanov, M. S., Pribnow, D., Magun, J. L., Dinh, T. H., Pearson, J. A., & Magun, B. E. (1998). Ultraviolet radiation triggers the ribotoxic stress response in mammalian cells. *The Journal of Biological Chemistry*, *273*(25), 15794–15803. https://doi.org/10.1074/jbc.273.25.15794

Ito, S., Hara, Y., & Kubota, T. (2014). CARD8 is a negative regulator for NLRP3 inflammasome, but mutant NLRP3 in cryopyrin-associated periodic syndromes escapes the restriction. *Arthritis Research & Therapy*, *16*(1), R52. https://doi.org/10.1186/ar4483

Jakobs, C., Bartok, E., Kubarenko, A., Bauernfeind, F., & Hornung, V. (2013). Immunoblotting for Active Caspase-1. In *Methods Mol Biol.* (pp. 103–115). https://doi.org/10.1007/978-1-62703-523-1_9

Javanmard Khameneh, H., Leong, K. W. K., Mencarelli, A., Vacca, M., Mambwe, B., Neo, K., Tay, A., Zolezzi, F., Lee, B., & Mortellaro, A. (2019). The Inflammasome Adaptor ASC Intrinsically Limits CD4+ T-Cell Proliferation to Help Maintain Intestinal Homeostasis. *Frontiers in Immunology*, *10*. https://doi.org/10.3389/fimmu.2019.01566

Johnson, D. C., Okondo, M. C., Orth, E. L., Rao, S. D., Huang, H.-C., Ball, D. P., & Bachovchin, D. A. (2020). DPP8/9 inhibitors activate the CARD8 inflammasome in resting lymphocytes. *Cell Death & Disease*, *11*(8), 628. https://doi.org/10.1038/s41419-020-02865-4

Johnson, D. C., Taabazuing, C. Y., Okondo, M. C., Chui, A. J., Rao, S. D., Brown, F. C., Reed, C., Peguero, E., de Stanchina, E., Kentsis, A., & Bachovchin, D. A. (2018). DPP8/DPP9 inhibitor-induced pyroptosis for treatment of acute myeloid leukemia. *Nature Medicine*, *24*(8), 1151–1156. https://doi.org/10.1038/s41591-018-0082-y

Johnson, J. L., Yaron, T. M., Huntsman, E. M., Kerelsky, A., Song, J., Regev, A., Lin, T.-Y., Liberatore, K., Cizin, D. M., Cohen, B. M., Vasan, N., Ma, Y., Krismer, K., Robles, J. T., van de Kooij, B., van Vlimmeren, A. E., Andrée-Busch, N., Käufer, N. F., Dorovkov, M. V., … Cantley, L. C. (2023). An atlas of substrate specificities for the human serine/threonine kinome. *Nature*, *613*(7945), 759–766. https://doi.org/10.1038/s41586-022-05575-3

Jose, J., Snyder, J. E., & Kuhn, R. J. (2009). A structural and functional perspective of alphavirus replication and assembly. *Future Microbiology*, *4*(7), 837–856. https://doi.org/10.2217/fmb.09.59

Kabelitz, D. (2007). Expression and function of Toll-like receptors in T lymphocytes. *Current Opinion in Immunology*, *19*(1), 39–45. https://doi.org/10.1016/j.coi.2006.11.007

Kafai, N. M., Diamond, M. S., & Fox, J. M. (2022). Distinct Cellular Tropism and Immune Responses to Alphavirus Infection. *Annual Review of Immunology*, *40*, 615–649. https://doi.org/10.1146/annurev-immunol-101220-014952

Kamura, T., Maenaka, K., Kotoshiba, S., Matsumoto, M., Kohda, D., Conaway, R. C., Conaway, J. W., & Nakayama, K. I. (2004). VHL-box and SOCS-box domains determine binding specificity for Cul2-Rbx1 and Cul5-Rbx2 modules of ubiquitin ligases. *Genes & Development*, *18*(24), 3055–3065. https://doi.org/10.1101/gad.1252404

Kant, S., Swat, W., Zhang, S., Zhang, Z.-Y., Neel, B. G., Flavell, R. A., & Davis, R. J. (2011). TNF-stimulated MAP kinase activation mediated by a Rho family GTPase signaling pathway. *Genes & Development*, *25*(19), 2069–2078. https://doi.org/10.1101/gad.17224711

Karliuk, Y., vom Hemdt, A., Wieseler, J., Pfeffer, M., & Kümmerer, B. M. (2021). Characterization and Vector Competence Studies of Chikungunya Virus Lacking Repetitive Motifs in the 3′ Untranslated Region of the Genome. *Viruses*, *13*(3), 403. https://doi.org/10.3390/v13030403

Karran, P., & Brem, R. (2016). Protein oxidation, UVA and human DNA repair. *DNA Repair*, *44*, 178–185. https://doi.org/10.1016/j.dnarep.2016.05.024

Kayagaki, N., Kornfeld, O. S., Lee, B. L., Stowe, I. B., O'Rourke, K., Li, Q., Sandoval, W., Yan, D., Kang, J., Xu, M., Zhang, J., Lee, W. P., McKenzie, B. S., Ulas, G., Payandeh, J., Roose-Girma, M., Modrusan, Z., Reja, R., Sagolla, M., … Dixit, V. M. (2021). NINJ1 mediates plasma membrane rupture during lytic cell death. *Nature*, *591*(7848), 131–136. https://doi.org/10.1038/s41586-021-03218-7

Kayagaki, N., Stowe, I. B., Lee, B. L., O'Rourke, K., Anderson, K., Warming, S., Cuellar, T., Haley, B., Roose-Girma, M., Phung, Q. T., Liu, P. S., Lill, J. R., Li, H., Wu, J., Kummerfeld, S., Zhang, J., Lee, W. P., Snipas, S. J., Salvesen, G. S., … Dixit, V. M. (2015). Caspase-11 cleaves gasdermin D for non-canonical inflammasome signalling. *Nature*, *526*(7575), 666–671. https://doi.org/10.1038/nature15541

Kayagaki, N., Warming, S., Lamkanfi, M., Walle, L. Vande, Louie, S., Dong, J., Newton, K., Qu, Y., Liu, J., Heldens, S., Zhang, J., Lee, W. P., Roose-Girma, M., & Dixit, V. M. (2011). Non-canonical inflammasome activation targets caspase-11. *Nature*, *479*(7371), 117–121. https://doi.org/10.1038/nature10558

Kelley, N., Jeltema, D., Duan, Y., & He, Y. (2019). The NLRP3 Inflammasome: An Overview of Mechanisms of Activation and Regulation. *International Journal of Molecular Sciences*, *20*(13), 3328. https://doi.org/10.3390/ijms20133328

Kelsall, I. R. (2022). Non-lysine ubiquitylation: Doing things differently. *Frontiers in Molecular Biosciences*, *9*. https://doi.org/10.3389/fmolb.2022.1008175

Kim, D., & Kim, J. Y. (2014). Anti-CD14 antibody reduces LPS responsiveness via TLR4 internalization in human monocytes. *Molecular Immunology*, *57*(2), 210–215. https://doi.org/10.1016/j.molimm.2013.09.009

Kirchhofer, A., Helma, J., Schmidthals, K., Frauer, C., Cui, S., Karcher, A., Pellis, M., Muyldermans, S., Casas-Delucchi, C. S., Cardoso, M. C., Leonhardt, H., Hopfner, K.-

P., & Rothbauer, U. (2010). Modulation of protein properties in living cells using nanobodies. *Nature Structural & Molecular Biology*, *17*(1), 133–138. https://doi.org/10.1038/nsmb.1727

Kortmann, J., Brubaker, S. W., & Monack, D. M. (2015). Cutting Edge: Inflammasome Activation in Primary Human Macrophages Is Dependent on Flagellin. *The Journal of Immunology*, *195*(3), 815–819. https://doi.org/10.4049/jimmunol.1403100

Kozyulina, P. Y., Okorokova, L. S., Nikolsky, N. N., & Grudinkin, P. S. (2013). p38 MAP kinase enhances EGF-induced apoptosis in A431 carcinoma cells by promoting tyrosine phosphorylation of STAT1. *Biochemical and Biophysical Research Communications*, *430*(1), 331–335. https://doi.org/10.1016/j.bbrc.2012.11.041

Kuma, Y., Sabio, G., Bain, J., Shpiro, N., Márquez, R., & Cuenda, A. (2005). BIRB796 Inhibits All p38 MAPK Isoforms in Vitro and in Vivo. *Journal of Biological Chemistry*, *280*(20), 19472–19479. https://doi.org/10.1074/jbc.M414221200

Kumar, S., McDonnell, P. C., Gum, R. J., Hand, A. T., Lee, J. C., & Young, P. R. (1997). Novel homologues of CSBP/p38 MAP kinase: activation, substrate specificity and sensitivity to inhibition by pyridinyl imidazoles. *Biochemical and Biophysical Research Communications*, *235*(3), 533–538. https://doi.org/10.1006/bbrc.1997.6849

Kummer, J. A., Broekhuizen, R., Everett, H., Agostini, L., Kuijk, L., Martinon, F., Bruggen, R. van, & Tschopp, J. (2007). Inflammasome Components NALP 1 and 3 Show Distinct but Separate Expression Profiles in Human Tissues Suggesting a Site-specific Role in the Inflammatory Response. *Journal of Histochemistry & Cytochemistry*, *55*(5), 443–452. https://doi.org/10.1369/jhc.6A7101.2006

Kümmerer, B. M., Grywna, K., Gläsker, S., Wieseler, J., & Drosten, C. (2012). Construction of an infectious Chikungunya virus cDNA clone and stable insertion of mCherry reporter genes at two different sites. *Journal of General Virology*, *93*(9), 1991–1995. https://doi.org/10.1099/vir.0.043752-0

Lage, S. L., Dominical, V. M., Wong, C.-S., & Sereti, I. (2019). Evaluation of Canonical Inflammasome Activation in Human Monocytes by Imaging Flow Cytometry. *Frontiers in Immunology*, *10*. https://doi.org/10.3389/fimmu.2019.01284

Lauwereys, M., Arbabi Ghahroudi, M., Desmyter, A., Kinne, J., Hölzer, W., De Genst, E., Wyns, L., & Muyldermans, S. (1998). Potent enzyme inhibitors derived from dromedary heavy-chain antibodies. *The EMBO Journal*, *17*(13), 3512–3520. https://doi.org/10.1093/emboj/17.13.3512

Lebre, M. C., van der Aar, A. M. G., van Baarsen, L., van Capel, T. M. M., Schuitemaker, J. H. N., Kapsenberg, M. L., & de Jong, E. C. (2007). Human Keratinocytes Express Functional Toll-Like Receptor 3, 4, 5, and 9. *Journal of Investigative Dermatology*, *127*(2), 331–341. https://doi.org/10.1038/sj.jid.5700530

Lech, M., Avila-Ferrufino, A., Skuginna, V., Susanti, H. E., & Anders, H.-J. (2010). Quantitative expression of RIG-like helicase, NOD-like receptor and inflammasome-related mRNAs in humans and mice. *International Immunology*, *22*(9), 717–728. https://doi.org/10.1093/intimm/dxq058

Lefrancois, L., & Lyles, D. S. (1982). The interaction of antibody with the major surface glycoprotein of vesicular stomatitis virus. I. Analysis of neutralizing epitopes with monoclonal antibodies. *Virology*, *121*(1), 157–167.

Levandowski, C. B., Mailloux, C. M., Ferrara, T. M., Gowan, K., Ben, S., Jin, Y., McFann, K. K., Holland, P. J., Fain, P. R., Dinarello, C. A., & Spritz, R. A. (2013). NLRP1 haplotypes associated with vitiligo and autoimmunity increase interleukin-1β processing via the NLRP1 inflammasome. *Proceedings of the National Academy of*

Sciences of the United States of America, *110*(8), 2952–2956. https://doi.org/10.1073/pnas.1222808110

Levine, B., Huang, Q., Isaacs, J. T., Reed, J. C., Griffin, D. E., & Hardwick, J. M. (1993). Conversion of lytic to persistent alphavirus infection by the bcl-2 cellular oncogene. *Nature*, *361*(6414), 739–742. https://doi.org/10.1038/361739a0

Levinsohn, J. L., Newman, Z. L., Hellmich, K. A., Fattah, R., Getz, M. A., Liu, S., Sastalla, I., Leppla, S. H., & Moayeri, M. (2012). Anthrax lethal factor cleavage of Nlrp1 is required for activation of the inflammasome. *PLoS Pathogens*, *8*(3). https://doi.org/10.1371/journal.ppat.1002638

Li, M., Lay, K., Zimmer, A., Technau-Hafsi, K., Wong, J., Reimer-Taschenbrecker, A., Rohr, J., Abdalla, E., Fischer, J., Reversade, B., & Has, C. (2023). A homozygous p.Leu813Pro gain-of-function NLRP1 variant causes phenotypes of different severity in two siblings. *British Journal of Dermatology*, *188*(2), 259–267. https://doi.org/10.1093/bjd/ljac039

Li, X., Tang, L., Ye Myat Thu, & Chen, D. (2020). Titanium Ions Play a Synergistic Role in the Activation of NLRP3 Inflammasome in Jurkat T Cells. *Inflammation*, *43*(4), 1269–1278. https://doi.org/10.1007/s10753-020-01206-z

Liao, K. C., & Mogridge, J. (2009). Expression of Nlrp1b inflammasome components in human fibroblasts confers susceptibility to anthrax lethal toxin. *Infection and Immunity*, *77*(10), 4455–4462. https://doi.org/10.1128/IAI.00276-09

Lim, K.-H., Chen, L.-C., Hsu, K., Chang, C.-C., Chang, C.-Y., Kao, C.-W., Chang, Y.-F., Chang, M.-C., & Chen, C. G. (2020). BAFF-driven NLRP3 inflammasome activation in B cells. *Cell Death & Disease*, *11*(9), 820. https://doi.org/10.1038/s41419-020-03035-2

Linder, A., Bauernfried, S., Cheng, Y., Albanese, M., Jung, C., Keppler, O. T., & Hornung, V. (2020). CARD8 inflammasome activation triggers pyroptosis in human T cells. *The EMBO Journal*, *39*(19). https://doi.org/10.15252/embj.2020105071

Liston, A., & Masters, S. L. (2017). Homeostasis-altering molecular processes as mechanisms of inflammasome activation. In *Nature Reviews Immunology* (Vol. 17, Issue 3, pp. 208–214). Nature Publishing Group. https://doi.org/10.1038/nri.2016.151

Liu, X., Zhang, Z., Ruan, J., Pan, Y., Magupalli, V. G., Wu, H., & Lieberman, J. (2016). Inflammasome-activated gasdermin D causes pyroptosis by forming membrane pores. *Nature*, *535*(7610), 153–158. https://doi.org/10.1038/nature18629

Liu, Y., Ge, J., Li, Q., Gu, L., Guo, X., Ma, Z. G., & Zhu, Y. P. (2012). Anisomycin Induces Apoptosis of Glucocorticoid Resistant Acute Lymphoblastic Leukemia CEM-C1 Cells via Activation of Mitogen-Activated Protein Kinases p38 and JNK. *Neoplasma*, *60*(01), 101–110. https://doi.org/10.4149/neo_2013_014

Lozano-Ruiz, B., Tzoumpa, A., Martínez-Cardona, C., Moreno, D., Aransay, A. M., Cortazar, A. R., Picó, J., Peiró, G., Lozano, J., Zapater, P., Francés, R., & González-Navajas, J. M. (2022). Absent in Melanoma 2 (AIM2) Regulates the Stability of Regulatory T Cells. *International Journal of Molecular Sciences*, *23*(4), 2230. https://doi.org/10.3390/ijms23042230

Lutz, L. M., Pace, C. R., & Arnold, M. M. (2016). Rotavirus NSP1 Associates with Components of the Cullin RING Ligase Family of E3 Ubiquitin Ligases. *Journal of Virology*, *90*(13), 6036–6048. https://doi.org/10.1128/JVI.00704-16

Maass, D. R., Sepulveda, J., Pernthaner, A., & Shoemaker, C. B. (2007). Alpaca (Lama pacos) as a convenient source of recombinant camelid heavy chain antibodies

(VHHs). *Journal of Immunological Methods*, *324*(1–2), 13–25. https://doi.org/10.1016/j.jim.2007.04.008

Magnotti, F., Lefeuvre, L., Benezech, S., Malsot, T., Waeckel, L., Martin, A., Kerever, S., Chirita, D., Desjonqueres, M., Duquesne, A., Gerfaud-Valentin, M., Laurent, A., Sève, P., Popoff, M.-R., Walzer, T., Belot, A., Jamilloux, Y., & Henry, T. (2019). Pyrin dephosphorylation is sufficient to trigger inflammasome activation in familial Mediterranean fever patients. *EMBO Molecular Medicine*, *11*(11), e10547. https://doi.org/10.15252/emmm.201910547

Mansson, A., Adner, M., Hockerfelt, U., & Cardell, L.-O. (2006). A distinct Toll-like receptor repertoire in human tonsillar B cells, directly activated by Pam3CSK4, R-837 and CpG-2006 stimulation. *Immunology*, *0*(0), 060616085813002-??? https://doi.org/10.1111/j.1365-2567.2006.02392.x

Mao, L., Kitani, A., Similuk, M., Oler, A. J., Albenberg, L., Kelsen, J., Aktay, A., Quezado, M., Yao, M., Montgomery-Recht, K., Fuss, I. J., & Strober, W. (2018). Loss-of-function CARD8 mutation causes NLRP3 inflammasome activation and Crohn's disease. *Journal of Clinical Investigation*, *128*(5), 1793–1806. https://doi.org/10.1172/JCI98642

Marie, J., Kovacs, D., Pain, C., Jouary, T., Cota, C., Vergier, B., Picardo, M., Taieb, A., Ezzedine, K., & Cario-André, M. (2014). Inflammasome activation and vitiligo/nonsegmental vitiligo progression. *British Journal of Dermatology*, *170*(4), 816–823. https://doi.org/10.1111/bjd.12691

Marleaux, M., Anand, K., Latz, E., & Geyer, M. (2020). Crystal structure of the human NLRP9 pyrin domain suggests a distinct mode of inflammasome assembly. *FEBS Letters*, *594*(15), 2383–2395. https://doi.org/10.1002/1873-3468.13865

Marsh, M., Bolzau, E., & Helenius, A. (1983). Penetration of semliki forest virus from acidic prelysosomal vacuoles. *Cell*, *32*(3), 931–940. https://doi.org/10.1016/0092-8674(83)90078-8

Martin, B. N., Wang, C., Zhang, C., Kang, Z., Gulen, M. F., Zepp, J. A., Zhao, J., Bian, G., Do, J., Min, B., Pavicic, P. G., El-Sanadi, C., Fox, P. L., Akitsu, A., Iwakura, Y., Sarkar, A., Wewers, M. D., Kaiser, W. J., Mocarski, E. S., … Li, X. (2016). T cell–intrinsic ASC critically promotes TH17-mediated experimental autoimmune encephalomyelitis. *Nature Immunology*, *17*(5), 583–592. https://doi.org/10.1038/ni.3389

Martinon, F., Burns, K., & Tschopp, J. (2002). The inflammasome: a molecular platform triggering activation of inflammatory caspases and processing of proIL-beta. *Molecular Cell*, *10*(2), 417–426. https://doi.org/10.1016/s1097-2765(02)00599-3

Mascarenhas, D. P. A., Cerqueira, D. M., Pereira, M. S. F., Castanheira, F. V. S., Fernandes, T. D., Manin, G. Z., Cunha, L. D., & Zamboni, D. S. (2017). Inhibition of caspase-1 or gasdermin-D enable caspase-8 activation in the Naip5/NLRC4/ASC inflammasome. *PLoS Pathogens*, *13*(8), e1006502. https://doi.org/10.1371/journal.ppat.1006502

Masters, S. L., Gerlic, M., Metcalf, D., Preston, S., Pellegrini, M., O'Donnell, J. A., McArthur, K., Baldwin, T. M., Chevrier, S., Nowell, C. J., Cengia, L. H., Henley, K. J., Collinge, J. E., Kastner, D. L., Feigenbaum, L., Hilton, D. J., Alexander, W. S., Kile, B. T., & Croker, B. A. (2012). NLRP1 Inflammasome Activation Induces Pyroptosis of Hematopoietic Progenitor Cells. *Immunity*, *37*(6), 1009–1023. https://doi.org/10.1016/j.immuni.2012.08.027

Mathea, S., Abdul Azeez, K. R., Salah, E., Tallant, C., Wolfreys, F., Konietzny, R., Fischer, R., Lou, H. J., Brennan, P. E., Schnapp, G., Pautsch, A., Kessler, B. M., Turk, B. E., & Knapp, S. (2016). Structure of the Human Protein Kinase ZAK in Complex with Vemurafenib. *ACS Chemical Biology*, *11*(6), 1595–1602. https://doi.org/10.1021/acschembio.6b00043

Matthijnssens, J., Ciarlet, M., Heiman, E., Arijs, I., Delbeke, T., McDonald, S. M., Palombo, E. A., Iturriza-Gómara, M., Maes, P., Patton, J. T., Rahman, M., & Van Ranst, M. (2008). Full Genome-Based Classification of Rotaviruses Reveals a Common Origin between Human Wa-Like and Porcine Rotavirus Strains and Human DS-1-Like and Bovine Rotavirus Strains. *Journal of Virology*, *82*(7), 3204–3219. https://doi.org/10.1128/JVI.02257-07

Matthijnssens, J., Ciarlet, M., Rahman, M., Attoui, H., Bányai, K., Estes, M. K., Gentsch, J. R., Iturriza-Gómara, M., Kirkwood, C. D., Martella, V., Mertens, P. P. C., Nakagomi, O., Patton, J. T., Ruggeri, F. M., Saif, L. J., Santos, N., Steyer, A., Taniguchi, K., Desselberger, U., & Van Ranst, M. (2008). Recommendations for the classification of group A rotaviruses using all 11 genomic RNA segments. *Archives of Virology*, *153*(8), 1621–1629. https://doi.org/10.1007/s00705-008-0155-1

Matthijnssens, J., De Grazia, S., Piessens, J., Heylen, E., Zeller, M., Giammanco, G. M., Bányai, K., Buonavoglia, C., Ciarlet, M., Martella, V., & Van Ranst, M. (2011). Multiple reassortment and interspecies transmission events contribute to the diversity of feline, canine and feline/canine-like human group A rotavirus strains. *Infection, Genetics and Evolution*, *11*(6), 1396–1406. https://doi.org/10.1016/j.meegid.2011.05.007

McKee, C. M., & Coll, R. C. (2020). NLRP3 inflammasome priming: A riddle wrapped in a mystery inside an enigma. *Journal of Leukocyte Biology*, *108*(3), 937–952. https://doi.org/10.1002/JLB.3MR0720-513R

McKee, C. M., Fischer, F. A., Bezbradica, J. S., & Coll, R. C. (2021). PHOrming the inflammasome: phosphorylation is a critical switch in inflammasome signalling. *Biochemical Society Transactions*, *49*(6), 2495–2507. https://doi.org/10.1042/BST20200987

Meerbrey, K. L., Hu, G., Kessler, J. D., Roarty, K., Li, M. Z., Fang, J. E., Herschkowitz, J. I., Burrows, A. E., Ciccia, A., Sun, T., Schmitt, E. M., Bernardi, R. J., Fu, X., Bland, C. S., Cooper, T. A., Schiff, R., Rosen, J. M., Westbrook, T. F., & Elledge, S. J. (2011). The pINDUCER lentiviral toolkit for inducible RNA interference in vitro and in vivo. *Proceedings of the National Academy of Sciences*, *108*(9), 3665–3670. https://doi.org/10.1073/pnas.1019736108

Meunier, E., & Broz, P. (2017). Evolutionary Convergence and Divergence in NLR Function and Structure. *Trends in Immunology*, *38*(10), 744–757. https://doi.org/10.1016/j.it.2017.04.005

Mittelstadt, P. R., Yamaguchi, H., Appella, E., & Ashwell, J. D. (2009). T Cell Receptor-mediated Activation of p38α by Mono-phosphorylation of the Activation Loop Results in Altered Substrate Specificity. *Journal of Biological Chemistry*, *284*(23), 15469–15474. https://doi.org/10.1074/jbc.M901004200

Miura, H., Kondo, Y., Matsuda, M., & Aoki, K. (2018). Cell-to-Cell Heterogeneity in p38-Mediated Cross-Inhibition of JNK Causes Stochastic Cell Death. *Cell Reports*, *24*(10), 2658–2668. https://doi.org/10.1016/j.celrep.2018.08.020

Mizutani, H., Black, R., & Kupper, T. S. (1991). Human keratinocytes produce but do not process pro-interleukin-1 (IL-1) beta. Different strategies of IL-1 production and

processing in monocytes and keratinocytes. *The Journal of Clinical Investigation*, *87*(3), 1066–1071. https://doi.org/10.1172/JCI115067

Moayeri, M., Sastalla, I., & Leppla, S. H. (2012). Anthrax and the inflammasome. In *Microbes and Infection* (Vol. 14, Issue 5, pp. 392–400). https://doi.org/10.1016/j.micinf.2011.12.005

Moecking, J., Laohamonthonkul, P., Chalker, K., White, M. J., Harapas, C. R., Yu, C. H., Davidson, S., Hrovat-Schaale, K., Hu, D., Eng, C., Huntsman, S., Calleja, D. J., Horvat, J. C., Hansbro, P. M., O'Donoghue, R. J. J., Ting, J. P., Burchard, E. G., Geyer, M., Gerlic, M., & Masters, S. L. (2021). NLRP1 variant M1184V decreases inflammasome activation in the context of DPP9 inhibition and asthma severity. *Journal of Allergy and Clinical Immunology*, *147*(6), 2134-2145.e20. https://doi.org/10.1016/j.jaci.2020.12.636

Moore, K. P., Schwaid, A. G., Tudor, M., Park, S., Beshore, D. C., Converso, A., Shipe, W. D., Anand, R., Lan, P., Moningka, R., Rothman, D. M., Sun, W., Chi, A., Cornella-Taracido, I., Adam, G. C., Bahnck-Teets, C., Carroll, S. S., Fay, J. F., Goh, S. L., … Balibar, C. J. (2022). A Phenotypic Screen Identifies Potent DPP9 Inhibitors Capable of Killing HIV-1 Infected Cells. *ACS Chemical Biology*, *17*(9), 2595–2604. https://doi.org/10.1021/acschembio.2c00515

Mousset, C. M., Hobo, W., Woestenenk, R., Preijers, F., Dolstra, H., & van der Waart, A. B. (2019). Comprehensive Phenotyping of T Cells Using Flow Cytometry. *Cytometry Part A*, *95*(6), 647–654. https://doi.org/10.1002/cyto.a.23724

Muñoz-Planillo, R., Kuffa, P., Martínez-Colón, G., Smith, B. L., Rajendiran, T. M., & Núñez, G. (2013). K+ Efflux Is the Common Trigger of NLRP3 Inflammasome Activation by Bacterial Toxins and Particulate Matter. *Immunity*, *38*(6), 1142–1153. https://doi.org/10.1016/j.immuni.2013.05.016

Muyldermans, S. (2021). Applications of Nanobodies. *Annual Review of Animal Biosciences*, *9*, 401–421. https://doi.org/10.1146/annurev-animal-021419-083831

Nadkarni, R., Chu, W. C., Lee, C. Q. E., Mohamud, Y., Yap, L., Toh, G. A., Beh, S., Lim, R., Fan, Y. M., Zhang, Y. L., Robinson, K., Tryggvason, K., Luo, H., Zhong, F., & Ho, L. (2022). Viral proteases activate the CARD8 inflammasome in the human cardiovascular system. *Journal of Experimental Medicine*, *219*(10). https://doi.org/10.1084/jem.20212117

Nagar, A., DeMarco, R. A., & Harton, J. A. (2019). Inflammasome and Caspase-1 Activity Characterization and Evaluation: An Imaging Flow Cytometer–Based Detection and Assessment of Inflammasome Specks and Caspase-1 Activation. *The Journal of Immunology*, *202*(3), 1003–1015. https://doi.org/10.4049/jimmunol.1800973

Nakatsue, T., Katoh, I., Nakamura, S., Takahashi, Y., Ikawa, Y., & Yoshinaka, Y. (1998). Acute Infection of Sindbis Virus Induces Phosphorylation and Intracellular Translocation of Small Heat Shock Protein HSP27 and Activation of p38 MAP Kinase Signaling Pathway. *Biochemical and Biophysical Research Communications*, *253*(1), 59–64. https://doi.org/10.1006/bbrc.1998.9724

Nandi, D., Tahiliani, P., Kumar, A., & Chandu, D. (2006). The ubiquitin-proteasome system. *Journal of Biosciences*, *31*(1), 137–155. https://doi.org/10.1007/BF02705243

Nayak, T. K., Mamidi, P., Sahoo, S. S., Kumar, P. S., Mahish, C., Chatterjee, S., Subudhi, B. B., Chattopadhyay, S., & Chattopadhyay, S. (2019). P38 and JNK Mitogen-Activated Protein Kinases Interact With Chikungunya Virus Non-structural Protein-2 and Regulate TNF Induction During Viral Infection in Macrophages. *Frontiers in Immunology*, *10*. https://doi.org/10.3389/fimmu.2019.00786

Neiman-Zenevich, J., Liao, K.-C., & Mogridge, J. (2014). Distinct Regions of NLRP1B Are Required To Respond to Anthrax Lethal Toxin and Metabolic Inhibition. *Infection and Immunity*, *82*(9), 3697–3703. https://doi.org/10.1128/IAI.02167-14

Nestle, F. O., Di Meglio, P., Qin, J.-Z., & Nickoloff, B. J. (2009). Skin immune sentinels in health and disease. *Nature Reviews Immunology*, *9*(10), 679–691. https://doi.org/10.1038/nri2622

Netea, M. G., Domínguez-Andrés, J., Barreiro, L. B., Chavakis, T., Divangahi, M., Fuchs, E., Joosten, L. A. B., van der Meer, J. W. M., Mhlanga, M. M., Mulder, W. J. M., Riksen, N. P., Schlitzer, A., Schultze, J. L., Stabell Benn, C., Sun, J. C., Xavier, R. J., & Latz, E. (2020). Defining trained immunity and its role in health and disease. *Nature Reviews Immunology*, *20*(6), 375–388. https://doi.org/10.1038/s41577-020-0285-6

Newman, Z. L., Crown, D., Leppla, S. H., & Moayeri, M. (2010). Anthrax lethal toxin activates the inflammasome in sensitive rat macrophages. *Biochemical and Biophysical Research Communications*, *398*(4), 785–789. https://doi.org/10.1016/j.bbrc.2010.07.039

Newman, Z. L., Printz, M. P., Liu, S., Crown, D., Breen, L., Miller-Randolph, S., Flodman, P., Leppla, S. H., & Moayeri, M. (2010). Susceptibility to anthrax lethal toxin-induced rat death is controlled by a single chromosome 10 locus that includes rNlrp1. *PLoS Pathogens*, *6*(5), 1–8. https://doi.org/10.1371/journal.ppat.1000906

Ng, L. F. P., Chow, A., Sun, Y.-J., Kwek, D. J. C., Lim, P.-L., Dimatatac, F., Ng, L.-C., Ooi, E.-E., Choo, K.-H., Her, Z., Kourilsky, P., & Leo, Y.-S. (2009). IL-1β, IL-6, and RANTES as Biomarkers of Chikungunya Severity. *PLoS ONE*, *4*(1), e4261. https://doi.org/10.1371/journal.pone.0004261

Okondo, M. C., Johnson, D. C., Sridharan, R., Go, E. Bin, Chui, A. J., Wang, M. S., Poplawski, S. E., Wu, W., Liu, Y., Lai, J. H., Sanford, D. G., Arciprete, M. O., Golub, T. R., Bachovchin, W. W., & Bachovchin, D. A. (2017). DPP8 and DPP9 inhibition induces pro-caspase-1-dependent monocyte and macrophage pyroptosis. *Nature Chemical Biology*, *13*(1), 46–53. https://doi.org/10.1038/nchembio.2229

Okondo, M. C., Rao, S. D., Taabazuing, C. Y., Chui, A. J., Poplawski, S. E., Johnson, D. C., & Bachovchin, D. A. (2018). Inhibition of Dpp8/9 Activates the Nlrp1b Inflammasome. *Cell Chemical Biology*, *25*(3), 262-267.e5. https://doi.org/10.1016/j.chembiol.2017.12.013

Omatola, C. A., & Olaniran, A. O. (2022). Rotaviruses: From Pathogenesis to Disease Control—A Critical Review. *Viruses*, *14*(5), 875. https://doi.org/10.3390/v14050875

Orth-He, E. L., Huang, H. C., Rao, S. D., Wang, Q., Chen, Q., O'Mara, C. M., Chui, A. J., Saoi, M., Griswold, A. R., Bhattacharjee, A., Ball, D. P., Cross, J. R., & Bachovchin, D. A. (2023). Protein folding stress potentiates NLRP1 and CARD8 inflammasome activation. *Cell Reports*, *42*(1). https://doi.org/10.1016/j.celrep.2022.111965

Ozfiliz Kilbas, P., Sonmez, O., Uysal-Onganer, P., Coker Gurkan, A., Obakan Yerlikaya, P., & Arisan, E. D. (2020). Specific c-Jun N-Terminal Kinase Inhibitor, JNK-IN-8 Suppresses Mesenchymal Profile of PTX-Resistant MCF-7 Cells through Modulating PI3K/Akt, MAPK and Wnt Signaling Pathways. *Biology*, *9*(10), 320. https://doi.org/10.3390/biology9100320

Papa, G., Borodavka, A., & Desselberger, U. (2021). Viroplasms: Assembly and Functions of Rotavirus Replication Factories. *Viruses*, *13*(7), 1349. https://doi.org/10.3390/v13071349

Park, S.-H., Ham, S., Lee, A., Möller, A., & Kim, T. S. (2019). NLRP3 negatively regulates Treg differentiation through Kpna2-mediated nuclear translocation. *Journal of*

Biological Chemistry, *294*(47), 17951–17961. https://doi.org/10.1074/jbc.RA119.010545

Park, Y. H., Wood, G., Kastner, D. L., & Chae, J. J. (2016). Pyrin inflammasome activation and RhoA signaling in the autoinflammatory diseases FMF and HIDS. *Nature Immunology*, *17*(8), 914–921. https://doi.org/10.1038/ni.3457

Patel, R. K., Burnham, A. J., Gebhart, N. N., Sokoloski, K. J., & Hardy, R. W. (2013). Role for subgenomic mRNA in host translation inhibition during Sindbis virus infection of mammalian cells. *Virology*, *441*(2), 171–181. https://doi.org/10.1016/j.virol.2013.03.022

Perez-Lopez, A., Rosales-Reyes, R., Alpuche-Aranda, C. M., & Ortiz-Navarrete, V. (2013). Salmonella Downregulates Nod-like Receptor Family CARD Domain Containing Protein 4 Expression To Promote Its Survival in B Cells by Preventing Inflammasome Activation and Cell Death. *The Journal of Immunology*, *190*(3), 1201–1209. https://doi.org/10.4049/jimmunol.1200415

Petterson, T., Månsson, A., Riesbeck, K., & Cardell, L. O. (2011). Nucleotide-binding and oligomerization domain-like receptors and retinoic acid inducible gene-like receptors in human tonsillar T lymphocytes. *Immunology*, *133*(1), 84–93. https://doi.org/10.1111/j.1365-2567.2011.03414.x

Phan, M. V. T., Anh, P. H., Cuong, N. Van, Munnink, B. B. O., van der Hoek, L., My, P. T., Tri, T. N., Bryant, J. E., Baker, S., Thwaites, G., Woolhouse, M., Kellam, P., Rabaa, M. A., & Cotten, M. (2016). Unbiased whole-genome deep sequencing of human and porcine stool samples reveals circulation of multiple groups of rotaviruses and a putative zoonotic infection. *Virus Evolution*, *2*(2), vew027. https://doi.org/10.1093/ve/vew027

Phulphagar, K., Kühn, L. I., Ebner, S., Frauenstein, A., Swietlik, J. J., Rieckmann, J., & Meissner, F. (2021). Proteomics reveals distinct mechanisms regulating the release of cytokines and alarmins during pyroptosis. *Cell Reports*, *34*(10), 108826. https://doi.org/10.1016/j.celrep.2021.108826

Planès, R., Pinilla, M., Santoni, K., Hessel, A., Passemar, C., Lay, K., Paillette, P., Valadão, A. L. C., Robinson, K. S., Bastard, P., Lam, N., Fadrique, R., Rossi, I., Pericat, D., Bagayoko, S., Leon-Icaza, S. A., Rombouts, Y., Perouzel, E., Tiraby, M., … Meunier, E. (2022). Human NLRP1 is a sensor of pathogenic coronavirus 3CL proteases in lung epithelial cells. *Molecular Cell*, *82*(13), 2385-2400.e9. https://doi.org/10.1016/j.molcel.2022.04.033

Powers, A. M., Brault, A. C., Shirako, Y., Strauss, E. G., Kang, W., Strauss, J. H., & Weaver, S. C. (2001). Evolutionary relationships and systematics of the alphaviruses. *Journal of Virology*, *75*(21), 10118–10131. https://doi.org/10.1128/JVI.75.21.10118-10131.2001

Prakash, S., Inobe, T., Hatch, A. J., & Matouschek, A. (2009). Substrate selection by the proteasome during degradation of protein complexes. *Nature Chemical Biology*, *5*(1), 29–36. https://doi.org/10.1038/nchembio.130

Prakash, S., Tian, L., Ratliff, K. S., Lehotzky, R. E., & Matouschek, A. (2004). An unstructured initiation site is required for efficient proteasome-mediated degradation. *Nature Structural & Molecular Biology*, *11*(9), 830–837. https://doi.org/10.1038/nsmb814

Próchnicki, T., Vasconcelos, M. B., Robinson, K. S., Mangan, M. S. J., De Graaf, D., Shkarina, K., Lovotti, M., Standke, L., Kaiser, R., Stahl, R., Duthie, F. G., Rothe, M., Antonova, K., Jenster, L.-M., Lau, Z. H., Rösing, S., Mirza, N., Gottschild, C.,

Wachten, D., … Latz, E. (2023). Mitochondrial damage activates the NLRP10 inflammasome. *Nature Immunology*, *24*(4), 595–603. https://doi.org/10.1038/s41590-023-01451-y

Prozzillo, Y., Fattorini, G., Santopietro, M. V., Suglia, L., Ruggiero, A., Ferreri, D., & Messina, G. (2020). Targeted Protein Degradation Tools: Overview and Future Perspectives. *Biology*, *9*(12), 421. https://doi.org/10.3390/biology9120421

Puiprom, O., Morales Vargas, R. E., Potiwat, R., Chaichana, P., Ikuta, K., Ramasoota, P., & Okabayashi, T. (2013). Characterization of chikungunya virus infection of a human keratinocyte cell line: Role of mosquito salivary gland protein in suppressing the host immune response. *Infection, Genetics and Evolution*, *17*, 210–215. https://doi.org/10.1016/j.meegid.2013.04.005

Puren, A. J., Fantuzzi, G., & Dinarello, C. A. (1999). Gene expression, synthesis, and secretion of interleukin 18 and interleukin 1beta are differentially regulated in human blood mononuclear cells and mouse spleen cells. *Proceedings of the National Academy of Sciences of the United States of America*, *96*(5), 2256–2261. https://doi.org/10.1073/pnas.96.5.2256

Raingeaud, J., Whitmarsh, A. J., Barrett, T., Dérijard, B., & Davis, R. J. (1996). MKK3- and MKK6-Regulated Gene Expression Is Mediated by the p38 Mitogen-Activated Protein Kinase Signal Transduction Pathway. *Molecular and Cellular Biology*, *16*(3), 1247–1255. https://doi.org/10.1128/MCB.16.3.1247

Rao, S. D., Chen, Q., Wang, Q., Orth-He, E. L., Saoi, M., Griswold, A. R., Bhattacharjee, A., Ball, D. P., Huang, H.-C., Chui, A. J., Covelli, D. J., You, S., Cross, J. R., & Bachovchin, D. A. (2022). M24B aminopeptidase inhibitors selectively activate the CARD8 inflammasome. *Nature Chemical Biology*, *18*(5), 565–574. https://doi.org/10.1038/s41589-021-00964-7

Rauch, I., Tenthorey, J. L., Nichols, R. D., Al Moussawi, K., Kang, J. J., Kang, C., Kazmierczak, B. I., & Vance, R. E. (2016). NAIP proteins are required for cytosolic detection of specific bacterial ligands in vivo. *Journal of Experimental Medicine*, *213*(5), 657–665. https://doi.org/10.1084/jem.20151809

Razmara, M., Srinivasula, S. M., Wang, L., Poyet, J.-L., Geddes, B. J., DiStefano, P. S., Bertin, J., & Alnemri, E. S. (2002). CARD-8 Protein, a New CARD Family Member That Regulates Caspase-1 Activation and Apoptosis. *Journal of Biological Chemistry*, *277*(16), 13952–13958. https://doi.org/10.1074/jbc.M107811200

Rice, C. M., Levis, R., Strauss, J. H., & Huang, H. V. (1987). Production of infectious RNA transcripts from Sindbis virus cDNA clones: mapping of lethal mutations, rescue of a temperature-sensitive marker, and in vitro mutagenesis to generate defined mutants. *Journal of Virology*, *61*(12), 3809–3819. https://doi.org/10.1128/jvi.61.12.3809-3819.1987

Rincon, M., Enslen, H., Raingeaud, J., Recht, M., Zapton, T., Su, M., Penix, LA., Davis, RJ., & Flavell, RA. (1998). Interferon-gamma expression by Th1 effector T cells mediated by the p38 MAP kinase signaling pathway. *The EMBO Journal*, *17*(10), 2817–2829. https://doi.org/10.1093/emboj/17.10.2817

Robinson, K. S., Teo, D. E. T., Tan, K. Sen, Toh, G. A., Ong, H. H., Lim, C. K., Lay, K., Au, B. V., Lew, T. S., Chu, J. J. H., Chow, V. T. K., Wang, D. Y., Zhong, F. L., & Reversade, B. (2020). Enteroviral 3C protease activates the human NLRP1 inflammasome in airway epithelia. *Science*, *370*(6521). https://doi.org/10.1126/science.aay2002

Robinson, K. S., Toh, G. A., Rozario, P., Chua, R., Bauernfried, S., Sun, Z., Firdaus, M. J., Bayat, S., Nadkarni, R., Poh, Z. S., Tham, K. C., Harapas, C. R., Lim, C. K., Chu, W., Tay, C. W. S., Tan, K. Y., Zhao, T., Bonnard, C., Sobota, R., … Zhong, F. L. (2022). ZAKα-driven ribotoxic stress response activates the human NLRP1 inflammasome. *Science (New York, N.Y.)*, *377*(6603), 328–335. https://doi.org/10.1126/science.abl6324

Rothbauer, U., Zolghadr, K., Tillib, S., Nowak, D., Schermelleh, L., Gahl, A., Backmann, N., Conrath, K., Muyldermans, S., Cardoso, M. C., & Leonhardt, H. (2006). Targeting and tracing antigens in live cells with fluorescent nanobodies. *Nature Methods*, *3*(11), 887–889. https://doi.org/10.1038/nmeth953

Rousseau, A., & Bertolotti, A. (2018). Regulation of proteasome assembly and activity in health and disease. *Nature Reviews Molecular Cell Biology*, *19*(11), 697–712. https://doi.org/10.1038/s41580-018-0040-z

Rühl, S., & Broz, P. (2015). Caspase-11 activates a canonical NLRP3 inflammasome by promoting K+ efflux. *European Journal of Immunology*, *45*(10), 2927–2936. https://doi.org/10.1002/eji.201545772

Sadiq, A., Bostan, N., Yinda, K. C., Naseem, S., & Sattar, S. (2018). Rotavirus: Genetics, pathogenesis and vaccine advances. *Reviews in Medical Virology*, *28*(6). https://doi.org/10.1002/rmv.2003

Sagulenko, V., Thygesen, S. J., Sester, D. P., Idris, A., Cridland, J. A., Vajjhala, P. R., Roberts, T. L., Schroder, K., Vince, J. E., Hill, J. M., Silke, J., & Stacey, K. J. (2013). AIM2 and NLRP3 inflammasomes activate both apoptotic and pyroptotic death pathways via ASC. *Cell Death and Differentiation*, *20*(9), 1149–1160. https://doi.org/10.1038/cdd.2013.37

Salvador, J. M., Mittelstadt, P. R., Guszczynski, T., Copeland, T. D., Yamaguchi, H., Appella, E., Fornace, A. J., & Ashwell, J. D. (2005). Alternative p38 activation pathway mediated by T cell receptor–proximal tyrosine kinases. *Nature Immunology*, *6*(4), 390–395. https://doi.org/10.1038/ni1177

Sand, J., Haertel, E., Biedermann, T., Contassot, E., Reichmann, E., French, L. E., Werner, S., & Beer, H. D. (2018). Expression of inflammasome proteins and inflammasome activation occurs in human, but not in murine keratinocytes article. *Cell Death and Disease*, *9*(2). https://doi.org/10.1038/s41419-017-0009-4

Sandstrom, A., Mitchell, P. S., Goers, L., Mu, E. W., Lesser, C. F., & Vance, R. E. (2019). Functional degradation: A mechanism of NLRP1 inflammasome activation by diverse pathogen enzymes. *Science*, *364*(6435). https://doi.org/10.1126/science.aau1330

Santos, J. C., Boucher, D., Schneider, L. K., Demarco, B., Dilucca, M., Shkarina, K., Heilig, R., Chen, K. W., Lim, R. Y. H., & Broz, P. (2020). Human GBP1 binds LPS to initiate assembly of a caspase-4 activating platform on cytosolic bacteria. *Nature Communications*, *11*(1), 3276. https://doi.org/10.1038/s41467-020-16889-z

Sanz, M. A., Castelló, A., & Carrasco, L. (2007). Viral Translation Is Coupled to Transcription in Sindbis Virus-Infected Cells. *Journal of Virology*, *81*(13), 7061–7068. https://doi.org/10.1128/JVI.02529-06

Sanz, M. A., García-Moreno, M., & Carrasco, L. (2015). Inhibition of host protein synthesis by Sindbis virus: correlation with viral RNA replication and release of nuclear proteins to the cytoplasm. *Cellular Microbiology*, *17*(4), 520–541. https://doi.org/10.1111/cmi.12381

Sastalla, I., Crown, D., Masters, S. L., McKenzie, A., Leppla, S. H., & Moayeri, M. (2013). Transcriptional analysis of the three Nlrp1 paralogs in mice. *BMC Genomics*, *14*(1), 188. https://doi.org/10.1186/1471-2164-14-188

Scheffner, M., Nuber, U., & Huibregtse, J. M. (1995). Protein ubiquitination involving an E1–E2–E3 enzyme ubiquitin thioester cascade. *Nature*, *373*(6509), 81–83. https://doi.org/10.1038/373081a0

Schmid-Burgk, J. L., Gaidt, M. M., Schmidt, T., Ebert, T. S., Bartok, E., & Hornung, V. (2015). Caspase-4 mediates non-canonical activation of the NLRP3 inflammasome in human myeloid cells. *European Journal of Immunology*, *45*(10), 2911–2917. https://doi.org/10.1002/eji.201545523

Schmid-Burgk, J. L., Schmidt, T., Gaidt, M. M., Pelka, K., Latz, E., Ebert, T. S., & Hornung, V. (2014). OutKnocker: a web tool for rapid and simple genotyping of designer nuclease edited cell lines. *Genome Research*, *24*(10), 1719–1723. https://doi.org/10.1101/gr.176701.114

Schmidt, F. I., Hanke, L., Morin, B., Brewer, R., Brusic, V., Whelan, S. P. J., & Ploegh, H. L. (2016). Phenotypic lentivirus screens to identify functional single domain antibodies. *Nature Microbiology*, *1*(8), 16080. https://doi.org/10.1038/nmicrobiol.2016.80

Schmidt, F. I., Lu, A., Chen, J. W., Ruan, J., Tang, C., Wu, H., & Ploegh, H. L. (2016). A single domain antibody fragment that recognizes the adaptor ASC defines the role of ASC domains in inflammasome assembly. *Journal of Experimental Medicine*, *213*(5), 771–790. https://doi.org/10.1084/jem.20151790

Schoenlaub, L., Cherla, R., Zhang, Y., & Zhang, G. (2016). Coxiella burnetii Avirulent Nine Mile Phase II Induces Caspase-1-Dependent Pyroptosis in Murine Peritoneal B1a B Cells. *Infection and Immunity*, *84*(12), 3638–3654. https://doi.org/10.1128/IAI.00694-16

Schonborn, J., Oberstraβ, J., Breyel, E., Tittgen, J., Schumacher, J., & Lukacs, N. (1991). Monoclonal antibodies to double-stranded RNA as probes of RNA structure in crude nucleic acid extracts. *Nucleic Acids Research*, *19*(11), 2993–3000. https://doi.org/10.1093/nar/19.11.2993

Sester, D. P., Thygesen, S. J., Sagulenko, V., Vajjhala, P. R., Cridland, J. A., Vitak, N., Chen, K. W., Osborne, G. W., Schroder, K., & Stacey, K. J. (2015). A Novel Flow Cytometric Method To Assess Inflammasome Formation. *The Journal of Immunology*, *194*(1), 455–462. https://doi.org/10.4049/jimmunol.1401110

Sfriso, P., Caso, F., Tognon, S., Galozzi, P., Gava, A., & Punzi, L. (2012). Blau syndrome, clinical and genetic aspects. *Autoimmunity Reviews*, *12*(1), 44–51. https://doi.org/10.1016/j.autrev.2012.07.028

Sharif, H., Hollingsworth, L. R., Griswold, A. R., Hsiao, J. C., Wang, Q., Bachovchin, D. A., & Wu, H. (2021). Dipeptidyl peptidase 9 sets a threshold for CARD8 inflammasome formation by sequestering its active C-terminal fragment. *Immunity*, *54*(7), 1392-1404.e10. https://doi.org/10.1016/j.immuni.2021.04.024

Sheahan, B. J., McGee, M. M., Mooney, D. A., Atkins, G. J., Glasgow, G. M., & Tarbatt, C. J. (1998). The Semliki Forest virus vector induces p53-independent apoptosis. *Journal of General Virology*, *79*(10), 2405–2410. https://doi.org/10.1099/0022-1317-79-10-2405

Shen, C., Li, R., Negro, R., Cheng, J., Vora, S. M., Fu, T.-M., Wang, A., He, K., Andreeva, L., Gao, P., Tian, Z., Flavell, R. A., Zhu, S., & Wu, H. (2021). Phase separation drives

RNA virus-induced activation of the NLRP6 inflammasome. *Cell*, *184*(23), 5759-5774.e20. https://doi.org/10.1016/j.cell.2021.09.032

Sheriff, S., & Constantine, K. L. (1996). Redefining the minimal antigen-binding fragment. *Nature Structural Biology*, *3*(9), 733–736. https://doi.org/10.1038/nsb0996-733

Sherpa, D., Chrustowicz, J., & Schulman, B. A. (2022). How the ends signal the end: Regulation by E3 ubiquitin ligases recognizing protein termini. *Molecular Cell*, *82*(8), 1424–1438. https://doi.org/10.1016/j.molcel.2022.02.004

Shi, J., Zhao, Y., Wang, K., Shi, X., Wang, Y., Huang, H., Zhuang, Y., Cai, T., Wang, F., & Shao, F. (2015). Cleavage of GSDMD by inflammatory caspases determines pyroptotic cell death. *Nature*, *526*(7575), 660–665. https://doi.org/10.1038/nature15514

Shi, J., Zhao, Y., Wang, Y., Gao, W., Ding, J., Li, P., Hu, L., & Shao, F. (2014). Inflammatory caspases are innate immune receptors for intracellular LPS. *Nature*, *514*(7521), 187–192. https://doi.org/10.1038/nature13683

Shifrin, V. I., & Anderson, P. (1999). Trichothecene Mycotoxins Trigger a Ribotoxic Stress Response That Activates c-Jun N-terminal Kinase and p38 Mitogen-activated Protein Kinase and Induces Apoptosis. *Journal of Biological Chemistry*, *274*(20), 13985–13992. https://doi.org/10.1074/jbc.274.20.13985

Sidrauski, C., Acosta-Alvear, D., Khoutorsky, A., Vedantham, P., Hearn, B. R., Li, H., Gamache, K., Gallagher, C. M., Ang, K. K.-H., Wilson, C., Okreglak, V., Ashkenazi, A., Hann, B., Nader, K., Arkin, M. R., Renslo, A. R., Sonenberg, N., & Walter, P. (2013). Pharmacological brake-release of mRNA translation enhances cognitive memory. *ELife*, *2*. https://doi.org/10.7554/eLife.00498

Siepe, D. H., Picton, L. K., & Garcia, K. C. (2023). Receptor Elimination by E3 Ubiquitin Ligase Recruitment (REULR): A Targeted Protein Degradation Toolbox. *ACS Synthetic Biology*, *12*(4), 1081–1093. https://doi.org/10.1021/acssynbio.2c00587

Skidmore, A. M., & Bradfute, S. B. (2023). The life cycle of the alphaviruses: From an antiviral perspective. *Antiviral Research*, *209*, 105476. https://doi.org/10.1016/j.antiviral.2022.105476

Smits, J. P. H., Niehues, H., Rikken, G., van Vlijmen-Willems, I. M. J. J., van de Zande, G. W. H. J. F., Zeeuwen, P. L. J. M., Schalkwijk, J., & van den Bogaard, E. H. (2017). Immortalized N/TERT keratinocytes as an alternative cell source in 3D human epidermal models. *Scientific Reports*, *7*(1), 11838. https://doi.org/10.1038/s41598-017-12041-y

Sollberger, G., Strittmatter, G. E., Grossi, S., Garstkiewicz, M., Auf Dem Keller, U., French, L. E., & Beer, H. D. (2015). Caspase-1 activity is required for UVB-induced apoptosis of human keratinocytes. *Journal of Investigative Dermatology*, *135*(5), 1395–1404. https://doi.org/10.1038/jid.2014.551

Soucy, T. A., Smith, P. G., Milhollen, M. A., Berger, A. J., Gavin, J. M., Adhikari, S., Brownell, J. E., Burke, K. E., Cardin, D. P., Critchley, S., Cullis, C. A., Doucette, A., Garnsey, J. J., Gaulin, J. L., Gershman, R. E., Lublinsky, A. R., McDonald, A., Mizutani, H., Narayanan, U., … Langston, S. P. (2009). An inhibitor of NEDD8-activating enzyme as a new approach to treat cancer. *Nature*, *458*(7239), 732–736. https://doi.org/10.1038/nature07884

Squires, R. C., Muehlbauer, S. M., & Brojatsch, J. (2007). Proteasomes control caspase-1 activation in anthrax lethal toxin-mediated cell killing. *Journal of Biological Chemistry*, *282*(47), 34260–34267. https://doi.org/10.1074/jbc.M705687200

Srinivasula, S. M., Poyet, J.-L., Razmara, M., Datta, P., Zhang, Z., & Alnemri, E. S. (2002). The PYRIN-CARD Protein ASC Is an Activating Adaptor for Caspase-1. *Journal of Biological Chemistry*, *277*(24), 21119–21122. https://doi.org/10.1074/jbc.C200179200

Staples, C. J., Owens, D. M., Maier, J. V., Cato, A. C. B., & Keyse, S. M. (2010). Cross-talk between the p38α and JNK MAPK Pathways Mediated by MAP Kinase Phosphatase-1 Determines Cellular Sensitivity to UV Radiation. *Journal of Biological Chemistry*, *285*(34), 25928–25940. https://doi.org/10.1074/jbc.M110.117911

Stein, R., Kapplusch, F., Heymann, M. C., Russ, S., Staroske, W., Hedrich, C. M., Rösen-Wolff, A., & Hofmann, S. R. (2016). Enzymatically Inactive Procaspase 1 stabilizes the ASC Pyroptosome and Supports Pyroptosome Spreading during Cell Division. *Journal of Biological Chemistry*, *291*(35), 18419–18429. https://doi.org/10.1074/jbc.M116.718668

Stutz, A., Horvath, G. L., Monks, B. G., & Latz, E. (2013). ASC speck formation as a readout for inflammasome activation. *Methods in Molecular Biology (Clifton, N.J.)*, *1040*, 91–101. https://doi.org/10.1007/978-1-62703-523-1_8

Sugasti-Salazar, M., Llamas-González, Y. Y., Campos, D., & González-Santamaría, J. (2021). Inhibition of p38 Mitogen-Activated Protein Kinase Impairs Mayaro Virus Replication in Human Dermal Fibroblasts and HeLa Cells. *Viruses*, *13*(6), 1156. https://doi.org/10.3390/v13061156

Sun, X., Zhou, C., Xia, S., & Chen, X. (2023). Small molecule-nanobody conjugate induced proximity controls intracellular processes and modulates endogenous unligandable targets. *Nature Communications*, *14*(1), 1635. https://doi.org/10.1038/s41467-023-37237-x

Svensson, A., Patzi Churqui, M., Schlüter, K., Lind, L., & Eriksson, K. (2017). Maturation-dependent expression of AIM2 in human B-cells. *PLOS ONE*, *12*(8), e0183268. https://doi.org/10.1371/journal.pone.0183268

Takeuchi, O., & Akira, S. (2010). Pattern Recognition Receptors and Inflammation. *Cell*, *140*(6), 805–820. https://doi.org/10.1016/j.cell.2010.01.022

Tang, G., & Leppla, S. H. (1999). Proteasome Activity Is Required for Anthrax Lethal Toxin To Kill Macrophages. In *INFECTION AND IMMUNITY* (Vol. 67, Issue 6).

Tang, H. K., Tang, H. Y., Hsu, S. C., Chu, Y. R., Chien, C. H., Shu, C. H., & Chen, X. (2009). Biochemical properties and expression profile of human prolyl dipeptidase DPP9. *Archives of Biochemistry and Biophysics*, *485*(2), 120–127. https://doi.org/10.1016/j.abb.2009.02.015

Terra, J. K., Cote, C. K., France, B., Jenkins, A. L., Bozue, J. A., Welkos, S. L., LeVine, S. M., & Bradley, K. A. (2010). Cutting Edge: Resistance to Bacillus anthracis Infection Mediated by a Lethal Toxin Sensitive Allele of Nalp1b/Nlrp1b . *The Journal of Immunology*, *184*(1), 17–20. https://doi.org/10.4049/jimmunol.0903114

Thomas, G. D., Hamers, A. A. J., Nakao, C., Marcovecchio, P., Taylor, A. M., McSkimming, C., Nguyen, A. T., McNamara, C. A., & Hedrick, C. C. (2017). Human Blood Monocyte Subsets: a new gating strategy defined using cell surface markers identified by mass cytometry. *Arteriosclerosis, Thrombosis, and Vascular Biology*, *37*(8), 1548–1558. https://doi.org/10.1161/ATVBAHA.117.309145

Timms, R. T., & Koren, I. (2020). Tying up loose ends: the N-degron and C-degron pathways of protein degradation. *Biochemical Society Transactions*, *48*(4), 1557–1567. https://doi.org/10.1042/BST20191094

Timms, R. T., Zhang, Z., Rhee, D. Y., Harper, J. W., Koren, I., & Elledge, S. J. (2019). A glycine-specific N-degron pathway mediates the quality control of protein N-myristoylation. *Science*, *365*(6448). https://doi.org/10.1126/science.aaw4912

Ting, J. P.-Y., Lovering, R. C., Alnemri, E. S., Bertin, J., Boss, J. M., Davis, B. K., Flavell, R. A., Girardin, S. E., Godzik, A., Harton, J. A., Hoffman, H. M., Hugot, J.-P., Inohara, N., MacKenzie, A., Maltais, L. J., Nunez, G., Ogura, Y., Otten, L. A., Philpott, D., … Ward, P. A. (2008). The NLR Gene Family: A Standard Nomenclature. *Immunity*, *28*(3), 285–287. https://doi.org/10.1016/j.immuni.2008.02.005

Tobiume, K., Matsuzawa, A., Takahashi, T., Nishitoh, H., Morita, K., Takeda, K., Minowa, O., Miyazono, K., Noda, T., & Ichijo, H. (2001). ASK1 is required for sustained activations of JNK/p38 MAP kinases and apoptosis. *EMBO Reports*, *2*(3), 222–228. https://doi.org/10.1093/embo-reports/kve046

Toribio, R., Díaz-López, I., Boskovic, J., & Ventoso, I. (2016). An RNA trapping mechanism in Alphavirus mRNA promotes ribosome stalling and translation initiation. *Nucleic Acids Research*, *44*(9), 4368–4380. https://doi.org/10.1093/nar/gkw172

Tracz, M., & Bialek, W. (2021). Beyond K48 and K63: non-canonical protein ubiquitination. *Cellular & Molecular Biology Letters*, *26*(1), 1. https://doi.org/10.1186/s11658-020-00245-6

Tran, T. A. T., Grievink, H. W., Lipinska, K., Kluft, C., Burggraaf, J., Moerland, M., Tasev, D., & Malone, K. E. (2019). Whole blood assay as a model for in vitro evaluation of inflammasome activation and subsequent caspase-mediated interleukin-1 beta release. *PLOS ONE*, *14*(4), e0214999. https://doi.org/10.1371/journal.pone.0214999

Trefzer, U., Brockhaus, M., Lötscher, H., Parlow, F., Budnik, A., Grewe, M., Christoph, H., Kapp, A., Schöpf, E., & Luger, T. A. (1993). The 55-kD tumor necrosis factor receptor on human keratinocytes is regulated by tumor necrosis factor-alpha and by ultraviolet B radiation. *Journal of Clinical Investigation*, *92*(1), 462–470. https://doi.org/10.1172/JCI116589

Trzupek, D., Dunstan, M., Cutler, A. J., Lee, M., Godfrey, L., Jarvis, L., Rainbow, D. B., Aschenbrenner, D., Jones, J. L., Uhlig, H. H., Wicker, L. S., Todd, J. A., & Ferreira, R. C. (2020). Discovery of CD80 and CD86 as recent activation markers on regulatory T cells by protein-RNA single-cell analysis. *Genome Medicine*, *12*(1), 55. https://doi.org/10.1186/s13073-020-00756-z

Tsu, B. V., Beierschmitt, C., Ryan, A. P., Agarwal, R., Mitchell, P. S., & Daugherty, M. D. (2021). Diverse viral proteases activate the nlrp1 inflammasome. *ELife*, *10*, 1–76. https://doi.org/10.7554/eLife.60609

Tupik, J. D., Nagai-Singer, M. A., & Allen, I. C. (2020). To protect or adversely affect? The dichotomous role of the NLRP1 inflammasome in human disease. *Molecular Aspects of Medicine*, *76*, 100858. https://doi.org/10.1016/j.mam.2020.100858

Tye, H., Yu, C.-H., Simms, L. A., de Zoete, M. R., Kim, M. L., Zakrzewski, M., Penington, J. S., Harapas, C. R., Souza-Fonseca-Guimaraes, F., Wockner, L. F., Preaudet, A., Mielke, L. A., Wilcox, S. A., Ogura, Y., Corr, S. C., Kanojia, K., Kouremenos, K. A., De Souza, D. P., McConville, M. J., … Masters, S. L. (2018). NLRP1 restricts butyrate producing commensals to exacerbate inflammatory bowel disease. *Nature Communications*, *9*(1), 3728. https://doi.org/10.1038/s41467-018-06125-0

van der Linden, R., de Geus, B., Stok, W., Bos, W., van Wassenaar, D., Verrips, T., & Frenken, L. (2000). Induction of immune responses and molecular cloning of the heavy chain antibody repertoire of Lama glama. *Journal of Immunological Methods*, *240*(1–2), 185–195. https://doi.org/10.1016/S0022-1759(00)00188-5

van der Linden, R. H. J., Frenken, L. G. J., de Geus, B., Harmsen, M. M., Ruuls, R. C., Stok, W., de Ron, L., Wilson, S., Davis, P., & Verrips, C. T. (1999). Comparison of physical chemical properties of llama VHH antibody fragments and mouse monoclonal antibodies. *Biochimica et Biophysica Acta (BBA) - Protein Structure and Molecular Enzymology*, *1431*(1), 37–46. https://doi.org/10.1016/S0167-4838(99)00030-8

Van Opdenbosch, N., Gurung, P., Vande Walle, L., Fossoul, A., Kanneganti, T. D., & Lamkanfi, M. (2014). Activation of the NLRP1b inflammasome independently of ASC-mediated caspase-1 autoproteolysis and speck formation. *Nature Communications*, *5*. https://doi.org/10.1038/ncomms4209

Van Opdenbosch, N., & Lamkanfi, M. (2019). Caspases in Cell Death, Inflammation, and Disease. *Immunity*, *50*(6), 1352–1364. https://doi.org/10.1016/j.immuni.2019.05.020

Varghese, F. S., Thaa, B., Amrun, S. N., Simarmata, D., Rausalu, K., Nyman, T. A., Merits, A., McInerney, G. M., Ng, L. F. P., & Ahola, T. (2016). The Antiviral Alkaloid Berberine Reduces Chikungunya Virus-Induced Mitogen-Activated Protein Kinase Signaling. *Journal of Virology*, *90*(21), 9743–9757. https://doi.org/10.1128/JVI.01382-16

Ventoso, I., Sanz, M. A., Molina, S., Berlanga, J. J., Carrasco, L., & Esteban, M. (2006). Translational resistance of late alphavirus mRNA to eIF2α phosphorylation: a strategy to overcome the antiviral effect of protein kinase PKR. *Genes & Development*, *20*(1), 87–100. https://doi.org/10.1101/gad.357006

Venuprasad, K., & Theiss, A. L. (2021). NLRP6 in host defense and intestinal inflammation. *Cell Reports*, *35*(4), 109043. https://doi.org/10.1016/j.celrep.2021.109043

Vind, A. C., Genzor, A. V., & Bekker-Jensen, S. (2020). Ribosomal stress-surveillance: three pathways is a magic number. *Nucleic Acids Research*, *48*(19), 10648–10661. https://doi.org/10.1093/nar/gkaa757

Vind, A. C., Snieckute, G., Blasius, M., Tiedje, C., Krogh, N., Bekker-Jensen, D. B., Andersen, K. L., Nordgaard, C., Tollenaere, M. A. X., Lund, A. H., Olsen, J. V., Nielsen, H., & Bekker-Jensen, S. (2020). ZAKα Recognizes Stalled Ribosomes through Partially Redundant Sensor Domains. *Molecular Cell*, *78*(4), 700-713.e7. https://doi.org/10.1016/j.molcel.2020.03.021

von Kampen, O., Lipinski, S., Till, A., Martin, S. J., Nietfeld, W., Lehrach, H., Schreiber, S., & Rosenstiel, P. (2010). Caspase Recruitment Domain-containing Protein 8 (CARD8) Negatively Regulates NOD2-mediated Signaling. *Journal of Biological Chemistry*, *285*(26), 19921–19926. https://doi.org/10.1074/jbc.M110.127480

Vrentas, C. E., Boggiatto, P. M., Olsen, S. C., Leppla, S. H., & Moayeri, M. (2020). Characterization of the NLRP1 inflammasome response in bovine species. *Innate Immunity*, *26*(4), 301–311. https://doi.org/10.1177/1753425919886649

Walsh, J. G., Logue, S. E., Lüthi, A. U., & Martin, S. J. (2011). Caspase-1 Promiscuity Is Counterbalanced by Rapid Inactivation of Processed Enzyme. *Journal of Biological Chemistry*, *286*(37), 32513–32524. https://doi.org/10.1074/jbc.M111.225862

Wandel, M. P., Kim, B.-H., Park, E.-S., Boyle, K. B., Nayak, K., Lagrange, B., Herod, A., Henry, T., Zilbauer, M., Rohde, J., MacMicking, J. D., & Randow, F. (2020). Guanylate-binding proteins convert cytosolic bacteria into caspase-4 signaling platforms. *Nature Immunology*, *21*(8), 880–891. https://doi.org/10.1038/s41590-020-0697-2

Wang, C., Deng, L., Hong, M., Akkaraju, G. R., Inoue, J., & Chen, Z. J. (2001). TAK1 is a ubiquitin-dependent kinase of MKK and IKK. *Nature*, *412*(6844), 346–351. https://doi.org/10.1038/35085597

Wang, Q., Gao, H., Clark, K. M., Mugisha, C. S., Davis, K., Tang, J. P., Harlan, G. H., DeSelm, C. J., Presti, R. M., Kutluay, S. B., & Shan, L. (2021). CARD8 is an inflammasome sensor for HIV-1 protease activity. *Science*, *371*(6535). https://doi.org/10.1126/science.abe1707

Wang, Q., Hsiao, J. C., Yardeny, N., Huang, H. C., O'Mara, C. M., Orth-He, E. L., Ball, D. P., Zhang, Z., & Bachovchin, D. A. (2023). The NLRP1 and CARD8 inflammasomes detect reductive stress. *Cell Reports*, *42*(1). https://doi.org/10.1016/j.celrep.2022.111966

Wang, X., Mader, M. M., Toth, J. E., Yu, X., Jin, N., Campbell, R. M., Smallwood, J. K., Christe, M. E., Chatterjee, A., Goodson, T., Vlahos, C. J., Matter, W. F., & Bloem, L. J. (2005). Complete inhibition of anisomycin and UV radiation but not cytokine induced JNK and p38 activation by an aryl-substituted dihydropyrrolopyrazole quinoline and mixed lineage kinase 7 small interfering RNA. *The Journal of Biological Chemistry*, *280*(19), 19298–19305. https://doi.org/10.1074/jbc.M413059200

Waterhouse, A. M., Procter, J. B., Martin, D. M. A., Clamp, M., & Barton, G. J. (2009). Jalview Version 2—a multiple sequence alignment editor and analysis workbench. *Bioinformatics*, *25*(9), 1189–1191. https://doi.org/10.1093/bioinformatics/btp033

Whelan, S. P., Ball, L. A., Barr, J. N., & Wertz, G. T. (1995). Efficient recovery of infectious vesicular stomatitis virus entirely from cDNA clones. *Proceedings of the National Academy of Sciences*, *92*(18), 8388–8392. https://doi.org/10.1073/pnas.92.18.8388

White, L. K., Sali, T., Alvarado, D., Gatti, E., Pierre, P., Streblow, D., & DeFilippis, V. R. (2011). Chikungunya Virus Induces IPS-1-Dependent Innate Immune Activation and Protein Kinase R-Independent Translational Shutoff. *Journal of Virology*, *85*(1), 606–620. https://doi.org/10.1128/JVI.00767-10

Wickliffe, K. E., Leppla, S. H., & Moayeri, M. (2008). Killing of macrophages by anthrax lethal toxin: involvement of the N-end rule pathway. *Cellular Microbiology*, *10*(6), 1352–1362. https://doi.org/10.1111/j.1462-5822.2008.01131.x

Windheim, M., Lang, C., Peggie, M., Plater, L. A., & Cohen, P. (2007). Molecular mechanisms involved in the regulation of cytokine production by muramyl dipeptide. *Biochemical Journal*, *404*(2), 179–190. https://doi.org/10.1042/BJ20061704

Witola, W. H., Mui, E., Hargrave, A., Liu, S., Hypolite, M., Montpetit, A., Cavailles, P., Bisanz, C., Cesbron-Delauw, M. F., Fournié, G. J., & McLeod, R. (2011). NALP1 influences susceptibility to human congenital toxoplasmosis, proinflammatory cytokine response, and fate of Toxoplasma gondii-infected monocytic cells. *Infection and Immunity*, *79*(2), 756–766. https://doi.org/10.1128/IAI.00898-10

Wu, C. C.-C., Peterson, A., Zinshteyn, B., Regot, S., & Green, R. (2020). Ribosome Collisions Trigger General Stress Responses to Regulate Cell Fate. *Cell*, *182*(2), 404-416.e14. https://doi.org/10.1016/j.cell.2020.06.006

Xu, H., Shi, J., Gao, H., Liu, Y., Yang, Z., Shao, F., & Dong, N. (2019). The N-end rule ubiquitin ligase UBR2 mediates NLRP1B inflammasome activation by anthrax lethal toxin. *The EMBO Journal*, *38*(13). https://doi.org/10.15252/embj.2019101996

Xu, H., Yang, J., Gao, W., Li, L., Li, P., Zhang, L., Gong, Y.-N., Peng, X., Xi, J. J., Chen, S., Wang, F., & Shao, F. (2014). Innate immune sensing of bacterial modifications of Rho GTPases by the Pyrin inflammasome. *Nature*, *513*(7517), 237–241. https://doi.org/10.1038/nature13449

Xu, Z., Deng, S., Huang, Y., Yang, Y., Sun, L., Liu, H., Zhao, D., Zeng, W., Yin, X., Zheng, P., Wang, Y., Liu, M., Zhao, W., Xiao, T. S., Zhou, Y., & Jin, T. (2022). The CARD8 T60 variant associates with NLRP1 and negatively regulates its activation. *Frontiers in Immunology*, *13*. https://doi.org/10.3389/fimmu.2022.1047922

Xu, Z., Zhou, Y., Liu, M., Ma, H., Sun, L., Zahid, A., Chen, Y., Zhou, R., Cao, M., Wu, D., Zhao, W., Li, B., & Jin, T. (2021). Homotypic CARD-CARD interaction is critical for the activation of NLRP1 inflammasome. *Cell Death & Disease*, *12*(1), 57. https://doi.org/10.1038/s41419-020-03342-8

Yang, J., Shibu, M. A., Kong, L., Luo, J., BadrealamKhan, F., Huang, Y., Tu, Z.-C., Yun, C.-H., Huang, C.-Y., Ding, K., & Lu, X. (2020). Design, Synthesis, and Structure–Activity Relationships of 1,2,3-Triazole Benzenesulfonamides as New Selective Leucine-Zipper and Sterile-α Motif Kinase (ZAK) Inhibitors. *Journal of Medicinal Chemistry*, *63*(5), 2114–2130. https://doi.org/10.1021/acs.jmedchem.9b00664

Yang, J., Zhao, Y., Shi, J., & Shao, F. (2013). Human NAIP and mouse NAIP1 recognize bacterial type III secretion needle protein for inflammasome activation. *Proceedings of the National Academy of Sciences*, *110*(35), 14408–14413. https://doi.org/10.1073/pnas.1306376110

Yang, X., Zhou, J., Liu, C., Qu, Y., Wang, W., Xiao, M. Z. X., Zhu, F., Liu, Z., & Liang, Q. (2022). KSHV-encoded ORF45 activates human NLRP1 inflammasome. *Nature Immunology*, *23*(6), 916–926. https://doi.org/10.1038/s41590-022-01199-x

Yu, F., White, S. B., Zhao, Q., & Lee, F. S. (2001). HIF-1alpha binding to VHL is regulated by stimulus-sensitive proline hydroxylation. *Proceedings of the National Academy of Sciences of the United States of America*, *98*(17), 9630–9635. https://doi.org/10.1073/pnas.181341498

Yue, J., & López, J. M. (2020). Understanding MAPK Signaling Pathways in Apoptosis. *International Journal of Molecular Sciences*, *21*(7), 2346. https://doi.org/10.3390/ijms21072346

Zanoni, I., Ostuni, R., Marek, L. R., Barresi, S., Barbalat, R., Barton, G. M., Granucci, F., & Kagan, J. C. (2011). CD14 Controls the LPS-Induced Endocytosis of Toll-like Receptor 4. *Cell*, *147*(4), 868–880. https://doi.org/10.1016/j.cell.2011.09.051

Zawada, A. M., Rogacev, K. S., Schirmer, S. H., Sester, M., Böhm, M., Fliser, D., & Heine, G. H. (2012). Monocyte heterogeneity in human cardiovascular disease. *Immunobiology*, *217*(12), 1273–1284. https://doi.org/10.1016/j.imbio.2012.07.001

Zhang, C., Song, J.-W., Huang, H.-H., Fan, X., Huang, L., Deng, J.-N., Tu, B., Wang, K., Li, J., Zhou, M.-J., Yang, C.-X., Zhao, Q.-W., Yang, T., Wang, L.-F., Zhang, J.-Y., Xu, R.-N., Jiao, Y.-M., Shi, M., Shao, F., … Wang, F.-S. (2021). NLRP3 inflammasome induces CD4+ T cell loss in chronically HIV-1–infected patients. *Journal of Clinical Investigation*, *131*(6). https://doi.org/10.1172/JCI138861

Zhang, H., Gao, J., Tang, Y., Jin, T., & Tao, J. (2023). Inflammasomes cross-talk with lymphocytes to connect the innate and adaptive immune response. *Journal of Advanced Research*. https://doi.org/10.1016/j.jare.2023.01.012

Zhao, C., Gu, Y., Zeng, X., & Wang, J. (2018). NLRP3 inflammasome regulates Th17 differentiation in rheumatoid arthritis. *Clinical Immunology*, *197*, 154–160. https://doi.org/10.1016/j.clim.2018.09.007

Zhao, Y., Yang, J., Shi, J., Gong, Y.-N., Lu, Q., Xu, H., Liu, L., & Shao, F. (2011). The NLRC4 inflammasome receptors for bacterial flagellin and type III secretion apparatus. *Nature*, *477*(7366), 596–600. https://doi.org/10.1038/nature10510

Zhao, Z., Xu, B., Wang, S., Zhou, M., Huang, Y., Guo, C., Li, M., Zhao, J., Sung, S.-S. J., Gaskin, F., Yang, N., & Fu, S. M. (2022). Tfh cells with NLRP3 inflammasome activation are essential for high-affinity antibody generation, germinal centre formation and autoimmunity. *Annals of the Rheumatic Diseases*, *81*(7), 1006–1012. https://doi.org/10.1136/annrheumdis-2021-221985

Zhong, F. L., Mamaï, O., Sborgi, L., Boussofara, L., Hopkins, R., Robinson, K., Szeverényi, I., Takeichi, T., Balaji, R., Lau, A., Tye, H., Roy, K., Bonnard, C., Ahl, P. J., Jones, L. A., Baker, P., Lacina, L., Otsuka, A., Fournie, P. R., … Reversade, B. (2016). Germline NLRP1 Mutations Cause Skin Inflammatory and Cancer Susceptibility Syndromes via Inflammasome Activation. *Cell*, *167*(1), 187-202.e17. https://doi.org/10.1016/j.cell.2016.09.001

Zhong, F. L., Robinson, K., Teo, D. E. T., Tan, K. Y., Lim, C., Harapas, C. R., Yu, C. H., Xie, W. H., Sobota, R. M., Au, V. B., Hopkins, R., D'Osualdo, A., Reed, J. C., Connolly, J. E., Masters, S. L., & Reversade, B. (2018). Human DPP9 represses NLRP1 inflammasome and protects against autoinflammatory diseases via both peptidase activity and FIIND domain binding. *Journal of Biological Chemistry*, *293*(49), 18864–18878. https://doi.org/10.1074/jbc.RA118.004350

Zhou, H.-R., He, K., Landgraf, J., Pan, X., & Pestka, J. (2014). Direct Activation of Ribosome-Associated Double-Stranded RNA-Dependent Protein Kinase (PKR) by Deoxynivalenol, Anisomycin and Ricin: A New Model for Ribotoxic Stress Response Induction. *Toxins*, *6*(12), 3406–3425. https://doi.org/10.3390/toxins6123406

Zhou, J. Y., Sarkar, M. K., Okamura, K., Harris, J. E., Gudjonsson, J. E., & Fitzgerald, K. A. (2023). Activation of the NLRP1 inflammasome in human keratinocytes by the dsDNA mimetic poly(dA:dT). *Proceedings of the National Academy of Sciences*, *120*(5). https://doi.org/10.1073/pnas.2213777120

Zhu, S., Ding, S., Wang, P., Wei, Z., Pan, W., Palm, N. W., Yang, Y., Yu, H., Li, H.-B., Wang, G., Lei, X., de Zoete, M. R., Zhao, J., Zheng, Y., Chen, H., Zhao, Y., Jurado, K. A., Feng, N., Shan, L., … Flavell, R. A. (2017). Nlrp9b inflammasome restricts rotavirus infection in intestinal epithelial cells. *Nature*, *546*(7660), 667–670. https://doi.org/10.1038/nature22967

Zhu, S., Romano, P. R., & Wek, R. C. (1997). Ribosome Targeting of PKR Is Mediated by Two Double-stranded RNA-binding Domains and Facilitates in Vivo Phosphorylation of Eukaryotic Initiation Factor-2. *Journal of Biological Chemistry*, *272*(22), 14434–14441. https://doi.org/10.1074/jbc.272.22.14434

Ziegler-Heitbrock, L. (2015). Blood Monocytes and Their Subsets: Established Features and Open Questions. *Frontiers in Immunology*, *6*. https://doi.org/10.3389/fimmu.2015.00423

11. Acknowledgments

First of all, I want to thank Florian and Eicke for providing me the opportunity to do my PhD at the Institute of Innate Immunity. The III has always offered a great scientific and joyful environment and I am grateful that I was able to spend my PhD time here.
I want to thank Florian for being a great supervisor who has always been supportive, encouraging, and sympathetic. I am grateful that I was able to learn from a scientist as passionate as you, you definitely taught me a lot. Thank you for all your help with the paper, for proofreading this thesis and every important text that I have written, and for your support with the Autumn School in Japan. Thank you for always believing in me, for every word of encouragement, and for making me a better scientist.

Next, I want to thank all the people who have accompanied me throughout my PhD time, who made this time so much more fun and enjoyable, and without whom I probably would have resigned at some point.

I start with my “best office” members and PhD companions Lisa, Florian and Yonas:
Lisa, thank you for all the conversations that helped me to forget about the stressful lab routine, for all your encouraging words, and for all the hugs whenever everything became too much. I will always remember our hiking holidays in Munich, completed with the best burger I ever had in the restaurant that turned out to be an illegal club.
Florian, thank you for all the conversations that started as a brief chat but turned into never-ending discussions about topics like AoE or “krasse Specks”. Also a big thanks for all the help with setting up my thesis in Word, for always sharing your licorice with me, and for bringing kohlrabi to our Janeway club.
Yonas, even though the office was constantly dark because of you, you were always able to compensate for it with your cheerful personality. Thank you for always making me laugh and for sacrificing your e-mail address to get me the Peprotech lab penguin. I will forgive you that you dropped my sausages (several times) and that you tried to trash your plant.
I hope we can keep our promise that we all meet once a year, no matter where we live and what we are up to!

Next, I want to thank Jen and Damien for all the support and encouragement throughout the last years:
Jen, I cannot thank you enough for all your kind words, for the countless hugs, and for just being an irreplaceable support since you joined our lab. I was only able to attend the Autumn School in Japan because you persuaded me to apply for it, so thank you for persistently pushing me in the right direction.
Damien, since my time at IFM you have always supported me, boosting my confidence in myself and my work, and cheering me up whenever necessary. Thank you for accompanying and supporting me for so long.
Also thank you both for sacrificing your free time to proofread this thesis. Thank you for all the corrections and the useful comments, these really improved my thesis. Thank you for teaching me English comma rules and how to use “whereas”, and for pointing out that I wrote “it was shown” way too often and that I don´t express proteins myself.

Next, I want to thank the “new generation” of PhD students, Doro, Stefan and Jose:
Doro, thank you for continuing the work on the NLRP1 project, even though it is probably more of a patchwork of individual projects. I think the project is in really good hands, and I am sure that you will unravel some of the remaining mysteries of this inflammasome. And don´t forget you are really hip, as NLRP1 is the new NLRP3.
Stefan, thank you for establishing all the skin processing and primary keratinocyte generation, as this will help a lot in future NLRP1 experiments. I am sure that your work will also lead to great discoveries regarding immune responses in the skin, and you are of course always welcome to join Team NLRP1.
Jose, thank you for being the first lab member who is willing to discuss the current Anime season or the best arcs of Naruto with me. I really enjoyed our regular nerd-talks. As a sign of my gratitude, I promise that I will watch One Piece until the end and I will keep you updated about the journey.
Thank all of you for initiating more activities outside the lab, like the monthly dinner or Pride cocktail parties. I really had a great time with all of you.

Of course, I want to thank Sabine, Moni, Jan, and Steffen for the continual help in the lab, for answering all my questions, and for organizing the everyday lab-life. Special thanks go

to Sabine who performed many of the specking assays and Western blots for the paper and therefore helped me a lot during the pre-submission and revision phase.

I want to thank my lab rotation students who helped me with different projects throughout my PhD. But I have to especially thank Laura, for being an enormous help during the pre-submission phase. Thank you for performing countless infections and specking assays, for never complaining about last-minute additional treatments, and for your great vibes and positivity in these stressful times.

In general, I want to thank every current and past member of the Schmidt lab for the great working atmosphere in the lab. I really appreciate that we are working as a team without competition and jealousy between the students. I always knew that I could ask everyone for help, which was verified in the times of the “NLRP1 purge”. I cannot thank you enough for all the help and support in the pre-submission and revision phase of the paper.

I also want to thank Ibrahim for all the encouraging and helpful conversations throughout my PhD, be it about experiments with primary monocytes or about the PhD guidelines of the medical faculty. Thank you for all your advice about writing the thesis, this really helped me a lot.

Next, I want to thank all the people outside of the lab and the institute who accompanied me throughout my PhD time, who helped me to forget about NLRP1, experiments, and deadlines for once, and who helped me to relax in my free time.

Even though we started our tandem only at the beginning of this year, I want to thank Wiebke for the weekly motivation and support. It was so helpful to share my doubts and problems with you and to know that I am not the only one suffering from thesis stress at the moment. I am looking forward to celebrate the thesis submission with you.

I want to thank Jasmin for all the way too long Positiv-Tagebuch podcasts that always made me smile whatever the circumstances. Thank you for always believing in me and

for always encouraging me. Thanks to you, this thesis has “Sinn und Fuß”, Do Not Ask why.

I want to thank the penguins, Jenny, Inga, and KleinLea, for our long-lasting friendship, for the constant support, and all the penguin meetings including the traditional cookie baking and Kniffel sessions. I really enjoyed our short penguin vacation and it gave me additional motivation to finish the discussion of chapter 3.

I want to thank Celina and Stephi for all the times you made me forget about work and everything work-related. Being with you always feels like vacation, as we can talk about all the nerdy things for hours, eliminating every depressing thought and anxiety. Our annual weekends at Dokomi, Animagic, and other conventions were always highlights of my last years, giving me something to look forward to and distracting me successfully with last-minute cosplays. Thank you for being part of my life and for all the support and motivation you gave me.

I want to thank Shimi for all his love and support throughout the last years. Thank you for always being there for me, for always believing in me, and for always encouraging me. Thank you for preparing all the oishi dinners every day, for accepting me working probably way too much, and for listening to all my presentations although you “don´t know what a proteasome is”. いつもそばにいてくれてありがとう.

12. Curriculum Vitae

Personal data

Name Lea-Marie Jenster

Current position

Since 05/2018 PhD candidate in the laboratory of Prof. Dr. Florian Schmidt
Institute of Innate Immunity
University hospital, University of Bonn, Germany

Education

10/2015-12/2017 Master of Science in Microbiology, University of Bonn, Germany

09/2011-02/2015 Bachelor of Science in Bio-and Nanotechnology, University of Applied Sciences Südwestfalen, Iserlohn, Germany

09/2002-07/2011 Abitur, Willibrord Gymnasium, Emmerich am Rhein, Germany

Research and work experience

11/2017-05/2018 Technical assistant, IFM Therapeutics GmbH, Bonn, Germany

03/2017-10/2017
11/2016 Internship and Master Thesis in the laboratory of Dr. Beatrix Schumak
Project: Characterisation of eosinophils in *Plasmodium berghei* ANKA-induced experimental cerebral malaria in susceptible and protected mice
Institute of Medical Microbiology, Parasitology and Immunology
University hospital, University of Bonn, Germany

01/2017-02/2017 Internship in the laboratory of Dr. Beate Kümmerer
Project: Characterisation of Flavivirus and host cell protein interactions in infected insect cells
Institute of Virology
University hospital, University of Bonn, Germany

04/2015-06/2015 Internship in the Institute of clinical pathology and microbiology, Ev. Krankenhaus Oberhausen GmbH, Oberhausen, Germany

04/2014-12/2014 Bachelor Thesis in the laboratory of Dr. Killian Hennes
Project: Analysis of IL-β secretion by HaCaT cells as potential signal of skin sensitization in a skin 3D culture model
University of Applied Sciences Südwestfalen, Iserlohn, Germany

Publications

1. **Jenster, L,** Ribeiro, LS, Franklin, BS, Bertheloot, D (2023). Measuring NLR Oligomerization II: Detection of ASC Speck Formation by Confocal Microscopy and Immunofluorescence. In: Pelegrín, P, Di Virgilio, F (eds) NLR Proteins. Methods in Molecular Biology, vol 2696. Humana, New York.

2. Próchnicki, T, Vasconcelos, MB, Robinson, KS, Mangan MSJ, De Graaf D, Shkarina K, Lovotti M, Standke L, Kaiser R, Stahl R, Duthie FG, Rothe M, Antonova K, **Jenster LM**, Heng Lau Z, Rösing S, Mirza N, Gottschild C, Wachten D, Günther C, Kufer TA, Schmidt FI, Zhong FL, Latz E (2023). Mitochondrial damage activates the NLRP10 inflammasome. *Nature Immunology.* 24, 595–603.

3. **Jenster LM**, Lange KE, Normann S, vom Hemdt A, Wuerth JD, Schiffelers LDJ, Tesfamariam YM, Gohr FN, Klein L, Kaltheuner IH, Ebner S, Lapp DJ, Mayer J, Moecking J, Ploegh HL, Latz E, Meissner F, Geyer M, Kümmerer BM, Schmidt FI (2023). P38 kinases mediate NLRP1 inflammasome activation after ribotoxic stress response and virus infection. *Journal of Experimental Medicine.* 220(1):e20220837

4. Bertheloot D, Wanderley CWS, Schneider AH, Schiffelers LDJ, Wuerth JD, Tödtmann JMP, Maasewerd S, Hawwari I, Duthie F, Rohland C, Ribeiro LS, **Jenster LM**, Rosero N, Tesfamariam YM, Cunha FQ, Schmidt FI, Franklin BS (2022). Nanobodies dismantle post-pyroptotic ASC specks and counteract inflammation *in vivo*. *EMBO Molecular Medicine.* 14: e15415

5. Scheunemann JF, Reichwald JJ, Korir PJ, Kuehlwein JM, **Jenster LM**, Hammerschmidt-Kamper C, Lewis MD, Klocke K, Borsche M, Schwendt KE, Soun C, Thiebes S, Limmer A, Engel DR, Mueller A-K, Hoerauf A, Hübner MP, Schumak B (2021). Eosinophils Suppress the Migration of T Cells Into the Brain of *Plasmodium berghei*-Infected Ifnar1-/- Mice and Protect Them From Experimental Cerebral Malaria. *Frontiers in Immunology.* 12:711876

6. Koenig PA, Das H, Liu H, Kümmerer BM, Gohr FN, **Jenster LM**, Schiffelers LDJ, Tesfamariam YM, Uchima M, Wuerth JD, Gatterdam K, Ruetalo N, Christensen MH, Fandrey CI, Normann S, Tödtmann JMP, Pritzl S, Hanke L, Boos J, Yuan M, Zhu X, Schmid-Burgk JL, Kato H, Schindler M, Wilson IA, Geyer M, Ludwig KU, Hällberg BM, Wu NC, Schmidt FI (2021). Structure-guided multivalent nanobodies block SARS-CoV-2 infection and suppress mutational escape. *Science*. 371. eabe6230

13. Appendix

List of cell lines used in this thesis

Name in this thesis	Lab intern name	Parental cell line	Transgene	Plasmid	Generation and selection	Medium
HEK^{ASC}	H1	HEK 293T	ASC-EGFP	pRRL pUbC ASC-EGFP Puro	Transduction with a dilution series of lentivirus to achieve single insertion, selection of clone based on minimal ASC speck background	DMEM/10 % FBS, 1 µg/mL puromycin,
$HEK^{NLRP1+ASC}$	H8-1	H1	NLRP1-HA	pRRL pUbC NLRP1-HA Hygromycin B	Transduction with a dilution series of lentivirus to achieve single insertion, selection of clone based on optimal signal-to-noise ratio after talabostat stimulation	DMEM/10 % FBS, 1 µg/mL puromycin, 50 µg/mL hygromycin B
$HEK^{NLRP3+ASC}$	H98	H1	NLRP3-HA	pRRL pUbC NLRP3-HA Hygromycin B	Transduction with a dilution series of lentivirus to achieve single insertion, selection of clone based on optimal signal-to-noise ratio after LPS and nigericin stimulation	DMEM/10 % FBS, 1 µg/mL puromycin, 50 µg/mL hygromycin B

HEK^{ASC} + NLRP1	H151	H1	NLRP1-HA	pRRL pUbC NLRP1-HA Hygromycin B	Transduction with lentivirus MOIs that permit multiple insertions, polyclonal cell line	DMEM/10 % FBS, 1 µg/mL puromycin, 50 µg/mL hygromycin B
HEK^{ASC} + mNlrp1b1	H152	H1	mNlrp1b1-HA	pRRL pUbC mNlrp1b1-HA Hygromycin B	Transduction with lentivirus MOIs that permit multiple insertions, polyclonal cell line	DMEM/10 % FBS, 1 µg/mL puromycin, 50 µg/mL hygromycin B
HEK^{ASC} + mNlrp1b2	H153	H1	mNlrp1b2-HA	pRRL pUbC mNlrp1b2-HA Hygromycin B	Transduction with lentivirus MOIs that permit multiple insertions, polyclonal cell line	DMEM/10 % FBS, 1 µg/mL puromycin, 50 µg/mL hygromycin B
HEK^{ASC} + mNlrp1b3	H154	H1	mNlrp1b3-HA	pRRL pUbC mNlrp1b3-HA Hygromycin B	Transduction with lentivirus MOIs that permit multiple insertions, polyclonal cell line	DMEM/10 % FBS, 1 µg/mL puromycin, 50 µg/mL hygromycin B
HEK^{ASC} + mNlrp1b5	H155	H1	mNlrp1b5-HA	pRRL pUbC mNlrp1b5-HA Hygromycin B	Transduction with lentivirus MOIs that permit multiple insertions, polyclonal cell line	DMEM/10 % FBS, 1 µg/mL puromycin, 50 µg/mL hygromycin B
HEK^{ASC} + NLRP1 SP-AP TP-AP [PYD+linker]	H156	H1	NLRP1-HA SP-AP TP-AP [PYD+linker]	pRRL pUbC NLRP1-HA SP-AP TP-AP PYD+linker Hygromycin B	Transduction with lentivirus MOIs that permit multiple insertions, polyclonal cell line	DMEM/10 % FBS, 1 µg/mL puromycin, 50 µg/mL hygromycin B

HEK^{ASC} + NLRP1 SA TA [linker]	H157	H1	NLRP1-HA SA TA [linker]	pRRL pUbC NLRP1-HA SA TA linker Hygromycin B	Transduction with lentivirus MOIs that permit multiple insertions, polyclonal cell line	DMEM/10 % FBS, 1 µg/mL puromycin, 50 µg/mL hygromycin B
HEK^{ASC} + NLRP1 KR [PYD]	H158	H1	NLRP1-HA KR [PYD]	pRRL pUbC NLRP1-HA KR PYD Hygromycin B	Transduction with lentivirus MOIs that permit multiple insertions, polyclonal cell line	DMEM/10 % FBS, 1 µg/mL puromycin, 50 µg/mL hygromycin B
HEK^{ASC} + NLRP1 KR [linker]	H159	H1	NLRP1-HA KR [linker]	pRRL pUbC NLRP1-HA KR linker Hygromycin B	Transduction with lentivirus MOIs that permit multiple insertions, polyclonal cell line	DMEM/10 % FBS, 1 µg/mL puromycin, 50 µg/mL hygromycin B
HEK^{ASC} + NLRP1 D1401R	H160	H1	NLRP1-HA D1401R	pRRL pUbC NLRP1-HA D1401R Hygromycin B	Transduction with lentivirus MOIs that permit multiple insertions, polyclonal cell line	DMEM/10 % FBS, 1 µg/mL puromycin, 50 µg/mL hygromycin B
HEK^{ASC} + NLRP1 T41A	H162	H1	NLRP1-HA T41A	pRRL pUbC NLRP1-HA T41A Hygromycin B	Transduction with lentivirus MOIs that permit multiple insertions, polyclonal cell line	DMEM/10 % FBS, 1 µg/mL puromycin, 50 µg/mL hygromycin B
HEK^{ASC} + NLRP1 S107A	H163	H1	NLRP1-HA S107A	pRRL pUbC NLRP1-HA S107A Hygromycin B	Transduction with lentivirus MOIs that permit multiple insertions, polyclonal cell line	DMEM/10 % FBS, 1 µg/mL puromycin, 50 µg/mL hygromycin B

HEK^{ASC} + NLRP1 T240A	H164	H1	NLRP1-HA T240A	pRRL pUbC NLRP1-HA T240A Hygromycin B	Transduction with lentivirus MOIs that permit multiple insertions, polyclonal cell line	DMEM/10 % FBS, 1 µg/mL puromycin, 50 µg/mL hygromycin B
HEK^{ASC} + NLRP1 S1371A	H166	H1	NLRP1-HA S1371A	pRRL pUbC NLRP1-HA S1371A Hygromycin B	Transduction with lentivirus MOIs that permit multiple insertions, polyclonal cell line	DMEM/10 % FBS, 1 µg/mL puromycin, 50 µg/mL hygromycin B
HEK^{ASC} + NLRP1 SP-AP TP-AP A107S	H172	H1	NLRP1-HA SP-AP TP-AP A107S	pRRL pUbC NLRP1-HA SP-AP TP-AP A107S Hygromycin B	Transduction with lentivirus MOIs that permit multiple insertions, polyclonal cell line	DMEM/10 % FBS, 1 µg/mL puromycin, 50 µg/mL hygromycin B
-	HFT9	HEK 293 Flp-In T-REx	NLRP1-SH	pEXPR TO FRT NLRP1-SH	Flp-In recombination after plasmid transfection	DMEM/10 % FBS, 50 µg/mL hygromycin B, 4 µg/mL blasticidin
-	HFT44	HEK 293 Flp-In T-REx	NLRX1-SH	pEXPR TO FRT NLRX1-SH	Flp-In recombination after plasmid transfection	DMEM/10 % FBS, 50 µg/mL hygromycin B, 4 µg/mL blasticidin
N/TERT-1 C1C-EGFP	K14	N/TERT-1	caspase-1^{CARD}-EGFP (C1C-EGFP)	pRRL pUbC caspase-1^{CARD}-EGFP Puro	Transduction with lentivirus MOIs that permit multiple insertions, polyclonal cell line	K-sfm (fully supplemented), 1 µg/mL puromycin

N/TERT-1 C1C-EGFP ΔASC (p)	K17	K14	sgRNA ASC #5 + Cas9	pLentiCRISPR v2 delta sgRNA ASC #5 Blasticidin	Transduction with lentivirus MOIs that permit multiple insertions, polyclonal cell line	K-sfm (fully supplemented), 1 µg/mL puromycin, 5 µg/mL blasticidin
N/TERT-1 C1C-EGFP ΔASC (m)	K17-1	K14	sgRNA ASC #5 + Cas9	pLentiCRISPR v2 delta sgRNA ASC #5 Blasticidin	Limiting dilution of polyclonal K17 cell line and selection of successful knockout clone	K-sfm (fully supplemented), 1 µg/mL puromycin, 5 µg/mL blasticidin
N/TERT-1 C1C-EGFP ΔNLRP1 (m)	K20-6	K14	sgRNA NLRP1 #2 + Cas9	pLentiCRISPR v2 delta sgRNA NLRP1 #2 Blasticidin	Limiting dilution of polyclonal K20 cell line and selection of successful knockout clone	K-sfm (fully supplemented), 1 µg/mL puromycin, 5 µg/mL blasticidin
N/TERT-1 C1C-EGFP Δp38α 1 (p)	K23	K14	sgRNA p38α #1 + Cas9	pLentiCRISPR v2 delta sgRNA p38α #1 Blasticidin	Transduction with lentivirus MOIs that permit multiple insertions, polyclonal cell line	K-sfm (fully supplemented), 1 µg/mL puromycin, 5 µg/mL blasticidin
N/TERT-1 C1C-EGFP Δp38α 2 (p)	K24	K14	sgRNA p38α #2 + Cas9	pLentiCRISPR v2 delta sgRNA p38α #2 Blasticidin	Transduction with lentivirus MOIs that permit multiple insertions, polyclonal cell line	K-sfm (fully supplemented), 1 µg/mL puromycin, 5 µg/mL blasticidin

N/TERT-1 C1C-EGFP Δp38β 1 (p)	K27	K14	sgRNA p38β #2 + Cas9	pLentiCRISPR v2 delta sgRNA p38β #2 Blasticidin	Transduction with lentivirus MOIs that permit multiple insertions, polyclonal cell line	K-sfm (fully supplemented), 1 µg/mL puromycin, 5 µg/mL blasticidin
N/TERT-1 C1C-EGFP Δp38β 2 (p)	K28	K14	sgRNA p38β #3 + Cas9	pLentiCRISPR v2 delta sgRNA p38β #3 Blasticidin	Transduction with lentivirus MOIs that permit multiple insertions, polyclonal cell line	K-sfm (fully supplemented), 1 µg/mL puromycin, 5 µg/mL blasticidin
N/TERT-1 (VHL-)VHH+C1C-EGFP	K44	N/TERT-1	VHL-VHH_{NP}-HA MB C1C-EGFP	pInducer20bi-NA VHL-VHH52-HA MB C1C-EGFP G418	Transduction with lentivirus MOIs that permit multiple insertions, polyclonal cell line	K-sfm (fully supplemented), 500 µg/mL geneticin
N/TERT-1 (VHL-)VHH+C1C-EGFP	K45	N/TERT-1	$VHH_{PYD\ 1}$-HA MB C1C-EGFP	pInducer20bi-NA VHH AF-F08a-HA MB C1C-EGFP G418	Transduction with lentivirus MOIs that permit multiple insertions, polyclonal cell line	K-sfm (fully supplemented), 500 µg/mL geneticin
N/TERT-1 (VHL-)VHH+C1C-EGFP	K46	N/TERT-1	VHL-$VHH_{PYD\ 1}$-HA MB C1C-EGFP	pInducer20bi-NA VHL-VHH AF-F08a-HA MB C1C-EGFP G418	Transduction with lentivirus MOIs that permit multiple insertions, polyclonal cell line	K-sfm (fully supplemented), 500 µg/mL geneticin
N/TERT-1 (VHL-)VHH+C1C-EGFP	K47	N/TERT-1	$VHH_{PYD\ 2}$-HA MB C1C-EGFP	pInducer20bi-NA VHH LJ-03-G12-HA MB C1C-EGFP G418	Transduction with lentivirus MOIs that permit multiple insertions, polyclonal cell line	K-sfm (fully supplemented), 500 µg/mL geneticin
N/TERT-1 (VHL-)VHH+C1C-EGFP	K48	N/TERT-1	VHL-$VHH_{PYD\ 2}$-HA MB C1C-EGFP	pInducer20bi-NA VHL-VHH LJ-03-G12-HA MB C1C-EGFP G418	Transduction with lentivirus MOIs that permit multiple insertions, polyclonal cell line	K-sfm (fully supplemented), 500 µg/mL geneticin

N/TERT-1 C1C-EGFP ΔZAKα 1 (p)	K63	K14	sgRNA ZAKα #1 + Cas9	pLentiCRISPR v2 sgRNA ZAKα 1 Neomycin	Transduction with lentivirus MOIs that permit multiple insertions, polyclonal cell line	K-sfm (fully supplemented), 1 µg/mL puromycin, 500 µg/mL geneticin
N/TERT-1 C1C-EGFP ΔZAKα 2 (p)	K64	K14	sgRNA ZAKα #2 + Cas9	pLentiCRISPR v2 sgRNA ZAKα 2 Neomycin	Transduction with lentivirus MOIs that permit multiple insertions, polyclonal cell line	K-sfm (fully supplemented), 1 µg/mL puromycin 500 µg/mL geneticin
N/TERT-1 C1C-EGFP ΔZAKα 3 (p)	K65	K14	sgRNA ZAKα #3 + Cas9	pLentiCRISPR v2 sgRNA ZAKα 3 Neomycin	Transduction with lentivirus MOIs that permit multiple insertions, polyclonal cell line	K-sfm (fully supplemented), 1 µg/mL puromycin 500 µg/mL geneticin
N/TERT-1 C1C-EGFP ΔTAOK2 1 (p)	K66	K14	sgRNA TAOK2 #1 + Cas9	pLentiCRISPR v2 sgRNA TAO 1 Neomycin	Transduction with lentivirus MOIs that permit multiple insertions, polyclonal cell line	K-sfm (fully supplemented), 1 µg/mL puromycin 500 µg/mL geneticin
N/TERT-1 C1C-EGFP ΔTAOK2 2 (p)	K67	K14	sgRNA TAOK2 #2 + Cas9	pLentiCRISPR v2 sgRNA TAO 2 Neomycin	Transduction with lentivirus MOIs that permit multiple insertions, polyclonal cell line	K-sfm (fully supplemented), 1 µg/mL puromycin 500 µg/mL geneticin

N/TERT-1 C1C-EGFP ΔTAOK2 3 (p)	K68	K14	sgRNA TAOK2 #3 + Cas9	pLentiCRISPR v2 sgRNA TAO 3 Neomycin	Transduction with lentivirus MOIs that permit multiple insertions, polyclonal cell line	K-sfm (fully supplemented), 1 µg/mL puromycin 500 µg/mL geneticin
N/TERT-1 C1C-EGFP ΔNLRP1 (m) + NLRP1	K100	K20-6	NLRP1-HA sg2 mut	pInducer20 NLRP1-HA sg2 mut	Transduction with lentivirus MOIs that permit multiple insertions, polyclonal cell line	K-sfm (fully supplemented), 1 µg/mL puromycin, 5 µg/mL blasticidin, 500 µg/mL geneticin
N/TERT-1 C1C-EGFP ΔNLRP1 (m) + NLRP1 S107A	K101	K20-6	NLRP1-HA S107A sg2 mut	pInducer20 NLRP1-HA S107A sg2 mut	Transduction with lentivirus MOIs that permit multiple insertions, polyclonal cell line	K-sfm (fully supplemented), 1 µg/mL puromycin, 5 µg/mL blasticidin, 500 µg/mL geneticin
N/TERT-1 C1C-EGFP ΔNLRP1 (m) + NLRP1 KR [PYD]	K102	K20-6	NLRP1-HA KR [PYD] sg2 mut	pInducer20 NLRP1-HA KR PYD sg2 mut	Transduction with lentivirus MOIs that permit multiple insertions, polyclonal cell line	K-sfm (fully supplemented), 1 µg/mL puromycin, 5 µg/mL blasticidin, 500 µg/mL geneticin